

**AQUEOUS PHASE REACTION KINETICS OF ORGANIC
SULFUR COMPOUNDS OF ATMOSPHERIC INTEREST**

A Dissertation
Presented to
The Academic Faculty

By

Lei Zhu

In Partial Fulfillment
of the Requirement for the Degree
Doctor of Philosophy in
the School of Earth and Atmospheric Sciences

GEORGIA INSTITUTE OF TECHNOLOGY

Nov. 2004

Aqueous Phase Reaction Kinetics of Organic Sulfur Compounds of Atmospheric Interest

Approved by:

Dr. Paul H. Wine, Advisor

Dr. Douglas Davis

Dr. Greg Huey

Dr. Athanasios Nenes

Dr. Rodney Weber

Dr. Robert Whetten

Date Approved: **Nov. 15th 2004**

To My Dearest Mother

And

Beloved Xiaobing

ACKNOWLEDGEMENTS

This work was sponsored by NSF through grants No. ATM-99-10912 and ATM-03-50185.

At first I must give the acknowledgement to my advisor Dr. Paul H. Wine, for providing me such a good topic for my PhD project, for offering his time to inspire me in both my research and my studies. The next person I would like to thank is Dr. J. Mike Nicovich for helping me so much in setting up my experiment and solving all the problems I encountered during my work. I should say without their kind help I could never have finished this work. I appreciate Dr. Athanasios Nenes for sharing the wonderful, state-of-the-art model with me to finish the last part of the thesis and for his great help during my thesis writing. I need also thank Dr. Bob Stickel for writing a very handy program for data collecting during my experiment.

I want to thank my thesis committee members: Drs. Douglas Davis, Greg Huey, Athanasios Nenes, Rodney Weber and Robert Whetten for being very accommodating and supportive throughout my time here.

Members of the Wine, Huey and Tan groups have been of great support for me during my graduate study. Special gratitude goes to former graduate students Edgar Estupinan and Rafal Strekowski; to my officemates Anne Case, Venus Dookwah, Carissa Howard, and Darlene Slusher; and to postdocs Patrice Bell and Raenell Soller. Thank you all for helping me in my English speaking and writing, for helping me overcome all

challenges since my first day here, and for sharing research and study experiences with me.

Finally I want to thank my family and friends who are always the most important in my life. Because of their friendship and love, my life becomes colorful and full of joy. I truly appreciate the faith they have in me, though I don't always feel deserving. But I do know one thing: Because of your support, I will overcome all the difficulties in my life.

TABLE OF CONTENTS

ACKNOWLEDGEMENTS.....	iv
TABLE OF CONTENTS.....	vi
LIST OF FIGURES	viii
LIST OF TABLES.....	xi
SUMMARY.....	xiii
CHAPTER I INTRODUCTION.....	1
Sulfur in the Atmosphere.....	1
Atmospheric DMS Cycling.....	6
DMS and Climate	19
Aqueous Kinetics of Organic Sulfur Species.....	25
CHAPTER II EXPERIMENTAL TECHNIQUES.....	32
Introduction.....	32
Experimental Approach	33
Chemicals and Solution Preparation.....	37
CHAPTER III TEMPERATURE DEPENDENT KINETICS STUDIES OF SO_4^- REACTIONS WITH DMSO, DMSO ₂ AND MS.....	39
SO_4^- in the Atmosphere	39
Experimental Method.....	42
Results and Discussion	47
CHAPTER IV TEMPERATURE DEPENDENT KINETICS STUDIES OF OH REACTIONS WITH DMSO, DMSO ₂ AND MS.....	66
OH Radicals in the Atmospheric Aqueous Phase.....	66
Experimental Method.....	69
Results and Discussion	75
Evaluation of Absolute Rate Coefficients.....	75
Possible Sources of Systematic Error	84
Comparison with Previous Work.....	86
Reaction Mechanisms	89
CHAPTER V KINETICS STUDIES OF $\text{Cl} \leftrightarrow \text{Cl}_2^-$ REACTIONS WITH DMSO, DMSO ₂ AND MS.....	92

Cl \leftrightarrow Cl $_2^-$ Radicals in the Atmospheric Aqueous Phase	92
Experimental Method.....	95
Results and Discussion	99
Kinetics of Cl \leftrightarrow Cl $_2^-$ degradation in Water.....	99
Kinetics of Cl \leftrightarrow Cl $_2^-$ Reactions with DMSO, DMSO $_2$ and MS.....	103
Kinetic and Spectroscopic Studies of the Aqueous Phase DMSO-Cl Adduct Radical	120
Analysis of Systematic Errors.....	136
CHAPTER VI KINETICS STUDIES OF METHANE SULFINATE (MSI) REACTIONS WITH OH AND Cl $_2^-$ RADICALS.....	141
Kinetics Studies of the OH + MSI Reaction.....	143
Determination of k_4 , k_5 , k'_7 and k'_8	146
Determination of k_3	154
Possible Sources of Systematic Errors.....	159
Reaction Mechanisms	161
Kinetics Studies of Cl \leftrightarrow Cl $_2^-$ Reactions with MSI	164
CHAPTER VII SUMMARY OF KINETICS STUDIES	170
CHAPTER VIII EFFECTS OF UPDATED AQUEOUS ORGANO-SULFUR CHEMISTRY ON SPECIATION AND PARTICULATE MS-TO-NSS RATIOS	174
Introduction.....	174
Model Description and Chemical Mechanism.....	179
Physical Description	179
Chemical Mechanism.....	182
Simulations	189
Simulation of the “Primary Scenario”	194
Contribution of Aqueous Phase Reactions to MS and NSS Production.....	198
Temperature Dependence of MS and NSS Production.....	205
Comparison of Stratocumulus and Cumulus Clouds	212
Comparison with Field Observations	220
CHAPTER IX SUMMARY AND CONCLUSIONS.....	228
Recommendations for Future Kinetics Studies.....	234
References.....	235

LIST OF FIGURES

Figure 1 An abbreviated atmospheric DMS oxidation scheme	11
Figure 2 A simplified representation of the CLAW Hypothesis, an example of a negative climate feedback loop.....	23
Figure 3 A simplified DMS cycling in the marine boundary layer atmosphere.....	24
Figure 4 Schematic diagram of the LFP-LPA apparatus.....	35
Figure 5 The absorption spectrum of SO_4^- from studies of Yu et al. (2004).....	45
Figure 6 Typical plots of $\ln(A)$ at 445 nm versus time in the study of the $\text{SO}_4^- +$ DMSO reaction at 293 K	51
Figure 7 Plots of k' versus $[\text{DMSO}]$ at $T = 278 \text{ K}$, 293 K and 308 K	52
Figure 8 Plot of initial and corrected (to 0 ionic strength) ($k' - k_{\text{bg}}$) vs. $[\text{MS}]$ at 293 K ...	53
Figure 9 Arrhenius plots for SO_4^- reactions with DMSO, DMSO2 and MS	61
Figure 10 Comparison of the Arrhenius plots of k_{diff} , k_{obs} and k_{react} for the DMSO $+ \text{SO}_4^-$ reaction	64
Figure 11 The absorption spectrum of $(\text{SCN})_2^-$ from Dogliotti and Hayon (1968)	73
Figure 12 Typical temporal profiles of $(\text{SCN})_2^-$ absorbance at 475 nm in the DMSO/ $\text{H}_2\text{O}_2/\text{SCN}^-$ system.....	74
Figure 13 Plots of A_0/A_R versus $[\text{R}]/[\text{SCN}^-]$ ($\text{R} = \text{DMSO}$, DMSO_2 or MS) for data obtained at $T = 298 \text{ K}$	77
Figure 14 Arrhenius plots for $\text{OH}(\text{aq})$ reactions with DMSO, DMSO2 and MS	79
Figure 15 Arrhenius plots of k_{obs} , k_{diff} and k_{react} for the DMSO + OH reaction	83
Figure 16 The absorption spectra of Cl_2^- (Yu et al., 2004) and Cl (Wicktor et al., 2003).....	98
Figure 17 Temporal absorption profiles detected at 340 nm in the $\text{S}_2\text{O}_8^{2-}/\text{Cl}^-/\text{water}$ $/h\nu$ system	104
Figure 18 Plot of measured first order decay rates (k'_{measured}) versus $[\text{Cl}^-]$ in the studies of Cl and Cl_2^- reactions with water	105

Figure 19 Temporal profiles of absorbance at 340 nm in the $S_2O_8^{2-}/Cl^-/DMSO$ system	106
Figure 20 Plots of $k' - k'_0$ versus [DMSO] and [DMSO2] for different $[Cl^-]$	109
Figure 21 Comparison of original k_{MS} and that after corrected to 0 ionic strength	117
Figure 22 Plot of measured k_{DMSO} vs. $[Cl^-]$	118
Figure 23 Temporal profiles of detected absorbance at 430 nm in the $S_2O_8^{2-}/Cl^-/DMSO/h\nu$ system.....	122
Figure 24 Plots of maximum absorbance (A_{peak}) at 430 nm vs. [DMSO]	123
Figure 25 Temporal profiles of detected absorbance at 430 nm in the $S_2O_8^{2-}/Cl^-/DMSO/h\nu$ system.....	124
Figure 26 Plot of A_0/A at 430 nm versus $1/[Cl^-]$ in the studies of $DMSO^+ + Cl^- \leftrightarrow DMSO-Cl$	127
Figure 27 Absorption spectrum of the DMSO-Cl adduct determined from this work (top) and from Kishore and Asmus, 1991 (bottom).....	135
Figure 28 Typical temporal profiles of $(SCN)_2^-$ absorbance observed at 475 nm and fits of exponential decay of radicals	148
Figure 29 Plots of measured pseudo-first-order decay rates ($k'_{measured}$) versus [MSI] ...	150
Figure 30 Plot of S and I versus $[SCN^-]$	151
Figure 31 Analytical fits of $(SCN)_2^-$ absorbance at 475 nm using the two-parameter fitting routine	155
Figure 32 Plots of a_3 versus [MSI] at $[SCN^-] = 3.0 \times 10^{-5}$ M (red) and 3.3×10^{-6} M (black)	158
Figure 33 Plots of $k' - k'_0$ versus [MSI] at all $[Cl^-]$ studied.....	167
Figure 34 Lagrangian trajectories derived from the LES used to “drive” the cloud parcel model for (a) stratocumulus clouds and (b) cumulus clouds.....	181
Figure 35 Average liquid water content for (a) 1-hour simulation of the stratocumulus cloud, and (b) 30-minute simulation of the cumulus cloud considered.....	193
Figure 36 Vertical profiles of (a) DMSO(g), (b) SO_2 (g), (c) MS(aq) and (d) NSS(aq) after 1, 5, 10, and 15 simulation cycles of the “primary scenario”.....	196

Figure 37 Temporal evolution of (a) DMSO(g), (b) DMSO(aq), (c) SO ₂ (g), (d) MS(aq), (e) NSS(aq) and (f) MS/NSS from the simulations of the “primary scenario”	197
Figure 38 Temporal evolution of (a) MS, (b) NSS and (c) MS/NSS for simulations of the “primary scenario” at different temperatures	209
Figure 39 Temporal evolution of (a) DMSO(g), (b) DMSO(aq) and (c) SO ₂ (g) for simulations of the “primary scenario” at different temperatures	210
Figure 40 Vertical distribution of (a) MS, (b) NSS and (c) MS/NSS after 15 simulation cycles of the ASTEX-1(red) and the ASTEX-2 (blue) cloud	214
Figure 41 Temporal evolution of (a) MS, (b) NSS and (c) MS/NSS for simulations of ASTEX-1 (red) and ASTEX-2 (blue).....	215
Figure 42 Temporal evolution of MS (a), NSS (b) and MS/NSS (c) for simulations of CF-Cloud (green) and ASTEX-1 (red).....	219

LIST OF TABLES

Table 1	Estimated global emissions of important sulfur species.....	3
Table 2	Observed concentrations of important atmospheric sulfur gases (pptv).....	5
Table 3	Important radical oxidants for gas phase DMS in the marine boundary layer atmosphere	10
Table 4	Henry's Law Constants for the sulfur species of atmospheric interest.....	22
Table 5	Comparison of reported Extinction Coefficients of SO_4^- ($\epsilon_{\text{SO}_4^-}$) around 440 nm	46
Table 6	Summary of kinetic data for the $\text{DMSO} + \text{SO}_4^-$ reaction (R3-11).....	55
Table 7	Summary of kinetic data for the $\text{DMSO}_2 + \text{SO}_4^-$ reaction (R3-12).....	57
Table 8	Summary of kinetic data for the $\text{MS} + \text{SO}_4^-$ reaction (R3-13).....	59
Table 9	Rate coefficient ratios ($k_{\text{R}}/k_{\text{SCN}^-}$) determined in this study	78
Table 10	Summary of k_{obs} , k_{diff} and k_{react} for the $\text{DMSO} + \text{OH}$ reaction at all studied temperatures in units of $10^9 \text{ M}^{-1} \text{ s}^{-1}$	82
Table 11	Comparison of 295 K rate coefficients obtained in this study with literature values	88
Table 12	Summary of measured rate coefficients (k_{R}) for the reactions of $\text{Cl} \leftrightarrow \text{Cl}_2^-$ with water, DMSO, DMSO ₂ and MS.....	107
Table 13	Summary of kinetics results on the $(\text{Cl} \leftrightarrow \text{Cl}_2^-) + \text{R}$ reactions	110
Table 14	Summary of the kinetics data obtained at 430 nm in DMSO-Cl studies.....	132
Table 15	Reference extinction coefficients of SO_4^- and $\epsilon_{\text{DMSO-Cl}} / \epsilon_{\text{SO}_4^-}$ ratios obtained from this work.....	133
Table 16	Comparison of $A_0 / A_{\text{Cl}_2^-}$ and $\epsilon_{\text{SO}_4^-} / \epsilon_{\text{Cl}_2^-}$ at all wavelengths studied.....	140
Table 17	Literature values of k_1 , k_2 and K_2 at room temperature.....	152
Table 18	Summary of the kinetics results from the two-parameter fitting routine.....	156

Table 19 Measured rate coefficients for $\text{MSI} + \text{Cl} \leftrightarrow \text{Cl}_2^-$ at different $[\text{Cl}^-]$	166
Table 20 Summary of kinetic data at $295 \pm 1 \text{ K}$	172
Table 21 Gas phase kinetic mechanism	184
Table 22 Aqueous phase kinetic mechanism	185
Table 23 Acid-base equilibria for aqueous phase species	186
Table 24 Henry's Law's constant (H) and Mass Accommodation Coefficient (α) for semi-volatile species	187
Table 25 Concentrations of steady-state radicals used in the simulation	188
Table 26 Production yields of $\text{SO}_2(\text{g})$, $\text{DMSO}(\text{g})$ (pptv) and aqueous phase MS and NSS (pmol m^{-3}) after 15 simulation cycles for scenarios (1), (2), (3), (4), (5) and (6)	204
Table 27 Contributions of aqueous phase reactions to MS and NSS production for simulations of the "primary scenario" at different temperatures	211
Table 28 Change of of MS, NSS and MS/NSS due to the $\text{MS} + \text{OH}$ reaction for simulations of the "primary scenario" at different temperatures	211
Table 29 Examples of field measurements of DMS, SO_2 (pptv), MS, NSS (nmol m^{-3}) and MS/NSS in the marine atmosphere	227
Table 30 Estimated lifetimes of DMSO, DMSO_2 , MSI and MS at 295 K.....	230

SUMMARY

Dimethyl Sulfide (CH_3SCH_3 , DMS) is the most important reduced sulfur compound emitted from the ocean into the atmosphere. It has been proposed that the oxidation of DMS in the atmosphere could play an important role in climate modification because several products from DMS oxidation are highly non-volatile and could participate in particle formation and growth processes, thus affecting the albedo of the atmosphere and the solar radiation budget at the Earth's surface. Also the observed MS (methanesulfonate)-to-NSS (non-seasalt sulfate) ratios in aerosols have been used to evaluate the contribution of DMS to the global sulfur burden because MS is believed to be generated primarily from DMS oxidation while NSS has multiple sources. While DMS oxidation has been of great interest to atmospheric scientists for several decades, most of the work has focused on gas phase studies. Hence the kinetics database for aqueous phase transformations is rather limited, although it has been demonstrated by numerous field observations and model studies that aqueous phase reactions are potentially important for understanding MS and NSS production from DMS and the atmospheric sulfur cycle.

In this work, a laser flash photolysis (LFP) – long path UV-visible absorption (LPA) technique was employed to investigate the kinetics of the aqueous phase reactions of four important stable organic sulfur compounds produced from DMS oxidation, i.e., dimethyl sulfoxide (DMSO), dimethyl sulfone (DMSO_2), methanesulfinate (MSI) and

methanesulfonate (MS). Kinetics studies of the reactions of these organic sulfur compounds with four important aqueous phase radicals, OH, SO₄⁻, Cl and Cl₂⁻, are presented in this dissertation. The temperature dependent kinetics of the OH and SO₄⁻ reactions with DMSO, DMSO₂ and MS were studied for the first time. OH radical is found to be the most reactive, while Cl₂⁻ radical is the least reactive toward all the sulfur species studied. The less oxidized species DMSO and MSI are found to be more reactive than the more oxidized species DMSO₂ and MS for each radical. The rate coefficients in units of M⁻¹ s⁻¹ at 295 K are found to be $(6.4 \pm 0.5) \times 10^9$, $(6.3 \pm 0.6) \times 10^9$, $(3.2 \pm 0.3) \times 10^9$, and $(1.6 \pm 0.8) \times 10^7$, for reactions of DMSO with OH, Cl, SO₄⁻ and Cl₂⁻; $(7.7 \pm 0.7) \times 10^9$ and $(8.0 \pm 1.0) \times 10^8$ for MSI reactions with OH and Cl₂⁻ radicals; $(1.7 \pm 0.2) \times 10^7$, $(8.2 \pm 1.6) \times 10^5$, $(3.8 \pm 0.4) \times 10^6$, and $(8.2 \pm 5.5) \times 10^3$ for reactions of DMSO₂ with OH, Cl, SO₄⁻ and Cl₂⁻; and $(1.2 \pm 0.2) \times 10^7$, $(4.9 \pm 0.2) \times 10^5$, $(1.0 \pm 0.2) \times 10^4$, and $(4.8 \pm 0.8) \times 10^3$ for reactions of MS with OH, Cl, SO₄⁻ and Cl₂⁻. Activation energies in units of kJ mol⁻¹ are found to be 11.6 ± 0.8 , 11.3 ± 1.3 , and 20.7 ± 4.3 for SO₄⁻ reactions with DMSO, DMSO₂ and MS, and 10.6 ± 0.3 , 14.1 ± 0.4 , and 21.9 ± 0.3 for OH reactions with DMSO, DMSO₂ and MS. All uncertainties reported above are 2σ and represent precision only. The absorption spectrum of the DMSO-Cl adduct generated from the DMSO + Cl₂⁻ reaction was studied and the peak extinction coefficient was found to be $\sim 5760 \text{ M}^{-1} \text{ cm}^{-1}$ at $\lambda_{\text{max}} \approx 390 \text{ nm}$.

The kinetics data obtained from this work are employed in a Trajectory Ensemble Model to simulate DMS oxidation in the marine atmosphere as a means of assessing the contribution of aqueous phase reactions to the growth of particulate matter and to control of MS/NSS ratios. For the first time, aqueous phase oxidation of organic sulfur

compounds by SO_4^- , Cl and Cl_2^- is included in the model to simulate DMS chemistry. Our simulations suggest that Cl_2^- -initiated oxidation of methanesulfinate (MSI) is the dominant source of MS in particles and accounts for 65% of MS production; while $\text{OH} + \text{MSI}$ contributes 25% to total MS in the condensed phase. Our simulations also suggest that aqueous phase reactions of the sulfur compounds contribute about 97% of MS and 91% of NSS in particles at 300 K. Aqueous phase reactions of the organic sulfur compounds could contribute about 30% to total particle mass growth during 3 days of in-cloud processing. When the temperature dependent kinetic data for the $\text{MS} + \text{OH}$ reaction obtained in this work was used in the model, it was found that $\text{MS} + \text{OH}$ could consume 20% of MS and produce 8% of NSS, thereby changing the MS/NSS ratio by about 25%, within 3 days under typical marine atmospheric conditions.

CHAPTER I

INTRODUCTION

Sulfur in the Atmosphere

Sulfur compounds play an important role in the environment and in the climate. The volatile sulfur emitted into the atmosphere can be transformed into highly oxidized, non-volatile species, such as sulfuric acid, which could be involved in the formation of new aerosols or the growth of pre-existing particles. Within the boundary layer these aerosols could reduce visibility and enter the respiration system to harm human health; additionally, the aerosols serve as cloud condensation nuclei and cause severe acidic rain in some polluted areas; the aerosols also impact the backscattering of the solar radiation and affect the cloud albedo. In the stratosphere, these particles provide surfaces for heterogeneous chemical reactions, which convert inactive halogens (HCl, HBr, ClONO₂, BrONO₂) into HOCl, HOBr, Cl₂, Br₂, and BrCl, which are photolytic precursors to Cl, ClO, Br, and BrO. These radicals play important roles in catalytic cycles that destroy stratospheric ozone (Molina et al., 1996 and references therein).

Atmospheric sulfur species are normally divided into two categories based on their sources: anthropogenic and natural. Anthropogenic emissions are currently thought

to be the more important source of sulfur in the atmosphere. Important anthropogenic sources include fossil fuel combustion, coal refining and ore smelting for SO_2 as well as automobiles, chemical industry and sulfur recovery processes for of OCS and CS_2 . Natural emissions of SO_2 are mainly from volcanoes and biomass burning, while the biosphere and oceans are dominant natural sources for H_2S , OCS, dimethyl sulfide (DMS), and CS_2 (Chin and Davis 1993; Berresheim et al., 1995; Pham et al., 1995). Fluxes of each species from their specific sources as well as the total sulfur emissions have been widely studied. Estimates of the total global sulfur flux range from ~80 to over 150 Tg S/yr (Warneck 1988; Langner and Rodhe 1991; Andreae and Jaeschke 1992; Bates et al., 1992; Spiro et al., 1992; Penner et al., 1994; Pham et al., 1995; Chin and Jacob 1996; Lelieveld et al., 1997). Table 1 lists results from a study by Pham et al. (1995), which basically represents the current understanding of the global sulfur emission inventory. Based on the above-mentioned studies, the global anthropogenic emissions of sulfur species are relatively well quantified and are estimated to range from 71 to 103 Tg S/yr with an average of about 90 Tg S/yr. Large uncertainties remain in the flux of sulfur to the atmosphere from natural sources, especially from the ocean and the tropical biosphere, which are the most important natural sources of atmospheric H_2S , DMS, OCS and CS_2 . As listed in Table 1, DMS is the most abundant natural reduced sulfur species and its primary source is emission from the ocean. Estimates of DMS flux vary by nearly a factor of 5 from 12 to 58 Tg S/yr, and current wisdom suggests an average global DMS flux from the ocean of the order of 15-20 Tg S/yr (Erickson et al., 1990; Bates et al., 1992).

Table 1 Estimated global emissions of important sulfur species

Sources	SO ₂	H ₂ S	OCS	DMS	CS ₂	Total
Volcanoes	9.2	—	—	—	—	9.2
Biosphere	—	0.52	0.35	0.3	0.0064	1.18
Biomass Burning	2.9	—	0.11	—	—	3
Ocean	—	—	0.30	19.2	0.2	19.7
Man-made	92	—	0.07	—	0.3	92.4
Total	104.1	0.52	0.83	19.5	0.5	125.5

After Pham et al. (1995).

Numerous atmospheric concentration measurements of sulfur species have been carried out and have found that the mixing ratios change dramatically with time, latitude, climate parameters and location. Table 2 lists the widely accepted average concentrations for the most important sulfur gases in the atmosphere generalized from the work of Berresheim et al. (1995) and Lelieveld et al. (1997). The atmospheric concentration of a sulfur species depends on its source strength, transport, reactivity and deposition velocity. In the most polluted urban areas SO_2 is the dominant species with mixing ratios ranging from ~ 100 pptv to over several hundred ppbv, while in the unpolluted marine boundary layer SO_2 concentrations drop to less than one hundred pptv. DMS is the primary species in the marine boundary layer due to large emissions from the ocean. Relatively reactive species, such as DMS, H_2S and CS_2 , are oxidized within the boundary layer and have low concentrations in areas far away from their emission sources and in the free troposphere. OCS is the most abundant sulfur gas in the global background atmosphere because of its low reactivity in the troposphere and its correspondingly long residence time (global atmospheric lifetime of ~ 7 years). It is the only sulfur compound that survives to enter the stratosphere, with an exception of the direct injection of SO_2 into the stratosphere in volcanic eruptions. The input of OCS into the stratosphere is considered to be responsible for the maintenance of the background stratospheric sulfate aerosol layer (Chin and Davis 1993; Seinfeld and Pandis 1998).

Table 2 Observed concentrations of important atmospheric sulfur gases (pptv)

Species	Marine air	Remote continental	Urban continental	Free troposphere
DMS	<10 – 2000	<1 – 500	2 - 560	< 0.1 – 15
SO ₂	<4 – 160	70 - 200	100 - 10000	10 - 300
H ₂ S	<0.4 – 75	5 – 6400	80 – 810	1 – 140
CS ₂	1 – 420	5 – 560	65 – 370	1 – 170
OCS	400 – 800	500 - 7000	300 – 1800	510 ± 60

After Berresheim et al. (1995) and Lelieveld et al. (1997).

Atmospheric DMS Cycling

About 90% of anthropogenic sulfur emissions occur in the northern hemisphere; the other 10% contribution from southern latitudes accounts for roughly half the total atmospheric sulfur budget in the Southern Hemisphere (Langner and Rodhe 1991), because the ocean, which is the largest source of natural sulfur into the atmosphere, covers more than 80% of the total surface areas of the southern hemisphere. As mentioned earlier, DMS is the most important natural sulfur species emitted from the ocean to the atmosphere and it accounts for almost half of the total sulfur flux in the southern hemisphere. Currently, there is considerable interest in understanding the transport and atmospheric oxidation of DMS for several reasons. First, it facilitates our understanding of past climate as interpreted from ice core data analyses: It is thought that the release of DMS from the ocean and its oxidation are both affected by climate, so records of sulfur species concentrations in ice cores could be used to infer past climatic conditions. Second, it facilitates the current understanding of the role sulfur compounds play in particle formation and growth in the atmosphere and its impact on current and future climate: The products from DMS oxidation are relatively non-volatile and could be involved in the formation and growth of atmospheric aerosols, which are important in affecting climate. The third is the use of field observations of MS-to-NSS ratios (MS \equiv methanesulfonate, $\text{CH}_3(\text{O})\text{S}(\text{O})\text{O}^-$; NSS \equiv non-sea-salt sulfate) to infer the relative amounts of natural versus anthropogenic sulfur in atmospheric particulate matter: In theory, the NSS observed in marine aerosols could represent any mixture of possible gas

phase precursor origins, i.e., oxidation of anthropogenic SO₂, oxidation of DMS (or other natural reduced sulfur species), and volcanic sulfur emissions, whereas MS is thought to originate exclusively from the oxidation of DMS.

DMS was first discovered in the surface ocean by Lovelock et al. in 1972 (Lovelock et al., 1972). As early as 1948, Challenger reported DMS production from the decomposition of dimethyl-sulfoniopropionate (DMSP), which is released by planktonic marine organisms (Challenger and Simpson 1948). DMS concentrations in sea water have been measured widely and the results show substantial variability, both in space and in time. In particular, seasonal studies of oceanic DMS concentrations (Bates et al., 1987; Turner et al., 1988; Leck et al., 1990; Nguyen et al., 1990; Berresheim et al., 1991; Turner et al., 1996a; Turner et al., 1996b; Dacey et al., 1998) have shown that average surface seawater DMS concentrations can vary by as much as a factor of 50 between summer and winter in the mid and high latitudes. Overall, DMS concentrations in sea water measured from different studies range from <1 nM in winter to over 15 nM in summer (Holligan et al., 1987; Turner et al., 1988; Berresheim et al., 1998; De Bruyn et al., 1998; Kettle et al., 1999; Putaud et al., 1999). DMS is removed from sea water mainly through bacterial consumption, photochemical oxidation and sea-air exchange (Liss et al., 1997). The first two processes account for more than 90% of the total DMS consumption and mainly will result in the recycling of DMS in the ocean, while the later process leads to the release of DMS into the atmosphere.

Given such high concentration levels of DMS in surface sea water, very low average atmospheric concentrations of 80-110 ppt (Seinfeld and Pandis 1998), and a low Henry's law constant (De Bruyn et al., 1995), a huge DMS flux from the ocean to the

atmosphere is generated. The sea-air exchange of DMS is a function of gas transfer velocity and surface seawater DMS concentration. The gas transfer velocity is controlled primarily by surface turbulence, seawater temperature, gas diffusivity and surface windspeed (Liss and Merlivat 1986; Wanninkhof 1992). The mixing ratio of DMS in the marine boundary layer has been widely studied since the first demonstration of this species in the marine atmosphere and it was found that the atmospheric DMS concentration varies dramatically with season and location (Berresheim et al., 1993; Berresheim et al., 1998; Davis et al., 1998; De Bruyn et al., 1998; Putaud et al., 1999; Ayers and Gillett 2000; Sciare et al., 2000c; Jourdain and Legrand 2001; Legrand et al., 2001; Nowak et al., 2001) due to the large variability in the ocean surface DMS concentration, as well as the parameters affecting the DMS sea-to-air flux. DMS mixing ratios in the atmosphere could reach 2 ppb over eutrophic waters because of rapid production *via* the phytoplanktonic activity in these areas. However, in the continental boundary layer, DMS mixing ratios are normally lower than 100 ppt. In the free troposphere DMS mixing ratios drop to <15 ppt because DMS is readily oxidized by the radicals within the boundary layer and, once transferring across the sea-air interface, it has a short atmospheric lifetime of 1-2 days.

In the marine atmosphere, OH radicals were thought to be predominantly responsible for DMS oxidation during daytime, but at night DMS is most likely to be consumed by NO₃ radicals (Barnes et al., 1989; Hynes and Wine 1989; Butkovskaya and Lebras 1994; Barone et al., 1996; Sorensen et al., 1996; Turnipseed et al., 1996; Patroescu et al., 1999). However, these ideas have become less and less supported as more and more studies were carried out. Some recent studies have shown that Cl and

BrO radicals may also play significant roles in DMS oxidation under specific atmospheric conditions (Toumi 1994; Butkovskaya et al., 1995; Spicer et al., 1998; Ingham et al., 1999; Urbanski and Wine 1999; Diaz-de-Mera et al., 2002). In addition, reaction with O₃ at the air/water interface may be an important atmospheric DMS removal process (Lee and Zhou 1994; Gershenzon et al., 2001). In order to assess the importance of the above-mentioned radicals in DMS oxidation, their typical atmospheric radical concentrations, radical + DMS reaction rate coefficients, and resulting DMS lifetimes toward reactions with these radicals are summarized in Table 3. Due to wide variations of radical concentrations in the atmosphere, all these radicals are potentially important for DMS oxidation under certain conditions.

Although the initial steps of DMS oxidation by the above radicals are well documented, the atmospheric fate of intermediates produced from the initial reactions and subsequent reactions which result in stable end products are very complicated and not well understood yet. Figure 1 presents an abbreviated atmospheric DMS oxidation scheme including both gas and aqueous phase transformations. The gas phase mechanism is a simplified and updated adaptation of the one proposed by Davis et al. (1999). Aqueous phase reactions in the scheme are from the present study and other published kinetic and mechanistic studies (Veltwisch et al., 1980; Milne et al., 1989; Olson and Fessenden 1992; Sehested and Holcman 1996; Flyunt et al., 2001; Bardouki et al., 2002). The dashed lines represent transformations that remain speculative, and question marks represent reactions with unknown branching ratios or product yields.

Table 3 Important radical oxidants for gas phase DMS in the marine boundary layer atmosphere

Radicals	Conc. (molecule cm ⁻³)	<i>k</i> at 298 K (cm ³ molecule ⁻¹ s ⁻¹)	$\tau_{\text{(DMS)}}$ (hours)
OH	^a (0.5 – 5)×10 ⁶	^b 6.5×10 ⁻¹²	8 - 80
NO ₃	^c (5 - 250)×10 ⁶	^b 1.1×10 ⁻¹²	1-50
Cl	^d (0.1 - 10)×10 ⁴	^b 5.5×10 ⁻¹⁰	5-500
BrO	^e (0.5 - 10)×10 ⁷	^b 4.4×10 ⁻¹³	6-126

^a (Davis et al., 1999);

^b (Atkinson et al., 2001);

^c (Carslaw et al., 1997);

^d (Vogt et al., 1996; Spicer et al., 1998);

^e (Sander and Crutzen 1996; Vogt et al., 1996)

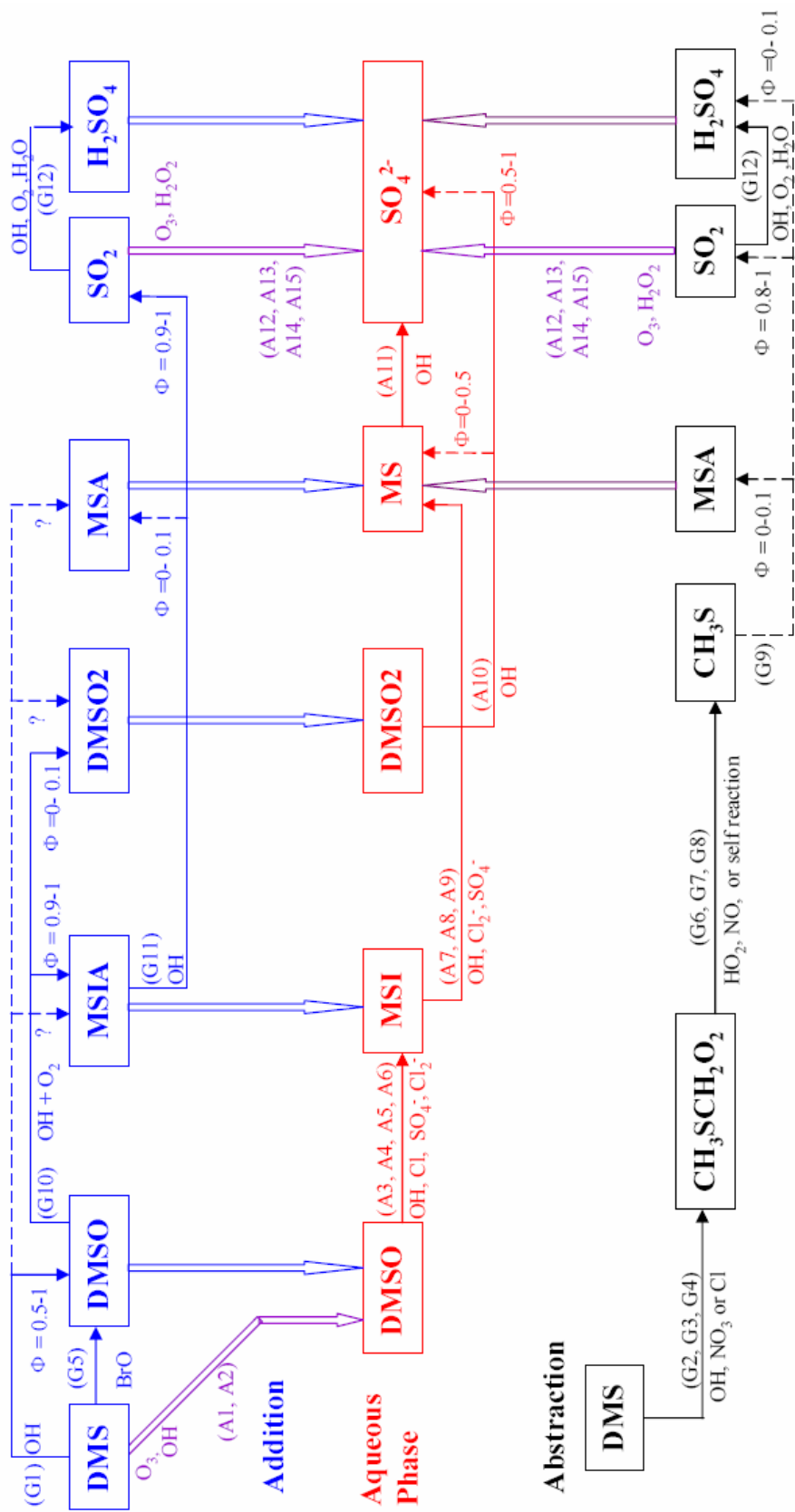


Figure 1 An abbreviated atmospheric DMS oxidation scheme

Chemical notations are the same as in the text. The dashed lines represent those mechanisms still elusive or from speculations, and question marks represent reactions with unknown branching ratios or product yields. The reactions in black and blue are abstraction and addition channels of gas phase DMS oxidation, respectively; the reactions in red are aqueous phase reactions and those in purple represent the heterogeneous reactions.

In the gas phase, the DMS oxidation process begins through either the addition of radicals to the central sulfur atom (for OH, Cl and BrO, shown as blue fonts) or by the H-abstraction from the methyl group (for OH, NO₃ and Cl, shown as black fonts).

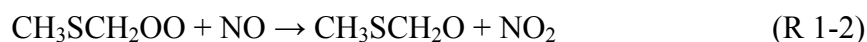
OH + DMS is the most studied DMS reaction and it has been demonstrated that OH-induced oxidation of DMS proceeds through both addition and abstraction channels. The OH + DMS addition reaction is O₂-dependent, because the reaction of O₂ with the DMS-OH adduct competes with adduct decomposition to regenerate OH and DMS (Hynes et al., 1986; Hynes et al., 1995; Barone et al., 1996; Turnipseed et al., 1996). While the abstraction channel of the OH + DMS reaction is O₂-independent, the CH₃SCH₂ radical produced after H-abstraction reacts rapidly with O₂ to produce CH₃SCH₂OO, which will be discussed in detail later. The abstraction channel dominates the OH + DMS reaction at room temperature, and the addition channel is favored at lower temperature (Hynes et al., 1986; Williams et al., 2001).

Even though the NO₃ + DMS reaction rate coefficient is lower than that for the OH + DMS reaction, NO₃-induced oxidation of DMS at night is thought to be important due to the accumulation of NO₃ after sunset. Studies of Vrekoussis et al. (2004) have claimed that the loss of DMS by NO₃ during night is about 75% of that by OH radical during daytime. The NO₃ + DMS reaction mechanism has been well studied and there is strong evidence that H-transfer is the only important channel (Dlugokencky and Howard 1988; Daykin and Wine 1990; Tyndall and Ravishankara 1991; Jensen et al., 1992; Butkovskaya and Lebras 1994; Langer et al., 1996) and the reaction gets faster at lower temperatures (Dlugokencky and Howard 1988).

The importance of Cl atom in oxidizing DMS in the remote marine boundary layer is a subject of ongoing debate. Two model studies quantifying contributions of the Cl + DMS reaction to DMS removal give consistent estimates: Davis et al. (1999) indicated that the Cl reaction constitutes 5-10% of DMS removal in the remote equatorial Pacific boundary layer, and Singh et al. (1996) concluded that Cl atoms account for no more than 3% of total DMS removal on a global average. Like the OH reaction with DMS, the Cl + DMS reaction also proceeds *via* two distinct channels: pressure-independent hydrogen abstraction channel and pressure-dependent addition channel. Studies of Stickel et al. (1992) and Butkovskaya & LeBras (1995) both found that the abstraction channel is dominant to produce HCl and CH₃SCH₂ with yields of unit as the pressure approaches zero, but accounts for only 40-50% at one atmosphere pressure and room temperature. In some later studies (Langer et al., 1996; Zhao et al., 1996; Urbanski and Wine 1999; Enami et al., 2004), production of the DMS-Cl adduct and its fragmentation radicals, i.e., CH₃Cl, CH₃S, CH₃, were observed. Though possible decays of DMSO-Cl due to photolysis, thermal decomposition, as well as its reactions with some possible oxidants, such as NO, NO₂ and O₂, were studied (Urbanski and Wine 1999; Enami et al., 2004), the atmospheric fate of this adduct is not well understood yet.

Some recent studies have found that BrO is another potentially important oxidant to remove DMS from the marine boundary layer atmosphere, and indicated that the BrO + DMS reaction proceeds primarily *via* the CH₃S(BrO)CH₃ intermediate adduct (Barnes et al., 1991; Bedjanian et al., 1996; Ingham et al., 1999; Nakano et al., 2001) and produce dimethylsulfoxide (DMSO) with a high yield.

As mentioned above, the intermediate produced from the first step of DMS oxidation *via* the abstraction channel is the CH₃SCH₂ radical. It has been demonstrated that CH₃SCH₂ reacts rapidly with O₂, and the following mechanism has been proposed and validated by laboratory investigations (Wallington et al., 1993; Butkovskaya and Lebras 1994; Turnipseed et al., 1996; Urbanski et al., 1997):



Because of the efficient scavenging of CH₃SCH₂ by O₂ (R1-1) and fast decomposition of CH₃SCH₂O through R1-3, these two radicals were ignored in the scheme shown in Figure 1 to simplify the mechanism. In the marine boundary layer, NO concentrations are typically very low (<10 pptv) and reactions with other species, such as HO₂ or RO₂, may represent important degradation pathways for CH₃SCH₂OO. By analogy with the oxidation processes of other alkyl peroxy radicals, the CH₃SCH₂OO + HO₂ reaction will produce CH₃SCH₂OOH with a high yield, which photolyzes or reacts with OH radicals to produce CH₃S radicals (by analogy with CH₃OOH decay in the atmosphere) (Lightfoot et al., 1992; Wallington et al., 1992; Butkovskaya et al., 1995; Urbanski et al., 1997; Tyndall et al., 2001). Further studies on the CH₃SCH₂OO + HO₂ reaction are necessary to facilitate our understanding of the production of CH₃S, which is an important intermediate during DMS oxidation. The fate of CH₃S in the atmosphere is believed to hold an important key to the eventual formation of end products such as SO₂ (important precursor of sulfuric acid), sulfuric acid and methane sulfonic acid (MSA).

Unfortunately, the studies of CH₃S oxidation in the atmosphere are far from being able to show a complete picture of the mechanism. Some studies find that O₃, NO₂, O₂ and HO₂ might play important roles in the oxidation of CH₃S and subsequent intermediates (e.g., CH₃SO, CH₃SO₂, CH₃SO₃) to produce the final products SO₂, H₂SO₄ and MSA, (Tyndall and Ravishankara 1989a; 1989b; Turnipseed et al., 1993; Martinez et al., 1999; 2000), while the detailed mechanisms are needed for understanding the ratio of MS to NSS from DMS oxidation. Of special interest, the CH₃S → H₂SO₄ reaction without going through SO₂ would, if it occurred, make DMS oxidation a much more important source of new particles in the marine atmosphere.

While the BrO + DMS reaction produces DMSO as the dominant product, as mentioned earlier, studies found that the reaction of the OH + DMS adduct with O₂ appears to produce DMSO with a yield of only 50% - 100% (Hynes et al., 1993; Barnes et al., 1994; Sorensen et al., 1996; Turnipseed et al., 1996; Arsene et al., 1999; Patroescu et al., 1999; Arsene et al., 2001), although all of these studies have confirmed that the DMSO yield is quite substantial. The studies of Arsene et al. (1999; 2001) showed that the DMSO product yield from DMS oxidation by OH is sensitive to the NO concentration and the absolute yield of DMSO under atmospheric conditions is still uncertain. The other up to 50% yield of the DMSO + OH reaction remains un-identified to date; dimehtylsulfone (DMSO₂), SO₂, methane sulfinic acid (MSIA) and MSA are all quite possibly produced from further oxidation of DMS-OH by O₂ and NO_x, and all have been observed in some smog chamber studies of products (Sorensen et al., 1996; Turnipseed et al., 1996; Arsene et al., 1999; Patroescu et al., 1999).

The only identified product from the OH + DMS addition channel, DMSO, is oxidized by OH radicals with a rate coefficient approximately 15 times faster than the OH + DMS reaction: $k_{\text{DMSO}+\text{OH}} \sim 9.4 \times 10^{-11}$ (Hynes and Wine 1996; Kukui et al., 2003) compared to $k_{\text{DMS}+\text{OH}} \sim 6.5 \times 10^{-12}$ (Hynes et al., 1986) in units of $\text{cm}^3 \text{ molecule}^{-1} \text{ s}^{-1}$. Different from the DMS + OH reaction, several recent studies strongly support that the DMSO + OH reaction proceeds primarily *via* the addition of OH to sulfur, followed by rapid methyl elimination to produce MSIA in high yield (Urbanski et al., 1998; Arsene et al., 2002; Kukui et al., 2003). However, in some earlier studies of Barnes et al. (1989) and Sorensen et al. (1996) significant yields of SO₂ and DMSO₂ were observed. In the studies of Arsene et al. (2002) production of SO₂, DMSO₂ and MSA were also observed, but pronounced delays were found in the formation of these species when compared to that of MSIA; such results show that these compounds are not main primary products of the DMSO + OH reaction, instead, they are formed from the secondary reactions. As analyzed by Arsene et al. (2002), the different experimental conditions and sampling methods employed by these authors are possibly responsible for the apparent discrepancy. It is expected that MSIA will be very susceptible to both the physical removal due to its high solubility, i.e., wall/aerosol loss processes, and the fast further oxidation by OH radicals to form secondary products, such as SO₂, DMSO₂ and MSA. It is not surprising that in the studies of Sorensen et al. (1996), where samples were collected at the end of the irradiation period, SO₂ and DMSO₂ were identified as the primary products; while in the studies of Arsene et al. (2002), where samples were analyzed during the irradiation, MSIA was found to be the dominant primary product. The above analysis can also be used to explain products other than DMSO that are observed in the studies of the DMS +

OH addition reaction. Therefore, in the scheme presented in Figure 1, the primary product from the DMS + OH addition channel is DMSO, and MSIA is shown as the dominant direct product from the DMSO oxidation by OH radicals.

The other potentially important oxidants of DMSO in the gas phase include Cl atoms, NO₃ radicals and O₃. Two kinetics studies (Barnes et al., 1989; Falbe-Hansen et al., 2000) of the DMSO reactions with these species have agreed that O₃ does not play significant roles in DMSO oxidation in the atmosphere, and the NO₃ + DMSO rate coefficient is over two orders of magnitude slower than the OH + DMSO reaction. Although the rate coefficient for the Cl + DMSO reaction is close to that for OH + DMSO, much lower concentrations of Cl atoms make this reaction of little atmospheric importance compared to the DMSO + OH reaction.

As mentioned above, DMSO₂, MSA and SO₂ are all possibly produced from the fast oxidation of MSIA by OH radicals in the gas phase (Barnes et al., 1989; Arsene et al., 1999; Falbe-Hansen et al., 2000; Arsene et al., 2001; Arsene et al., 2002; Kukui et al., 2003), although the branching ratios of each product and their detailed mechanisms are not clear. In a recent study of Kukui et al. (2003), SO₂ was found to be the only dominant product (with a yield of 0.9 ± 0.2) of the gas phase MSIA + OH reaction and the formation yield of MSA would be less than 5% of that of SO₂. Therefore, SO₂ is the main gas phase product from both addition and abstraction channels of DMS oxidation. While the study by Kukui et al. (2003) was carried out in N₂, further studies of this reaction in air are necessary for a better understanding of the addition channel of DMS oxidation. As the primary source of NSS, SO₂ can be either oxidized by OH to form H₂SO₄ in the gas phase (Wine et al., 1984; Atkinson et al., 1997 and references therein)

or taken-up into the condensed phase and oxidized by O_3 and H_2O_2 to produce S(VI) (Kreidenweis et al., 2003 and references therein).

DMSO₂ and MSA have been measured in many field and laboratory studies, however, their detailed production mechanisms are not well known yet. The only available kinetics study (Falbe-Hansen et al., 2000) of the gas phase DMSO₂ have found that OH, NO₃, Cl and O₃ are all not efficient in removing DMSO₂ from the atmosphere. There are no kinetics studies of gas phase MSA reactions available, although it is believed that MSA is quite stable in the gas phase. Therefore, the only significant sink of gas phase DMSO₂ and MSA is through heterogeneous processes (will be discussed later) and dry deposition.

DMS and Climate

As discussed earlier, DMS undergoes a complicated oxidation process once transferring across the sea-air interface. It has been demonstrated from both field observations and laboratory studies that the important stable oxidation intermediate species produced from DMS oxidation, i.e., DMSO, DMSO₂, MSIA, MSA, SO₂, and H₂SO₄, are all more water soluble than DMS. In Table 4 the Henry's Law constants for DMS and the most important stable soluble products from its atmospheric oxidation are compared. Due to their low volatility, these sulfur species may be involved in the formation (in case of H₂SO₄) of new aerosols and the growth of pre-existing aerosols, or be dissolved into cloud droplets directly. It is well-established that clouds, aerosols and atmospheric molecules have an important impact on the earth-atmosphere radiation budget and could scatter about 23% of incident solar radiation back to space. Clouds comprise *ca.* 75% of this atmospheric albedo (Kiehl and Trenberth 1997). Aerosols impact the earth's energy budget by either scattering solar radiation back to space (direct effect) or by serving as cloud condensation nuclei (CCN) and altering the properties and lifetimes of clouds (indirect effect) (Shaw 1983; Charlson et al., 1987; Shaw 1987; Albrecht 1989; Charlson et al., 1991; Andreae and Crutzen 1997; Lohmann and Feichter 1997).

Charlson et al. (1987) have proposed that DMS cycling in the atmosphere could form a negative feedback loop in climate modification, which is known as the famous CLAW hypothesis (named after the authors of the paper), as shown in Figure 2. In the 1960's the scientist Jim Lovelock and his co-worker Lynn Margulis proposed that

all living matter on Earth has the ability to act together to react to changes in conditions in such a way as to correct itself and keep our planet a fit place for life. Lovelock named this control system, Gaia, after the Greek Goddess of the Earth. The CLAW hypothesis is one example of the Gaia theory. According to the CLAW hypothesis, atmospheric cycling of DMS could counteract the perturbation of global temperatures because as temperature increases, phytoplankton grows faster and the phytoplanktonic activity becomes more productive and increases DMS emissions from the ocean. Oxidation of DMS in the atmosphere will lead to more production of aerosols and CCN, faster growth rate of pre-existing particles during the evaporation/condensation cycles, and thus, the cloud coverage and albedo in the marine atmosphere will be increased. Therefore the initial temperature increase is decelerated because of a higher albedo induced by more cloud coverage. On the other hand, as the global temperature decreases, emission of DMS decreases due to slower phytoplanktonic activities, then less aerosols and CCN formation from DMS oxidation will reduce the cloud coverage and the albedo at the earth surface. In that sense, emission of DMS from the ocean and its oxidation in the atmosphere act as a moderator of the abrupt change of global climate, and counteract the global warming effect from green house gases.

The negative feedback climate modification loop discussed above involves the gas phase oxidation of DMS and its subsequent products, heterogeneous processes, as well as the chemical transformations of the soluble products in the condensed phases. A simplified scheme of DMS cycling in the marine boundary layer atmosphere is shown in Figure 3. As mentioned earlier, ~ 10% of the DMS produced from phytoplanktonic activity are emitted into the atmosphere. Once transferring across the sea-air interface,

DMS is readily oxidized by radicals in the atmosphere, and the relatively stable oxidation products, i.e., DMSO, DMSO₂, MSIA, MS, SO₂ and H₂SO₄, are much more water soluble compared to DMS. Therefore, if given time to equilibrate with the atmospheric condensed phase, all of the above mentioned stable DMS oxidation products will be partitioned partially or primarily (almost exclusively in the cases of MSA and H₂SO₄) into the condensed phase. These species have been measured in atmospheric condensed phases, e.g., rain water, aerosols and cloud droplets, in many studies (Harvey and Lang 1986; Watts et al., 1987; Brimblecombe and Clegg 1988; Watts et al., 1990; Eisele and Tanner 1993; De Bruyn et al., 1994; De Bruyn et al., 1995; Jefferson et al., 1997; Berresheim and Eisele 1998; Davis et al., 1998; Davis et al., 1999; Sciare et al., 2000a; Sciare et al., 2001).

During droplet evaporation/condensation cycles, condensed phase chemical transformations of these sulfur species are potentially important for the growth of aerosols (which serve as CCN) and cloud droplets, because most of these reactions convert more volatile species into less volatile species and these compounds stay in particles as cloud droplets evaporate and contribute to mass growth of particulate matter in the atmosphere. Eventually they could play important roles in the earth surface solar radiation budget, as the albedo of both the aerosols and clouds are affected by changes in number density, size distribution, and composition of atmospheric particulate matter.

Table 4 Henry's Law Constants for the sulfur species of atmospheric interest

Sulfur	DMS	DMSO	DMSO ₂	MSIA	MSA	SO ₂	H ₂ SO ₄
K_H^0 (M atm ⁻¹)	^a 0.5	^b >5 × 10 ⁴ ^c 1 × 10 ⁶	^b >5 × 10 ⁴	^b >5 × 10 ⁴	^b >5 × 10 ⁴ ^d 8.9 × 10 ¹¹	^e 1.2	^f >10 ¹¹

^a (De Bruyn et al., 1995).

^b (De Bruyn et al., 1994), and all K_H^0 from this work are for the species itself.

^c (Lee and Zhou 1994).

^d $K_H^0 = 6.3 \times 10^{13} / K_a$, and is the “effective” Henry's law constant for MSA in acid-base equilibrium, where $K_a = 73$ M (Clegg and Brimblecombe 1985; Brimblecombe and Clegg 1988).

^e (Hoffmann and Jacob 1984; Pandis and Seinfeld 1989), for the SO₂ itself.

^f (Gmitro and Vermeulen 1964), for H₂SO₄ in acid-base equilibrium.

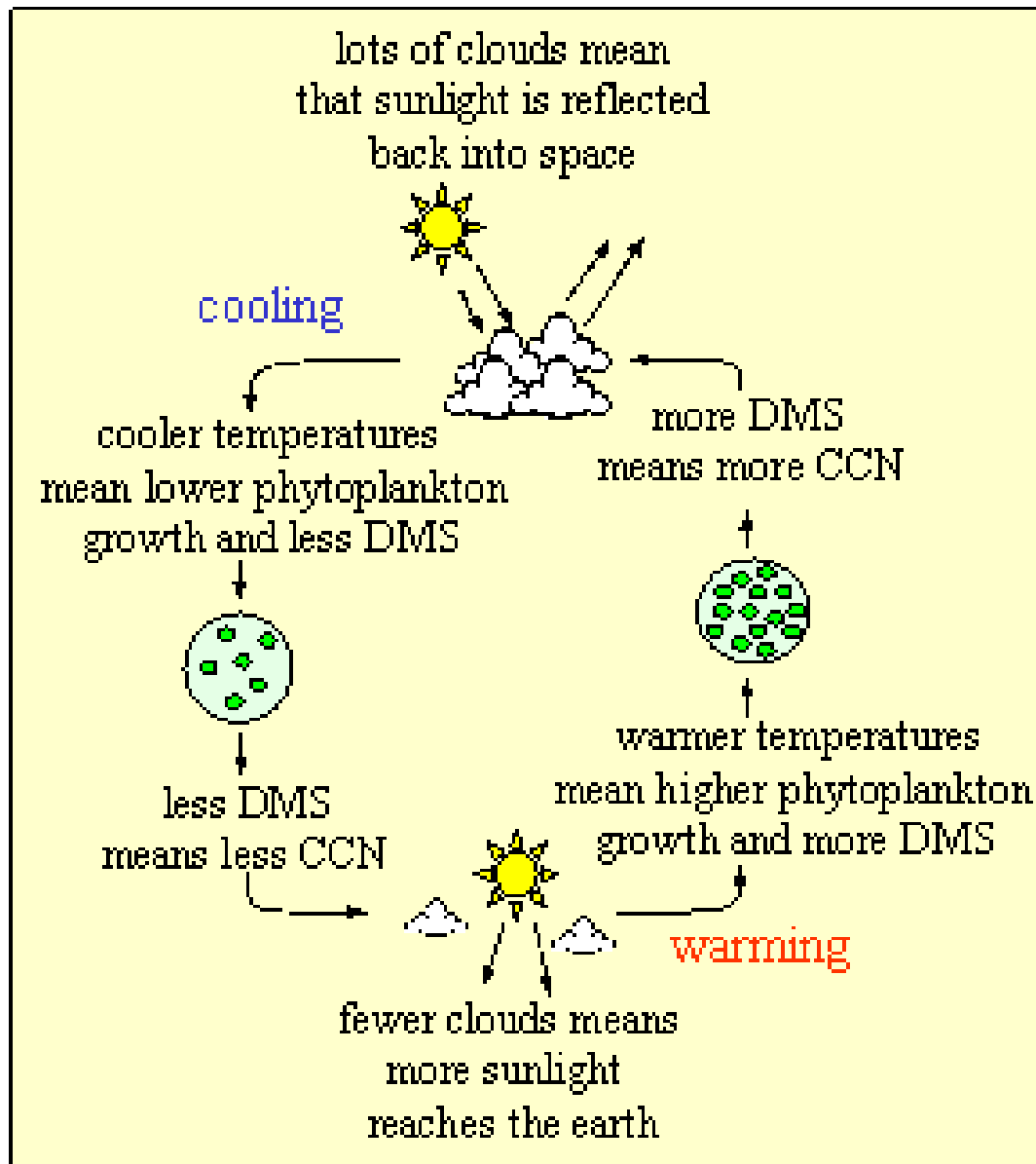


Figure 2 A simplified representation of the CLAW Hypothesis, an example of a negative climate feedback loop

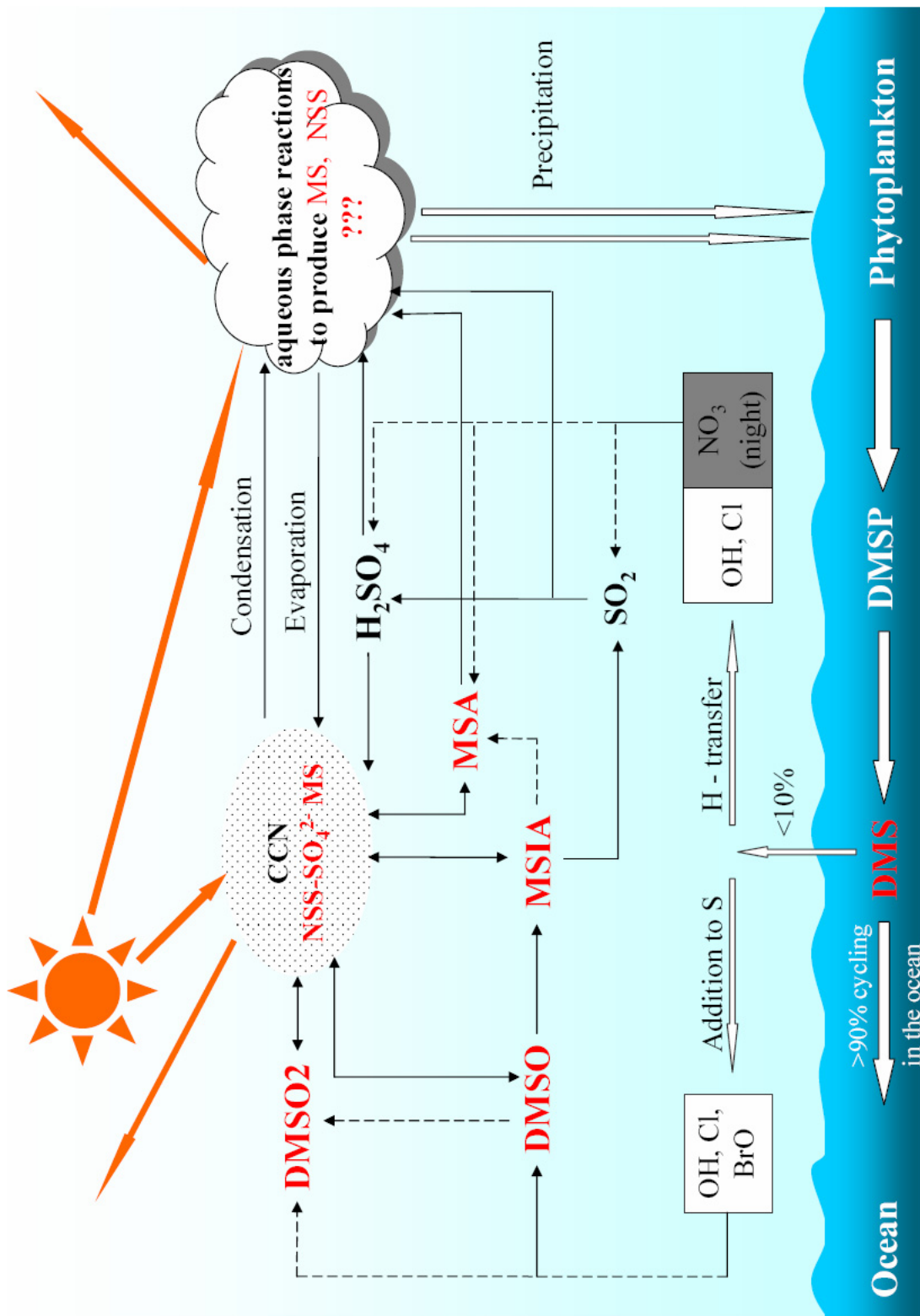


Figure 3 A simplified DMS cycling in the marine boundary layer atmosphere

Aqueous Kinetics of Organic Sulfur Species

Ever since the first proposal of the link between DMS and climate modification, the DMS oxidation mechanism has been of great interest to the atmospheric chemistry community. Although most studies have focused on gas phase processes, more and more recent field measurements, model simulations, and laboratory studies have demonstrated that heterogeneous processes and aqueous phase transformations are potentially important for our understanding of DMS chemistry and its effect on climate modification, as well as assessment of observed MS/NSS ratios in the atmospheric condensed phase.

Heterogeneous processes and condensed phase transformations are very important in the atmospheric sulfur cycle, especially when researchers attempt to explain the levels of certain stable species in particulate matter. For instance, Davis et al. (1999) compared their field observations at an equatorial Pacific site near Christmas Island with model calculations and reported that gas phase production accounts for only 1% of MS and 20% of non-sea-salt sulfate (NSS) measured in atmospheric aerosols. They proposed that the oxidation of DMSO and MSI in the aqueous phase is most likely responsible for the implied substantial production of MS in the condensed phase, and they also believed that about 80% of observed NSS results from the heterogeneous oxidation of SO₂ and other DMS oxidation products. Another study, which investigated the diurnal and seasonal variation of DMSO at Amsterdam Island in the southern Indian Ocean (Sciare et al., 2000b), found that in order to reproduce the observed gaseous DMSO concentrations, about 38-58% of atmospheric DMSO should be removed by heterogeneous processes, which are linked to the photochemical activity in the atmosphere with a maximum

efficiency at noon and a minimum at night. Similar conclusions were obtained by Legrand et al. (2001) in their studies of subdaily variations of DMSO at Dumont d'Uville, a coastal Antarctic site. A recent simulation of sulfur cycling in the remote, high-latitude Southern Hemisphere (Cosme et al., 2002) overestimated gas phase DMSO by a factor of 2 while underestimating aerosol MS compared to observed concentrations when only gas phase chemistry was simulated. Also in this study, DMSO concentration levels were reproduced well by model calculations when the uptake of DMSO into the condensed phase was included in the model. All of the above mentioned studies suggest the existence of a heterogeneous sink for DMSO that leads to the production of more stable sulfur species, i.e., MS and SO_4^{2-} . The efficient uptake of DMSO and its low concentration observed in the condensed phase strongly suggest a fast removal of DMSO in the condensed phase. However, the detailed mechanism involved in this process is not well known. The database for the relevant aqueous phase transformations is still rather limited.

Potentially important atmospheric aqueous phase oxidants include O_3 , H_2O_2 , HO_2 , OH , SO_4^- , Cl , Cl_2^- and NO_3 . Studies have demonstrated that O_3 and H_2O_2 are the oxidants that are primarily responsible for aqueous phase SO_2 oxidation (Kreidenweis et al., 2003 and references therein). Two studies of the $\text{O}_3 + \text{DMS}$ reaction (Lee and Zhou 1994; Gershenzon et al., 2001) demonstrated that the simultaneous uptake of DMS and O_3 and the subsequent surface reaction might play important roles in DMS oxidation. The study by Lee and Zhou (1994) employed a bubbler-type gas-liquid reactor and reported a rate coefficient of $(4 \pm 40\%) \times 10^8 \text{ M}^{-1} \text{ s}^{-1}$ at 287 K for the $\text{DMS} + \text{O}_3$ reaction. The temperature dependence of this reaction was studied by Gershenzon et al. (2001) in a

bubble train flow reactor and a rate coefficient of about $(8.6 \pm 3.6) \times 10^8 \text{ M}^{-1} \text{ s}^{-1}$ was obtained at 293 K, which is in agreement with the previous one when uncertainties are considered. However, for oxygenated organic sulfur compounds, the most important oxidants in the aqueous phase appear to be radicals, because two studies of the $\text{O}_3 + \text{DMSO}$ reaction have shown this reaction to be very slow (Pryor et al., 1984; Lee and Zhou 1994) and one study of DMSO reactions with a series of hydroperoxides (Amels et al., 1997) also demonstrated that hydroperoxides do not play significant roles in DMSO oxidation in the aqueous phase. On the other hand, studies on reactions of organic sulfur compounds have shown that radicals, such as OH , SO_4^- , Cl , Cl_2^- and NO_3 , are potentially important in oxidizing the organic species in the aqueous phase (see below).

The most studied aqueous phase reactions are those with the OH radical, a key gas phase and aqueous phase atmospheric oxidant. The aqueous phase $\text{OH} + \text{DMS}$ rate coefficient has been found to be close to the diffusion-controlled limit, $1.9 \times 10^{10} \text{ M}^{-1} \text{ s}^{-1}$, from the studies by Bonifacic et al. (1975) and Schoneich & Bobrowski (1993) using pulse radiolysis and UV-vis absorption techniques.

To the best of the author's knowledge, the first kinetics study of the $\text{OH} + \text{DMSO}$ reaction was carried out by Meissner et al. (1967) using a pulse radiolysis technique. A rate coefficient of $7.0 \times 10^9 \text{ M}^{-1} \text{ s}^{-1}$, close to the diffusion controlled limit, was reported by the competitive kinetics method using SCN^- as the competitor. The study also claimed that the DMSO-OH adduct is the only important product. A later study of the $\text{DMSO} + \text{OH}$ reaction by Reuvers et al. (1973) used the same experimental technique and data analysis method, and reported a rate coefficient about 20% lower than the above mentioned data. The study by Veltwisch et al. (1980) combined the pulse radiolysis and

conductivity technique and reported a result in excellent agreement with the work by Meissner et al. (1967). This work also demonstrated that the DMSO-OH adduct is a short-lived intermediate and decomposes very rapidly to produce $\text{CH}_3\text{S(O)OH}$ (MSIA) and the CH_3 radical. MSIA dissociates almost completely at $\text{pH} > 3.5$ and produces the de-protonated anion, CH_3SO_2^- (MSI), because of its low pK_a (~ 2.3) (Wudl et al., 1967). A more recent study by Milne et al. (Milne et al., 1989) employed the flash photolysis method to produce radicals and the competitive kinetics to investigate OH reactions with DMSO, DMSO₂ and MS. They reported a rate coefficient for the DMSO + OH reaction in good agreement with Meissner et al. (1967). Different from all above studies, Bardouki et al. (2002) employed a continuous photolysis method to produce OH radicals and ion/gas chromatography to monitor the reactants or products, and used either MSI or benzoate as competitors in their studies of the DMSO + OH kinetics. The rate coefficient from this method is about a factor of 1.5 lower than most other studies, probably because their rate coefficient determinations are subject to complications from slow secondary chemical and photochemical reactions that would not present a problem in real-time flash photolysis or pulse radiolysis studies. It is also worth pointing out that for those studies employing SCN^- as a competitor, the different values for $k_{\text{OH}+\text{SCN}^-}$ used could make some difference in the reported rate coefficient. This factor will be taken into account when we compare our results with literature values.

The only available study on DMSO₂ + OH kinetics (Milne et al., 1989) reports a relatively slow rate coefficient of $3.0 \times 10^7 \text{ M}^{-1} \text{ s}^{-1}$, over two orders of magnitude slower than the DMSO + OH reaction.

Three studies on the MSI + OH reaction are in reasonable agreement and indicate that this is a very fast reaction with a room temperature rate coefficient near the diffusion-controlled limit. Sehested & Holcman (1996) and Flyunt et al. (2001) both employed pulse radiolysis and UV absorption techniques to investigate the kinetics and mechanism of the MSI + OH reaction. They each reported a rate coefficient of about $6 \times 10^9 \text{ M}^{-1} \text{ s}^{-1}$. However, both studies focused on the reaction mechanism and no details of the kinetics analyses were available in their papers. The above mentioned work by Bardouki et al (2002) reported a rate coefficient of $1.2 \times 10^{10} \text{ M}^{-1} \text{ s}^{-1}$ for MSI + OH, twice the rate coefficients from the other two studies; the continuous photolysis method and the detection technique are also the possible reason for the discrepancy between this work and the other two studies.

Interestingly, the room temperature rate coefficients for the potentially atmospherically important OH + MS reaction reported from three studies (Lind and Eriksen 1975; Milne et al., 1989; Olson and Fessenden 1992) are in very poor agreement with each other, varying from 1.3×10^7 to $1.4 \times 10^9 \text{ M}^{-1} \text{ s}^{-1}$. The study by Lind and Eriksen (1975) employed the pulse radiolysis technique and reported an extremely fast rate coefficient. The more recent study by Olson and Fessenden (1992) used the same experimental method and reported the lowest value, $1.3 \times 10^7 \text{ M}^{-1} \text{ s}^{-1}$. The rate of the aqueous phase MS + OH reaction could directly affect the interpretation of MS/NSS ratios in atmospheric particulate matter, which is often used to evaluate the relative contribution of natural versus anthropogenic sulfur in atmospheric particles. An important assumption of such an assessment is that MS is as stable as SO_4^{2-} in the atmosphere after being produced, while the huge uncertainty in the reactivity of MS

makes it hard to evaluate the effect of the MS + OH reaction on the measured MS/NSS ratios, and therefore, further investigation of this reaction is needed.

Besides OH radical kinetics, the other available aqueous kinetics data base includes the above mentioned two studies of the O₃ + DMS reaction (Lee and Zhou 1994; Gershenzon et al., 2001), as well as one study each of the reactions of DMS with Cl₂⁻, Br₂⁻ (Bonifacic and Asmus 1980) and a series of hydroperoxides (Amels et al., 1997). The only reaction important for DMS oxidation was demonstrated to be the simultaneous uptake of DMS and O₃ and the subsequent surface reaction. The DMSO data base includes two studies of the O₃ + DMSO reaction (which show this reaction to be very slow) (Pryor et al., 1984; Lee and Zhou 1994), one study of DMSO reactions with a series of hydroperoxides (Amels et al., 1997), and one study each of the reactions of DMSO with SO₄⁻ (Kishore and Asmus 1989) and Cl₂⁻ (Kishore and Asmus 1991). The study by Flyunt et al. (2001) on the reaction of methanesulfinate (MSI; CH₃S(O)O⁻) with SO₄⁻ is the only available study of the reactions of MSI with radicals other than OH. These studies have shown that not only OH, but also SO₄⁻ and Cl₂⁻ could play potentially important roles in aqueous phase sulfur oxidation. In addition to the aqueous phase kinetics studies mentioned above, NO₃ reactions with DMS and DMSO (Akiho et al., 1989), and the Cl reactions with DMS and DMSO (Sumiyoshi and Katayama 1987) have been studied in non-aqueous solvents. It is worth noting that all rate coefficients for the above mentioned reactions of organic sulfur compounds reported to date have been measured at room temperature (293 – 298 K).

To enrich the data base of the aqueous phase oxidation of the organic sulfur compounds, further kinetics studies are necessary, especially for those having potential

atmospheric importance and for those which have not been well documented. Additionally the temperature dependent kinetics of some potentially important reactions are required to quantitatively understand the role of condensed phase reactions in the sulfur cycle under different atmospheric conditions.

The focus of this dissertation is a series of laboratory kinetics studies of the reactions of free radicals with organic sulfur species that are of atmospheric importance using a laser flash photolysis – long path UV-Vis absorption technique. The studied kinetics include: Temperature dependent kinetics studies of the $\text{SO}_4^- + \text{R}$ reactions ($\text{R} = \text{DMSO}$, DMSO_2 and MS , in Chapter III) and the $\text{OH} + \text{R}$ reactions (Chapter IV) over the temperature range of 275 – 310 K, room temperature kinetics studies of the $\text{Cl} \leftrightarrow \text{Cl}_2^- + \text{R}$ reactions (Chapter V), and room temperature kinetics studies of the $\text{OH} + \text{MSI}$ and $\text{Cl}_2^- + \text{MSI}$ reactions (Chapter VI). Chapter VIII incorporates the kinetics data obtained in Chapters III – VI into a Trajectory Ensemble Model to simulate DMS oxidation in cloudy marine atmosphere in order to assess the importance of the aqueous phase reactions in the DMS oxidation and its contribution to particulate matter mass growth and MS/NSS ratios.

CHAPTER II

EXPERIMENTAL TECHNIQUES

Introduction

A thorough understanding of the mechanism of any complicated system requires a quantitative knowledge of elementary reaction kinetics and product yields for a range of relevant conditions. By properly controlling experimental conditions, choosing a selective detection technique for the compounds of interest, a single elementary reaction can be isolated from a complicated system and thus studied in the laboratory. By studying the variation of reaction rate coefficients and product yields with experimental conditions, such as temperature, pH, and ionic strength (in the case of aqueous phase studies) the precise mechanism can be determined. The basic goal of this dissertation involves the measurement of rate coefficients of some reactions of organic sulfur compounds with aqueous phase radicals in order to ascertain their importance in atmospheric DMS oxidation. The general experimental approach employed in these studies involves the in-situ generation of free radicals using Laser Flash Photolysis (LFP), in combination with time resolved detection of reactants or products (mainly radicals) using Long Path UV-Visible Absorption Spectroscopy (LPA).

Experimental Approach

The general experimental approach of the LFP-LPA technique involves the following steps: A flowing solution consisting of water solvent, an organic sulfur reactant, a photolytic precursor for the radical of interest, and a competitor to the organic sulfur reactant if necessary (details in Chapter IV), was passed through a reaction cell. The free radical chemistry was initiated by laser flash photolysis of an appropriate photolytic precursor. The desired free radical reactant could be generated either directly from the photolysis of the precursor or through rapid secondary chemistry. The reaction mixture was then probed using UV-Visible absorption spectroscopy, and temporal absorption profiles of either the radical reactant or a product were monitored under pseudo-first order conditions with the concentration of the stable reactant in large excess over that of the radical reactant. A schematic diagram of the LFP-LPA apparatus is shown in Figure 4. It consists of a pulsed excimer laser photolysis light source, a continuous wavelength xenon arc lamp probe light source, optics to direct the photolysis and probe beams, a set of White cell optics (White 1942) to obtain multiple passes of the probe beam through the photolyzed region of the sample, a Teflon reactor with anti-reflection coated quartz windows, a liquid flow system, a monochromator to isolate the probe wavelength, an oscilloscope to record the temporal evolution of the transmitted probe radiation immediately before and after each laser flash, a photodiode to detect the laser flash and trigger the oscilloscope, a computer connected to the oscilloscope to store and average the waveforms from the oscilloscope, a thermostated bath to control the temperature of the liquid reservoir, and a Teflon-coated thermocouple to measure the temperature of the solution in the reactor.

Important features of the methodology include the following: (1) Reactive intermediates are probed in “real-time”, i.e., on time scales corresponding to their lifetimes under the experimental conditions employed (10^{-6} - 10^{-2} s); and (2) Very low radical concentrations (5 - 100 nanomolar) are employed. These two features eliminate many potential side reactions that could seriously complicate the interpretation of kinetic data. The experimental methodology was first developed in our laboratory in the late 1980s, and has been employed successfully in several previous studies of aqueous phase free radical kinetics (Tang et al., 1988; Wine et al., 1988; Wine et al., 1989; Chin and Wine 1992; Chin and Wine 1994).

The photolysis laser employed in this study was a Lambda Physik Compex 102 excimer laser operating with a KrF gas fill ($\lambda = 248$ nm, pulse width = 25 ns). After adjustment of the height, distance and size of the laser beam by some mirrors and lenses, the laser was directed through the reaction cell. The laser beam fairly uniformly covers an area of $2.5\text{cm} \times 2.5\text{cm}$ in the center of windows. The laser fluence at the entrance of the reaction cell was typically 1.5×10^{16} photons per cm^2 per pulse, and changed by less than 10% from the center to the edge of the laser beam. The laser power after the reaction cell was less than 3% different than the power before the cell when the reaction cell is displaced. This indicates that there is no significant divergence/convergence of the laser beam while it passes through the reaction cell. Variations of laser power for the averaged shots were typically less than 2%. The laser pulse repetition rate was controlled by a small pulse generator, and in most experiments, the repetition rate was 0.03 Hz, in order to allow enough time to refresh the solution in the reaction cell.

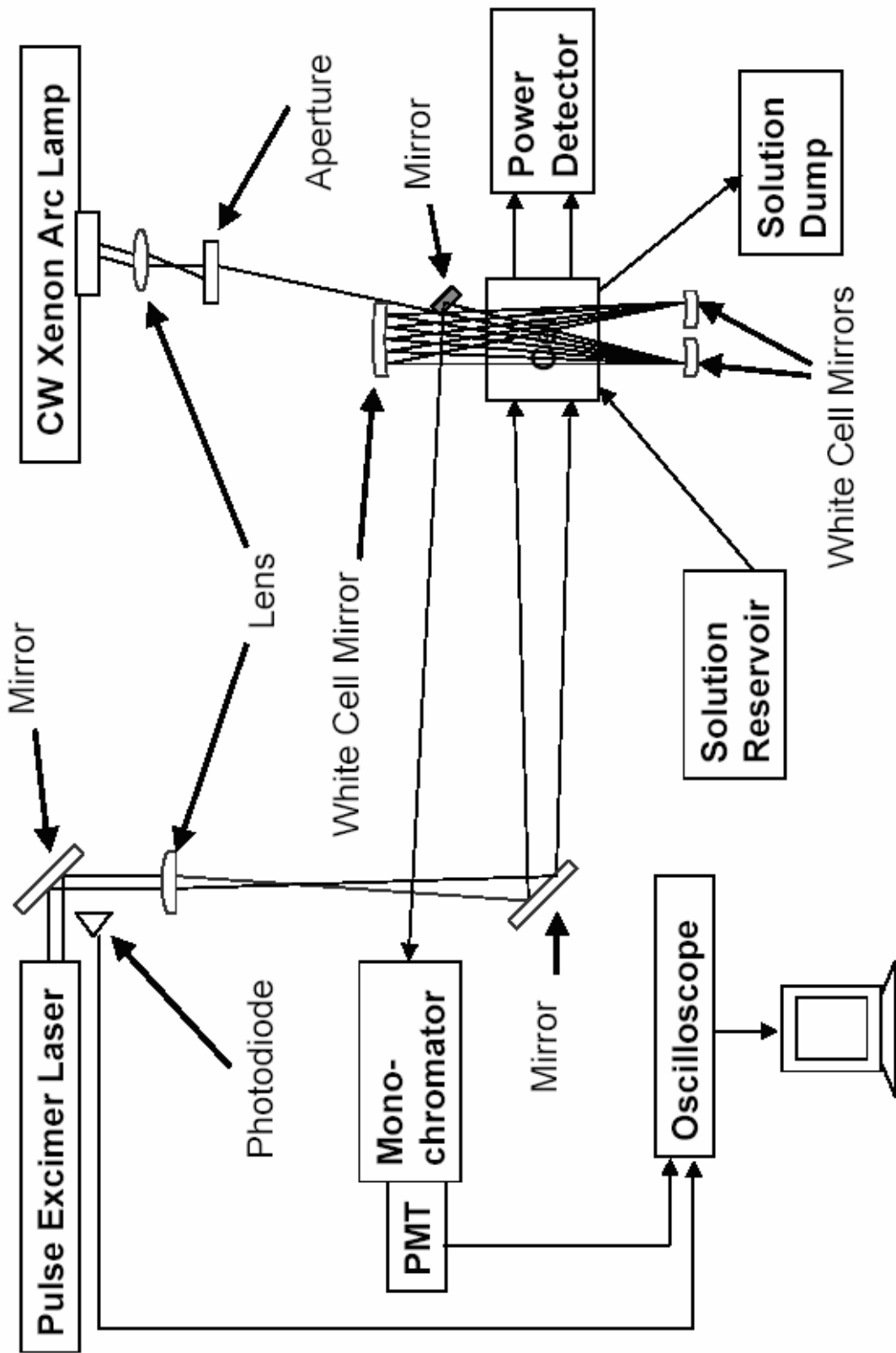


Figure 4 Schematic diagram of the LFP-LPA apparatus

The reactor is a 55 cm³ cubic Teflon cell with broad band anti-reflection coated (BBAR) quartz windows on four sides. The BBAR coated windows minimize the loss of light as the probe light beam travels through the reaction cell. The windows have to be exchanged for different detection wavelengths during the studies as the BBAR coat functions best within a short range of wavelengths. Solutions from the reservoir were flowed through the reaction cell using a quick load pump (Master Flex) at the rate of ~ 2.5 cm³/s. At this flow rate no air bubbles are generated in the reaction cell and the solution in the reaction cell is completely replaced between laser shots.

The detection light source is a high pressure 150 W continuous wave Xenon arc lamp with an LSP-250 power supply and an LPS-221 Lamp Igniter (Photon Technologies Incorporated). Two lenses were used (one is at the window of the light source housing) to minimize divergence of the probe light beam. An aperture was used to select a small part of the light beam, which was then multipassed through the reaction cell using the White Cell optics. The White Cell mirrors were adjusted to optimize the number of passes the probe radiation traversed through the region of the reaction cell irradiated by the excimer laser (~2.5 cm wide). The White Cell mirrors were coated to have high reflectivity over a small range of wavelengths, therefore they have to be exchanged depending on the absorption wavelength being monitored. For studies at 410-500 nm wavelength range, 46 passes of the detection light beam could be obtained, while for studies at shorter wavelengths, only 26-34 passes were obtained, because coatings are not as good in the UV and the output radiant energy from the Xenon arc lamp is weak in that region. With an electronic time constant of 1 μ s for this experimental setup, the detection limit is about 0.03% absorption (64 flashes averaged). The actual detection limit of the

target radical varies with each experimental setup, because it depends on the absorption path length (which changes with the number of passes of the probe light beam) and the wavelength (probe light intensity depends on the wavelength) and the extinction coefficient of that radical at the monitoring wavelength. This will be discussed further for each study in the following chapters separately.

The detection light beam leaving the White Cell Mirrors was directed into a monochromator to isolate the desired probe wavelength and detected by a photomultiplier tube to convert the optical signals into electrical signals. Then a TDS210 two channel digital real-time oscilloscope (Tektronix) was used to digitize and record the signals. The oscilloscope is triggered by the laser pulse detected by a photodiode, and a computer is connected to the oscilloscope to average and store the data using the data collecting program (SCOPE) designed in our lab.

Chemicals and Solution Preparation

The stated minimum purities of the chemicals used in this study are as follows: sodium peroxydisulfate ($\text{Na}_2\text{S}_2\text{O}_8$), 98%; sodium thiocyanate (NaSCN), 99.99%; sodium chloride (NaCl), 99.999%; sodium methane sulfonate (NaMS), 98% and 99%; sodium methane sulfinate (NaMSI), 97% (aqueous solutions were colorless for MSA and MSIA); DMSO₂, 98%; DMSO, 99.9%; 30% H_2O_2 in H_2O (unstabilized with total ionic

impurities less than 5 ppm), and perchloric acid (HClO₄), 99.99%. All of these chemicals were used without further purification.

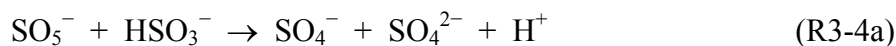
The water used for preparing solutions was purified by a Millipore Milli-Q system equipped with filters to remove particles, ions and organics. In most studies solutions were unbuffered with pH in the 5-6 range; and in some pH dependence studies HClO₄ was used to adjust the pH. Solutions were prepared in Pyrex volumetric flasks and were stored in 4-liter Pyrex flasks. All solutions were prepared at room temperature, but during temperature dependent kinetics studies a thermostated water bath was used to control temperature. The tubings to flow the solution from the reservoir to the reaction cell were covered by insulation in order to keep temperature more constant. The temperature of solution was measured both in the flask and in the reaction cell throughout the experiment. In all studies, the difference between these two temperature measurements was less than 0.5 °C. As mentioned above, solutions were pumped through the reactor at a typical flow rate of 2.5 cm³ s⁻¹ without recycling. The laser repetition rate was 0.03 Hz, and the reactor volume was ~55 cm³; hence, no aliquot of solution was subjected to more than one laser flash. All reported kinetic data were obtained using air saturated solutions, as preliminary experiments showed that data obtained using N₂-saturated solutions gave identical results to data obtained using air saturated solutions. In most experiments, solutions were used immediately after preparation, although kinetics results were found to be unaffected by allowing the solution to sit overnight before being used in an experiment.

CHAPTER III

TEMPERATURE DEPENDENT KINETICS STUDIES OF SO₄⁻ REACTIONS WITH DMSO, DMSO₂ AND MS

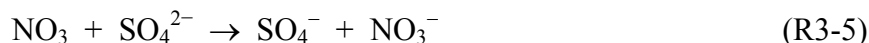
SO₄⁻ in the Atmosphere

SO₄⁻ is an important radical produced during the autoxidation of S(IV) to S(VI) in the atmospheric condensed phase. The principal pathway for generating SO₄⁻ radicals is thought to be *via* the OH-initiated oxidation of S(IV), followed by one branch of the reaction of peroxymonosulfate radical, SO₅⁻, with bisulfite, HSO₃⁻ (Dogliotti and Hayon 1967a; 1967b; 1968; Hayon et al., 1972; Chameides and Davis 1982; Chameides 1984; 1986; Jacob 1986; Jacob et al., 1989; Chameides and Stelson 1992; Herrmann et al., 2000):





The following reactions have also been suggested as sources of SO_4^- in cloud water (Chameides 1986; Tang et al., 1988),



although it has been suggested that the solubility of NO_3 in water might be too low for R3-5 to be important for SO_4^- production in the atmospheric aqueous phase (Berdniko.Vm and Bazhin 1970; Mozurkewich 1986)

SO_4^- is well established as a strong one-electron oxidant that very efficiently oxidizes many anions in the atmospheric aqueous phase (Chawla and Fessenden 1975; Huie and Clifton 1990). The main sink for SO_4^- is the reaction with chloride, Cl^- , *via* the one electron transfer process, because the chloride concentration is higher than that of OH^- and, additionally, the reaction rate is nearly one order of magnitude higher than that of the corresponding reaction of SO_4^- and OH^- (Hayon et al., 1972; Chawla and Fessenden 1975; Wine et al., 1989; McElroy 1990; Huie et al., 1991; Herrmann et al., 1995b; 2000; Yu et al., 2004). SO_4^- also reacts with organic species, such as alcohols, alkanes, and ethers through hydrogen abstraction (Clifton and Huie 1989; Huie and Clifton 1989; George et al., 2001). The reaction of SO_4^- with carboxylate ions proceeds *via* electron transfer from the carboxylate group as well as by H-atom abstraction from C-H bonds (Chawla and Fessenden 1975; Madhavan et al., 1978; Wine et al., 1989). SO_4^- also reacts with a number of aromatic compounds at rates approaching the diffusion

controlled limit, which suggests that the reaction involves addition of SO_4^- to the aromatic ring (Herrmann et al., 1995a).

Even though SO_4^- is less reactive than OH toward most organics, higher concentrations of SO_4^- (Herrmann et al., 2000) in the atmospheric aqueous phase make it an oxidant comparable to OH, and, therefore, SO_4^- induced oxidation of sulfur compounds may play an important role in the atmospheric DMS oxidation process. In this work, temperature dependent kinetics of SO_4^- reactions with DMSO, DMSO₂ and MS are studied.

Experimental Method

The absorption spectrum of SO_4^- is well known (Heckel et al., 1966; Dogliotti and Hayon 1967a; Hayon and McGarvey 1967; Robke et al., 1969; Kim and Hamill 1976; Tang et al., 1988; McElroy and Waygood 1990; Herrmann et al., 1995b; Bao and Barker 1996; Yu et al., 2004); it consists of a relatively strong band with a peak absorbance around 450 nm and a weaker overlapping band with a peak absorbance around 330 nm. As an example, the absorption spectrum of SO_4^- reported by Yu et al. (2004) is shown in Figure 5. The extinction coefficient at maximum absorbance wavelength obtained from their work is at the upper end of reported values found in the literature. Table 5 consists of a summary of maximum extinction coefficients for the 440 nm band that are available in the literature; these works agree well on the maximum absorption wavelength and are in reasonable agreement on the determination of the extinction coefficient, giving an average value of $1400 \pm 20\% \text{ M}^{-1} \text{ cm}^{-1}$ at 445 nm (excluding the two very low extinction coefficients reported in the 1960s). In this study, SO_4^- radical absorbance at 445 nm was monitored in order to study SO_4^- kinetics; at this wavelength, no significant interference from other reactants or impurities was found.

The White Cell mirrors were adjusted to allow 46 passes of detection light through the region of the reactor irradiated by the laser beam in all studies. This gave an absorption path length of 115 cm. Given a 0.03% detection limit for this experimental setup, and $\epsilon_{\text{SO}_4^-} \sim 1400 \text{ M}^{-1} \text{ cm}^{-1}$, the detection limit of SO_4^- is about $1 \times 10^{-9} \text{ M}$.

It has been well-documented in the literature that UV photolysis of the peroxydisulfate anion results in production of sulfate radicals with a yield of 2 (Hayon and McGarvey 1967; Kraljic 1970; Tang et al., 1988; Yu et al., 2004):



The photolysis of $\text{S}_2\text{O}_8^{2-}$ was used as the source of SO_4^- , and concentrations of $\text{S}_2\text{O}_8^{2-}$ were $(0.3\text{-}3) \times 10^{-4}$ M in all experiments. The concentration of SO_4^- produced right after the laser flash was estimated using the following equation:

$$[\text{SO}_4^-] = \Phi \varepsilon_{\text{S}_2\text{O}_8^{2-}} F [\text{S}_2\text{O}_8^{2-}] / N_A \quad (3-1)$$

where $\Phi = 2$, the production yield of SO_4^- from the photolysis of $\text{S}_2\text{O}_8^{2-}$ (R3-7); $\varepsilon_{\text{S}_2\text{O}_8^{2-}} = 26 \text{ M}^{-1} \text{ cm}^{-1}$, the extinction coefficient of $\text{S}_2\text{O}_8^{2-}$ at 248 nm; F is the laser fluence at the reaction cell, typically 1.4×10^{16} photons/cm²/pulse; and N_A is Avogadro's number. Under the above experimental conditions, typical SO_4^- concentrations produced right after the laser flash were $(0.4 - 4) \times 10^{-7}$ M. Additionally, the SO_4^- concentration could be derived from the observed absorbance at 445 nm right after the laser flash. According the Beer-Lambert law, the absorbance is calculated from:

$$A = \log\left(\frac{I_0}{I}\right) = \varepsilon(\text{SO}_4^-) \cdot l \cdot [\text{SO}_4^-] \quad (3-2)$$

where I_0 and I are the transmitted probing light intensities before and after the laser flash, i.e., in the absence and presence of SO_4^- , A is the absorbance, and l is the absorption path length (115 cm). As an example, when $[\text{S}_2\text{O}_8^{2-}] = 1.60 \times 10^{-4}$ M, the detected absorbance

right after the laser flash is 0.027 (all absorbances in this text are base 10). The SO_4^- concentrations calculated using the two methods described above were 1.9×10^{-7} and 1.7×10^{-7} M, respectively. This consistency confirms that the absorbance detected is mainly from SO_4^- , and interference from any other species in the solution is negligible.

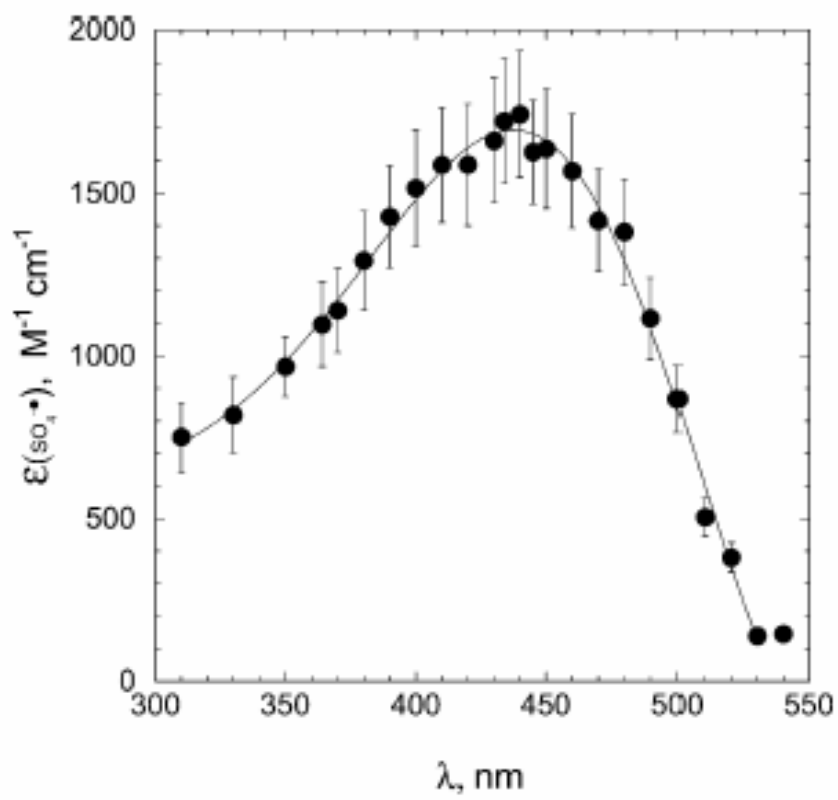


Figure 5 The absorption spectrum of SO₄²⁻ from studies of Yu et al. (2004)

Error bars are 1σ and correspond to precision only.

Table 5 Comparison of reported Extinction Coefficients of SO_4^- ($\epsilon_{\text{SO}_4^-}$) around 440 nm

$\epsilon_{\text{SO}_4^-}$ ($\text{M}^{-1} \text{cm}^{-1}$)	Method ^a	Reference
1050	PR	(Heckel et al., 1966)
1100 ^b	PR	(Roebke, Renz et al. 1969)
1100	PR	(Hayon et al., 1972)
1600	PR	(Chawla and Fessenden 1975)
1600 ± 100	PR	(McElroy and Waygood 1990)
1570 ± 130	PR	(Jiang et al., 1992)
1630 ± 120	PR	(Jiang et al., 1992)
1700 ± 150	PR	(Jiang et al., 1992)
1630 ± 50	PR	(Buxton et al., 1996)
450 ± 45	FP	(Hayon and McGarvey 1967)
460 ± 25	FP	(Dogliotti and Hayon 1967a; Dogliotti and Hayon 1967b)
1385 ± 140 ^c	FP	(Tang et al., 1988)
1385 ± 275 ^c	FP	(Wine et al., 1988)
1300 ± 300 ^d	FP	(Wine et al., 1989)
1630 ± 180	FP	(Yu et al., 2004)

^a PR, pulse radiolysis; FP, flash photolysis.

^b 460 nm;

^c 443 nm;

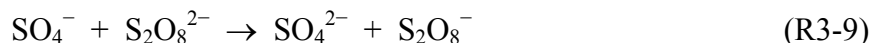
^d ~ 445 nm

Results and Discussion

All experiments were carried out under pseudo-first-order conditions with the concentration of radical precursor ($\text{S}_2\text{O}_8^{2-}$) and stable reactant (DMSO, DMSO₂ or MS) in large excess over that of SO_4^- . With the concentration of SO_4^- employed in the study, typically $< 2 \times 10^{-7}$ M, the recombination reaction,



was an insignificant removal process for SO_4^- , even though this reaction proceeds at a near-diffusion-controlled rate (Tang et al., 1988; Huie et al., 1989; McElroy and Waygood 1990; Herrmann et al., 1995b; Bao and Barker 1996; Yu et al., 2004). Another possible loss process for SO_4^- is reaction with $\text{S}_2\text{O}_8^{2-}$ (R3-9), which is also slow when compared to the loss rate of SO_4^- by reaction with water:



k_9 was reported to be $\sim 6.0 \times 10^5 \text{ M}^{-1} \text{ s}^{-1}$ at 298 K (McElroy and Waygood 1990; Jiang et al., 1992; Herrmann et al., 1995b; Yu et al., 2004), which gives a first order rate k'_9 of 20-200 s^{-1} for concentrations of $\text{S}_2\text{O}_8^{2-}$ employed in our studies; while k_{10} was found to be $400 \pm 100 \text{ s}^{-1}$ from this work, in agreement with other published studies (Tang et al., 1988; Herrmann et al., 1995b; Bao and Barker 1996). The results reported in this study suggest that k_{10} increases slightly as a function of temperature over the range 278 - 311 K

(see Tables 6 to 8). The very reactive OH radical is generated from R3-10, but it does not affect the kinetics analysis because of its extremely low concentration.

Under well controlled experimental conditions, the observed absorption temporal profiles could be analyzed using simple first-order kinetics:

$$\ln\left(\frac{A_0}{A_t}\right) = \left\{ k_{R_i} [R_i] + \sum_j k_{M_j} [M_j] + k_{bg} \right\} t \equiv k' t \quad (3-3)$$

where A_0 and A_t are the detected absorbances at 445 nm at time 0 and t , k_{bg} is the background first-order SO_4^- loss rate in the absence of organic sulfur compound R_i (dominated by R3-10 with a small contribution from reactions of SO_4^- with $S_2O_8^{2-}$ and solvent impurities), k_{R_i} is the bimolecular rate coefficient for the R_i studied, k_{M_j} is the bimolecular rate coefficient for the reaction of SO_4^- with impurity j in the sample of R_i , and k' is the pseudo first order rate coefficient.

As predicted by Equation. (3-3), exponential SO_4^- decays were observed for the following three reactions investigated:



Also linear dependencies of the first order decay rate k' on the concentration of organic sulfur compound R were observed in the studies of R3-11 and R3-12. Figure 6 shows the typical temporal profiles of SO_4^- absorbance observed at 445 nm in the studies

of DMSO + SO_4^- reaction kinetics. SO_4^- decays exponentially right after instantaneous generation from the laser flash and the pseudo-first order decay rate k' obtained from the linear least squares analysis of $\ln A$ versus time increases as the concentration of DMSO increases. As expected from Equation (3-3), a very good linear relationship between first order decay rate (k') and DMSO concentration was observed. In Figure 7 k' versus DMSO concentration for the studies at 278, 293 and 308 K are plotted and a linear relationship is observed for all studied temperatures. According to Equation (3-3), the second order reaction rate coefficient for R3-11 is obtained from the slopes of the linear relationship shown in Figure 7, and the intercepts are mainly due to the loss of SO_4^- from R3-10. For all reactions studied, observed SO_4^- decay rates were found to be independent of changes in photolysis laser power and $\text{S}_2\text{O}_8^{2-}$ concentration within the $(0.3-3) \times 10^{-4}$ M range, when SO_4^- self reaction (R3-8) and reaction with $\text{S}_2\text{O}_8^{2-}$ (R3-9) are insignificant compared to the reaction with water for SO_4^- background loss.

Similar single exponential decays of absorbance signals and linear relationships between k' and $[\text{R}]$ were observed for studies of DMSO2 + SO_4^- kinetics. However, during studies of the MS + SO_4^- reaction, a slightly non-linear relationship between pseudo-first order decay rate (k') and MS concentration was observed, even though the monitored absorbance showed excellent single exponential decay from which the first order rate k' could be derived. Sodium methansulfonate was used as the source of MS; it dissociates completely in water at the pH (~ 5.5) employed in the study and releases the deprotonated form of MSA (MS), given the high K_a of about 73 M (Clarke and Woodward 1966; Clegg and Brimblecombe 1985). Since the MS + SO_4^- reaction involves two negatively charged reactants, the measured rate coefficient is expected to increase with

increasing solution ionic strength. Furthermore, since R3-13 is quite slow, high concentrations of MS were employed to study the kinetics; thus the ionic strength of solutions increased with increasing [MS]. In relatively low ionic strength solutions ($\mu < 0.1$ M) such as those employed in this study, the following relationship is approximately obeyed if both reactants are singly charged (Espenson 1981):

$$\log k = \log k^0 + \frac{2X\mu^{1/2}}{(1 + \mu^{1/2})} \quad (3-4)$$

where k is the measured rate coefficient (at ionic strength μ), k^0 is the rate coefficient at the zero ionic strength limit; X is a collection of constants with values in water solvent that range from 0.492 at 278 K to 0.522 at 311 K (Manov et al., 1943); and μ is the ionic strength defined as:

$$\mu = 0.5 \sum_i (z_i^2 [i]) \quad (3-5)$$

where z_i is the charge of species i . Analysis of our kinetic data for R3-13 employed Equations (3-4) and (3-5) to convert each measured value of first order decay rate ($k' - k_{bg}$) to an appropriate value for the limit where $\mu \rightarrow 0$, thus allowing evaluation of the bimolecular rate coefficients $k_{13}^0(T)$ at zero ionic strength limit. Uncorrected and corrected values of ($k' - k_{bg}$) for data obtained at $T = 293$ K are plotted as a function of MS concentration in Figure 8. A slightly non-linear increase of observed ($k' - k_{bg}$) with increasing [MS] was observed for the initial data (open circles), while the corrected data (solid circles) show a better linear relationship between ($k' - k_{bg}$)₀ and [MS].

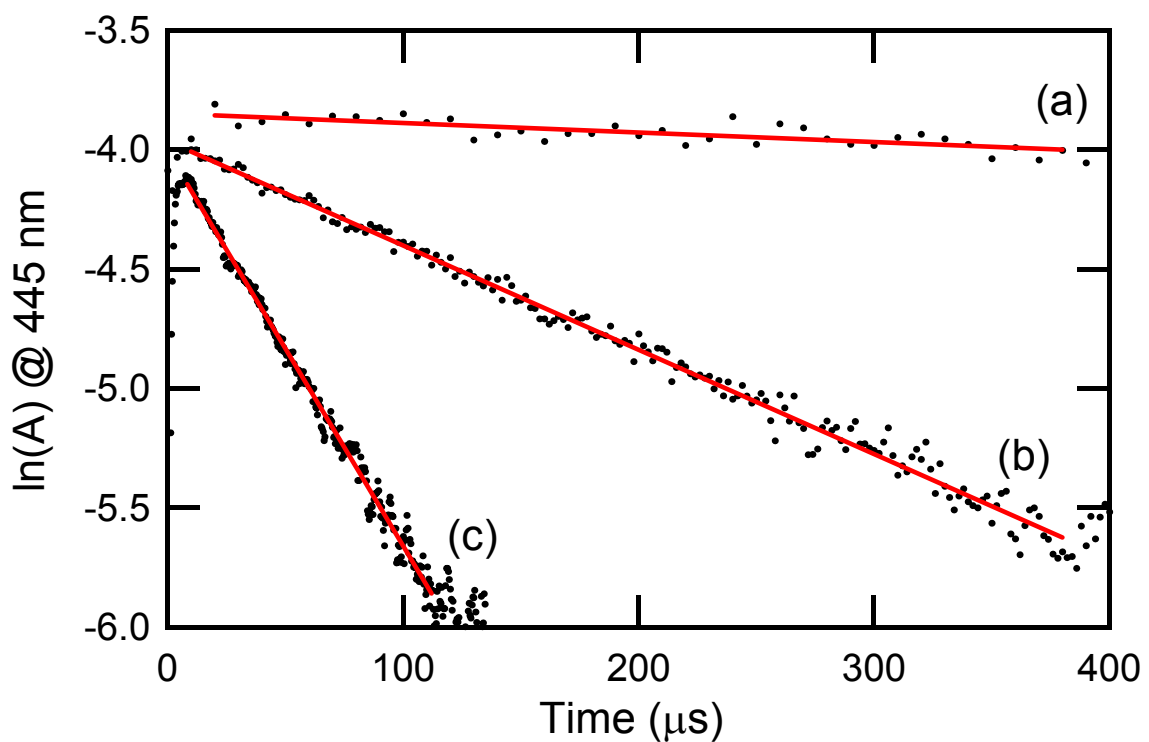


Figure 6 Typical plots of $\ln(A)$ at 445 nm versus time in the study of the $\text{SO}_4^- + \text{DMSO}$ reaction at 293 K

Experimental conditions: $[\text{S}_2\text{O}_8^{2-}] = 1.60 \times 10^{-4} \text{ M}$; $[\text{DMSO}] =$ (a) 0, (b) $1.58 \times 10^{-6} \text{ M}$, (c) $6.32 \times 10^{-6} \text{ M}$; solid lines are obtained from least squares analyses which give the following pseudo-first order decay rates (k'): (a) 378 s^{-1} , (b) 4770 s^{-1} , (c) 18300 s^{-1} .

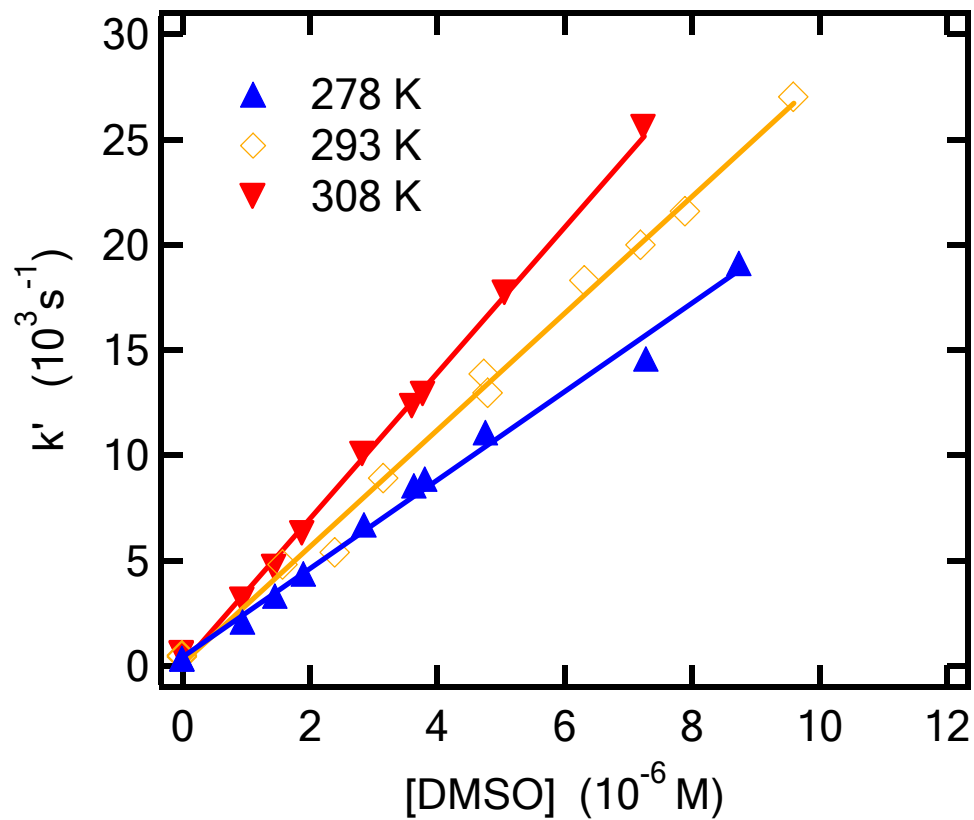


Figure 7 Plots of k' versus [DMSO] at $T = 278$ K, 293 K and 308 K

Solid lines are obtained from linear least-square analyses. The following bimolecular rate coefficients are obtained from the slopes of the solid lines (units are 10^9 M $^{-1}$ s $^{-1}$): 2.10 ± 0.12 at 278 K; 2.77 ± 0.12 at 293 K; 3.47 ± 0.11 at 308 K. Uncertainties are 2σ and represent precision only.

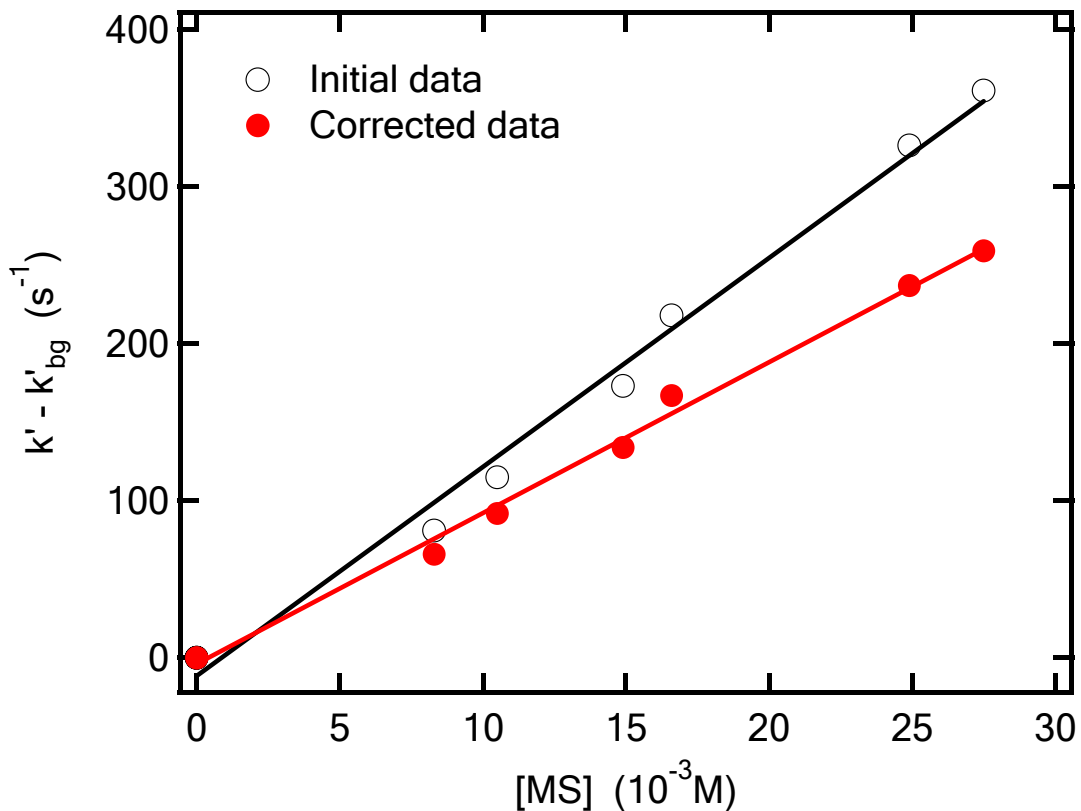


Figure 8 Plot of initial and corrected (to 0 ionic strength) ($k' - k_{bg}$) vs. [MS] at 293 K. Solid lines are obtained from linear least squares analyses. From the slopes of the solid lines, the uncorrected data give $k_{13} = (1.33 \pm 0.10) \times 10^4 \text{ M}^{-1} \text{ s}^{-1}$ whereas the data corrected to zero ionic strength give $k_{13}^0 = (9.59 \pm 0.53) \times 10^3 \text{ M}^{-1} \text{ s}^{-1}$. Uncertainties are 2σ and represent precision only.

Temperature dependent kinetics of the reactions of DMSO, DMSO₂ and MS with SO₄⁻ were studied over the temperature range 278-311 K, and all results are summarized in Tables 6 to 8. The solution reservoir was immersed in a thermostated bath (water and ethylene glycol) to control the temperature. The temperatures in the reservoir and reaction cell were measured using thermocouples and the differences between the two measurements were always less than 0.5 °C. The difference between temperatures at the inlet and outlet of the reaction cell is always less than 0.1 °C.

For the relatively volatile sulfur compounds DMSO and DMSO₂ the highest temperature employed in these studies is limited by the temperature dependent evaporation of the sulfur compounds from solution. At temperatures higher than 308 K, the evaporation of DMSO from the bulk solution affected the concentration of the solution so much that a nonlinear relationship between the first order decay rate k' and [DMSO] was observed, and the measured k' decreased as the solution stayed for longer time in the reservoir. At temperatures lower than 308 K, the kinetics results from solutions that were made right before the experiment and that sat in the thermal bath for two hours before being used in the experiment are identical, which demonstrated that the evaporation is not significant at these temperatures. Therefore the highest temperature studied for DMSO and DMSO₂ kinetics in this work is 308 K. For the less volatile sulfur species MS, evaporation is not a problem in the studies at higher temperatures. For consistency and atmospheric interest, the upper limit of the studies is 311 K for the MS reaction.

Table 6 Summary of kinetic data for the DMSO + SO₄⁻ reaction (R3-11)

T(K)	[S ₂ O ₈ ²⁻] (10 ⁻⁴ M)	[DMSO] (10 ⁻⁶ M)	A ₀ ^a	k' (s ⁻¹)	k ₁₁ ± 2σ ^b (10 ⁹ M ⁻¹ s ⁻¹)
278	0.988	0	0.024	311	
278	0.988	0.953	0.024	2040	
278	0.988	1.91	0.024	4320	
278	0.988	2.86	0.022	6660	
278	0.988	3.81	0.020	8840	
278	0.988	4.77	0.024	11000	
278	1.29	0	0.040	267	
278	1.29	1.46	0.040	3280	
278	1.29	3.64	0.029	8510	
278	1.29	7.29	0.030	14500	
278	1.29	8.75	0.030	19100	2.10 ± 0.30
287	0.988	0	0.023	358	
287	0.988	0.952	0.024	2390	
287	0.988	1.90	0.021	5200	
287	0.988	2.86	0.020	8010	
287	1.53	0	0.029	392	
287	1.53	0.728	0.027	2010	
287	1.53	1.46	0.023	4140	
287	1.53	2.19	0.026	5810	
287	1.53	2.91	0.025	7800	
287	1.53	3.64	0.025	9000	2.52 ± 0.15
294	1.60	0	0.042	378	
294	1.60	1.58	0.040	4770	
294	1.60	3.16	0.041	8880	
294	1.60	4.74	0.038	13800	
294	1.60	6.32	0.036	18300	
294	1.60	7.90	0.039	21600	
294	1.55	0	0.040	450	
294	1.55	2.40	0.041	5350	
294	1.55	4.80	0.038	12900	
294	1.55	7.20	0.039	20000	
294	1.55	9.60	0.035	27000	2.78 ± 0.12

Table 6 (continued)

T(K)	[S ₂ O ₈ ²⁻] (10 ⁻⁴ M)	[DMSO] (10 ⁻⁶ M)	A ₀ ^a	k' (s ⁻¹)	k ₁₁ ± 2σ ^b (10 ⁹ M ⁻¹ s ⁻¹)
298	1.29	0	0.036	400	
298	1.29	0.727	0.033	2260	
298	1.29	2.18	0.029	6630	
298	1.29	3.63	0.032	11200	
298	1.29	6.18	0.035	18300	
298	1.29	7.27	0.032	22100	
298	1.53	0	0.039	432	
298	1.53	0.950	0.034	2960	
298	1.53	1.90	0.032	5840	
298	1.53	2.85	0.030	8920	
298	1.53	3.80	0.034	11800	
298	1.53	5.09	0.030	16100	3.00 ± 0.07
308	1.29	0	0.052	498	
308	1.29	1.45	0.045	4640	
308	1.29	3.62	0.049	12300	
308	1.29	5.07	0.053	17700	
308	1.29	7.25	0.039	25600	
308	0.988	0	0.033	548	
308	0.988	0.947	0.034	3100	
308	0.988	1.90	0.032	6250	
308	0.988	2.84	0.026	10000	
308	0.988	3.79	0.028	12900	3.47 ± 0.11

^a A₀ ≡ the SO₄⁻ absorbance immediately after the laser flash, i.e., when SO₄⁻ production is complete but no significant SO₄⁻ decay has occurred.

^b Uncertainties represent precision only.

Table 7 Summary of kinetic data for the DMSO2 + SO₄⁻ reaction (R3-12)

T(K)	[S ₂ O ₈ ²⁻] (10 ⁻⁴ M)	[DMSO2] (10 ⁻⁴ M)	A ₀ ^a	k' (s ⁻¹)	k ₁₂ ± 2σ ^b (10 ⁶ M ⁻¹ s ⁻¹)
279	1.16	0	0.033	341	
279	1.16	2.46	0.032	980	
279	1.16	4.92	0.026	1910	
279	1.16	7.39	0.026	2520	
279	1.16	9.85	0.025	3180	
279	1.26	0	0.027	301	
279	1.26	3.15	0.056	1040	
279	1.26	6.31	0.032	2170	
279	1.26	9.46	0.024	3430	
279	1.26	12.6	0.03	3580	2.85 ± 0.33
286	1.26	0	0.029	353	
286	1.26	2.04	0.029	870	
286	1.26	4.08	0.028	1470	
286	1.26	6.13	0.024	2280	
286	1.26	8.17	0.027	2900	
286	1.26	10.1	0.026	3850	3.29 ± 0.20
289	1.26	0	0.033	308	
289	1.26	2.04	0.026	980	
289	1.26	4.08	0.026	1670	
289	1.26	6.12	0.026	2470	
289	1.26	8.16	0.025	3070	3.43 ± 0.15
294	1.58	0	0.028	387	
294	1.58	18.7	0.029	6130	
294	1.58	42.2	0.027	14900	
294	1.58	61.6	0.028	23300	
294	1.58	0	0.032	348	
294	1.58	10.3	0.031	4010	
294	1.58	25.7	0.029	10000	
294	1.58	35.9	0.029	14200	
294	1.57	0	0.035	364	
294	1.57	9.19	0.033	3790	
294	1.57	18.4	0.036	7250	
294	1.57	36.7	0.033	13200	
294	1.57	55.1	0.030	21700	3.73 ± 0.17

Table 7 (continued)

T(K)	[S ₂ O ₈ ²⁻] (10 ⁻⁴ M)	[DMSO ₂] (10 ⁻⁴ M)	A ₀ ^a	k' (s ⁻¹)	k ₁₂ ± 2σ ^b (10 ⁶ M ⁻¹ s ⁻¹)
298	1.16	0	0.028	394	
298	1.16	2.46	0.027	1140	
298	1.16	4.91	0.026	2130	
298	1.16	7.37	0.026	3190	
298	1.16	9.82	0.023	4120	
298	1.16	12.3	0.024	5040	
298	1.53	0	0.042	443	
298	1.53	3.15	0.035	1350	
298	1.53	6.29	0.035	2430	
298	1.53	9.43	0.035	3780	
298	1.53	12.6	0.035	5120	
298	1.53	15.7	0.032	6500	3.88 ± 0.17

^a A₀ ≡ the SO₄⁻ absorbance immediately after the laser flash, i.e., when SO₄⁻ production is complete but no significant SO₄⁻ decay has occurred;

^b Uncertainties represent precision only.

Table 8 Summary of kinetic data for the MS + SO₄⁻ reaction (R3-13)

T(K)	[S ₂ O ₈ ²⁻] (10 ⁻⁴ M)	[MS] (M)	A ₀ ^a	k' (s ⁻¹)	(k' - k _{bg}) (s ⁻¹)	(k' - k _{bg}) ₀ ^b (s ⁻¹)	k ₁₃ ⁰ ± 2σ ^c (10 ³ M ⁻¹ s ⁻¹)
293	1.58	0	0.050	343	0	0	
293	1.58	0.0105	0.047	458	115	92	
293	1.58	0.0149	0.046	516	173	134	
293	1.58	0.0275	0.050	704	361	259	
293	1.53	0	0.040	436	0	0	
293	1.53	0.0083	0.037	517	81	66	
293	1.53	0.0166	0.035	654	218	167	
293	1.53	0.0249	0.035	762	326	237	9.59 ± 0.53
298	1.26	0	0.028	419	0	0	
298	1.26	0.0115	0.027	592	173	137	
298	1.26	0.0209	0.028	743	324	240	
298	1.26	0.0317	0.029	913	494	346	10.9 ± 0.7
304	1.26	0	0.028	513	0	0	
304	1.26	0.0117	0.026	715	202	160	
304	1.26	0.0220	0.025	954	441	324	
304	1.26	0.0315	0.024	1150	637	446	
304	1.26	0.0409	0.025	1340	827	551	13.7 ± 0.9
311	1.16	0	0.022	469	0	0	
311	1.16	0.0122	0.022	750	281	221	
311	1.16	0.0335	0.023	1250	781	539	
311	1.16	0.0428	0.022	1470	1000	664	15.4 ± 1.1

^a A₀ ≡ the SO₄⁻ absorbance immediately after the laser flash, i.e., when SO₄⁻ production is complete but no significant SO₄⁻ decay has occurred;

^b (k' - k_{bg})₀ ≡ (k' - k_{bg}) in the zero-ionic strength limit;

^c Uncertainties represent precision only.

Arrhenius plots for R3-11 to R3-13 are shown in Figure 9. Linear least squares analyses of the $\ln k_{Ri}$ vs. $1/T$ data give the following Arrhenius expressions (units are $M^{-1} s^{-1}$):

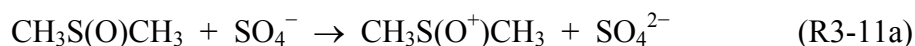
$$k_{11} = (3.7 \pm 0.6) \times 10^{11} \exp\{-(1400 \pm 100)/T\}$$

$$k_{12} = (3.8 \pm 1.9) \times 10^8 \exp\{-(1360 \pm 160)/T\}$$

$$k_{13} = (4.8 \pm 1.5) \times 10^7 \exp\{-(2490 \pm 520)/T\}$$

Uncertainties in the above expressions are 2σ and refer to the precision of the Arrhenius parameters only. Potential effects of systematic errors on the measured rate coefficients are discussed below.

The only kinetic study reported in the literature for SO_4^- reactions with organic sulfur compounds is a room temperature (not specified) measurement of the DMSO + SO_4^- rate coefficient (k_{11}) by Kishore and Asmus (1989) which was carried out using pulse radiolysis techniques. These authors report a rate coefficient of $(2.7 \pm 0.3) \times 10^9 M^{-1} s^{-1}$, which is in excellent agreement with the result at 294 K obtained in this study (see Table 6). The SO_4^- radical is a strong oxidant with a one-electron redox potential of about 2.5 V (Kim and Hamill 1976). Kishore and Asmus have demonstrated that R3-11 proceeds *via* one-electron transfer mechanism:



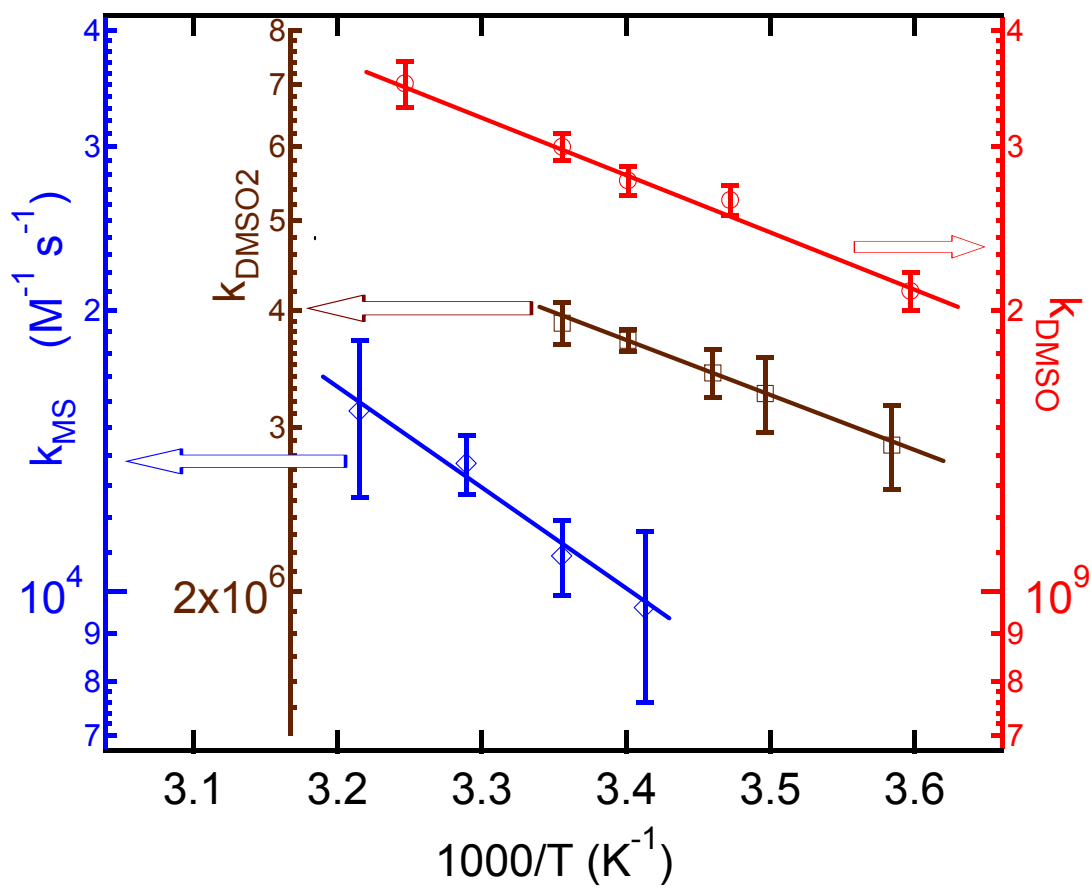


Figure 9 Arrhenius plots for SO_4^- reactions with DMSO, DMSO2 and MS

Solid lines are obtained from least square analyses which yield the Arrhenius expressions shown in the text.

Kishore and Asmus have also shown that the one-electron redox potential of DMSO is in the range 1.8 - 2.0 V. The more oxidized sulfur compounds DMSO₂ and MS are expected to have larger one-electron redox potentials than DMSO, and the much slower values for k_{12} and k_{13} (compared to k_{11}) observed in this study suggest that these two reactions probably proceed *via* an H-abstraction mechanism rather than *via* an electron transfer mechanism. This is similar to the reactions of SO_4^- with some organics, such as alcohols, alkanes and ethers (Clifton and Huie 1989; Huie and Clifton 1989; George et al., 2001).

The similar activation energies obtained for R3-11 and R3-12 can be rationalized using the relationship (Elliot et al., 1990)

$$k_{\text{obs}} = k_{\text{diff}} \left\{ 1 + \frac{k_{\text{diff}}}{k_{\text{react}}} \right\}^{-1} \quad (3-6)$$

where k_{obs} is the observed bimolecular rate coefficient, k_{diff} is the encounter rate coefficient of the two reacting species due to diffusion in water solution, and k_{react} is the rate coefficient that would be measured if diffusion was not rate-limiting. For the near-diffusion-controlled R3-11, the temperature dependence of k_{react} is presumably very small and the temperature dependence of k_{diff} exerts a strong influence on the observed activation energy. The value of k_{diff} for R3-11 can be estimated from the Smoluchowski equation (Espenson 1981)

$$k_{\text{diff}} = 4\pi(D_{\text{SO}_4^-} + D_{\text{DMSO}})(r_{\text{SO}_4^-} + r_{\text{DMSO}}) \cdot N_A \quad (3-7)$$

where $D_{\text{SO}_4^-}$ and D_{DMSO} are the reactant aqueous phase diffusion coefficients, $r_{\text{SO}_4^-}$ and r_{DMSO} are the reactant radii, and N_A is Avogadro's number. Using the diffusion coefficients and molecular radii tabulated by Elliot et al. (Elliot et al., 1990) as a guide, we estimate $D_{\text{SO}_4^-} \sim D_{\text{DMSO}} \sim 1.05 \times 10^{-9} \text{ m}^2 \text{ s}^{-1}$ and $r_{\text{SO}_4^-} \sim r_{\text{DMSO}} \sim 3.7 \times 10^{-10} \text{ m}$ at $T = 298 \text{ K}$. Substituting these parameters into Equation. (3-7) gives $k_{\text{diff}} \sim 1.2 \times 10^{10} \text{ M}^{-1} \text{ s}^{-1}$ for R3-11. Hence, it appears that for R3-11 at 298 K, $k_{\text{obs}} \sim k_{\text{diff}}/4$ and k_{react} could be estimated to be $\sim 4.0 \times 10^9 \text{ M}^{-1} \text{ s}^{-1}$ from Equation. (3-6). From the average effective activation energy for self-diffusion in water within the temperature range of 278 – 308 K, ($E_{\text{adiff}} \sim 20.3 \text{ kJ mol}^{-1}$) (Weingartner 1982), the pre-exponential factor for diffusion (A_{diff}) is estimated to be $4.2 \times 10^{13} \text{ M}^{-1} \text{ s}^{-1}$. Assuming that A_{diff} and E_{adiff} are constant within the temperature range studied (which is only approximately true), k_{diff} at each temperature can be evaluated, thus allowing $k_{\text{react}}(T)$ to be estimated using Equation (3-6). From a plot of k_{react} versus $1/T$, the following Arrhenius expression is derived:

$$k_{\text{react}} = (1.3 \pm 0.4) \times 10^{11} \exp(-(1040 \pm 96)/T)$$

Figure 10 shows the comparison of the Arrhenius plots of k_{diff} , k_{obs} and k_{react} for R-11. The true activation energy for the $\text{SO}_4^- + \text{DMSO}$ reaction is estimated to be $\sim 8.6 \text{ kJ mol}^{-1}$, about 25% lower than the observed E_a . The same analysis method was used for the data of R3-12 and R3-13, and k_{react} derived from such analyses were found to be exactly the same as k_{obs} , so that the observed temperature dependence of these two reactions should be due almost entirely to k_{react} , if impurity effects are not important.

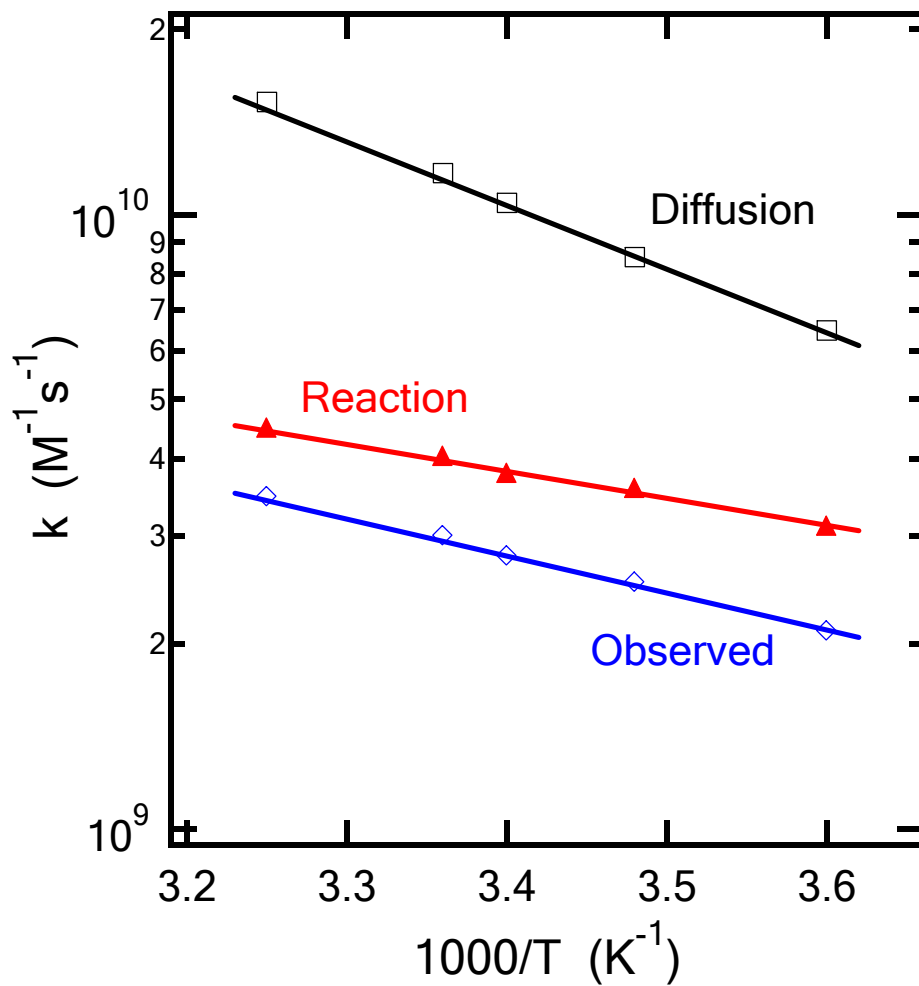


Figure 10 Comparison of the Arrhenius plots of k_{diff} , k_{obs} and k_{react} for the DMSO + SO_4^- reaction

The most likely source of systematic error in the rate coefficient determinations reported in this study is the significant contribution to SO_4^- loss from reactions with background impurities in the DMSO, DMSO₂, and/or MS samples. Because the DMSO sample purity is high (>99.9%) and the observed reaction rate coefficient is near the diffusion-controlled limit, impurity reactions can be ruled out as a source of error in the determination of k_{11} . The MS sample used in the study of R3-13 had a stated minimum purity of 98%. However, according to the manufacturer, the major impurity in the MS sample was water. The large observed activation energy for R3-13 argues against fast reaction of SO_4^- with a minor impurity as the source of observed reactivity; however, some contribution from impurity reactions cannot be completely ruled out, so the error bars for measured values of k_{13}^0 are adjusted upward to $\sim 30\%$. In the case of DMSO₂, all observed reactivity could result from reaction of SO_4^- with a trace impurity (0.11 % DMSO, for example); since this possibility cannot be ruled out, we consider the measured rate coefficients to represent upper limits to $k_{12}(T)$. Hence the low activation energy for R3-12 (close to that for R3-11) obtained from this work could be either from the reaction itself or reaction of SO_4^- with trace impurities in the DMSO₂ sample.

CHAPTER IV

TEMPERATURE DEPENDENT KINETICS STUDIES OF OH REACTIONS WITH DMSO, DMSO₂ AND MS

OH Radicals in the Atmospheric Aqueous Phase

OH radicals represent the most important atmospheric oxidant in both the gas and the aqueous phases. The principle primary source of gas phase OH is the photolysis of ozone in the presence of water vapor (Lelieveld and Crutzen 1991). Photolysis of nitrous acid (HONO) and reaction of HO₂ radicals with NO are also thought to be significant sources of gas phase OH production in the troposphere (Seinfeld and Pandis 1998, page 252) in the early morning and polluted areas, respectively. The production of HO₂ radicals from the photolysis of carbonyl species such as formaldehyde and acetone (Jaegle et al., 2000; Tan et al., 2001) is considered a potentially important source of OH because HO₂ is an important OH reservoir. Transfer of OH radicals from the gas phase is the most important source for the aqueous OH radicals and accounts for nearly 80% of its total flux (Jacob 1986; Herrmann et al., 2000). In the marine atmosphere, photolysis of H₂O₂ and the reactions of O₃ with OH⁻, H₂O₂ (Chameides and Davis 1982), and with O₂⁻ (Sehested et al., 1983) also play significant roles in the aqueous phase OH production. The main sinks for aqueous OH radicals are reactions with organics, such as

formaldehyde and acetate. Concentrations of these organic compounds are about one order of magnitude lower in the marine aqueous phase compared to polluted urban areas, so aqueous phase OH radical concentrations in the unpolluted marine atmosphere are generally higher than concentrations in polluted continental areas (Herrmann et al., 2000). Studies have shown that in the marine atmosphere, reactions with Br^- , H_2O_2 and Cl^- could account for about 50% of the total OH loss from the aqueous phase (Herrmann et al., 2000). However, in all above assessments, OH reactions with the organic sulfur compounds were not considered, although DMS and its oxidation products are a group of important components could potentially affect the OH budget in the marine atmosphere. In order to properly assess aqueous phase concentrations of OH radicals and/or organic sulfur compounds, it is important to examine OH-sulfur reactions, especially given their high reactivities and concentrations in the marine atmospheric condensed phase.

OH reactions with organics in the aqueous phase have been widely studied. The OH radical is an electrophile and readily adds to centers of unsaturation such as olefinic double bonds and aromatic rings, generally at close to diffusion rates. Its reactions with saturated organic molecules, such as alcohols, esters and carbonates proceed primarily *via* H-abstraction, and room temperature rate coefficients for such reactions are typically in the range of $10^7 - 5 \times 10^9 \text{ M}^{-1} \text{ s}^{-1}$ (Tuazon et al., 1999; Ervens et al., 2003; George et al., 2003), depending to some extent on the nature and position of functional groups (Buxton and Salmon 2003). OH reactions with some carboxylic acids / carboxylates were found to proceed *via* a one electron transfer mechanism, and the rate coefficients of these reactions are in the range of $10^7 - 5 \times 10^8 \text{ M}^{-1} \text{ s}^{-1}$ (Walling and El-Taliawi 1973; Cabelli and Bielski 1985; Logan 1989; Ervens et al., 2003). Only when the reduction

potentials of the organic anions are less than that of OH radical is the one electron transfer reaction possible, and the differences in reduction potentials for organics make the reactivity of the organic anions toward OH radicals vary widely.

The other mechanism for OH reaction is the very fast addition (near diffusion controlled limit) of OH with a reactant to form an adduct intermediate. In most cases the intermediate adduct is very unstable and either dissociates or reacts with other species in the system. Examples are that the adduct from the OH + SCN⁻ reaction dissociates to release OH⁻ and SCN radical (Chin and Wine 1992), and that the adduct from the OH + DMS reaction reacts with DMS and O₂ (if O₂ is available) (Bonifacic et al., 1975).

As the second part of a series of kinetics studies of the aqueous phase reactions of organic sulfur species with important atmospheric radicals, this chapter includes the first temperature-dependent kinetics investigation of reactions of three sulfur compounds of atmospheric interest, i.e., DMSO, DMSO₂ and MS with the OH radical using a laser flash photolysis (LFP) - long path UV-visible absorption (LPA) - competitive kinetics (CK) technique.

Experimental Method

The LFP - LPA - CK technique involves coupling OH radical production by laser flash photolysis of aqueous $\text{H}_2\text{O}_2/\text{SCN}^-/\text{R}$ (R = DMSO, DMSO₂ or MS) solutions with sensitive time-resolved detection of $(\text{SCN})_2^-$, the radical product of a competing reaction, by multipass absorption spectroscopy at $\lambda \sim 475$ nm. The schematic diagram of the experimental apparatus is the same as that described in Figure 4 and will not be repeated here. In all experiments, the White cell mirrors (White 1942) were adjusted to allow 46 passes of the probe radiation through the region of the reactor irradiated by the laser, giving an absorption path length of ~ 115 cm. With an electronic time constant of $1\ \mu\text{s}$, the detection limit is about 0.03% absorption (64 flashes averaged); assuming a peak $(\text{SCN})_2^-$ extinction coefficient of $\sim 7600\ \text{M}^{-1}\ \text{cm}^{-1}$ at 475 nm (Baxendale et al., 1968; Dogliotti and Hayon 1968; Hug 1981), the detection limit of $(\text{SCN})_2^-$ under the experimental conditions employed in this work is estimated to be $\sim 2 \times 10^{-10}$ M. As mentioned above, OH radicals were produced by laser flash photolysis of H_2O_2 :

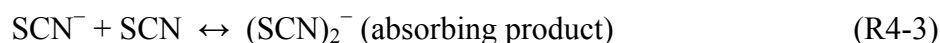


All experiments were carried out under pseudo-first order conditions with the concentration of H_2O_2 , SCN^- , and R (R = DMSO, DMSO₂, or MS) in large excess over that of OH. Typical concentrations of the OH photolytic precursor H_2O_2 were $(2 - 10) \times 10^{-5}$ M, and the concentration range of SCN^- was $(0.3 - 5) \times 10^{-5}$ M. The concentration of OH immediately after the laser flash is estimated to be in the range $(2 - 10) \times 10^{-8}$ M by using an equation similar to Equation (3-1):

$$[\text{OH}] = \Phi \varepsilon_{\text{H}_2\text{O}_2} F [\text{H}_2\text{O}_2] / N_A \quad (4-1)$$

where $\Phi = 2$, the production yield of OH from the photolysis of H_2O_2 (R4-1); $\varepsilon_{\text{H}_2\text{O}_2} = 26 \text{ M}^{-1} \text{ cm}^{-1}$ (<http://www.h2o2.com/intro/properties/radiation.html>), the extinction coefficient of H_2O_2 in water at 248 nm ; F is the laser fluence at the reaction cell, typically $1.4 \times 10^{16} \text{ photons/cm}^2/\text{pulse}$ in our experiments; and N_A is Avogadro's number. The use of such low radical concentrations avoided kinetic complications that could result from radical - radical side reactions.

Given the absence of aqueous phase OH fluorescence, the low OH extinction coefficient ($\varepsilon_{\text{max}} \approx 540 \text{ M}^{-1} \text{ cm}^{-1}$ at 188 nm) (Hug 1981), and the fact that OH (aq) absorbs radiation only in the far ultraviolet spectral region, directly monitoring OH radicals in aqueous phase kinetics studies is extremely difficult. Hence, a competitive kinetics method was employed to follow OH reaction kinetics subsequent to the laser flash. The thiocyanate anion, SCN^- , was used as the competitor for the present kinetics studies. In the presence of SCN^- and a given sulfur compound, R, the following chemistry occurs:



The absorption of the $(\text{SCN})_2^-$ radical anion at 475 nm (Baxendale et al., 1968; Dogliotti and Hayon 1968; Hug 1981) was followed as a function of time without significant interference from other absorbing species. The spectrum of $(\text{SCN})_2^-$ has been

studied previously, and Figure 10 shows one example of a reported $(\text{SCN})_2^-$ absorption spectrum from Dogliotti and Hayon (1968).

Experimental conditions were such that virtually all OH radicals produced by the laser flash react with either SCN^- or R, i.e., the fraction of OH removed by reaction with H_2O_2 or background solvent impurities is negligible. Therefore, the production of $(\text{SCN})_2^-$ is suppressed as the concentration of the sulfur species increases, since OH radicals react with either SCN^- or sulfur species R according to the product of the reaction rate coefficient and the competing reactant concentration, i.e., $k_{\text{SCN}^-}[\text{SCN}^-]$ and $k_{\text{R}}[\text{R}]$:

$$\frac{[(\text{SCN})_2^-]_0}{[(\text{SCN})_2^-]_{\text{R}}} = \frac{k_{\text{R}}[\text{R}] + k_{\text{SCN}^-}[\text{SCN}^-]}{k_{\text{SCN}^-}[\text{SCN}^-]} \quad (4-2)$$

where $[(\text{SCN})_2^-]_0$ is the concentration of $(\text{SCN})_2^-$ when SCN^- is the only species to react with OH, and $[(\text{SCN})_2^-]_{\text{R}}$ is the concentration of $(\text{SCN})_2^-$ when R is present in the system. Under the assumption that the $(\text{SCN})_2^-$ absorption signal per unit OH that reacts with SCN^- is independent of the concentration of sulfur species R (this assumption is discussed below), the above equation can then be rewritten as:

$$\frac{[(\text{SCN})_2^-]_0}{[(\text{SCN})_2^-]_{\text{R}}} = \frac{A_0}{A_{\text{R}}} = \frac{k_{\text{R}}[\text{R}]}{k_{\text{SCN}^-}[\text{SCN}^-]} + 1 \quad (4-3)$$

where A_0 is the absorbance that is observed after the production of $(\text{SCN})_2^-$ is complete but before significant $(\text{SCN})_2^-$ decay has occurred when SCN^- is the only species to react with OH, and A_{R} is the analogous absorbance when R is present in the solution.

According to Equation (4-3), a plot of A_0/A_R vs. $[R]/[SCN^-]$ should be linear with a slope equal to the rate coefficient ratio k_R/k_{SCN^-} .

Typical 475 nm absorbance temporal profiles observed following laser flash photolysis of $H_2O_2/SCN^-/DMSO$ aqueous solutions are shown in Figure 12. It is clear that the detected $(SCN)_2^-$ absorbance decreases with increasing DMSO concentration. The experimental conditions were such that absorbance rise times were always much faster than absorbance decay times. The pseudo-first order decay rate of radicals was found to be independent of concentrations of sulfur species in the studies of OH reactions with DMSO, DMSO₂ and MS. Therefore, values for A_0 and A_R could be obtained from the measurement of the peak absorbance without introducing significant error. Selected absorbance temporal profiles were fit to the triple-exponential function that was obtained as an analytical solution to the rate equations for the mechanism including R4-2, R4-3, and R4-4 as well as the loss of the free radicals (OH, SCN, and $(SCN)_2^-$) due to reactions with H_2O_2 , sulfur species R and background impurities (Chin and Wine 1992). The peak absorbance A_0 and A_R that would have been observed in the complete absence of radical decay could be derived from these fits. Further details of this method are described in Chapter VI. The rate coefficients obtained from this more rigorous analysis method were essentially identical to those obtained from the direct reading of A_0 and A_R maxima from the observed absorbance temporal profiles, like those shown in Figure 12. Typical plots of A_0/A_R vs. $[R]/[SCN^-]$ for studies of OH reactions with DMSO, DMSO₂ and MS at 298 K are shown in Figure 13. Good linear relationships were observed for all three reactions within the temperature range studied and, the rate coefficient ratios obtained from the slopes of these plots for all studied temperatures are summarized in Table 9.

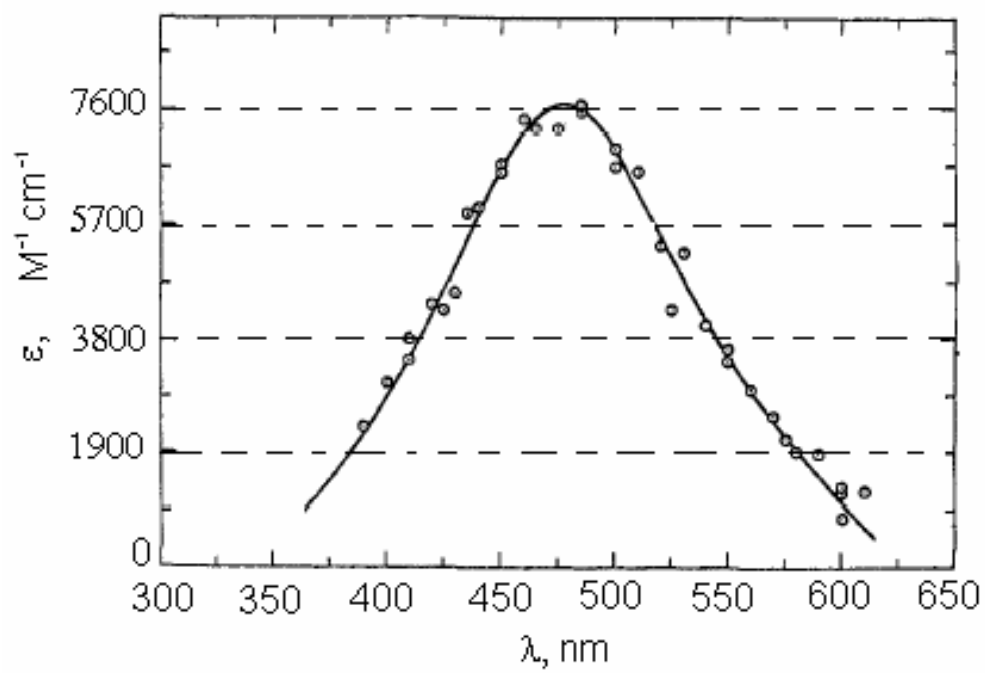


Figure 11 The absorption spectrum of $(\text{SCN})_2^-$ from Dogliotti and Hayon (1968)

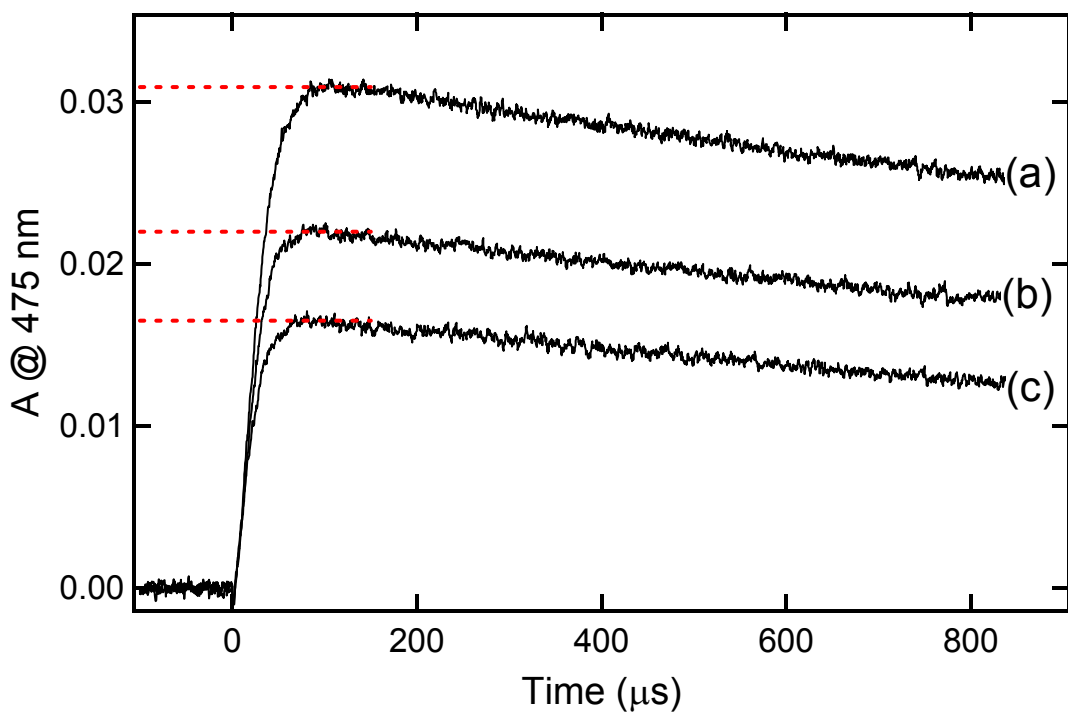


Figure 12 Typical temporal profiles of $(\text{SCN})_2^-$ absorbance at 475 nm in the **DMSO/H₂O₂/SCN⁻** system

Experimental conditions: $T = 298 \text{ K}$; $[\text{SCN}^-] = 4.8 \times 10^{-6} \text{ M}$; $[\text{H}_2\text{O}_2] = 4.3 \times 10^{-5} \text{ M}$; $[\text{DMSO}] =$ (a) 0, (b) $3.4 \times 10^{-6} \text{ M}$, and (c) $7.7 \times 10^{-6} \text{ M}$.

Results and Discussion

Evaluation of Absolute Rate Coefficients

In order to obtain temperature-dependent absolute rate coefficients from the results in Table 9, the OH + SCN⁻ reaction rate coefficient must be known as a function of temperature. To our knowledge, temperature-dependent kinetics studies of the OH + SCN⁻ reaction have been reported only by Elliot and Simsons (1984) over the temperature range 292 – 352 K and by Chin and Wine (1992) over the temperature range 277 – 321 K. Elliot and Simsons employed pulse radiolysis and competitive kinetics methods. In their study, the OH + SCN⁻ rate coefficient was measured relative to the rate coefficients for OH reactions with formate and t-butanol; the OH + formate and OH + t-butanol rate coefficients were measured relative to the rate coefficient for the OH + ferricyanide (Fe(CN)₆⁴⁻) reaction; and the OH + ferricyanide rate coefficient was measured directly. The approach employed by Chin and Wine was direct (no competitors) using the same technique described in this dissertation, but involved analysis of triple exponential temporal profiles of (SCN)₂⁻ absorbance. At low SCN⁻ concentrations, such experiments are sensitive to the OH + SCN⁻ rate coefficient (Baxendale et al., 1968; Chin and Wine 1992). At 297 K, the OH + SCN⁻ rate coefficients obtained from the two studies (Elliot and Simsons 1984; Chin and Wine 1992) agree very well. The activation energy reported by Chin and Wine, 15.8 kJ mol⁻¹, is somewhat larger than the activation energy reported by Elliot and Simsons, 11 kJ mol⁻¹, although the difference between the reported activation energies is reduced considerably if the highest temperature rate coefficient reported by Elliot and Simsons (T = 352 K, which is much higher than the

temperature range of interest in this study) is excluded from the analysis. Since there are advantages and disadvantages to both methods employed to obtain temperature-dependent rate coefficients for the OH + SCN⁻ reaction, we have decided to weigh the two data sets equally except that we ignored the highest temperature rate coefficient reported by Elliot and Simsons (see above). Adopting such an approach leads to the following temperature-dependent rate coefficient for the SCN⁻ + OH reaction:

$$k_{\text{SCN}^-} = 3.45 \times 10^{12} \exp(-1690/T)$$

in units of M⁻¹ s⁻¹. We estimate that the absolute uncertainty in k_{SCN^-} at the 95% confidence level is $\pm 11\%$ at 310 K, $\pm 8\%$ at 295 K, and $\pm 15\%$ at 275 K.

The above Arrhenius expression for k_{SCN^-} has been employed in combination with the relative rate data in Table 9 to obtain the temperature-dependent rate coefficients $k_{\text{R}}(T)$ (R = DMSO, DMSO₂, MS). The results are plotted in Arrhenius form in Figure 14. The dashed line is the temperature dependent kinetics of the SCN⁻ + OH reaction that was used to derive the $k_{\text{R}}(T)$ in this work, and the solid lines were obtained from least squares analyses of the $\ln k_{\text{R}}$ vs. $1/T$ data. These analyses give the following Arrhenius expressions in units of M⁻¹ s⁻¹:

$$k_{\text{DMSO}} = (4.72 \pm 0.66) \times 10^{11} \exp\{-(1270 \pm 40)/T\}$$

$$k_{\text{DMSO}_2} = (5.14 \pm 0.87) \times 10^9 \exp\{-(1690 \pm 50)/T\}$$

$$k_{\text{MS}} = (8.79 \pm 1.14) \times 10^{10} \exp\{-(2630 \pm 40)/T\}$$

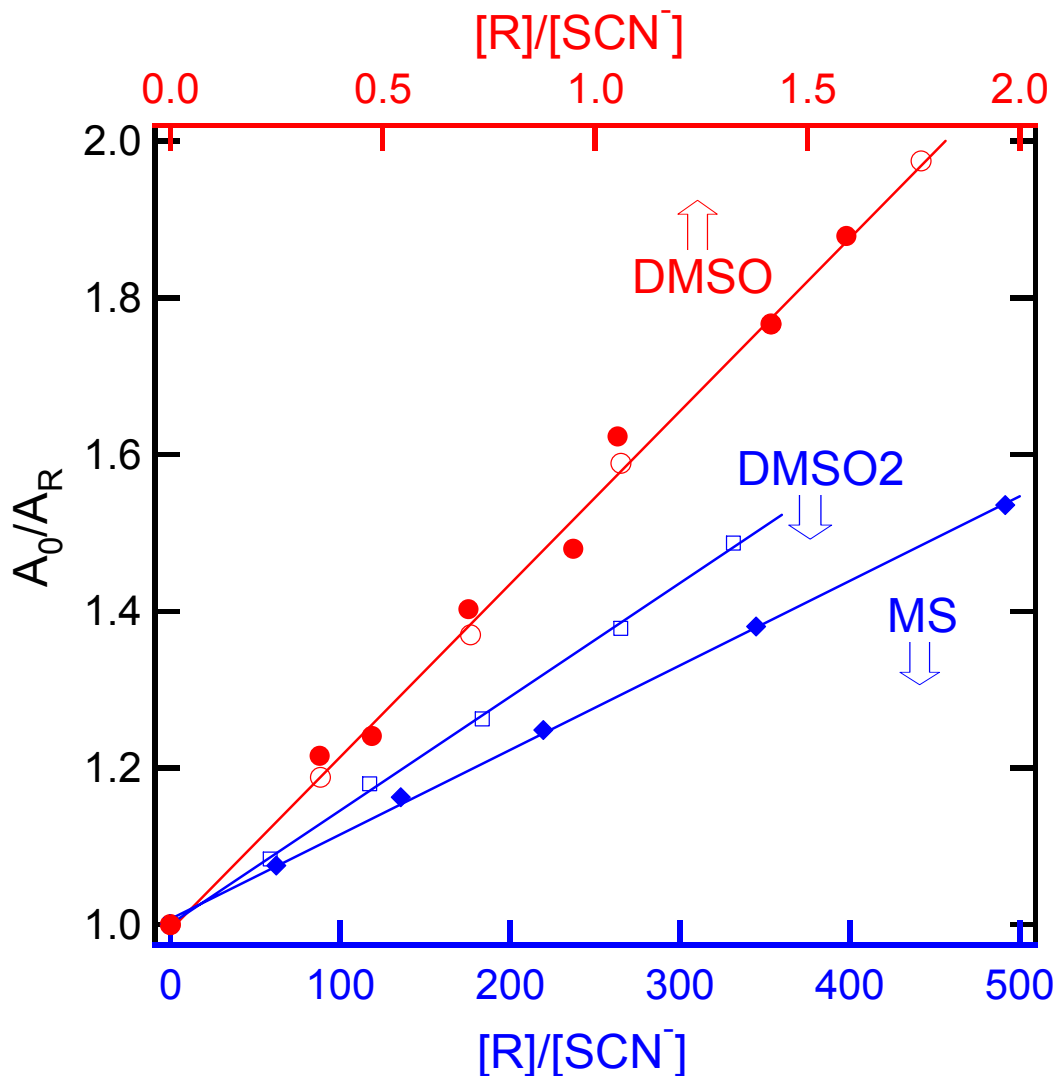


Figure 13 Plots of A_0/A_R versus $[R]/[SCN^-]$ ($R = \text{DMSO}, \text{DMSO}_2$ or MS) for data obtained at $T = 298 \text{ K}$

For $R = \text{DMSO}$, data are shown at two different SCN^- concentrations, $5 \times 10^{-5} \text{ M}$ (open circles) and $5 \times 10^{-6} \text{ M}$ (filled circles). The data shown for $R = \text{DMSO}_2$ and MS were obtained at an SCN^- concentration of $5 \times 10^{-6} \text{ M}$. Solid lines are obtained from linear least-squares analyses. The following rate coefficient ratios (k_R/k_{SCN^-}) are obtained from the slopes of the solid lines: 0.544 ± 0.017 for $R = \text{DMSO}$, 0.00143 ± 0.00009 for $R = \text{DMSO}_2$, and 0.00108 ± 0.00005 for $R = \text{MS}$. Uncertainties are 2σ and represent precision only.

Table 9 Rate coefficient ratios (k_R/k_{SCN^-}) determined in this study

T(K)	$10^5 k_R / k_{\text{SCN}^-}$ *		
	R= DMSO	R=DMSO2	R=MS
275		145 ± 5	82 ± 7
278	60600 ± 1600		
281		147 ± 6	89 ± 4
287	57500 ± 2200	147 ± 5	95 ± 3
293		148 ± 4	101 ± 3
294	56100 ± 1300		
298	54400 ± 1700	145 ± 6	108 ± 5
305	53100 ± 1100	147 ± 4	116 ± 5
310			120 ± 5

* Uncertainties are 2σ and represent precision only.

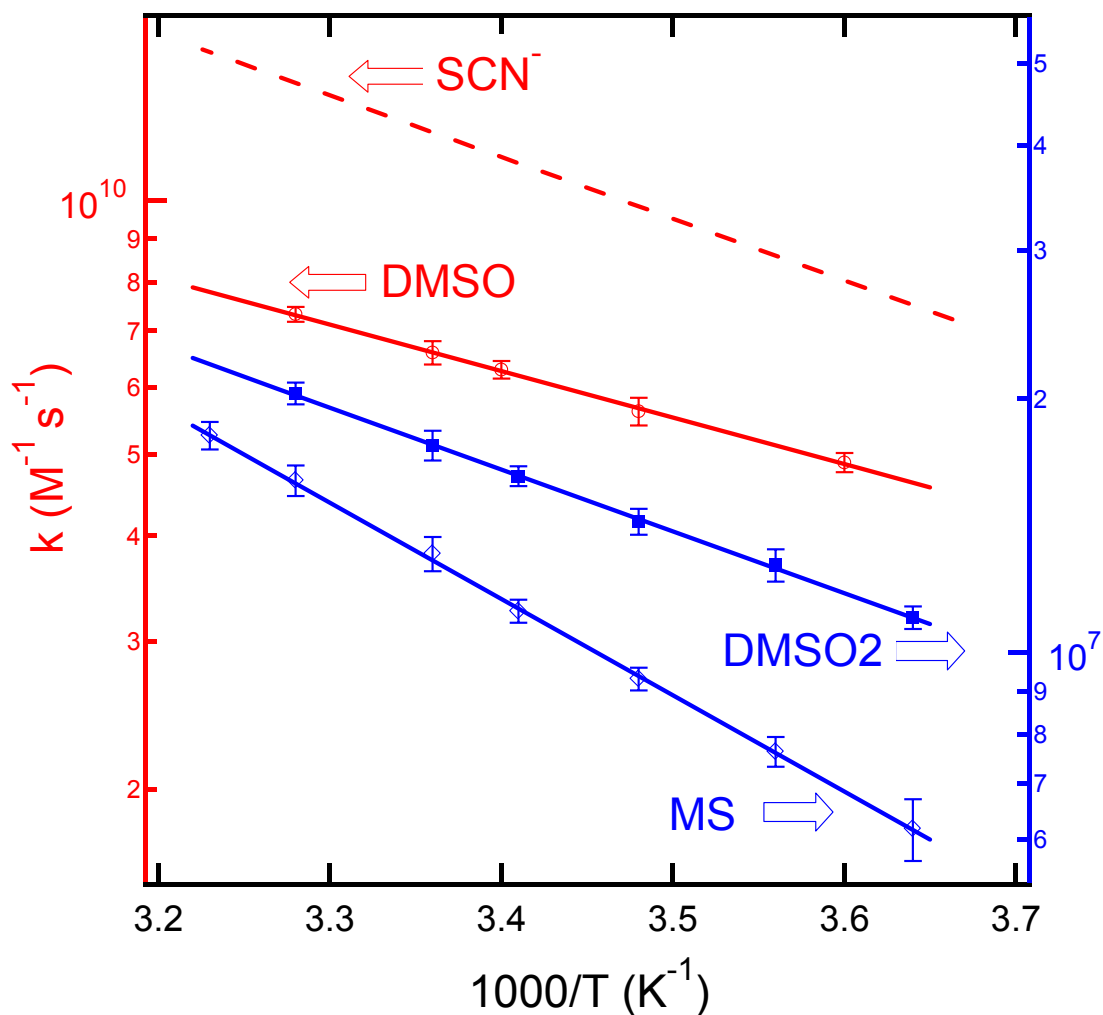


Figure 14 Arrhenius plots for OH(aq) reactions with DMSO, DMSO₂ and MS

The rate coefficients are the mean of all the experimental data for a given reactant at each temperature. Error bars are 2σ and represent the precision of the rate coefficient determination. Solid lines are obtained from least-squares analyses which yield the Arrhenius expressions given in the text. For completeness, the assumed Arrhenius plot for the competing OH + SCN⁻ reaction is shown by the dashed line.

Uncertainties in the above Arrhenius expressions are 2σ and represent precision only. Since the rate coefficient ratios have been determined with very good precision (Table 9), and since uncertainties in $[\text{SCN}^-]$ and $[\text{R}]$ are believed to be no more than a few percent, the absolute accuracies for $k_{\text{R}}(\text{T})$ derived from the above Arrhenius expressions appear to be limited by the accuracies of $k_{\text{SCN}^-}(\text{T})$, which were estimated above.

The measured rate coefficients for the $\text{DMSO} + \text{OH}(\text{aq})$ reaction are near the expected diffusion controlled limit, so the measured activation energy (E_a) is to a large extent affected by the effective E_a for molecular diffusion. As mentioned earlier in Chapter III, for diffusion-controlled reactions, the following equation applies here (Noyes 1961; North 1964; Elliot et al., 1990):

$$k_{\text{obs}} = k_{\text{diff}} \left\{ 1 + \frac{k_{\text{diff}}}{k_{\text{react}}} \right\}^{-1} \quad (4-4)$$

where k_{obs} is the observed rate coefficient, k_{diff} is the encounter rate coefficient of the two reactants due to diffusion in water solvent, and k_{react} is the true reaction rate coefficient. k_{diff} for the $\text{DMSO} + \text{OH}$ reaction can be estimated from the Smoluchowski equation (North 1964; Espenson 1981):

$$k_{\text{diff}} = 4\pi(D_{\text{OH}} + D_{\text{DMSO}})(r_{\text{OH}} + r_{\text{DMSO}}) \cdot N_{\text{A}} \quad (4-5)$$

Similar to analysis of $\text{DMSO} + \text{SO}_4^-$ reaction kinetics, using the diffusion coefficients (D) and radii (r) tabulated by Elliot et al. (1990) as a guide, the following

values are estimated for the parameters in Equation (4-5): $D_{\text{OH}} \sim 2.2 \times 10^{-9} \text{ m}^2/\text{s}$, $D_{\text{DMSO}} \sim 1.0 \times 10^{-9} \text{ m}^2/\text{s}$, $r_{\text{OH}} \sim 0.22 \text{ nm}$, $r_{\text{DMSO}} \sim 0.365 \text{ nm}$. Thus k_{diff} for the DMSO + OH reaction is estimated to be $\sim 1.4 \times 10^{10} \text{ M}^{-1} \text{ s}^{-1}$ at 298 K. From the average effective activation energy for self-diffusion in water within the temperature range 275 – 305 K, ($E_{\text{adiff}} \sim 20.3 \text{ kJ mol}^{-1}$) (Weingartner 1982), the pre-exponential factor for diffusion (A_{diff}) is estimated to be $5.2 \times 10^{13} \text{ M}^{-1} \text{ s}^{-1}$. Assuming that A_{diff} and E_{adiff} are constant within the temperature range studied (which is only approximately true), k_{diff} at each temperature can be evaluated, thus allowing $k_{\text{react}}(T)$ to be estimated from Equation (4-4). For the DMSO + OH reaction at all studied temperatures, values for k_{obs} , k_{diff} and k_{react} were estimated from this method, and are summarized in Table 10. Arrhenius plots of these data are presented in Figure 15, from which the true activation energy for the OH + DMSO reaction is estimated to be -1.1 kJ mol^{-1} . Although this estimate of the reaction activation energy (E_{areact}) is not very accurate, it is worth noting that it is very similar to the temperature dependence observed for the OH + DMSO reaction in the gas phase (Hynes and Wine 1996). The small negative E_a for the DMSO + OH reaction suggests that reaction proceeds *via* initial formation of the unstable DMSO-OH adduct; this will be discussed in detail later in the section discussing reaction mechanisms.

For the much slower DMSO₂ + OH(aq) and MS + OH(aq) reactions, it was found that when the same method was used to analyze the data, diffusion does not affect the reaction rate coefficients or the activation energies observed, i.e., the observed rate coefficients k_{obs} are essentially equal to k_{react} .

Table 10 Summary of k_{obs} , k_{diff} and k_{react} for the DMSO + OH reaction at all studied temperatures in units of $10^9 \text{ M}^{-1} \text{ s}^{-1}$

Temperature (K)	k_{obs}	k_{diff}	k_{react}
278	4.9	7.1	16.2
287	5.7	9.3	14.4
294	6.3	11	13.9
298	6.6	13	13.7
305	7.3	15	13.9

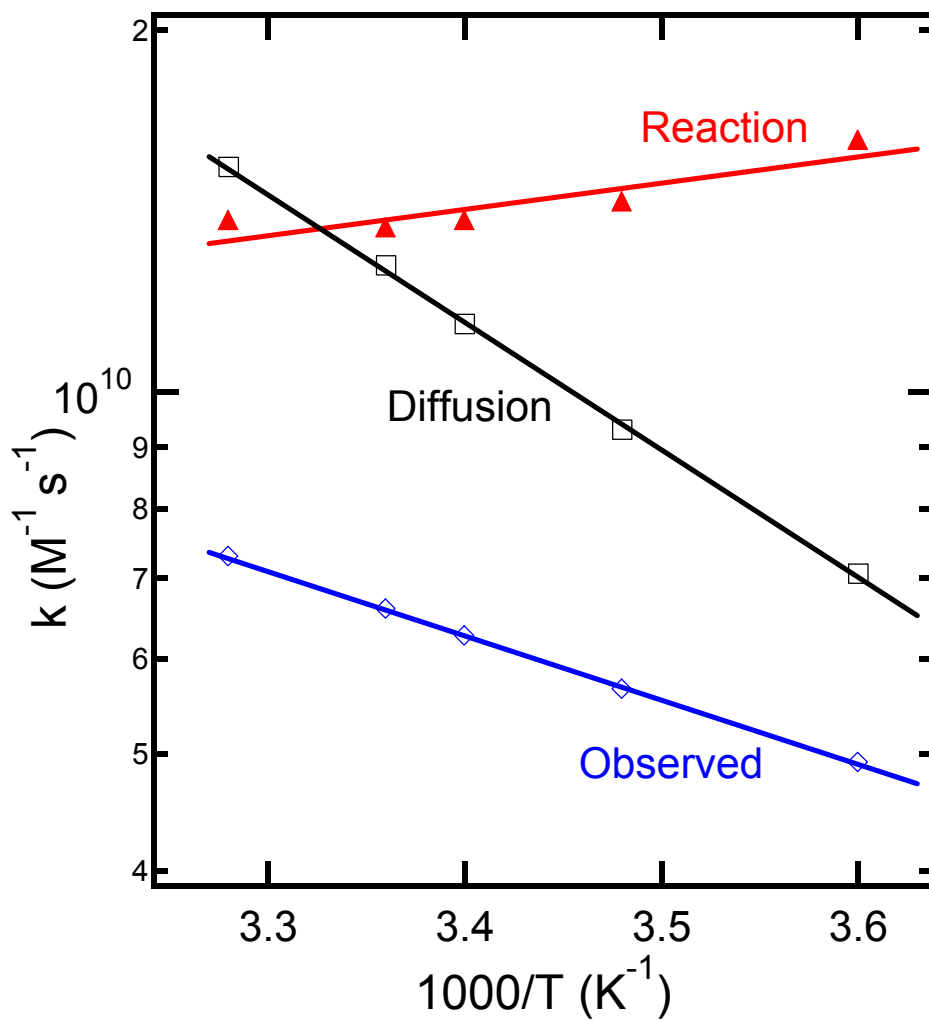


Figure 15 Arrhenius plots of k_{obs} , k_{diff} and k_{react} for the DMSO + OH reaction

Possible Sources of Systematic Error

An important experimental parameter in this competitive kinetics study is the SCN^- concentration. We have chosen to employ relatively low $[\text{SCN}^-]$ ranging from 3 to 50 μM . Use of low $[\text{SCN}^-]$ has two important advantages. First, production of reactive transient species *via* 248 nm laser flash photolysis of SCN^- is kept at a level where such species cannot perturb the chemistry under investigation (Dogliotti and Hayon 1968; Luria and Treinin 1968). Second, in air-saturated solutions, the radical products (X) of $\text{OH} + \text{R}$ reactions are expected to react with O_2 on a time scale that is sufficiently rapid to prevent X from reacting with SCN^- ; the peroxy radicals generated from $\text{X} + \text{O}_2$ reactions are relatively unreactive (for example, Neta et al., 1990) and are expected to be stable on the time scale for $(\text{SCN})_2^-$ appearance used in this study. The use of low $[\text{SCN}^-]$ does, in contrast to the advantages discussed above, have one potentially important disadvantage. Over the range of SCN^- concentrations employed in this study, the $\text{SCN} + \text{SCN}^- \leftrightarrow (\text{SCN})_2^-$ equilibrium (R4-3) is such that 10 – 65 % of the radicals exist as SCN (Baxendale et al., 1968; Baxendale and Bevan 1969; Elliot and Sopchyshyn 1984; Chin and Wine 1992; Wu et al., 2001). Hence, the occurrence of the following reaction



could lead to an overestimation of the rate coefficients of interest. While SCN^- appears to be a viable competitor for a wide range of $\text{OH}(\text{aq})$ kinetics, systematic errors due to R4-5 have been reported for $\text{R} =$ substituted carboxylic acids (Logan and Salmon 1984). Two pieces of experimental evidence lead us to conclude that R4-5 was not a problem in

this study. First, as exemplified by the data shown in Figure 13, no systematic trend in k_R/k_{SCN^-} as a function of $[\text{SCN}^-]$ is observed for any of the studied reactants. Second, the occurrence of R4-5 would manifest itself as an increase in the observed $(\text{SCN})_2^-$ decay rate with increasing $[\text{R}]$ at constant $[\text{SCN}^-]$ and as a decrease in the observed $(\text{SCN})_2^-$ decay rate with increasing $[\text{SCN}^-]$ at constant $[\text{R}]$. No such behavior was observed for any of the reactions studied.

A significant contribution to OH loss from impurities in the chemical samples represents another potential source of systematic errors in the reported rate coefficients. Because the DMSO and SCN^- sample purities were high and the rate coefficients for reactions of these species with OH are near the diffusion-controlled limit, it is not possible for impurity reactions to impact the determination of k_{DMSO} . Two different MS samples were used in this study, one with a stated minimum purity of 98% and the other with a stated minimum purity of 99%; in both cases, the major impurity was water, according to the manufacturer. Essentially identical results were obtained with these samples. The observed activation energy for the OH + MS reaction is much larger than one would expect if the observed reactivity was due to a minor impurity that reacted at a near-diffusion controlled rate with OH. Hence, we are confident that impurity reactions were not a problem in our study of the OH + MS reaction. The stated minimum purity of the DMSO2 sample used in this study was 98% and the observed activation energy is small enough that a significant contribution to the observed reactivity from a minor, highly reactive impurity cannot be completely ruled out. Hence, in the absence of detailed analyses that demonstrate very low levels of reactive impurities (like DMSO, for example), the reported rate coefficients $k_{\text{DMSO}_2}(\text{T})$ should be considered as upper limits.

Comparison with Previous Work

There are no temperature dependent kinetic data in the literature with which to compare the results reported in this study. Room temperature (295 K) rate coefficients determined in this study are compared with literature values in Table 11. All data summarized in Table 11 were obtained at a temperature of 295 ± 1 K (Lind and Eriksen 1975; Olson and Fessenden 1992; Bardouki et al., 2002), or at an unspecified “room temperature” (Meissner et al., 1967; Reuvers et al., 1973; Veltwisch et al., 1980; Milne et al., 1989). For those studies that employed $\text{OH} + \text{SCN}^-$ as a competing reaction, all results are scaled to the value for k_{SCN^-} (295 K) adopted in this study, i.e., $1.15 \times 10^{10} \text{ M}^{-1} \text{ s}^{-1}$; this rate coefficient differs by less than 5% from the values assumed in all other studies where SCN^- was employed as the competitor.

The value for k_{DMSO} (295 K) reported in this study agrees well with most published rate coefficients. The rate coefficient reported very recently by Bardouki et al. (2002) is about a factor of 1.5 slower than rate coefficients reported in all earlier studies and in this study. Unlike all other studies of $\text{OH} + \text{DMSO}$ aqueous phase kinetics, Bardouki et al. employed a continuous photolysis technique with analysis of end products and, in one set of experiments, the competitor benzoate. While this approach provides useful mechanistic information (see below), rate coefficient determinations are subject to complications from slow secondary chemical and photochemical reactions that would not present a problem in flash photolysis or pulse radiolysis studies.

The only literature value with which to compare our measurement of k_{DMSO_2} (295 K) comes from the laser flash photolysis study of Milne et al. (1989), who report a “room temperature” rate coefficient that is a factor of 1.8 faster than the 295 K rate coefficient reported in this study. The $[\text{DMSO}_2]/[\text{OH}]$ ratios employed in their study were about a factor of five smaller than those employed in this study, so interferences from radical-radical side reactions are less likely to be significant in our study. Also, as mentioned above, a significant contribution to OH removal *via* reaction with impurities in the DMSO₂ samples cannot be ruled out in this study or in the study of Milne et al. (1989), so higher impurity levels in the samples used by Milne et al. could account for the faster rate coefficient measured by these investigators.

The value for k_{MS} (295 K) obtained in this study is in excellent agreement with the value obtained in a pulse radiolysis study by Olsen and Fessenden (1992), which is the slowest of three literature values. The factors discussed above for the OH + DMSO₂ reaction could also explain why Milne et al. (1989) report a “room temperature” rate coefficient for the OH + MS reaction that is a factor of 4.7 faster than the value for k_{MS} (295 K) reported in this study. The extremely fast rate coefficient reported by Lind and Eriksen (1975) is not consistent with the expected relatively low reactivity of MS or with field observations and model simulations of MS levels observed in the atmospheric condensed phase (for examples, Saltzman et al., 1983; Capaldo and Pandis 1997; Legrand et al., 2001).

Table 11 Comparison of 295 K rate coefficients obtained in this study with literature values

k_R (10^7 M ⁻¹ s ⁻¹)			Method ^a	Competitor	Reference
DMSO	DMSO2	MS			
630 ^b	≤1.7 ^b	1.2 ^b	LFP-LPA	SCN ⁻	This work
730 ^d			PR-A	SCN ⁻	
610 ^c			PR-A	SCN ⁻	(Meissner et al., 1967; Reuvers et al., 1973)
700			PR-C	none	(Veltwisch et al., 1980)
680 ^c	3.0 ^c	5.6 ^c	LFP-A ^d	SCN ⁻	(Milne et al., 1989)
480			CP-GC/IC	benzionate	(Bardouki et al., 2002)
420			CP-GC/IC	MSI ^e	(Bardouki et al., 2002)
		140 ^c	PR-A	SCN ⁻	(Lind and Eriksen 1975)
		1.3 ^f	PR-A	SCN ⁻	(Olson and Fessenden 1992)

^a LFP: laser flash photolysis; LPA: long path absorption; PR: pulse radiolysis; A: absorption; C: conductivity; CP: continuous photolysis; GC: gas chromatography; IC: ion chromatography.

^b Rate coefficients are calculated from the reported Arrhenius expressions.

^c Rate coefficient reported in the literature scaled upward by a factor of 115/110 to account for a difference in the assumed reference rate coefficient compared to this study.

^d Time-resolved absorption spectra were captured using a gated diode array detector.

^e MSI ≡ methanesulfinate (CH₃S(O)O⁻).

^f Rate coefficient reported in the literature scaled upward by a factor of 115/114 to account for a difference in the assumed reference rate coefficient compared to this study.

Reaction Mechanisms

The research reported in this work does not provide information about reaction products. Information that is available in the literature and its consistency with the kinetic parameters reported in this study is discussed below.

The very fast observed rate coefficient and negative activation energy (E_a) for the aqueous phase OH + DMSO reaction suggests that reaction occurs mainly *via* addition of OH radical to the sulfur atom, not *via* hydrogen abstraction:



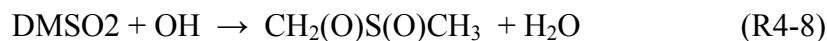
Mechanistic studies have demonstrated that the dissociation of DMSO-OH adduct proceeds *via* rapid fragmentation of one of the C-S bonds rather than the reverse reaction of R4-6 (Veltwisch et al., 1980; Sehested and Holcman 1996; Flyunt et al., 2001; Bardouki et al., 2002):



The same mechanism (i.e., methyl elimination following OH addition to the sulfur atom) is also operative in the gas phase OH + DMSO reaction (Urbanski et al., 1998; Arsene et al., 2002). A small (7%) yield for the H-abstraction pathway has been reported by Veltwisch et al. (1980).

Both the OH + DMSO₂ and OH + MS reactions are several hundred times slower than the OH + DMSO reaction. Initial attack of OH on both DMSO₂ and MS probably

involves abstraction of a hydrogen atom, as has been suggested previously by Harvey and Lang (1986) and Milne et al. (1989):



No detailed studies on reactions of the above two radical intermediates have been reported in the literature. The final products of $\text{CH}_2(\text{O})\text{S}(\text{O})\text{CH}_3$ oxidation could be either $\text{CH}_3(\text{O})\text{S}(\text{O})\text{O}^-$ (MS) or SO_4^{2-} (sulfate), while $\text{CH}_2(\text{O})\text{S}(\text{O})\text{O}^-$ oxidation almost certainly results in formation of sulfate, although the detailed reaction mechanisms remain poorly defined.

Ervens et al. (2003) have recently employed an experimental approach similar to the one employed in this study to measure temperature-dependent rate coefficients for OH reactions with a series of alcohols, aldehydes, ketones, carboxylic acids, and carboxylates. For these reactions, which are thought to occur primarily *via* H-abstraction mechanisms, Ervens et al. examined the correlations between the bond dissociation energies (BDEs) of the weakest C–H bond, which ranged from 381 to 412 kJ mol⁻¹ for the reactants studied, and observed A-factors, activation energies, and 298 K rate coefficients per abstractable H-atom. As mentioned above, the reactions of OH with DMSO₂ and MS probably proceed *via* H-abstraction mechanisms. The C–H BDEs in DMSO₂ and MS molecules do not appear to be well-known. For compounds where the abstracted H atom was known or estimated to be bound to carbon by 410-412 kJ mol⁻¹, activation energies observed by Ervens et al. ranged from 9 to 24 kJ mol⁻¹. The activation energies observed in this study for OH + DMSO₂ (R4-8) and OH + MS (R4-9)

are 14 kJ mol⁻¹ and 22 kJ mol⁻¹, respectively, i.e., within the range observed by Ervens et al. (2003). For compounds where the abstracted H atom was known or estimated to be bound to carbon by 410-412 kJ mol⁻¹, values for the 298 K rate coefficient per abstractable H atom observed by Ervens et al. ranged from 5×10^6 to 4×10^8 M⁻¹ s⁻¹, while in our study we find that this parameter is 3×10^6 M⁻¹ s⁻¹ for DMSO2 and 4×10^6 M⁻¹ s⁻¹ for MS, i.e., slightly below the lowest value observed by Ervens et al.. Since Ervens et al. find that the 298 K rate coefficient per abstractable H atom decreases with increasing C-H BDE, our kinetic results suggest large C-H BDEs in DMSO2 and MS, a suggestion that should be confirmable using high quality electronic structure calculations.

CHAPTER V
KINETICS STUDIES OF $\text{Cl} \leftrightarrow \text{Cl}_2^-$ REACTIONS WITH
DMSO, DMSO₂ AND MS

$\text{Cl} \leftrightarrow \text{Cl}_2^-$ Radicals in the Atmospheric Aqueous Phase

In addition to OH and SO_4^- , the Cl_2^- anion and the Cl atom are also potentially important radical oxidants for sulfur compounds in the atmospheric aqueous phase. Cl_2^- is formed *via* the fast equilibrium



so that the sources for Cl_2^- correspond to those for Cl. During the daytime, the two most important sources for Cl atoms are (Herrmann et al., 2000):



and



Hence the formation of Cl is pH-dependent and, as a consequence, no Cl is produced *via* R5-3 and R5-4 at higher pH values. Over the typical pH range 4-6 for the marine atmospheric condensed phase, R5-2 is thought to be the dominant source of Cl(aq). Nighttime Cl is mainly generated from the reaction of Cl⁻ with the elevated NO₃ in the condensed phase:



In the marine atmospheric condensed phase, typical concentrations of Cl⁻ are 10⁻⁴ – 10⁻³ M (Chameides 1984; Herrmann et al., 1996), and equilibrium R5-1 is shifted to the right hand side and favors the production of Cl₂⁻, so Cl₂⁻ is typically in significant excess over Cl in the marine atmosphere. Using the recommended equilibrium constant of R5-1 ($K_1 = 1.4 \times 10^5 \text{ M}^{-1}$) (Buxton et al., 1998; Yu et al., 2004), Cl₂⁻ is estimated to account for 93 – >99% of total radicals (Cl + Cl₂⁻) when Cl and Cl₂⁻ are in equilibrium.

Cl₂⁻ concentrations are higher in the marine atmosphere than in urban areas because of the higher initial concentration of chloride and the slower Cl ↔ Cl₂⁻ loss rate in the marine environment. The main destruction pathways for Cl₂⁻ in the marine atmosphere are its reactions with HO₂ ↔ O₂⁻ (65%) and with H₂O₂ (32%) (Herrmann et al., 2000). In urban environments, however, Cl₂⁻ destruction is thought to be dominated by its reactions with Fe²⁺ (50%) and HSO₃⁻ (37%) (Herrmann et al., 2000).

The maximum Cl₂⁻ concentration in the marine atmosphere occurs at noon and is estimated to be ~ 10⁻¹⁰ M, which is over two orders of magnitude higher than the concentration of OH (aq) (Jacob 1986; Herrmann et al., 2000). Studies of Cl and Cl₂⁻ reactions with unsaturated alcohols and hydrocarbons (Padmaja et al., 1992), aromatics

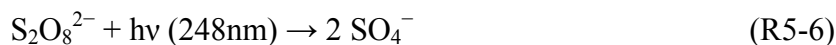
(Martire et al., 2001), and organic sulfides (Bonifacic and Asmus 1980) have demonstrated that Cl is very reactive toward H-abstraction or addition reactions and Cl_2^- is an effective electrophilic oxidant. Therefore, studies of reaction kinetics of these radicals with the organic sulfur species are potentially important for quantifying our understanding of the aqueous phase oxidation of sulfur compounds by free radicals. Unfortunately, as mentioned earlier in the literature review session of Chapter I, the database of kinetics studies of Cl and Cl_2^- reactions with sulfur compounds is rather limited. In this work the kinetics of Cl and Cl_2^- reactions with DMSO, DMSO₂ and MS are studied at room temperature ($295 \pm 1\text{K}$) using the laser flash photolysis (LFP) – long path UV-vis absorption (LPA) technique.

Experimental Method

The LFP - LPA technique involves coupling radical production by laser flash photolysis of aqueous $S_2O_8^{2-}/Cl^-/R$ ($R = \text{DMSO, DMSO}_2$ or MS) solutions with sensitive time-resolved detection of reactant or product radicals by multipass absorption spectroscopy. A schematic experimental apparatus is shown in Figure 4 and was described previously in Chapter II.

In most studies of $Cl \leftrightarrow Cl_2^-$ reaction kinetics, absorbance of $Cl \leftrightarrow Cl_2^-$ at 340 nm was monitored without significant interference from other species in the system. A significant spectral interference, however, was encountered in studies of the $Cl \leftrightarrow Cl_2^- + \text{DMSO}$ reactions; this interference will be discussed later in this chapter. In all experiments using 340 nm as the monitoring wavelength, the White cell mirrors (White 1942) were adjusted to allow at least 34 passes of the probe radiation through the region of the reactor irradiated by the laser. This gave an absorption path length of ~ 85 cm. With an electronic time constant of $1 \mu\text{s}$, the detection limit is about 0.03% absorption (64 flashes averaged); assuming a peak (340 nm) Cl_2^- extinction coefficient of $\sim 8800 \text{ M}^{-1} \text{ cm}^{-1}$ (Hug 1981; Yu et al., 2004), this corresponds to a Cl_2^- detection limit of $\sim 2 \times 10^{-10}$ M.

Different from the production of OH and SO_4^- radicals, Cl and Cl_2^- radicals are not directly generated from the photolysis of the precursor. Instead, the photolysis of persulfate ions ($S_2O_8^-$) at 248 nm produces SO_4^- , and subsequent reaction of SO_4^- with Cl^- generates Cl and Cl_2^- (Tang et al., 1988; Yu et al., 2004)



When high concentrations of Cl^- are employed in the system, self reaction and the reactions with $\text{S}_2\text{O}_8^{2-}$ and water are not important for SO_4^- loss because almost all SO_4^- is scavenged by Cl^- via R5-2.

The kinetics of reactions R5-1 and R5-2 are well-established (Huie et al., 1991; Buxton et al., 1999; Yu et al., 2004). Because of the low concentrations of Cl and SO_4^{2-} in the system, the forward reaction R5-2 dominates over its reverse reaction, and all SO_4^- radicals generated from the photolysis of $\text{S}_2\text{O}_8^{2-}$ are converted into Cl or Cl_2^- . In all studies, $\text{S}_2\text{O}_8^{2-}$ concentrations were in the range $(0.4 - 4.0) \times 10^{-5}$ M. For this $\text{S}_2\text{O}_8^{2-}$ concentration range, the total radical concentration immediately after the laser flash (primarily SO_4^-) is estimated to be $(0.5 - 5.0) \times 10^{-8}$ M.

The kinetics of Cl and Cl_2^- reactions with organic sulfur compounds, i.e., DMSO, DMSO2 and MS, were studied by observing the temporal evolution of $\text{Cl} \leftrightarrow \text{Cl}_2^-$ radicals. The spectrum of Cl_2^- is already well studied; its peak is around 340 nm, with a maximum extinction coefficient (ϵ) of $\sim 8800 \text{ M}^{-1} \text{ cm}^{-1}$ (Hug 1981; Yu et al., 2004). The left plot of Figure 16 is an example of the Cl_2^- absorbance spectrum reported in a recent study from Barker and coworkers (Yu et al., 2004). Also in their work, $\epsilon_{\text{SO}_4^-}$ is reported to be $< 800 \text{ M}^{-1} \text{ cm}^{-1}$ at 340 nm. The fast rate coefficient of R5-2 ($3 - 4 \times 10^8 \text{ M}^{-1} \text{ s}^{-1}$) gives a system SO_4^- lifetime of 0.3-30 μs when the Cl^- concentration ranges from 10^{-2} to 10^{-4} M. As a

result, SO_4^- does not affect the detection of $\text{Cl} \leftrightarrow \text{Cl}_2^-$ or the kinetic analysis under the experimental conditions employed in this work. One possible complication to monitoring Cl_2^- at 340 nm is that the extinction coefficient of Cl atom in aqueous solution at 340 nm is $\sim 3700 \text{ M}^{-1} \text{ cm}^{-1}$ (Nagarajan and Fessenden 1985; Wicktor et al., 2003), as shown in the right plot of Figure 16. Thus the detected absorbance at 340 nm is actually due to both Cl and Cl_2^- . However, as discussed in the following sections, this is not a problem in our kinetics studies.

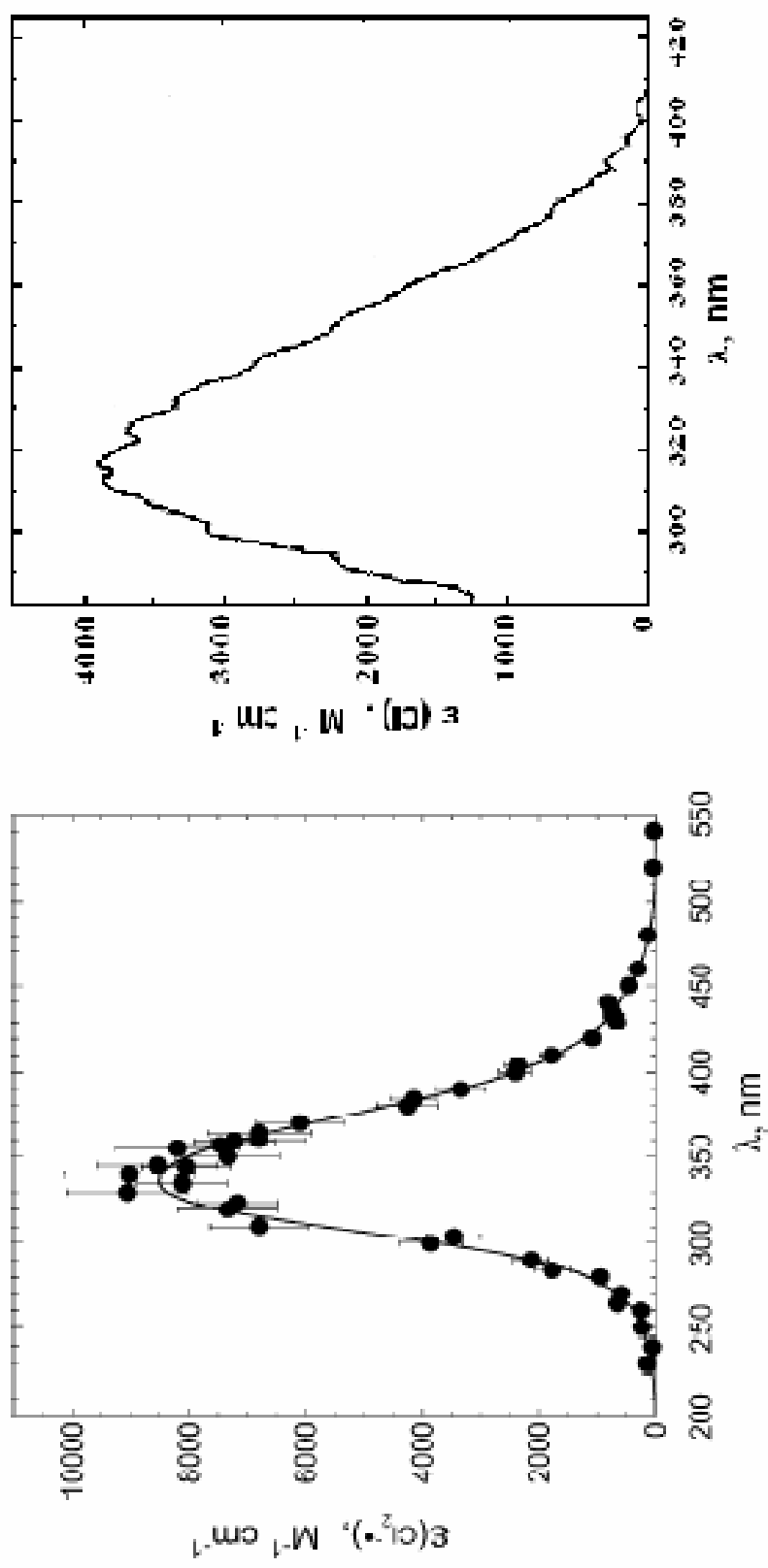


Figure 16 The absorption spectra of Cl_2^- (Yu et al., 2004) and Cl (Wicktor et al., 2003)

Results and Discussion

Kinetics of $\text{Cl} \leftrightarrow \text{Cl}_2^-$ degradation in Water

When $\text{S}_2\text{O}_8^{2-}$ and Cl^- are the only stable species in the solution, the main losses of Cl and Cl_2^- radicals include the following:



The kinetics for all of the above reactions have been studied before (Yu et al., 2004 and references therein). Considering the low $\text{S}_2\text{O}_8^{2-}$ concentration ($\sim 10^{-5}$ M) and the relatively slow reaction rate coefficients for R5-9 and R5-10 ($\sim 10^7$ and 10^4 $\text{M}^{-1}\text{s}^{-1}$, respectively) (Yu et al., 2004), these two reactions are of no significance under our experimental conditions; very low radical concentration [$(0.5 - 5.0) \times 10^{-8}$ M] makes R5-12 an un-important loss process for radicals in the system. The distribution of $\text{Cl} \leftrightarrow \text{Cl}_2^-$ is controlled by the equilibrium constant of R5-1 (K_1) and the $[\text{Cl}^-]$ in the system. When $[\text{Cl}^-]$ is relatively low, Cl concentrations are substantial and R5-7 is the dominant

pathway for $\text{Cl}_2^- \leftrightarrow \text{Cl}$ loss. At higher $[\text{Cl}^-]$, Cl_2^- is the dominant radical and reactions R5-8 and R5-11 both possibly contribute the background loss of $\text{Cl}_2^- \leftrightarrow \text{Cl}$.

Figure 17 shows typical temporal profiles of the detected absorbance at 340 nm in the $\text{Cl}^-/\text{S}_2\text{O}_8^{2-}/h\nu$ system when different Cl^- concentrations were employed but the $\text{S}_2\text{O}_8^{2-}$ concentration was kept constant. It is very clear that the absorbance increases quickly after the laser flash, and the rise times are relatively short when compared to the decay times. Hence, a simple first-order kinetics mechanism could be used and the pseudo-first order decay rate (k'_{measured}) of radicals at each Cl^- concentration could be obtained from the analysis of each temporal profile observed following laser flash photolysis. We find that, k'_{measured} increases from < 100 to $\sim 8000 \text{ s}^{-1}$ as the Cl^- concentration decreases from 0.25 M to 1.0×10^{-4} M. As mentioned above, at lower Cl^- concentrations, the $[\text{Cl}]/[\text{Cl}_2^-]$ ratio is high enough that R5-7 dominates the removal of radicals from the system. When the Cl^- concentration is high, loss of radical pool *via* R5-7 slows down and the slow reactions R5-8 and R5-11 may contribute significantly to radical loss. Under the assumption that R5-7, R5-8 and R5-11 are the only important processes to remove Cl and Cl_2^- radicals, the analysis of the system gives the following equation:

$$k'_{\text{measured}} = \alpha k'_7 + \beta k'_{\text{Cl}_2^-} \quad (5-1)$$

where $k'_{\text{Cl}_2^-}$ is the pseudo-first order loss rate of Cl_2^- primarily due to R5-8 and R5-11; α and β are fractions of Cl and Cl_2^- radicals defined as

$$\alpha = \frac{[\text{Cl}]}{[\text{Cl}] + [\text{Cl}_2^-]} \quad (5-2)$$

and

$$\beta = \frac{[\text{Cl}_2^-]}{[\text{Cl}] + [\text{Cl}_2^-]} \quad (5-3)$$

From equilibrium R5-1,

$$\frac{[\text{Cl}_2^-]}{[\text{Cl}]} = K_1[\text{Cl}^-] \quad (5-4)$$

Hence Equation (5-1) can be re-written as:

$$k'_{\text{measured}} = \frac{1}{1 + K_1[\text{Cl}^-]} k'_7 + \frac{K_1[\text{Cl}^-]}{1 + K_1[\text{Cl}^-]} k'_{\text{Cl}_2^-} \quad (5-5)$$

Therefore, the measured first order decay rates (k'_{measured}) could be plotted as a function of $[\text{Cl}^-]$, as shown in Figure 18. The solid sigmoid curve in Figure 18 is obtained from the best fit of k'_{measured} vs. $[\text{Cl}^-]$ using Equation (5-5) with the recommended value of $K_1 = 1.4 \times 10^5 \text{ M}^{-1}$ (Buxton et al., 1998; Yu et al., 2004). The rate coefficients $k'_7 = (1.4 \pm 0.1) \times 10^5 \text{ s}^{-1}$ and $k'_{\text{Cl}_2^-} = 40 \pm 20 \text{ s}^{-1}$, were obtained from the fit; uncertainties are 2σ and represent precision only. The value of k'_7 obtained from this work agrees very well with the studies from Klaning and Wolff (1985) and Yu et al (2004), but it is more than 40% lower than the values reported by Buxton et. al. (1998) and McElroy (1990). Our value of $k'_{\text{Cl}_2^-}$ is lower than most literature values of k'_8 (McElroy 1990; Buxton et al., 1998; Yu and Barker 2003a; Yu and Barker 2003b; Yu et al., 2004) and comparable to $2k_{11}[\text{Cl}_2^-]$ (Hynes and Wine 1988; Huie and Clifton 1990;

McElroy 1990; Yu et al., 2004) calculated using $[\text{Cl}_2^-] \sim 10^{-8}$ M. It is lower than the value of k'_8 reported from Buxton et. al. (1998) and McElroy (1990) by more than one order of magnitude. The discrepancies are quite likely from the different concentrations of both radicals and stable species. In the study of McElroy, $[\text{Cl}_2^-] \approx (1-5) \times 10^{-6}$ M, $[\text{S}_2\text{O}_8^{2-}] \approx (1-4) \times 10^{-2}$ M, approximately two orders of magnitude higher than those employed in our studies. Thus, the loss of Cl and Cl_2^- due to R5-9 and R5-10, as well as the radical-radical reactions R5-11 and R5-12, become non-negligible and result in higher decay rate of the radicals. While in our studies all of these reactions are very slow and the only possibly significant contributor to the observed $k'_{\text{Cl}_2^-}$ seem to be the Cl_2^- self reaction, for which the initial decay rate is expected to be $\sim 20-40 \text{ s}^{-1}$ when $[\text{Cl}_2^-] \sim (1-2) \times 10^{-8}$ M and $k_{11} = (9 \pm 1) \times 10^8 \text{ M}^{-1} \text{ s}^{-1}$ (Yu et al., 2004) are used.

$\text{Cl} + \text{H}_2\text{O}$ (R5-7) is a reversible reaction and the equilibrium is pH sensitive. Perchloric acid was added to the solution in order to investigate the pH effect on the kinetics. At pH = 2 and $[\text{Cl}^-] = 1 \times 10^{-4}$ M, the detected first order decay rate decreased from $\sim 8000 \text{ s}^{-1}$ (at pH = 5.5) to $\sim 200 \text{ s}^{-1}$. This detected decay rate is still higher than the measured $k'_{\text{Cl}_2^-}$ at pH ≈ 5.5 , because one of the products from R5-7, ClOH^- dissociates to produce Cl^- and OH radicals *via* the following reaction:



And when the Cl^- concentration is low, R5-13 shifts to the right hand side and facilitates the production ClOH^- *via* the $\text{Cl} + \text{H}_2\text{O}$ reaction (R5-7) (Kim and Hamill 1976). As a result, R5-7 contributes partially to the measured decay rates and makes k'_{measured} at pH = 2 greater than $k'_{\text{Cl}_2^-}$. Changing acidity of the solution in studies using higher Cl^-

concentrations does not affect the measured decay rate of the $\text{Cl}_2^- \leftrightarrow \text{Cl}$ radicals, since none of the reactions that potentially contribute to the observed Cl_2^- loss are pH sensitive.

Kinetics of $\text{Cl}^- \leftrightarrow \text{Cl}_2^-$ Reactions with DMSO, DMSO₂ and MS

After the introduction of sulfur species, R (R = DMSO, DMSO₂ or MS), into the system, the detected $\text{Cl}_2^- \leftrightarrow \text{Cl}$ decay rate is enhanced due to the reactions of $\text{Cl}_2^- \leftrightarrow \text{Cl}$ with the sulfur species. One important factor in these studies is the $[\text{Cl}^-]$ -to- $[\text{R}]$ ratio. Based on our studies of the kinetics of SO_4^- reactions with these organic sulfur species (Chapter III) and literature values for $\text{Cl}^- + \text{SO}_4^-$ kinetics (Wine et al., 1989; Buxton et al., 1999; George and Chovelon 2002; Yu et al., 2004), the experimental conditions in most kinetics studies were controlled such that most of the SO_4^- would react with Cl^- rather than R. Therefore, the yield of $\text{Cl}_2^- \leftrightarrow \text{Cl}$ radicals is maximized.

All experiments were carried out under pseudo first order conditions with the concentrations of stable species in large excess over the concentrations of radicals. Figure 19 shows a set of temporal profiles of absorbance detected at 340 nm in the $\text{S}_2\text{O}_8^{2-}/\text{Cl}^-/\text{DMSO}/h\nu$ system. The pseudo-first order decay rate, k' , increases with increasing DMSO concentration in the system while all other experimental conditions remain identical.

The linear least squares analysis of the measured k' versus the concentration of sulfur species R gives the second order reaction rate coefficient, k_R . Using this method, the second order rate coefficients for DMSO, DMSO₂ and MS reactions at different Cl^- concentrations were determined and all kinetic results are summarized in Table 12.

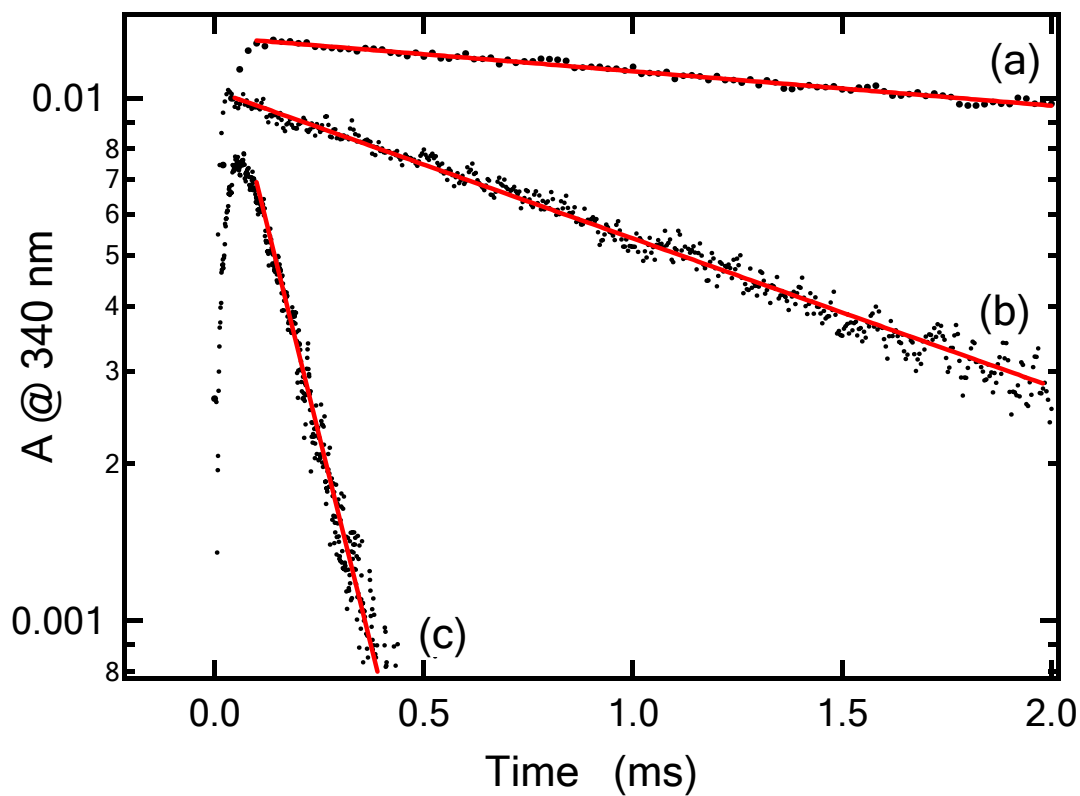


Figure 17 Temporal absorption profiles detected at 340 nm in the $\text{S}_2\text{O}_8^{2-}/\text{Cl}^-/\text{water}/h\nu$ system

Experimental conditions: $[\text{S}_2\text{O}_8^{2-}] = 1.45 \times 10^{-5}$ M, $[\text{Cl}^-] =$ (a) 1.0×10^{-2} , (b) 1.0×10^{-3} and (c) 1.0×10^{-4} M. The solid lines are the least-squares linear fitting of the data, which give $k'_{\text{measured}} =$ (a) 105, (b) 1050 and (c) 7800 in units of s^{-1} .

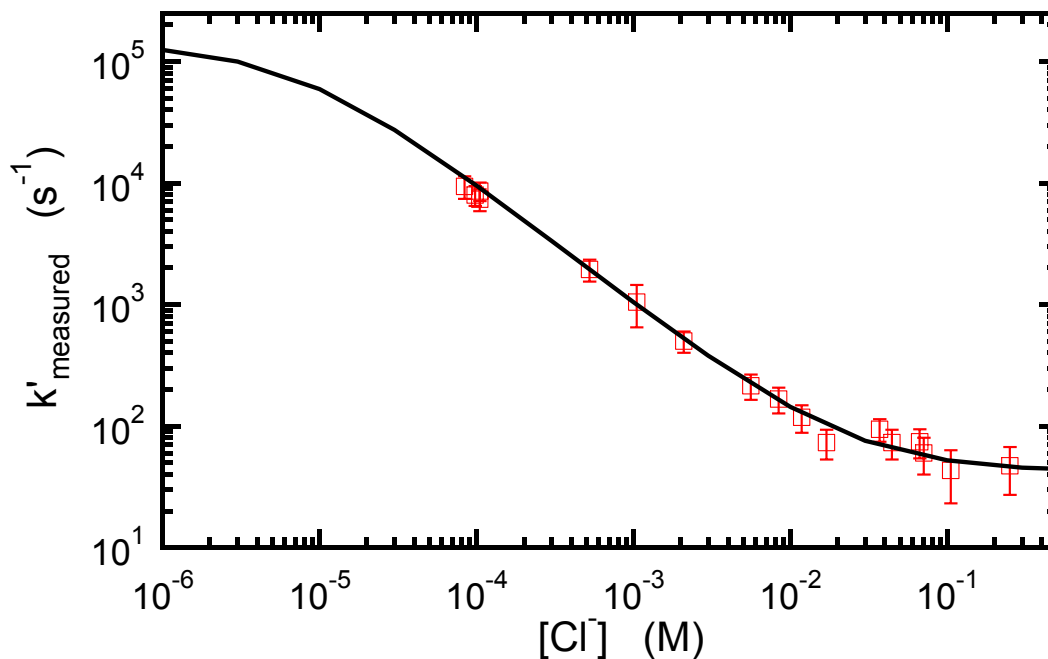


Figure 18 Plot of measured first order decay rates (k'_{measured}) versus $[\text{Cl}^-]$ in the studies of Cl and Cl_2^- reactions with water

The solid curve is the fit of data using Equation (5-5) in the text, and gives the rate coefficients k'_7 and $k'_{\text{Cl}_2^-}$ of $(1.4 \pm 0.1) \times 10^5$ and $40 \pm 20 \text{ s}^{-1}$, respectively; uncertainties are 2σ and represent precision only.

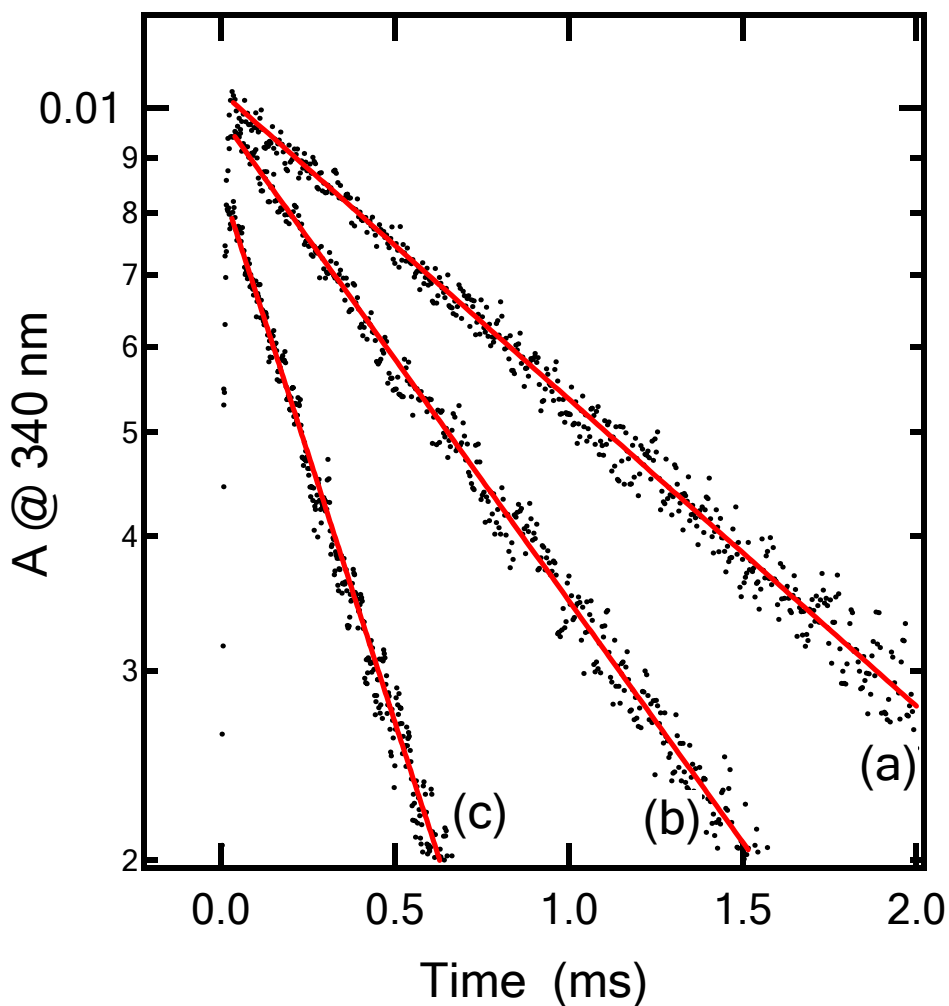


Figure 19 Temporal profiles of absorbance at 340 nm in the $\text{S}_2\text{O}_8^{2-}/\text{Cl}^-/\text{DMSO}$ system

Experimental conditions: $[\text{S}_2\text{O}_8^{2-}] = 1.4 \times 10^{-5} \text{ M}$, $[\text{Cl}^-] = 1.0 \times 10^{-3} \text{ M}$, $[\text{DMSO}] =$ (a) 0, (b) 5.67×10^{-6} and (c) $2.83 \times 10^{-5} \text{ M}$. The straight lines are best fits of the exponential decay of the absorbance, which give the first order decay rates of (a) 650, (b) 1043 and (c) 2590 in units of s^{-1} .

Table 12 Summary of measured rate coefficients (k_R) for the reactions of $\text{Cl} \leftrightarrow \text{Cl}_2^-$ with water, DMSO, DMSO2 and MS

[Cl ⁻] (M)	k_R (M ⁻¹ s ⁻¹)			
	Water*	R = DMSO	R = DMSO2	R = MS
1×10 ⁻⁴	8320	3.88×10 ⁸	61100	37600
2.0×10 ⁻⁴	4100			22600
2.5×10 ⁻⁴	3500	1.93×10 ⁸		
5×10 ⁻⁴	2050	9.56×10 ⁷	16400	
1×10 ⁻³	950	7.47×10 ⁷	18700	10300
2.5×10 ⁻³	460	3.43×10 ⁷		
5×10 ⁻³	250	1.42×10 ⁷	7780	
1×10 ⁻²	180	1.40×10 ⁷		6750
5×10 ⁻²	100			6210
0.1	50			
0.25	45			

* first order decay rate in unit of s⁻¹.

As an example, plots of measured first order decay rates $k' - k'_0$ vs. [DMSO] and [DMSO2] at three Cl^- concentrations each are shown in Figure 20, where k'_0 is the measured first order decay rate when sulfur compounds are not present in the solution. As mentioned above, k'_0 is a function of $[\text{Cl}^-]$, so it was subtracted from k' for a better data comparison. As typified by the data shown in Figure 20 and Table 12, the second order rate coefficient, k_R , obtained for each sulfur species decreases as the Cl^- concentration increases. Such a relationship between the measured k_R and Cl^- concentrations is anticipated because the following two reactions both contribute to the observed decay of 340 nm absorbance:



Each measured k_R is a mixture of k_{14} and k_{15} , and the relative contribution of each reaction is determined by the Cl^- concentration. Similar to the studies of $\text{Cl} \leftrightarrow \text{Cl}_2^-$ kinetics in water, fitting the measured k_R vs. $[\text{Cl}^-]$ with Equation (5-6)

$$k_R = \frac{1}{1 + K_1[\text{Cl}^-]} k_{14} + \frac{K_1[\text{Cl}^-]}{1 + K_1[\text{Cl}^-]} k_{15} \quad (5-6)$$

gives the second order reaction rate coefficients k_{14} and k_{15} . Using this method the rate coefficients for $(\text{Cl} \leftrightarrow \text{Cl}_2^-) + \text{R}$ ($\text{R} = \text{DMSO}$, DMSO_2 and MS) could be derived and all results for the studied reactions are summarized in Table 13.

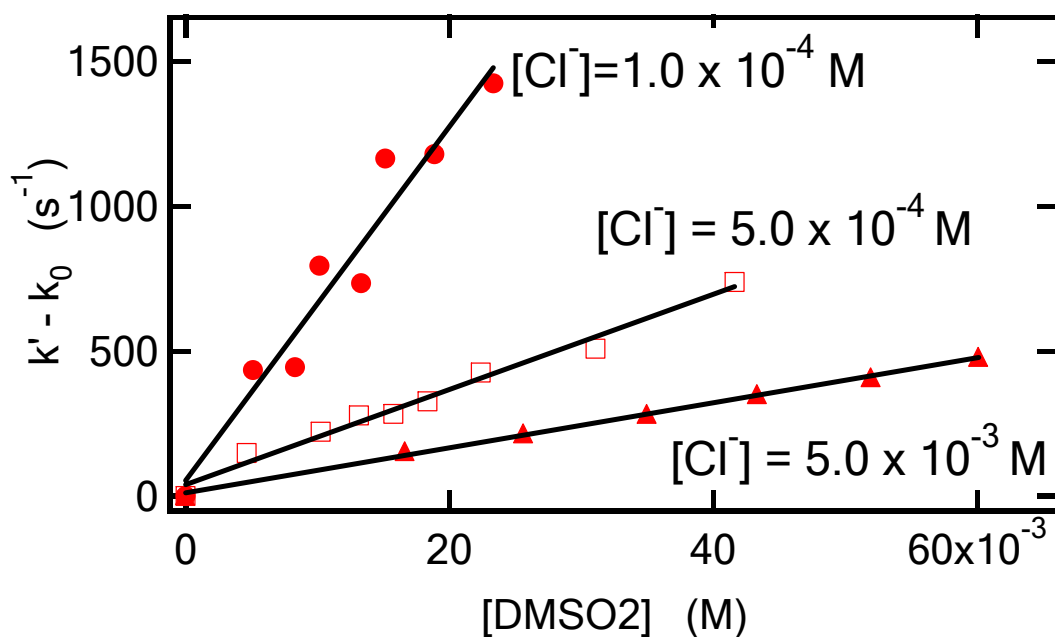
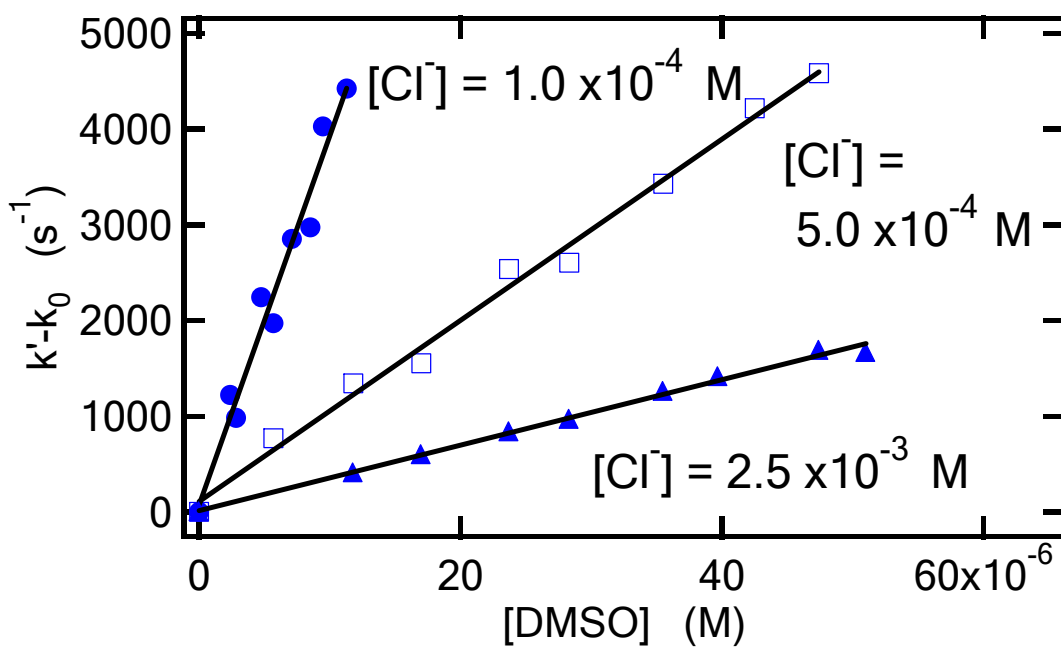


Figure 20 Plots of $k' - k_0$ versus $[DMSO]$ and $[DMSO_2]$ for different $[Cl^-]$

The second order rate coefficients derived from the linear least squares analyses of data are: $(3.88 \pm 0.70) \times 10^8$ (●), $(9.56 \pm 1.80) \times 10^7$ (□), and $(3.43 \pm 0.50) \times 10^7$ (▲) for DMSO reactions; 61100 ± 12400 (●), 16400 ± 1600 (□) and 7780 ± 320 (▲) for DMSO₂ reactions, in units of $M^{-1} s^{-1}$.

Table 13 Summary of kinetics results on the (Cl \leftrightarrow Cl $_2^-$) + R reactions

		k_R (M $^{-1}$ s $^{-1}$)	
		^a This work	^b Literature
Cl + R	R = H $_2$ O ^c	$(1.4 \pm 0.2) \times 10^5$ ^c	^{1,2} 2.5×10^5 ^c ^{3,4} 1.6×10^5 ^c
	R = DMSO	$(6.3 \pm 0.6) \times 10^9$	⁵ 7.0×10^9 ^d
	R = DMSO $_2$	$(8.2 \pm 1.6) \times 10^5$	
	R = MS	^d $(4.9 \pm 0.2) \times 10^5$	
Cl $_2^-$ + R	R = H $_2$ O ^c	< 80 ^c	^{1,2} 1.3×10^3 ^c ⁴ <100 ^c
	R = DMSO	$(1.6 \pm 0.8) \times 10^7$	⁶ 1.2×10^7
	R = DMSO $_2$	8240 ± 5480	
	R = MS	3890 ± 680 ^e	

^a All uncertainties are 2σ and represent precision of the least squares analysis of the data.

^b References: ¹ (McElroy 1990) ² (Buxton et al., 1998) ³ (Klaning and Wolff 1985) ⁴ (Yu et al., 2004) ⁵ (Sumiyoshi and Katayama 1987) ⁶ (Kishore and Asmus 1991).

^c First order rate coefficients are in unit of s $^{-1}$.

^d In CCl $_4$ solvent.

^e Data are corrected to the 0 ionic strength limit using the method described in the text.

Since the $\text{MS} + \text{Cl}_2^-$ reaction involves two negatively charged reactants, the measured rate coefficient is expected to increase with increasing ionic strength. Furthermore, high concentrations of MS were used because this reaction is extremely slow. Thus, the ionic strength is expected to affect the measurement of the reaction rate coefficient. As discussed in Chapter III, in relatively low ionic strength solutions such as those employed in this work, the following relationship is approximately obeyed if both reactants are singly charged (Espenson 1981):

$$\log k = \log k^0 + \frac{2X\mu^{1/2}}{1 + \mu^{1/2}} \quad (5-7)$$

where k is the measured rate coefficient, k^0 is the rate coefficient in the limit of zero ionic strength, X is a collection of constants with values in water solvent that range from 0.492 at 278 K to 0.522 at 311 K (Manov et al., 1943), and μ is the ionic strength defined as

$$\mu = 0.5 \sum_i (z_i^2 [i]) \quad (5-8)$$

where z_i is the charge of species i .

During analysis of our data, Equation (5-7) was used to convert each measured rate coefficient to an appropriate value for the limit where $\mu \rightarrow 0$. It is worth noting that k_{16} and k_{17} both contribute to each measured rate coefficient.



The rate coefficient k_{16} is not significantly affected by the ionic strength under the typical experimental conditions in this study, because R5-16 involves only one charged reactant (MS). Thus, the measured first order rate (k'_{MS}) is corrected to the zero ionic strength limit by assuming k_{16} is independent of ionic strength and correcting only k_{17} . The following iterative method was developed in order to account for the contribution of ionic strength to the measured k'_{MS} :

1. The initial measured second order rate coefficient $k_{MS}^{(0)}$ (the superscript means iteration i , and $i = 0 - n$) is obtained from the linear relationship between the first order rate $k'_{MS}^{(0)}$ and [MS] at each $[Cl^-]$, analogous to the plot shown in Figure 20.
2. $k_{16}^{(0)}$ and $k_{17}^{(0)}$ are obtained by fitting $k_{MS}^{(0)}$ vs. $[Cl^-]$ with Equation (5-6), shown as the black curve in Figure 21.
3. Then the actual contributions of R5-16 and R5-17 to the total measured first order rate $k'_{MS}^{(0)}$ at each $[Cl^-]$ and [MS] are calculated based on the equilibrium constant K_1 and the values of $k_{16}^{(0)}$ and $k_{17}^{(0)}$ obtained from step two:

$$k'_{16}{}^{(0)} = k'_{MS}{}^{(0)} \left[\frac{k_{16}{}^{(0)}}{\alpha k_{16}{}^{(0)} + \beta k_{17}{}^{(0)}} \right] \quad (5-9)$$

$$k'_{17}{}^{(0)} = k'_{MS}{}^{(0)} \left[\frac{k_{17}{}^{(0)}}{\alpha k_{16}{}^{(0)} + \beta k_{17}{}^{(0)}} \right] \quad (5-10)$$

where α and β are the fractions of Cl and Cl_2^- , defined as $\alpha = 1/(1 + K_1[Cl^-])$, and $\beta = K_1[Cl^-]/(1 + K_1[Cl^-])$.

4. Equation (5-7) is used to correct $k'_{17}{}^{(0)}$ to the 0 ionic strength limit giving a value of $k'_{17-0}{}^{(0)}$. Therefore the total first order reaction rate at the 0 ionic strength limit is calculated from:

$$k'_{\text{MS}}{}^{(1)} = \alpha k'_{16}{}^{(0)} + \beta k'_{17-0}{}^{(0)} \quad (5-11)$$

$k'_{\text{MS}}{}^{(1)}$ is then used as the initial first order rate to start the second round of iteration.

Step 1 through step 4 can then be repeated to obtain $k_{\text{MS}}{}^{(1)}$, $k_{16}{}^{(1)}$, $k_{17}{}^{(1)}$, $k'_{16}{}^{(1)}$ and $k'_{17}{}^{(1)}$, $k'_{17-0}{}^{(1)}$ as well as $k'_{\text{MS}}{}^{(2)}$. $k'_{\text{MS}}{}^{(2)}$ is used as the initial value for the third iteration. After iterating n times, $k_{16}{}^{(n)}$ and $k_{17-0}{}^{(n)}$ are compared to $k_{16}{}^{(n-1)}$ and $k_{17-0}{}^{(n-1)}$. If the difference is less than 2%, the iteration is terminated and $k_{16}{}^{(n)}$ and $k_{17-0}{}^{(n)}$ are adopted as the final results for the reaction rate coefficients of R16 and R17 at the 0 ionic strength limit. The kinetics data for MS reactions listed in Table 13 are the results corrected to the 0 ionic strength limit using the above iterative method, where 5 iterations were used.

Figure 21 shows the comparison of the original data (black squares) and those corrected to the zero ionic strength (red circles) limit using the iterative procedure described above. As expected, the differences between the original and the corrected data are evident only at the right side of the plot where R5-17 is the dominant reaction in the system, since R5-17 is the only reaction significantly affected by ionic strength. As a result, the corrected rate coefficient for R5-17 at 0 ionic strength limit, k_{17-0} , is about 40% lower than that obtained from the original data. However, the difference is negligible on

the left side of the plot, where R5-16 is more important in determining the measured k_{MS} . Therefore, the corrected k_{16} is very close to the one obtained from the original data.

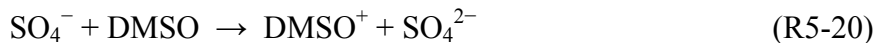
In the studies of DMSO reactions, two important features different from the studies of DMSO2 and MS reactions were observed when Cl^- concentrations were greater than 10^{-2} M. First, as the DMSO concentration increases, the appearance rate of the detected absorbance becomes slower and the maximum peak absorbance at 340 nm decreases. Second, decays of the absorbances appear to be non-exponential, i.e., the pseudo- first order decay rate is slower at longer time scales, particularly at high DMSO concentrations.

The most plausible explanation for the non-exponential decay of the observed absorbance is the accumulation of a product that absorbs at the probe wavelength, 340 nm. The study by Kishore and Asmus (1991) has demonstrated the following reaction mechanism:



According to the Kishore and Asmus study, the DMSO-Cl adduct is the main product of both reactions, and it absorbs at 340 nm with an extinction coefficient of $\sim 4000 \text{ M}^{-1} \text{ cm}^{-1}$, about half of that for Cl_2^- at the same wavelength (Hug 1981; Yu et al., 2004). Therefore the appearance of the DMSO-Cl adduct from both R5-18 and R5-19 can contribute to the detected absorbance and result in a non-exponential decay of the detected signal when compared to those reactions without interference from the products.

On the other hand, as the DMSO concentration increases, DMSO reacts more rapidly with $\text{SO}_4^{\cdot-}$ radicals:



Studies on R5-20 by Kishore and Asmus (1989) and our group (Zhu et al., 2003a) agree well and indicate $k_{20} = (3.0 \pm 0.3) \times 10^9 \text{ M}^{-1} \text{ s}^{-1}$ at room temperature. Therefore, it is estimated that over half of $\text{SO}_4^{\cdot-}$ radicals react with DMSO when $[\text{DMSO}]$ is over 10% of $[\text{Cl}^-]$, based on a rate coefficient of $(3.2 \pm 0.2) \times 10^8 \text{ M}^{-1} \text{ s}^{-1}$ (Wine et al., 1989; Buxton et al., 1999) for the $\text{SO}_4^{\cdot-} + \text{Cl}^-$ reaction (R5-2). At the same time, the DMSO^+ radical produced from R5-20 reacts with Cl^- at a diffusion controlled rate, i.e., $\sim 1.0 \times 10^{10} \text{ M}^{-1} \text{ s}^{-1}$, leading to the production of the DMSO-Cl adduct (Kishore and Asmus 1991):



Because of the high Cl^- concentration ($\geq 10^{-2} \text{ M}$) employed in this study, the equilibrium R5-21 facilitates the production of DMSO-Cl adduct. This explains why the production of $\text{Cl}_2^{\cdot-}$ is reduced as the DMSO concentration increases. The contribution of DMSO-Cl to the detected absorbance becomes dominant when $[\text{DMSO}] / [\text{Cl}^-] \geq 0.5$, i.e., more than 80% of $\text{SO}_4^{\cdot-}$ reacts with DMSO to produce DMSO-Cl through R5-20 and R5-21 without involving $\text{Cl}_2^{\cdot-}$ radicals. Under such conditions, the detected absorbance signal is primarily from DMSO-Cl; thus, the observed absorbance and decay rates cannot be used to derive the $\text{Cl}^- \leftrightarrow \text{Cl}_2^{\cdot-} + \text{DMSO}$ reaction kinetics (R5-18 and R5-19).

Another set of studies were carried out by monitoring the absorbance at 330 nm to reduce interference by DMSO-Cl absorbance. The experimental conditions were: $[\text{Cl}^-] =$

0.01 M, $[\text{S}_2\text{O}_8^{2-}] = 1.8 \times 10^{-5}$ M, and DMSO concentrations were varied from 0 to 10^{-5} M. A second order rate coefficient (k_{DMSO}) of $(1.4 \pm 0.4) \times 10^7 \text{ M}^{-1} \text{ s}^{-1}$ was obtained, which is very close to the rate coefficient for the $\text{DMSO} + \text{Cl}_2^-$ reaction reported by Kishore and Asmus (1991). Under the above experimental conditions, the $\text{DMSO} + \text{Cl}_2^-$ reaction is dominant in determining the measured k_{DMSO} . However, for studies with $[\text{Cl}^-]$ over 0.01 M, the measured k_{DMSO} is much slower than the value from Kishore and Asmus, suggesting that interference from DMSO-Cl is non-negligible even when absorbance at 330 nm is monitored.

In Figure 22, all measured k_{DMSO} are plotted as function of the Cl^- concentration, where the black curve is obtained from fitting all the data in the plot with Equation (5-6), and the red curve is obtained using the data for $[\text{Cl}^-] < 10^{-2}$ M. The two rate coefficients for $\text{DMSO} + \text{Cl}$ and $\text{DMSO} + \text{Cl}_2^-$ (k_{18} and k_{19} , respectively) obtained from the black curve analysis agree reasonably well with literature studies (Sumiyoshi and Katayama 1987; Kishore and Asmus 1991), but the error bar for k_{19} is over 100% and the fitting curve could not reproduce measurements well at high Cl^- concentrations. k_{19} obtained from the red curve analysis is about double that from the black curve and the error bar is reduced to 50%; k_{18} from both analyses agree well within the uncertainties. We believe that the two rate coefficients obtained from the red curve analysis, using only the data within the Cl^- concentration range of $10^{-4} - 10^{-2}$ M represent the kinetics of the DMSO reactions more precisely. Thus, we listed these values in Table 13 as the kinetics results for R5-18 and R5-19, i.e., $k_{18} = (6.3 \pm 0.6) \times 10^9$ and $k_{19} = (1.6 \pm 0.8) \times 10^7 \text{ M}^{-1} \text{ s}^{-1}$.

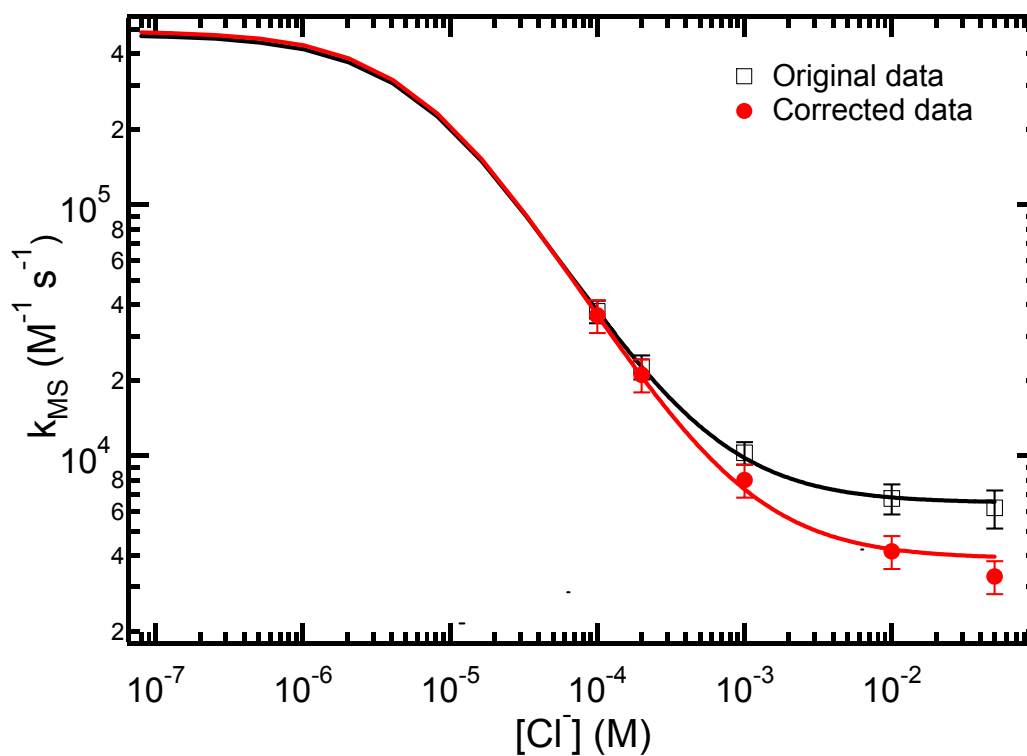


Figure 21 Comparison of original k_{MS} and that after corrected to 0 ionic strength

The corrected data were obtained using the procedure described in the text. Both curves are fitting of the data with equation (5-6). k_{16} and k_{17} are determined to be $(4.7 \pm 0.2) \times 10^5$ and 6490 ± 400 from the original data, and $(4.9 \pm 0.2) \times 10^5$ and 3890 ± 680 from the data corrected to 0 ionic strength, in units of $M^{-1} s^{-1}$.

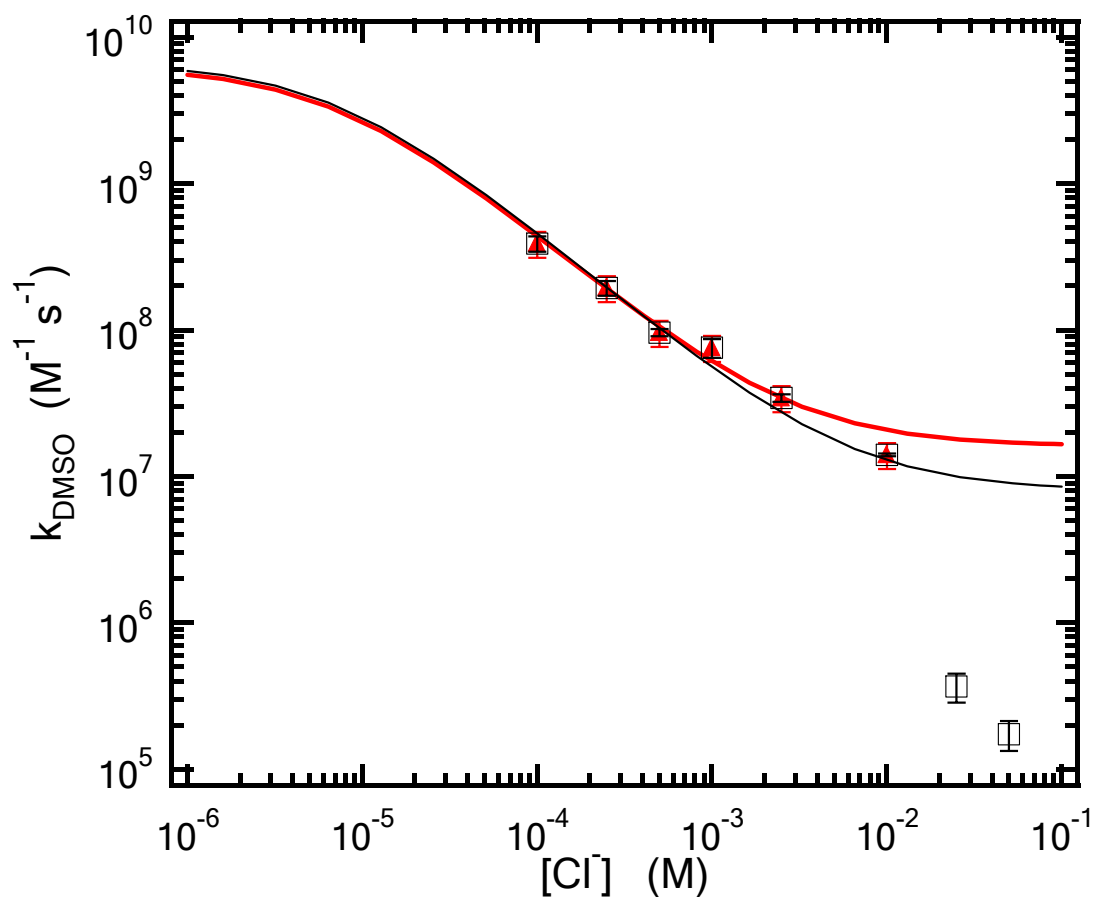


Figure 22 Plot of measured k_{DMSO} vs. $[\text{Cl}^-]$

The black curve is obtained from fitting all the data in the plot with Equation (5-6), and the red curve is the analysis of the data for $[\text{Cl}^-] < 10^{-2}$ M. k_{18} and k_{19} were obtained as $(6.74 \pm 0.67) \times 10^9$ and $(8.02 \pm 8.14) \times 10^6$ from the black curve and $(6.34 \pm 0.59) \times 10^9$ and $(1.61 \pm 0.85) \times 10^7$ from the red curve.

The only available data with which to compare our results are one study each on DMSO + Cl (Sumiyoshi and Katayama 1987) and DMSO + Cl₂⁻ (Kishore and Asmus 1991). Studies by Sumiyoshi and Katayama (1987) were carried out in carbon tetrachloride solvent using a pulse radiolysis method and reported a rate coefficient of $(7.0 \pm 0.5) \times 10^9 \text{ M}^{-1} \text{ s}^{-1}$ for the Cl + DMSO reaction. They also found that the reaction product is the three-electron-bonded DMSO-Cl adduct radical which possesses an absorption spectrum with a maximum around 400 nm. Kishore and Asmus (1991) used a pulse radiolysis technique and evaluated the DMSO + Cl₂⁻ kinetics from the pseudo first order decay of the Cl₂⁻ absorbance measured at 330 nm. They reported a rate coefficient of $(1.2 \pm 0.2) \times 10^7 \text{ M}^{-1} \text{ s}^{-1}$ for the DMSO + Cl₂⁻ reaction, about 25% lower than our value. However, they did not provide the details of the kinetics data analysis in the paper, such as concentrations of DMSO and the absorbance decay time scale. In our studies it was found that at high chloride concentrations (they used 0.05M [Cl⁻]), due to the slow DMSO + Cl₂⁻ reaction rate and the limit of DMSO concentrations (to suppress the occurrence of DMSO + SO₄⁻), a time scale to several ms was necessary to evaluate the absorbance decay. For that long time scale, production of the DMSO-Cl adduct is not negligible in the kinetics analysis of the first order decay of the Cl₂⁻ absorbance.

Similar spectra for the DMSO-Cl adduct were reported from the above two studies, and both studies have demonstrated that the DMSO-Cl adduct absorbs significantly at 340 nm. To obtain a better understanding of the complicated mechanisms involved in our studies of DMSO reactions with Cl \leftrightarrow Cl₂⁻, especially at high Cl⁻ concentrations, further studies of the DMSO-Cl adduct were necessary. These studies are described below.

Kinetic and Spectroscopic Studies of the Aqueous Phase DMSO-Cl Adduct Radical

A series of studies were carried out to understand the production and loss kinetics, as well as identify the absorption spectrum of the DMSO-Cl adduct radical in the aqueous phase.

In order to obtain the maximum DMSO-Cl and minimum Cl_2^- production in the solution, the $[\text{DMSO}]/[\text{Cl}^-]$ ratio was controlled so that all of the SO_4^- reacts with DMSO. As mentioned previously, when $[\text{DMSO}]/[\text{Cl}^-] > 0.5$, over 80% of the SO_4^- reacts with DMSO. Experiments were carried out at two different Cl^- concentrations: 0.002 and 0.01 M, and three wavelengths: 340, 430 and 480 nm. As an example, typical temporal profiles of the absorbance at 430 nm when $[\text{Cl}^-] = 0.01$ M are shown in Figure 23. It is easily seen that when $[\text{DMSO}] = 0$, the absorbance is primarily from Cl_2^- . As the DMSO concentration increases, the observed absorbance increases because of accumulation of the DMSO-Cl adduct, which has a greater extinction coefficient (ϵ) than Cl_2^- at 430 nm. In Figure 24, the detected maximum absorbance at 430 nm is plotted as a function of $[\text{DMSO}]$ when $[\text{Cl}^-] = 0.01$ M (filled circles) and 0.002 M (open circles). For both curves, the maximum absorbance becomes independent of $[\text{DMSO}]$ at $[\text{DMSO}]/[\text{Cl}^-] \geq 0.6$, as predicted based on the literature kinetics data (see above). These experiments were also carried out at 480 nm, where Cl_2^- absorbance is even lower; the results obtained are similar to those shown in Figures 23 and 24. For studies at 340 nm, as expected, curves are opposite to those in Figure 24, i.e., since $\epsilon_{\text{DMSO-Cl}}$ is lower than $\epsilon_{\text{Cl}_2^-}$, the observed absorbance drops as $[\text{DMSO}]$ increases and after $[\text{DMSO}]/[\text{Cl}^-] > 0.6$, absorbance reaches a minimum and becomes independent of $[\text{DMSO}]$. Therefore, in the

studies described below, we held $[\text{DMSO}]/[\text{Cl}^-] > 0.6$ in order to achieve maximum production of DMSO-Cl.

An important feature was found in Figure 24: the maximum absorbances at two Cl^- concentrations differ by more than a factor of 2, although the total SO_4^- radical concentrations in the two studies vary by no more than 15% (estimated from variations in precursor concentration, laser power, and other experimental parameters). The probable reason for such a big difference is that the different Cl^- concentrations employed resulted in significantly different DMSO-Cl concentrations because of a shift in the equilibrium reaction $\text{Cl}^- + \text{DMSO}^+ \leftrightarrow \text{DMSO-Cl}$ (R5-21).

In order to investigate the effect of R5-21 on the DMSO-Cl adduct production yield, $[\text{Cl}^-]$ and $[\text{DMSO}]$ were varied while maintaining $[\text{DMSO}] > 60\%[\text{Cl}^-]$ in a set of experiments with a constant $[\text{S}_2\text{O}_8^{2-}]$. Figure 25 shows a set of typical absorbance temporal profiles observed at 430 nm. When Cl^- and DMSO are absent in the solution, the detected absorbance (trace a) is mainly from SO_4^- ; when these two species are present in the solution with a ratio of $[\text{DMSO}]/[\text{Cl}^-] > 0.6$, $\text{DMSO-Cl} \leftrightarrow \text{DMSO}^+$ become the most important radicals in the system after fast decay of SO_4^- *via* $\text{DMSO} + \text{SO}_4^-$ (R5-20). Since the fractions of $\text{DMSO-Cl} \leftrightarrow \text{DMSO}^+$ of total radicals are dependent on the Cl^- concentration in the system, the observed absorbance is a function of $[\text{Cl}^-]$ if DMSO-Cl and DMSO^+ are the only important radicals in the system and have different extinction coefficients.

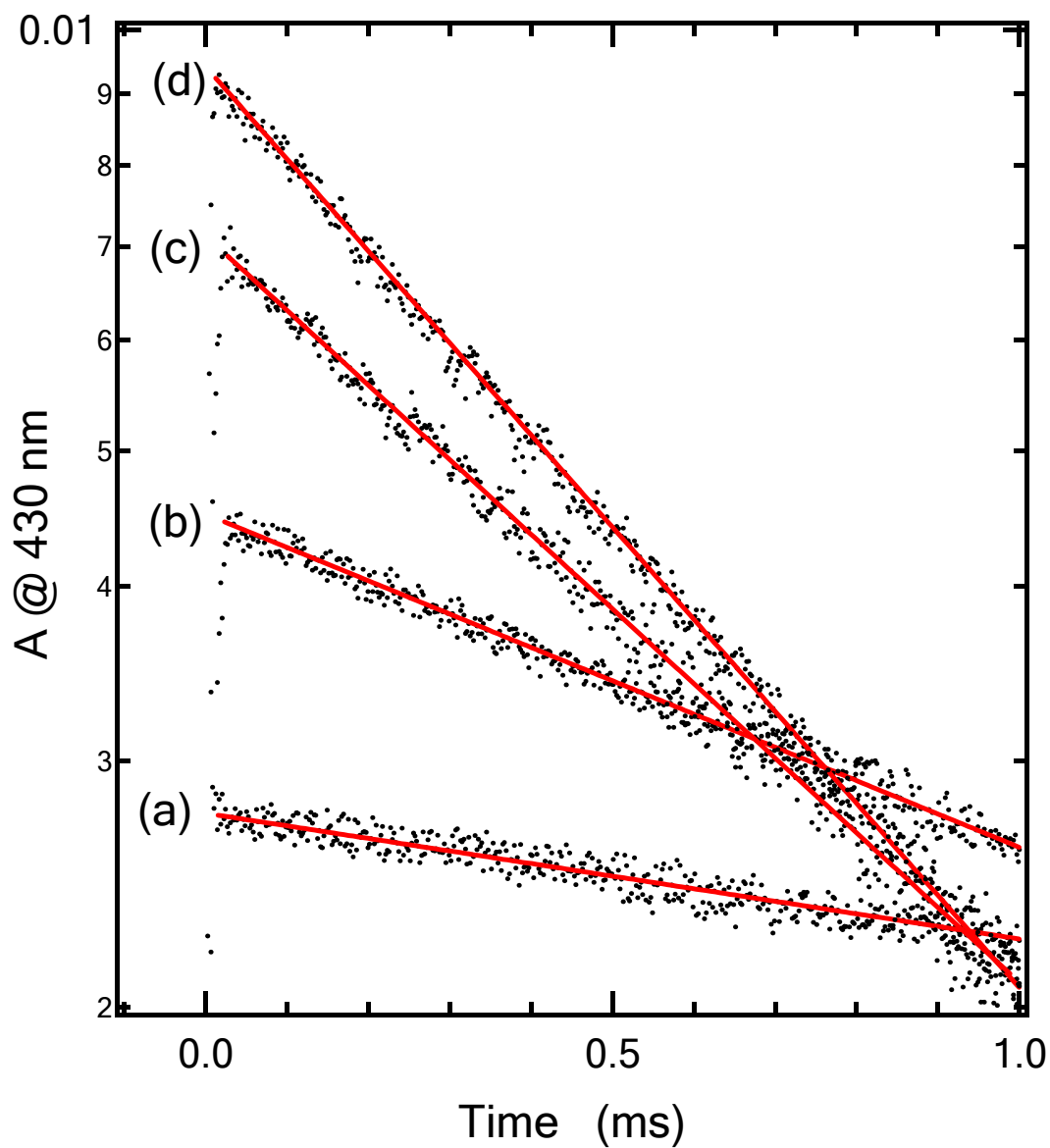


Figure 23 Temporal profiles of detected absorbance at 430 nm in the $\text{S}_2\text{O}_8^{2-}/\text{Cl}^-/\text{DMSO}/h\nu$ system

Experimental conditions: $[\text{S}_2\text{O}_8^{2-}] = 2.1 \times 10^{-5} \text{ M}$, $[\text{Cl}^-] = 0.01 \text{ M}$, $[\text{DMSO}] =$ (a) 0, (b) $8.8 \times 10^{-5} \text{ M}$, (c) $5.3 \times 10^{-4} \text{ M}$, and (d) $1.0 \times 10^{-2} \text{ M}$.

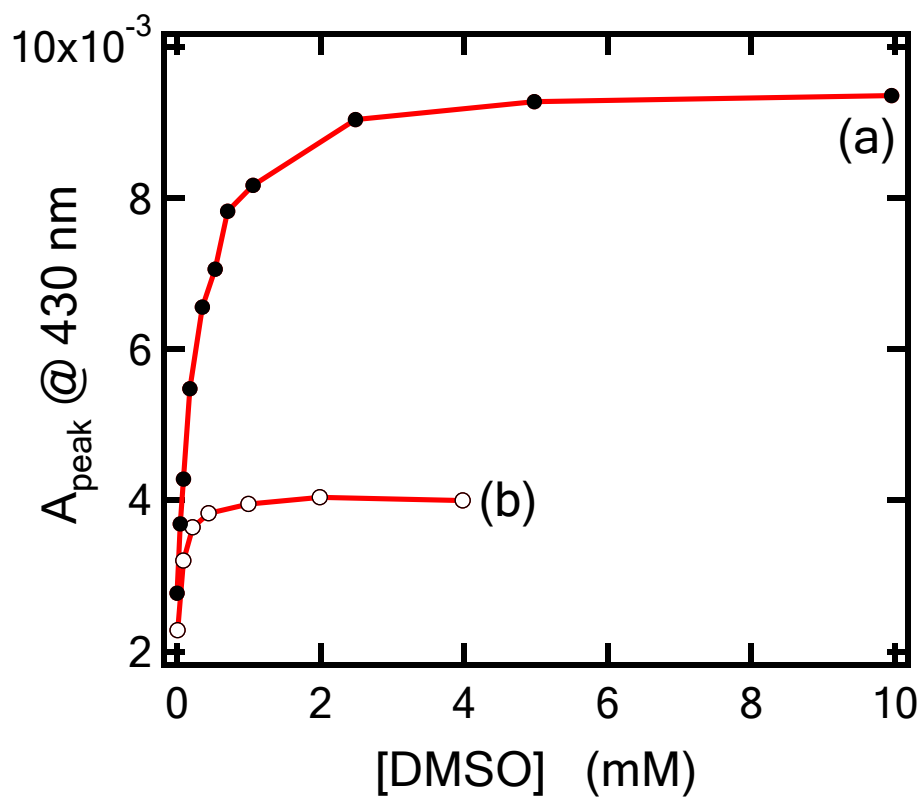


Figure 24 Plots of maximum absorbance (A_{peak}) at 430 nm vs. [DMSO]

Experimental conditions: (a) $[\text{S}_2\text{O}_8^{2-}] = 2.1 \times 10^{-5} \text{ M}$, $[\text{Cl}^-] = 0.01 \text{ M}$ (●) and (b) $[\text{S}_2\text{O}_8^{2-}] = 1.8 \times 10^{-5} \text{ M}$, $[\text{Cl}^-] = 0.002 \text{ M}$ (○).

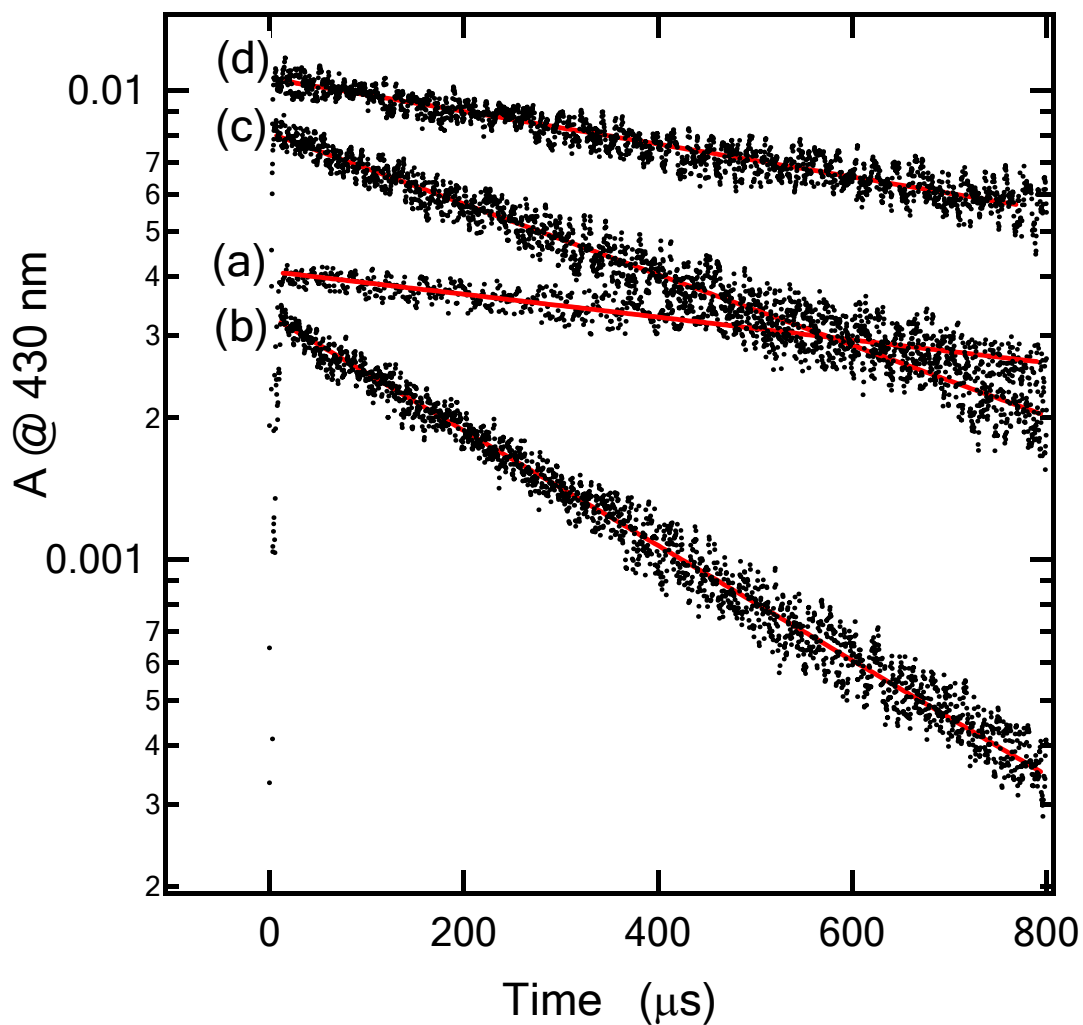


Figure 25 Temporal profiles of detected absorbance at 430 nm in the $\text{S}_2\text{O}_8^{2-}/\text{Cl}^-/\text{DMSO}/h\nu$ system

Experimental conditions: $[\text{S}_2\text{O}_8^{2-}] = 1.8 \times 10^{-5}$ M; (a): $[\text{Cl}^-] = 0$ M, $[\text{DMSO}] = 0$ M; (b): $[\text{Cl}^-] = 0.0015$ M, $[\text{DMSO}] = 0.0069$ M; (c): $[\text{Cl}^-] = 0.0075$ M, $[\text{DMSO}] = 0.0104$ M; (d): $[\text{Cl}^-] = 0.04$ M, $[\text{DMSO}] = 0.035$ M.

The spectrum of SO_4^- is well documented (see Figure 5 in chapter III); it consists of a relatively strong band with peak absorbance around 445 nm ($\epsilon \sim 1400 \text{ M}^{-1} \text{ cm}^{-1}$) and a weaker overlapping band with peak absorbance around 330 nm (Hug 1981; Tang et al., 1988). The spectrum of DMSO^+ was reported as a broad band with a peak absorbance around 300 nm and ϵ is about $1800 \text{ M}^{-1} \text{ cm}^{-1}$ (Kishore and Asmus 1989) at this peak wavelength. At 430 nm, $\epsilon_{\text{DMSO}^+} < 200 \text{ M}^{-1} \text{ cm}^{-1}$, so the detected absorbance is mainly from DMSO-Cl when Cl^- and DMSO are present in the system.

For each $[\text{Cl}^-]$ studied, at least two DMSO concentrations were used which differed by a factor of 2-5 in order to maximize the production of DMSO-Cl and check reproducibility of the experiments. The observed absorbance increases with $[\text{Cl}^-]$ at constant $\text{S}_2\text{O}_8^{2-}$ concentration, as shown in Figure 25. The photolysis of $\text{S}_2\text{O}_8^{2-}$ is the only source of free radicals in the system. Therefore, the total radical concentration remains unchanged if the laser power is constant during the experiment, based on the assumption that the only important loss of SO_4^- radicals in the system is from the reactions with DMSO and Cl^- (i.e., self reaction and reactions with $\text{S}_2\text{O}_8^{2-}$, water or any impurities in the solvents are negligible). Increases in production of DMSO-Cl occur *via* the equilibrium $\text{Cl}^- + \text{DMSO}^+ \leftrightarrow \text{DMSO-Cl}$ (R5-21), where initial Cl^- concentrations control the radical distribution between DMSO-Cl and DMSO^+ . The following expression could be derived for conditions where SO_4^- radical depletion has gone to completion but significant loss of DMSO-Cl and DMSO^+ has not yet occurred:

$$\frac{X}{[\text{DMSO-Cl}]} = 1 + \frac{1}{K_{21}[\text{Cl}^-]} \quad (5-12)$$

where $X = [\text{DMSO-Cl}] + [\text{DMSO}^+] = [\text{SO}_4^-]_0$. X is determined from the concentration of the radical precursor $\text{S}_2\text{O}_8^{2-}$ and laser power. By comparing the detected absorbance when DMSO and Cl^- are absent and present in the solution, the following equations apply:

$$A_0 = \varepsilon_{\text{SO}_4^-} \cdot l \cdot [\text{SO}_4^-]_0 = \varepsilon_{\text{SO}_4^-} \cdot l \cdot X \quad (5-13)$$

$$A = \varepsilon_{\text{DMSO-Cl}} \cdot l \cdot [\text{DMSO-Cl}] \quad (5-14)$$

where A_0 is the absorbance when Cl^- and DMSO are absent in the solution, A is the analogous absorbance when DMSO and Cl^- are present in the solution, ε is the extinction coefficient, and l is the absorption path length. The combination of equations (5-12), (5-13), and (5-14) leads to the following expression:

$$\frac{A_0}{A} = \chi + \frac{\chi}{K_{21}[\text{Cl}^-]} \quad (5-15)$$

where χ is a unitless constant defined as:

$$\chi = \frac{\varepsilon_{\text{SO}_4^-}}{\varepsilon_{\text{DMSO-Cl}}} \quad (5-16)$$

According to Equation (5-15), a plot of A_0/A versus $1/[\text{Cl}^-]$ is linear with intercept χ and slope χ/K_{21} . From a linear least squares analysis of the data shown in Figure 26, $\chi = 0.35 \pm 0.01$ and $K_{21} = 285 \pm 30 \text{ M}^{-1}$ were obtained at 430 nm. $\varepsilon_{\text{DMSO-Cl}}$ can then be derived from χ and $\varepsilon_{\text{SO}_4^-}$ at 430 nm.

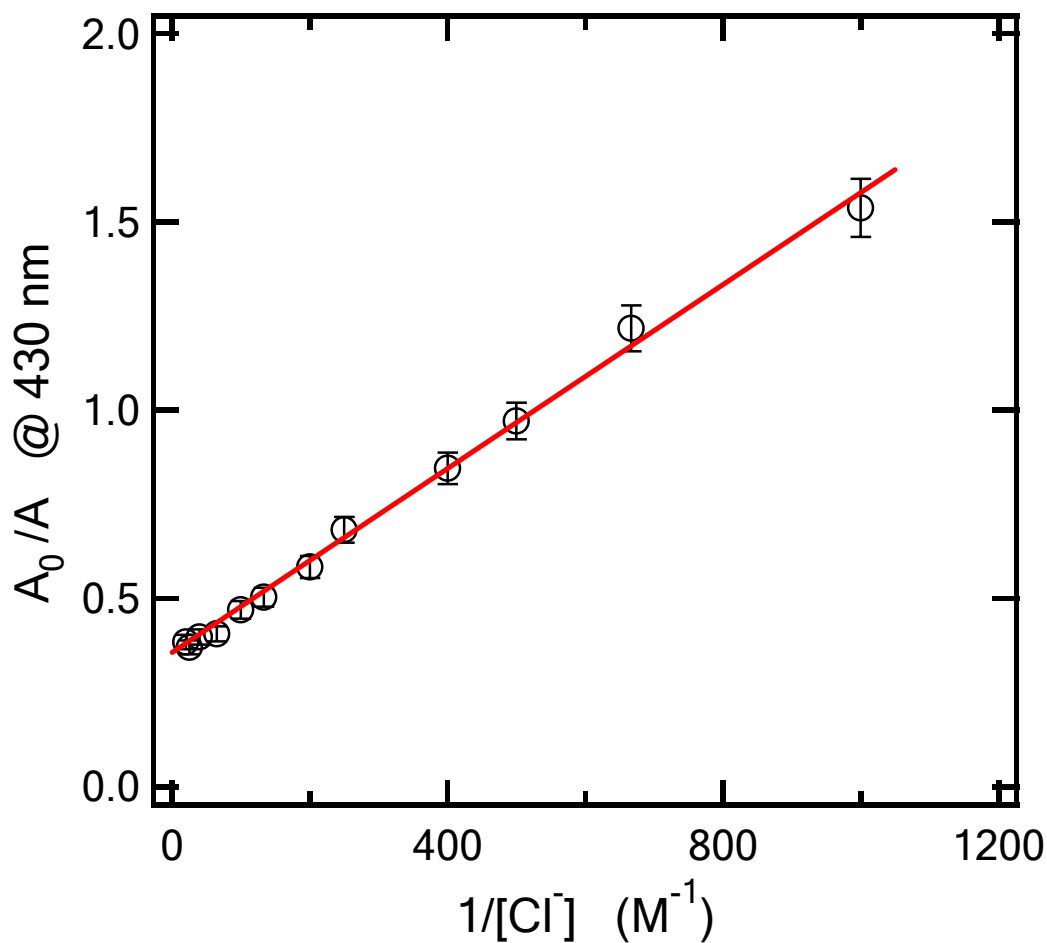


Figure 26 Plot of A_0/A at 430 nm versus $1/[Cl^-]$ in the studies of $DMSO^+ + Cl^- \leftrightarrow DMSO-Cl$

A_0 is the absorbance when Cl^- and DMSO are absent in the solution, A is the analogous absorbance when DMSO and Cl^- are present in the solution. Experimental conditions: $[S_2O_8^{2-}] = 1.8 \times 10^{-5} \text{ M}$, $[DMSO]/[Cl^-] > 60\%$. The solid straight line is the least squares linear fit of the data according to Equation (5-15) in the text, which gives $\epsilon_{SO_4} / \epsilon_{DMSO-Cl} = 0.35$ (intercept) and $K_{21} = 284 \text{ M}^{-1}$ (intercept/slope).

Another feature of the absorbance temporal profiles shown in Figure 25 is that the pseudo-first order decay rate (k') decreases as Cl^- concentration increases. Similar to the studies of $\text{Cl} \leftrightarrow \text{Cl}_2^-$ reaction kinetics, the following reactions both contribute to the detected decay of radicals:

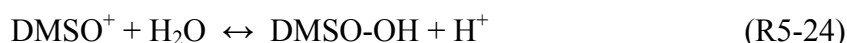


where M is any stable species or background impurities in the system.

All measured A/A_0 and first order decay rates k' at 430 nm with different $[\text{Cl}^-]$ are summarized in Table 14. k' vs. $[\text{Cl}^-]$ are fit using Equation (5-3) with three variable fitting coefficients: K_{21} , k_{22} and k_{23} . From this analysis K_{21} is derived as $360 \pm 90 \text{ M}^{-1}$, $\sim 25\%$ higher than the value obtained from Figure 24, and the loss rates of DMSO-Cl and DMSO^+ through R5-22 and R5-23 are found to be (780 ± 120) and $(4660 \pm 320) \text{ s}^{-1}$, respectively. The half-lives are estimated to be 0.9 ms for DMSO-Cl and 0.15 ms for DMSO^+ in our system, based on their pseudo-first order loss rates. These results disagree with the study by Kishore and Asmus (1991), who found that DMSO-Cl is a very short-lived species with a lifetime of about 4 μs at $\text{pH} \sim 5.5$. Our lifetime estimate is over 200 times longer than their result at the same acidity. The concentrations of DMSO and Cl^- are similar in the two studies, while radical concentrations are much higher in their work and their concentration of $\text{S}_2\text{O}_8^{2-}$ is over 200 times higher than ours. If reactions with DMSO, Cl^- and $\text{S}_2\text{O}_8^{2-}$, all contribute partially to the the loss of radicals *via* R5-22 and R5-23, such a difference in $\text{S}_2\text{O}_8^{2-}$ concentration will induce a huge difference in the

detected pseudo-first order decay rate of DMSO-Cl. Self reaction of DMSO-Cl, which is expected to occur at a near-diffusion-controlled rate, is another possible reason for the much shorter lifetime of DMSO-Cl observed in Kishore and Asmus studies.

Our reported equilibrium constant for R5-21 is the average of the two methods mentioned above, $K_{21} = (325 \pm 40) \text{ M}^{-1}$. This value is 40% lower than the value reported by Kishore and Asmus (1991). The most likely reason is the different pH conditions in two studies. In our studies, $\text{pH} \sim 5.5$ and the following equilibrium may have affected the distribution of radicals in the system:



$\text{p}K_{\text{a}24}$ is reported to be ~ 5.6 from the study of Kishore and Asmus (1991), so at the pH employed in our work, equilibrium R5-24 favors the loss of DMSO^+ radicals because the dissociation of DMSO-OH occurs at a rate of $\sim 10^7 \text{ s}^{-1}$ releasing a methyl group and generating $\text{CH}_3\text{S(O)}\text{O}^-$ (MSI):



As a result, the equilibrium of R5-21 is shifted to the production of DMSO^+ and DMSO-Cl production is reduced; therefore, the equilibrium constant K_{21} measured in our work is lower than the value obtained at a lower pH by Kishore and Asmus.

Based on the above analysis, it is more appropriate to define K_{21} obtained in our studies as the Effective Equilibrium Constant for $\text{Cl}^- + \text{DMSO}^+ \leftrightarrow \text{DMSO-Cl}$ (R5-21). As will be discussed later, K_{21} is an important parameter in deriving the absorption spectrum of the DMSO-Cl adduct, the determination of K_{21} under experimental

conditions similar to those employed in the spectroscopic studies is necessary, even though it does not represent the actual equilibrium constant for R5-21.

The absorption spectrum of DMSO-Cl was studied over the wavelength range 320 to 500 nm. All experiments were carried out under conditions where $[Cl^-] = 0.01$ M, $[S_2O_8^{2-}] = (1-2) \times 10^{-5}$ M, an unbuffered pH of ~ 5.5 , and $[DMSO] > 0.6[Cl^-]$ in order to achieve maximum production of DMSO-Cl. Since peak absorbances A_0 (from SO_4^-) and A (from DMSO-Cl), like those shown in Figures 23 and 24, were obtained under identical experimental conditions with the same absorption path length l , the following equation applies to the measurement of A_0 and A at any given wavelength:

$$\frac{A_0}{A} = \frac{\epsilon_{SO_4^-} \cdot l \cdot [SO_4^-]}{\epsilon_{DMSO-Cl} \cdot l \cdot [DMSO-Cl]} \quad (5-17)$$

Under the assumption that the total radical concentration is determined from the concentration of SO_4^- after the laser flash, i.e., all SO_4^- is converted into either DMSO-Cl or $DMSO^+$, substituting Equation (5-12) into (5-17) and rearranging leads to the following expression:

$$\frac{\epsilon_{DMSO-Cl}}{\epsilon_{SO_4^-}} = \left(1 + \frac{1}{K_{21}[Cl^-]} \right) \frac{A}{A_0} \quad (5-18)$$

Then $\epsilon_{DMSO-Cl}$ could be obtained from the observed peak absorbances A and A_0 as well as the extinction coefficient of SO_4^- at each studied wavelength. The spectrum of SO_4^- has been widely studied before, and since the extinction coefficients from these studies vary by nearly 30%, we have decided to use the average of the three studies by

Hayon et al. (1972), Tang et al. (1988), and Yu et al. (2004). The uncertainty for $\epsilon_{\text{SO}_4^-}$ obtained by this method is estimated to be $\sim 20\%$. When $[\text{Cl}^-] = 0.01 \text{ M}$, only 76% of total radicals exist as DMSO-Cl, and DMSO^+ accounts for 24% of total radicals after the depletion of SO_4^- radicals, estimated from the effective equilibrium constant of 325 M^{-1} for $\text{DMSO}^+ + \text{Cl}^- \leftrightarrow \text{DMSO-Cl}$ (R5-21). Therefore, the inclusion of K_{21} in Equation (5-18) is necessary to justify co-existence of $\text{DMSO}^+ \leftrightarrow \text{DMSO-Cl}$ radicals in the system. The reference extinction coefficient for SO_4^- and the obtained $\epsilon_{\text{DMSO-Cl}}/\epsilon_{\text{SO}_4^-}$ ratio at all wavelengths studied in this work are summarized in Table 15.

The results from the above simplified experimental approach were tested by using the more complicated method that was used to study the effective equilibrium constant (K_{21}) for $\text{DMSO}^+ + \text{Cl}^- \leftrightarrow \text{DMSO-Cl}$ (R5-21), where the $\epsilon_{\text{DMSO-Cl}}/\epsilon_{\text{SO}_4^-}$ ratio was obtained from the reciprocal ($1/\chi$) of the intercept of the A_0/A vs. $1/[\text{Cl}^-]$ plot, as shown in Figure 26. A value of 2.85 for $1/\chi$ was calculated from the linear least squares analysis of the data in Figure 26, which agrees within 5% with the value listed in Table 15 at 430 nm. This demonstrates that the simplified method is valid for obtaining the spectrum of DMSO-Cl without introducing significant systematic errors.

Table 14 Summary of the kinetics data obtained at 430 nm in DMSO-Cl studies

[Cl ⁻] (M)	^{a,b} A/A_0	^c k' (s ⁻¹)
0.001	0.65	3670 ± 180
0.002	0.82	3100 ± 180
0.0015	1.03	3100 ± 175
0.0025	1.82	3060 ± 165
0.004	1.47	2370 ± 150
0.005	1.71	2060 ± 130
0.0075	1.99	1790 ± 120
0.01	2.13	1590 ± 120
0.015	2.47	1390 ± 100
0.025	2.52	1160 ± 80
0.04	2.70	1070 ± 80
0.05	2.60	1015 ± 70

^a A_0 is the absorbance when Cl⁻ and DMSO are absent in the solution, A is the analogous absorbance when DMSO and Cl⁻ are present in the solution. Details are described in the text.

^b uncertainties are estimated to be less than 5%.

^c uncertainties are 2σ for the exponential fits of data typified in Figure 25 and represent precision only.

Table 15 Reference extinction coefficients of SO_4^- and $\epsilon_{\text{DMSO-Cl}} / \epsilon_{\text{SO}_4^-}$ ratios obtained from this work

Wavelength (nm)	$\epsilon_{\text{SO}_4^-}$ ($\text{M}^{-1} \text{cm}^{-1}$) *	$\epsilon_{\text{DMSO-Cl}} / \epsilon_{\text{SO}_4^-}$
320	666	1.8
330	694	2.6
340	730	3.4
350	760	4.3
360	805	5.1
370	865	6.0
380	946	5.9
390	1054	5.5
400	1161	4.8
410	1252	3.9
420	1313	3.3
430	1360	2.7
440	1388	2.3
450	1367	2.0
460	1324	1.8
470	1233	1.6
480	1096	1.6
490	960	1.4
500	805	1.2

* Obtained from the average of studies from Hayon et al. (1972), Tang et al. (1988) and Yu et al. (2004), errors of these data are estimated to be < 20%.

The DMSO-Cl absorption spectrum obtained from the data listed in Table 15 is shown as the top plot in Figure 27. For comparison, the spectrum from the study of Kishore and Asmus (1991) is shown in the bottom plot. Our DMSO-Cl spectrum has a broad band with a maximum absorbance around 390 nm and an extinction coefficient of $\sim 5760 \text{ M}^{-1} \text{ cm}^{-1}$ at the peak absorbance wavelength.

The shape of our spectrum resembles that from Kishore and Asmus (1991), but is not quite as broad. Kishore and Asmus used the pulse radiolysis technique and reported the spectrum in the form of $G \times \epsilon$, where G denotes the number of species generated or transformed per 100eV energy uptake and is approximately 2.8 in their work. They reported a maximum absorbance at 390 nm and estimated an extinction coefficient in the range of $5000\text{-}7000 \text{ M}^{-1} \text{ cm}^{-1}$; they also pointed out that this is a typical extinction coefficient range for the structurally similar $>\text{S} \cdot \text{X}$ type and other three-electron-bonded radical species (Bonifacic and Asmus 1980; Anklam et al., 1988; Anklam et al., 1990; Kishore and Asmus 1991).

From the above studies on DMSO-Cl, it is clear that formation of this species explains the observation that the pseudo-first order decay rates at 340 nm are slower than expected in the DMSO kinetics studies. In studies with high Cl^- concentrations, long time scales have to be used since the radical decay is very slow. Thus, the production of DMSO-Cl interferes with the detected absorbance at 340 nm ($\epsilon_{\text{DMSO-Cl}} \approx 0.3 \epsilon_{\text{Cl}_2}$) and makes observed absorbance decay rates slower due to the long DMSO-Cl lifetime under our experimental conditions.

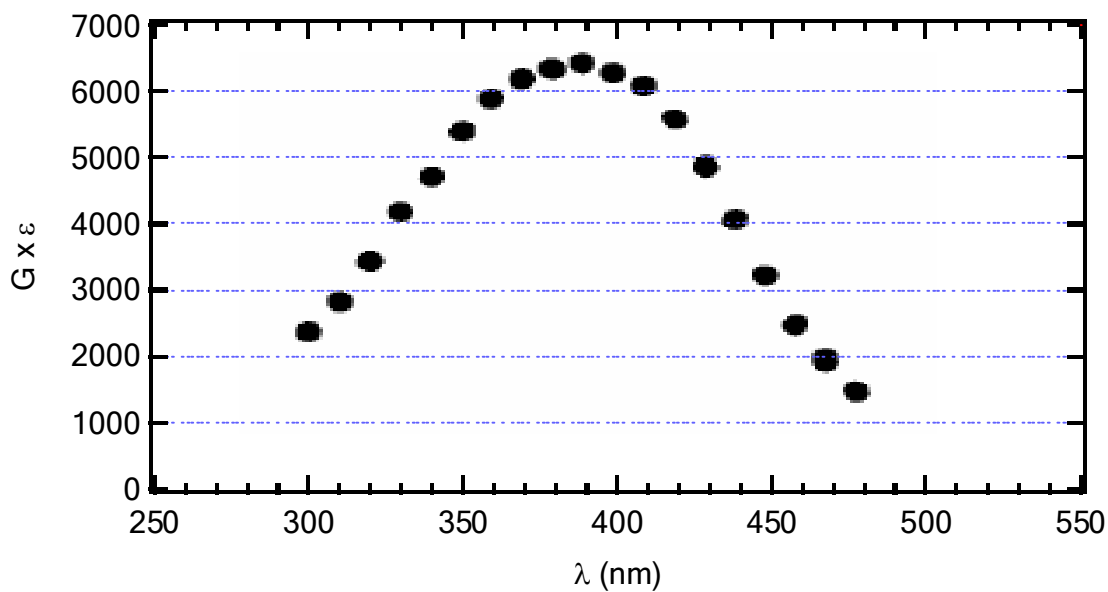
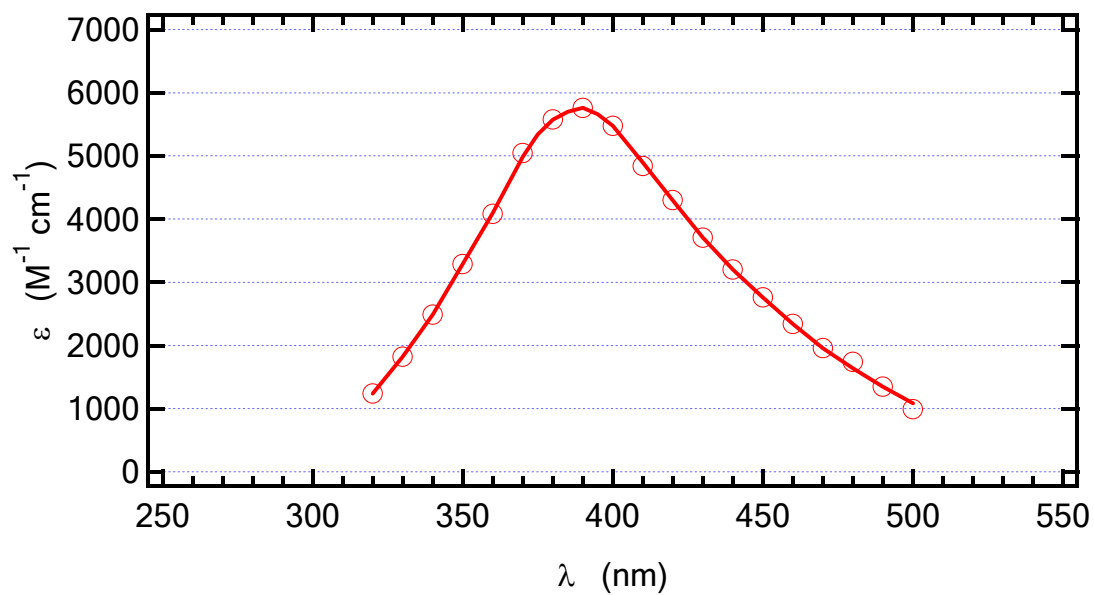


Figure 27 Absorption spectrum of the DMSO-Cl adduct determined from this work (top) and from Kishore and Asmus, 1991 (bottom)

Analysis of Systematic Errors

Derivation of the rate coefficients for all reactions used Equations (5-3) and (5-6), so the equilibrium constant of $\text{Cl} + \text{Cl}^- \leftrightarrow \text{Cl}_2^-$ (R5-1) is an important parameter in this kinetics study. $K_1 = 1.4 \times 10^5 \text{ M}^{-1}$ was adopted for all data analyses, based on a collection of studies (Jayson et al., 1973; Nagarajan and Fessenden 1985; McElroy 1990; Buxton et al., 1998; Yu et al., 2004), and the error for K_1 from this adoption is estimated to be $\sim 10\%$. Therefore, K_1 was adjusted by 10% for data analyses in order to investigate errors in kinetics data brought by this adjustment. It was found that for all reaction rate coefficients, errors are less than 10% for a 10% change in K_1 .

For two reasons, the concentration of Cl^- is another important experimental parameter in this study. First, the Cl^- concentration is important in determining the production rate of Cl and Cl_2^- radicals. Second, the Cl^- concentration determines the fractions of these two radicals in the system. In order to get sufficient number of data points to investigate the contribution of Cl reactions, the minimum Cl^- concentration was as low as possible. When the Cl^- concentration is low, Cl production from $\text{SO}_4^- + \text{Cl}^- \rightarrow \text{SO}_4^{2-} + \text{Cl}$ (R5-2) is too slow when compared to the decay of $\text{Cl} \leftrightarrow \text{Cl}_2^-$ radicals, making it impossible to derive the pseudo-first order decay rate of radicals from the observed absorbance signals. A $[\text{Cl}^-]$ range from 10^{-4} to $5 \times 10^{-2} \text{ M}$ was chosen to carry out the studies by considering the above two factors. Since both the forward and the reverse reaction rate coefficients of $\text{Cl} + \text{Cl}^- \leftrightarrow \text{Cl}_2^-$ are very fast ($\sim 8 \times 10^9 \text{ M}^{-1} \text{ s}^{-1}$) (Nagarajan and Fessenden 1985; Yu et al., 2004), it is appropriate to assume that Cl and Cl_2^- are always in equilibrium after SO_4^- has been depleted at the $[\text{Cl}^-]$ range employed. Cl_2^-

accounts for, therefore, $\sim 93\%$ of total radicals when $[\text{Cl}^-] = 10^{-4}$ M, and over 99.9% when $[\text{Cl}^-] = 10^{-2}$ M, which are estimated from the equilibrium constant of $\text{Cl} + \text{Cl}^- \leftrightarrow \text{Cl}_2^-$ mentioned above. In all studies, Cl_2^- is the dominant radical and all data are at the right hand side of the sigmoid curves. However, for all three species, rate coefficients for Cl reactions are over two orders of magnitude higher than those for Cl_2^- reactions, therefore, contributions from Cl reactions in the measured rate coefficients are non-negligible even at high Cl^- concentrations.

The loss of Cl and Cl_2^- radicals from reactions with impurities in the samples of Cl^- , $\text{S}_2\text{O}_8^{2-}$ and sulfur species is another potentially significant source of systematic error. From the very slow decay rate of radicals at high Cl^- concentrations where Cl_2^- is the dominant radical, reactions of Cl_2^- with impurities in $\text{S}_2\text{O}_8^{2-}$ and Cl^- samples are estimated to have an insignificant effect on kinetics. The DMSO sample purity was high (see chemical section in Chapter II) and the reaction of DMSO with Cl is near the diffusion-controlled limit, so it is not likely for impurity reactions from the DMSO sample to impact determination of rate coefficients. The MS and DMSO2 samples are both labeled 98% purity, and the reactions of these two species with $\text{Cl} \leftrightarrow \text{Cl}_2^-$ were found to be very slow; hence it can't be ruled out that the observed kinetics are affected by a minor reactive impurity in the sample (for example, DMSO). For this reason, the kinetics results obtained for DMSO2 and MS reactions should be strictly considered as upper limits.

In the studies of the DMSO-Cl spectrum, the most significant error comes from uncertainties in the extinction coefficients of SO_4^- adopted as the reference. We used the average of three studies (Hayon et al., 1972; Tang et al., 1988; Yu et al., 2004) for the full

spectrum of SO_4^- . The uncertainties on $\varepsilon_{\text{SO}_4^-}$ obtained with this method are estimated to be $\sim 20\%$. As mentioned earlier, the errors in absorbance ratios listed in Table 15 are $< 5\%$. The value of the effective equilibrium constant, K_{21} , which was used to calculate the extinction coefficients in Equation (5-18), is another potential source of systematic errors. An uncertainty of 15% in K_{21} brings a $< 5\%$ error in the determination of extinction coefficients, according to Equation (5-18).

Loss of SO_4^- from reactions with background species is another potential source of systematic error. In order to quantify the loss of SO_4^- , the absorbance obtained from the photolysis of $\text{S}_2\text{O}_8^{2-}$ solutions (A_0) and absorbance from the photolysis of solutions containing both $\text{S}_2\text{O}_8^{2-}$ and Cl^- ($A_{\text{Cl}_2^-}$) were compared at each studied wavelength. A_0 is primarily from SO_4^- , and $A_{\text{Cl}_2^-}$ is primarily from Cl_2^- . When the concentration of Cl^- is 0.01 M, all SO_4^- produced from the photolysis of $\text{S}_2\text{O}_8^{2-}$ is scavenged efficiently by Cl^- , and as a result Cl_2^- is the dominant radical in the system. Table 16 lists the absorbance ratio ($A_0/A_{\text{Cl}_2^-}$) obtained under experimental conditions identical to those in Table 15 and the extinction coefficient ratio ($\varepsilon_{\text{SO}_4^-} / \varepsilon_{\text{Cl}_2^-}$), where $\varepsilon_{\text{SO}_4^-}$ is the same as those listed in Table 15, and $\varepsilon_{\text{Cl}_2^-}$ was obtained from the average of studies of Jayson et al. (1973) and Yu et al. (2004). The errors of the two extinction coefficients obtained by this method are estimated to be $\sim 20\%$ each. As expected, the observed $A_0/A_{\text{Cl}_2^-}$ ratios agree well with $\varepsilon_{\text{SO}_4^-} / \varepsilon_{\text{Cl}_2^-}$ ratios at all wavelengths. These results indicate that the loss of SO_4^- from reactions with species other than Cl^- and DMSO will result in a systematic error of less than 5%; hence, the assumption of $[\text{SO}_4^-] = [\text{DMSO}^+] + [\text{DMSO-Cl}]$ at high DMSO concentrations is verified, and the errors introduced by this assumption are small.

Based on the above discussion, the uncertainty in the extinction coefficients reported in this work is estimated to be <30%, based on the sum of errors in extinction coefficients of SO_4^- , the measured absorbance ratio, determination of K_{21} in this work and loss of SO_4^- from reactions with species other than DMSO and Cl^- .

Table 16 Comparison of $A_0/A_{\text{Cl}_2^-}$ and $\varepsilon_{\text{SO}_4^-}/\varepsilon_{\text{Cl}_2^-}$ at all wavelengths studied

λ (nm)	^a $A_0/A_{\text{Cl}_2^-}$	^b $\varepsilon_{\text{SO}_4^-}/\varepsilon_{\text{Cl}_2^-}$
320	0.092	0.090
330	0.088	0.082
340	0.087	0.084
350	0.086	0.091
360	0.11	0.11
370	0.16	0.14
380	0.18	0.19
390	0.30	0.28
400	0.43	0.40
410	0.67	0.66
420	1.1	1.1
430	1.6	1.6
440	2.1	2.1
450	2.6	2.6
460	4.1	4.1
470	4.9	4.9
480	6.4	—
490	5.6	—
500	10	—

^a All absorbance ratios are the average of more than one experiment at different radical concentrations.

^b $\varepsilon_{\text{SO}_4^-}$ is same as those in Table 15; $\varepsilon_{\text{Cl}_2^-}$ is the average of works by Jayson et al. (1973) and Yu et al. (2004); uncertainties for both extinction coefficients are $\sim 10\%$.

CHAPTER VI

KINETICS STUDIES OF METHANE SULFINATE (MSI)

REACTIONS WITH OH AND Cl_2^- RADICALS

Methane sulfinic acid ($\text{CH}_3\text{S}(\text{O})\text{OH}$), MSIA, is another important intermediate formed during the atmospheric oxidation of DMS. Unlike the other sulfur species studied in this research project, i.e., DMSO, DMSO₂ and MSA (MS), MSIA has not been observed by any field experiments. It has been demonstrated, however, *via* laboratory investigations, that MSIA is the major product from DMSO oxidation by OH in both the gas phase (Urbanski et al., 1998; Arsene et al., 2002; Kukui et al., 2003) and the aqueous phase (Veltwisch et al., 1980; Scaduto 1995; Jahnke 1999; Bardouki et al., 2002). The study by Kukui et al. (2003) found that OH-initiated gas phase oxidation of DMSO generates MSIA as the predominant product and, in the absence of O₂, MSIA then undergoes further oxidation by OH radicals resulting in the formation of SO₂; the OH + MSIA reaction rate coefficient of $(9 \pm 3) \times 10^{-11} \text{ cm}^3 \text{ molecule}^{-1} \text{ s}^{-1}$ was reported from their work. Although the OH + MSIA reaction mechanism in the presence of atmospheric level of O₂ needs further investigation, the results from Kukui et al. (2003) suggest that the gas phase oxidation of DMS will lead primarily to the production of SO₂, eventually H₂SO₄, while the other important end product, methane sulfonic acid (MSA), is produced primarily *via* aqueous phase reactions. The very fast gas phase oxidation and

efficient uptake of MSIA into atmospheric condensed phases (assuming a Henry's Law constant and uptake coefficient close to those of MSA) should make the gas phase concentration of this species very low in the ambient atmosphere.

MSIA has a pK_a of 2.2-2.3 (Wudl et al., 1967), so it almost completely dissociates to release MSI (the de-protonated form of MSIA) in water at the typical atmospheric pH range 4-6. Several studies on the liquid phase oxidation of MSI by OH radicals report a very fast (essentially diffusion controlled) rate coefficient in the range of $(0.6-1.2) \times 10^{10} \text{ M}^{-1} \text{ s}^{-1}$ (Sehested and Holcman 1996; Flyunt et al., 2001; Bardouki et al., 2002), and the predominant product is demonstrated to be MSA. However, all these studies have focused on mechanistic studies, and no details concerning the derivation of rate coefficients were reported.

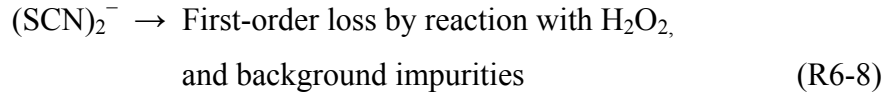
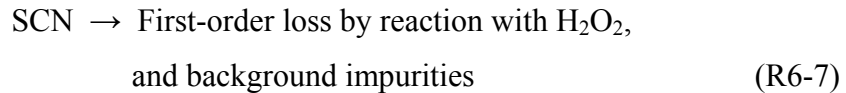
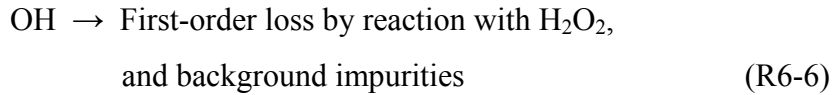
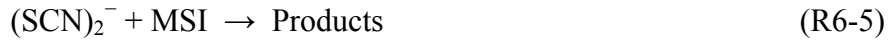
In our studies of the kinetics of MSI reactions with OH and $\text{Cl} \leftrightarrow \text{Cl}_2^-$, some interesting kinetic behavior was observed, so a separate chapter is devoted to a detailed description of studies of room temperature ($295 \pm 1 \text{ K}$) MSI reaction kinetics.

Kinetics Studies of the OH + MSI Reaction

The kinetics of the OH + MSI reaction were studied using the same technique as the one employed for studying reactions of OH with DMSO, DMSO₂ and MS, so the experimental method will not be repeated here.

However, the technique used for analyzing data from the OH + MSI reaction was modified as a result of MSI reacting with SCN and/or (SCN)₂⁻ radicals. This became evident when we found that the decay rates of the observed (SCN)₂⁻ absorbance (at 475 nm) increased dramatically with increasing MSI concentrations. During studies of OH reactions with DMSO, DMSO₂ and MS, reactions of the organic sulfur compounds R (R = DMSO, DMSO₂ or MS) with SCN and/or (SCN)₂⁻ radicals were sufficiently slow that they did not influence absorbance measurements. Thus, as discussed previously, peak absorbances were obtained directly from profiles of (SCN)₂⁻ absorbance and were used to determine k_R/k_{SCN^-} . On the other hand, during MSI + OH studies the concentration of SCN⁻ was found to be an important parameter in determining the $k_{\text{MSI}}/k_{\text{SCN}^-}$ ratio (obtained from the plot of A_0/A_{MSI} vs. $[\text{MSI}]/[\text{SCN}^-]$ as described in Chapter IV), if A_0 and A_{MSI} were obtained from the direct reading of the peak (SCN)₂⁻ absorbances. Because of the reaction(s) of MSI with SCN and/or (SCN)₂⁻ radicals, the data analysis method we used for the kinetics studies of OH reactions with other sulfur species are not applicable here. In that sense, a new analysis technique has to be pursued for MSI + OH kinetics data.

The new data analysis technique developed for examining OH + MSI kinetics involves fitting absorbance temporal profiles with a triple-exponential function. The fitting function is obtained as an analytical solution to the rate equations for the mechanism including both production and decay of all the free radicals in the system (Chin and Wine 1992), as follows:



The rate equations for the above kinetic scheme can be solved analytically to obtain the $(\text{SCN})_2^-$ absorbance temporal profile:

$$A_t = a_4 \left\{ \frac{\exp(-a_1 t)}{(a_2 - a_1)(a_3 - a_1)} + \frac{\exp(-a_2 t)}{(a_1 - a_2)(a_3 - a_2)} + \frac{\exp(-a_3 t)}{(a_1 - a_3)(a_2 - a_3)} \right\} \quad (6-1)$$

where

$$a_1 = 0.5[x - (x^2 - 4y)^{1/2}] \quad (6-2)$$

$$a_2 = 0.5[x + (x^2 - 4y)^{1/2}] \quad (6-3)$$

$$a_3 = k_1[\text{SCN}^-] + k_3[\text{MSI}] + k'_6 \quad (6-4)$$

$$a_4 = k_1 k_2 [\text{SCN}^-]^2 [\text{OH}]_0 \varepsilon l \quad (6-5)$$

$$x = a_1 + a_2 = k_2[\text{SCN}^-] + (k_4 + k_5)[\text{MSI}] + k'_{-2} + k'_7 + k'_8 \quad (6-6)$$

$$y = a_1 a_2 = k_2 (k_5[\text{MSI}] + k'_8) [\text{SCN}^-] + (k_4[\text{MSI}] + k'_7) (k_5[\text{MSI}] + k'_{-2} + k'_8) \quad (6-7)$$

In the above equations, A_t is the absorbance of $(\text{SCN})_2^-$ at time t , ε is the $(\text{SCN})_2^-$ extinction coefficient at the monitoring wavelength (475 nm), l is the absorption path length, k'_i and k_i are pseudo-first and second order rate coefficients for reaction i .

Equation (6-1) was used to fit the original data, and the fitting curves reproduced the data well. However, the four parameters (a_1 , a_2 , a_3 and a_4) obtained from this fit have large uncertainties. In order to increase the accuracy and precision of the fitting routine, one or two of the parameters need to be fixed during this procedure. From the definition of x and y in Equations (6-6) and (6-7), where rate coefficients k_1 , k_2 and k'_{-2} have been well studied before, if we could independently determine the rate coefficients for removal of SCN^- and $(\text{SCN})_2^-$, i.e., k_4 , k_5 , k'_7 and k'_8 , values for x and y as well as a_1 and a_2 could be derived for specific SCN^- and MSI concentrations. Therefore, the number of

coefficients in the fitting function is reduced, and a_3 and a_4 can be obtained with improved accuracy from such fits. The parameter a_3 is proportional to the MSI concentration when the concentration of SCN^- and other experimental conditions are held constant, and the slope of a plot of a_3 vs. $[\text{MSI}]$ is k_3 , the rate coefficient for the $\text{MSI} + \text{OH}$ reaction.

Determination of k_4 , k_5 , k'_7 and k'_8

As discussed above, k_4 , k_5 , k'_7 and k'_8 need to be evaluated independently in order to allow accurate determination of k_3 . Since all four rate coefficients involve the loss of SCN or $(\text{SCN})_2^-$ radicals, only the decay portion of absorption temporal profiles are important in providing the kinetics information.

All experiments were carried out under pseudo-first order conditions with concentrations of H_2O_2 , SCN^- and MSI in large excess over those of the radicals (OH , SCN and $(\text{SCN})_2^-$). Typical concentrations of H_2O_2 were $(0.5 - 3) \times 10^{-4}$ M, $[\text{SCN}^-]$ were in the range $(0.3 - 3) \times 10^{-5}$ M, and at each $[\text{SCN}^-]$, MSI concentrations varied from 0 to $<1.0 \times 10^{-5}$ M. Typical absorbance temporal profiles observed at 475 nm are plotted in Figure 28; the two graphs represent data sets at two different SCN^- concentrations, 3.3×10^{-6} M (top graph) and 3.0×10^{-5} M (bottom graph). For experiments at higher SCN^- concentrations, the signal rise times are much faster than the decay times for all MSI concentrations studied. At lower SCN^- concentrations, the signal rise times are much slower. For both plots, however, the observed signal decays exponentially after production is complete, and the decays gets faster as $[\text{MSI}]$ increases. The red lines in

the plots are least squares analyses of the decay portion of the profiles, and the slopes (on log scales) represent the pseudo-first order decay rates of the radicals (k'_{measured}).

After the depletion of OH radicals, i.e., after production of SCN and $(\text{SCN})_2^-$ has gone to completion, the only radicals in the system are SCN and $(\text{SCN})_2^-$. Within the time scale studied, R6-2 has attained equilibrium, and therefore the loss of SCN and $(\text{SCN})_2^-$ both contribute to the observed decay, even though only $(\text{SCN})_2^-$ contributes to absorbance at 475 nm, the monitoring wavelength. Similar to studies of $\text{Cl} \leftrightarrow \text{Cl}_2^-$ kinetics (Chapter V), the following equation applies for the measured first order decay:

$$k'_{\text{measured}} = \alpha k'_{\text{SCN}} + \beta k'_{(\text{SCN})_2^-} \quad (6-8)$$

where α and β are the fractions of SCN and $(\text{SCN})_2^-$ radicals defined as:

$$\alpha = \frac{[\text{SCN}]}{[\text{SCN}] + [\text{SCN}_2^-]} = \frac{1}{1 + K_2[\text{SCN}^-]} \quad (6-9)$$

$$\beta = \frac{[\text{SCN}_2^-]}{[\text{SCN}] + [\text{SCN}_2^-]} = \frac{K_2[\text{SCN}^-]}{1 + K_2[\text{SCN}^-]} \quad (6-10)$$

and k'_{SCN} and $k'_{(\text{SCN})_2^-}$ are pseudo-first-order loss rates of the two radicals:

$$k'_{\text{SCN}} = k_4[\text{MSI}] + k'_7 \quad (6-11)$$

$$k'_{(\text{SCN})_2^-} = k_5[\text{MSI}] + k'_8 \quad (6-12)$$

Substituting Equations (6-11) and (6-12) into Equation (6-8) gives:

$$k'_{\text{measured}} = (\alpha k_4 + \beta k_5)[\text{MSI}] + \alpha k'_7 + \beta k'_8 \quad (6-13)$$

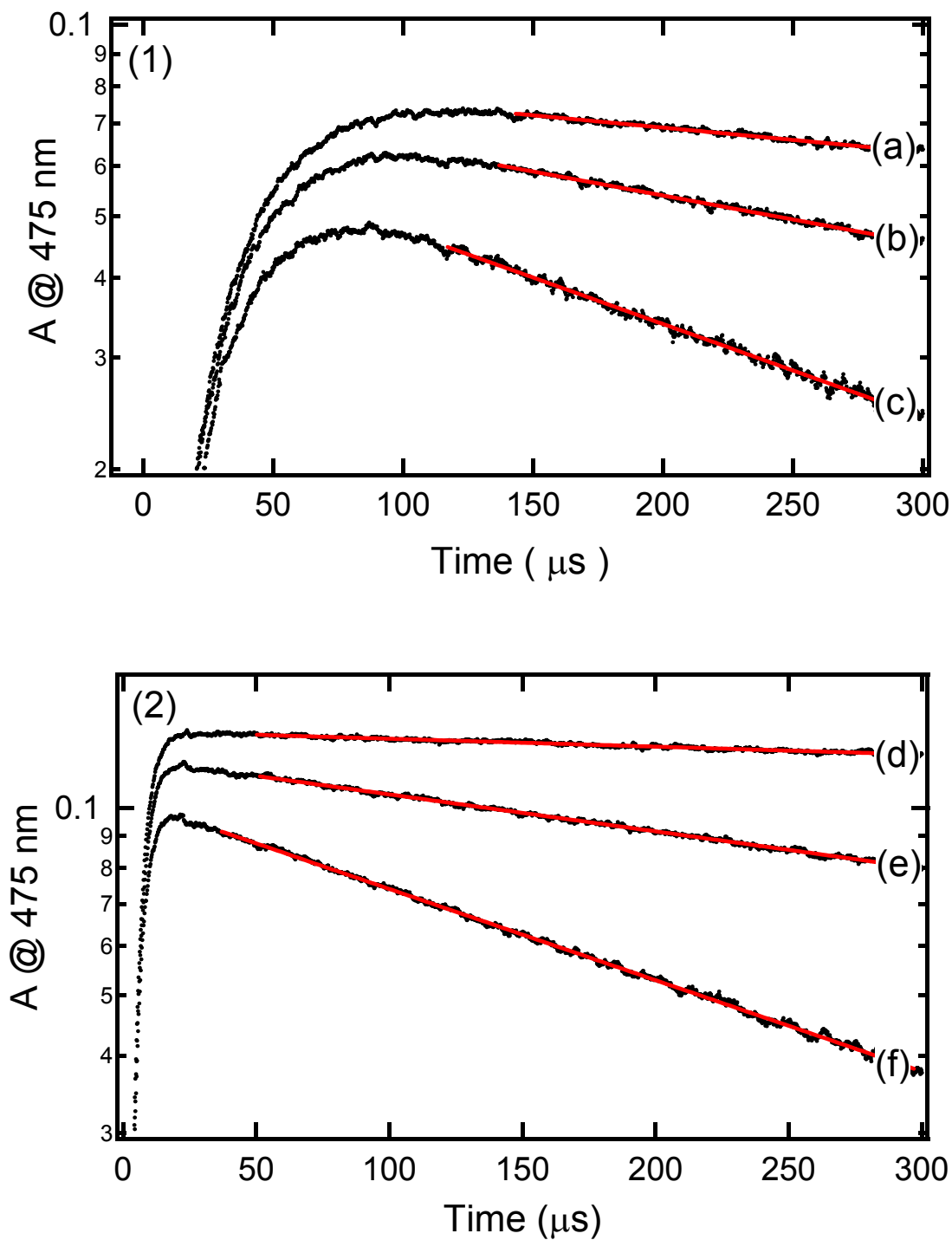


Figure 28 Typical temporal profiles of $(\text{SCN})_2^-$ absorbance observed at 475 nm and fits of exponential decay of radicals

Experimental conditions: $[\text{H}_2\text{O}_2] = 1.2 \times 10^{-4} \text{ M}$; in (1): $[\text{SCN}^-] = 3.3 \times 10^{-6} \text{ M}$, (a) $[\text{MSI}] = 0$, (b) $5.2 \times 10^{-7} \text{ M}$, (c) $1.6 \times 10^{-6} \text{ M}$; and in (2), $[\text{SCN}^-] = 3.0 \times 10^{-5} \text{ M}$, $[\text{MSI}] =$ (d) 0 M , (e) $2.4 \times 10^{-6} \text{ M}$, (f) $7.3 \times 10^{-6} \text{ M}$.

According to Equation (6-13), a plot of k'_{measured} versus [MSI] at a constant SCN^- concentration gives a straight line. The slope of the line (S) is $\alpha k_4 + \beta k_5$, and the intercept (I) corresponds to $\alpha k'_7 + \beta k'_8$. Plots of k'_{measured} versus [MSI] at two different SCN^- concentrations are compared in Figure 29. The data at both SCN^- concentrations show a very good linear relationship. As expected, S and I are both functions of $[\text{SCN}^-]$, because α and β are dependent on the concentration of SCN^- . Substituting Equations (6-9) and (6-10) into the definitions of S and I leads to the following expression:

$$S = \frac{1}{1 + K_2[\text{SCN}^-]} k_4 + \frac{K_2[\text{SCN}^-]}{1 + K_2[\text{SCN}^-]} k_5 \quad (6-14)$$

$$I = \frac{1}{1 + K_2[\text{SCN}^-]} k'_7 + \frac{K_2[\text{SCN}^-]}{1 + K_2[\text{SCN}^-]} k'_8 \quad (6-15)$$

In Figure 30, all slopes (S , black) and intercepts (I , red) are plotted as a function of the SCN^- concentration; the two curves were obtained by fitting S and I versus $[\text{SCN}^-]$ with Equations (6-14) and (6-15), respectively. An important parameter used in the fitting equation is the equilibrium constant for $\text{SCN}^- + \text{SCN} \leftrightarrow (\text{SCN})_2^-$ (R6-2), K_2 . The kinetics of R6-2 have been well studied, and Table 17 summarizes the room temperature ($295 \pm 1\text{K}$) kinetics data on R6-1 and R6-2 available in the literature. Since it is hard to choose any specific value from the literature, we have decided to use an average of all the data listed in Table 17 for k_1 , k_2 and K_2 . k'_{-2} is then calculated from k_2/K_2 using the average values listed in the table.

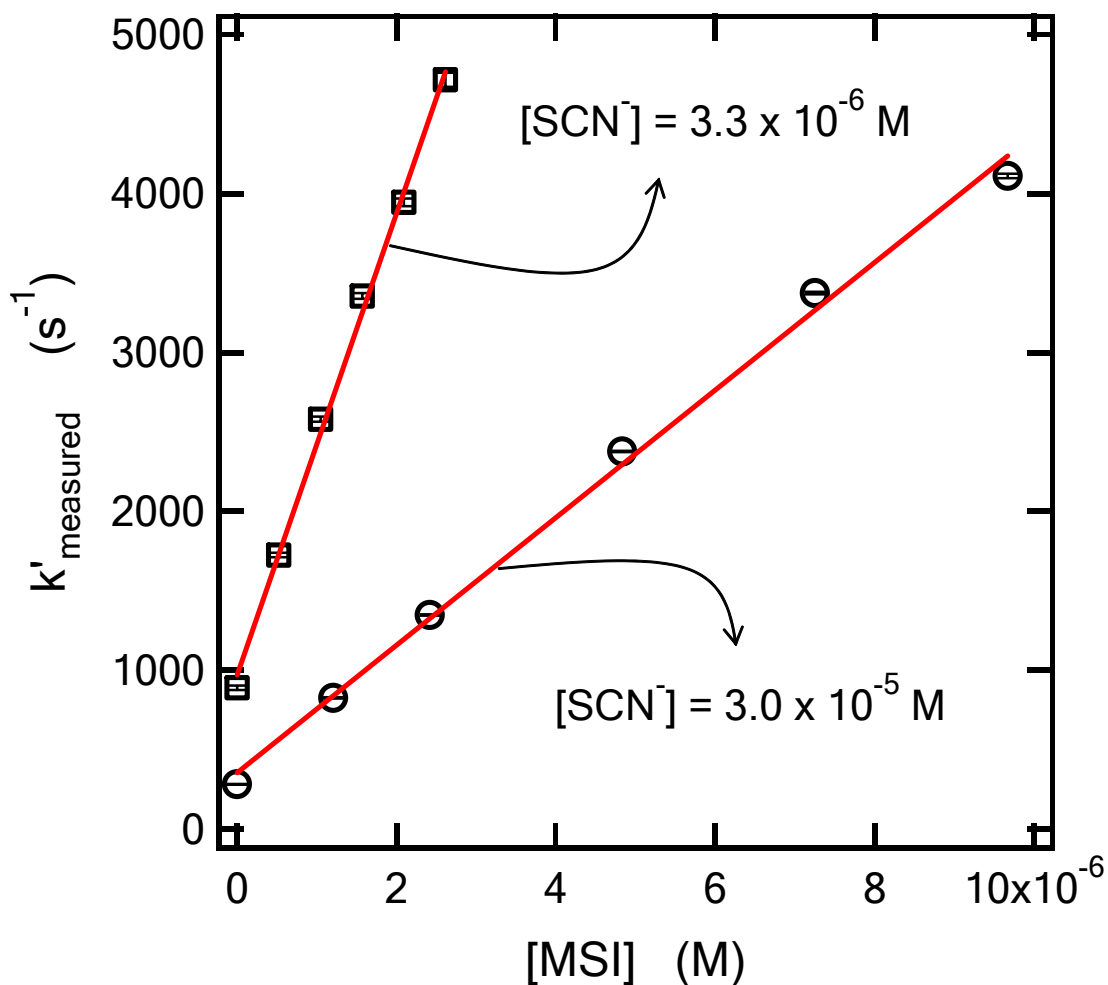


Figure 29 Plots of measured pseudo-first-order decay rates (k'_{measured}) versus [MSI]. Experimental conditions: $[\text{H}_2\text{O}_2] = 1.2 \times 10^{-4} \text{ M}$, $[\text{SCN}^-] = 3.3 \times 10^{-6}$ (squares) 3.0×10^{-5} (circles) M . The solid lines are linear least-squares analyses of the data and give the slopes (S) of $(1.45 \pm 0.08) \times 10^9$ (squares) and $(4.01 \pm 0.24) \times 10^8$ (circles) $\text{M}^{-1} \text{s}^{-1}$ and the intercepts (I) of 971 ± 131 (squares) and 356 ± 130 (circles) s^{-1} .

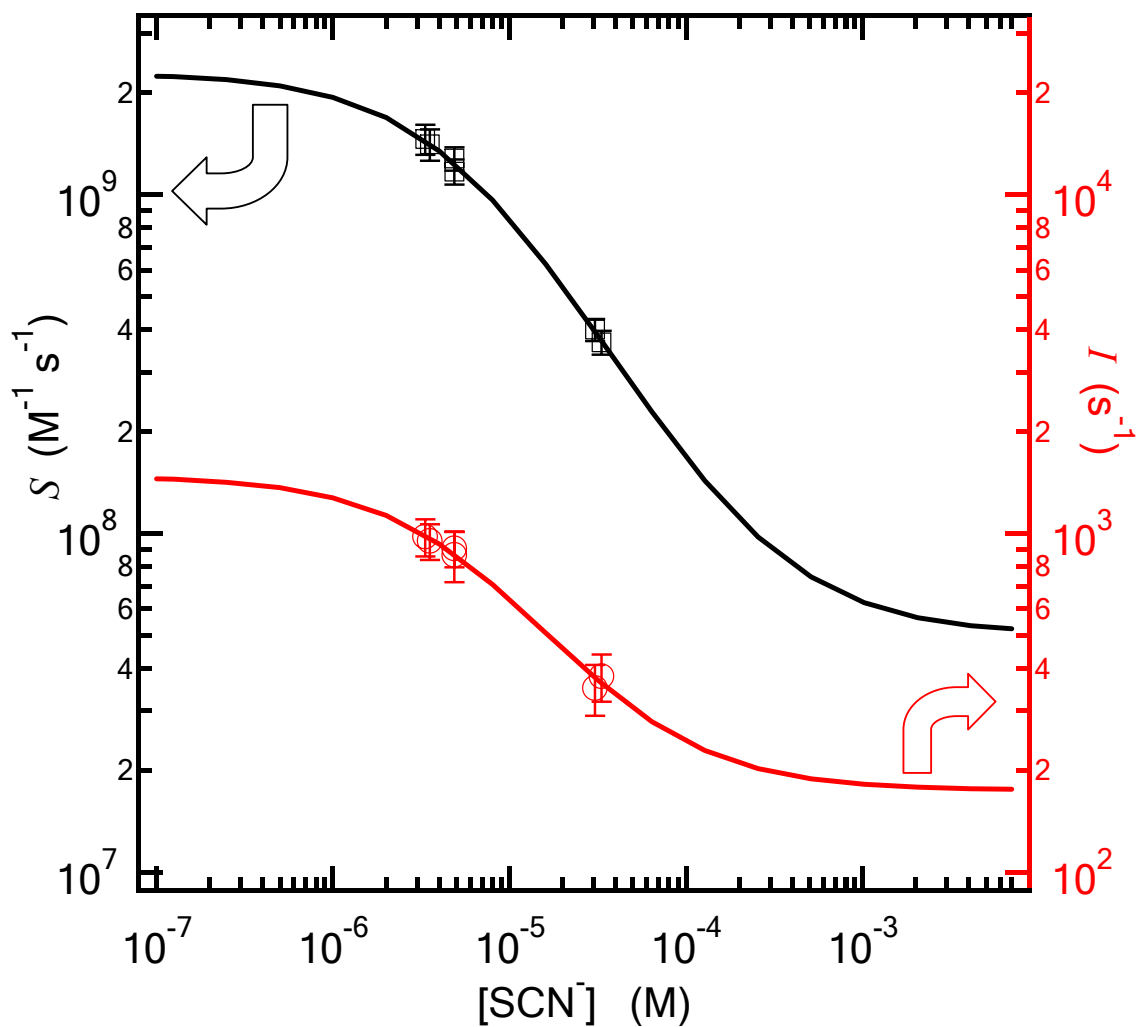


Figure 30 Plot of S and I versus $[\text{SCN}^-]$

The solid curves are from fitting the data with Equation (6-14) for S (black) and Equation (6-15) for I (red), which give values of k_4 , k_5 , k'_7 and k'_8 , as listed in the text. The error bars are two times standard deviations and represent precision only.

Table 17 Literature values of k_1 , k_2 and K_2 at room temperature

	k_i	References	Average
k_1 ($M^{-1}s^{-1}$)	1.10×10^{10}	(Elliot and Simsons 1984)	1.13×10^{10}
	1.16×10^{10}	(Chin and Wine 1992)	
k_2 ($M^{-1}s^{-1}$)	7.0×10^9	(Baxendale et al., 1968)	7.4×10^9
	6.8×10^9	(Behar et al., 1972)	
	9.0×10^9	(Nagarajan and Fessenden 1985)	
	6.9×10^9	(Chin and Wine 1992)	
K_2 (M^{-1})	2.1×10^5	(Baxendale et al., 1968)	1.8×10^5
	2.0×10^5	(Baxendale and Bevan 1969)	
	1.1×10^5	(Elliot and Sopchyshyn 1984)	
	1.8×10^5	(Chin and Wine 1992)	
k'_{-2} (s^{-1})			4.1×10^4

The 2σ uncertainties in k_1 , k_2 , K_2 and k'_{-2} obtained from this method are estimated to be around 20%. The curves shown in Figure 30 employed an average value of $1.8 \times 10^5 \text{ M}^{-1}$ from the literature for K_2 , and the following reaction rate coefficients were obtained:

$$k_4 = (2.3 \pm 0.1) \times 10^9 \text{ M}^{-1} \text{ s}^{-1}$$

$$k_5 = (5.1 \pm 2.5) \times 10^7 \text{ M}^{-1} \text{ s}^{-1}$$

$$k'_7 = 1500 \pm 100 \text{ s}^{-1}$$

$$k'_8 = 180 \pm 50 \text{ s}^{-1}$$

The uncertainties in the above results are 2σ from the fitting routine and represent precision only.

This represents the first determinations of the rate coefficients for MSI + SCN (R6-4) and MSI + (SCN) $_2^-$ (R6-5). k'_7 and k'_8 are the first order loss rates of SCN and (SCN) $_2^-$ radicals from reactions with H $_2$ O $_2$ and background impurities. Chin and Wine (1992) used the same technique and similar experimental conditions to study the loss of these two radicals in absence of MSI and reported values of (700 ± 160) and $(870 \pm 250) \text{ s}^{-1}$ for k'_7 and k'_8 , respectively, at 297 K. In studies by Chin and Wine, k'_7 and k'_8 at three temperatures were obtained from a plot of y (Equation 6-7, where [MSI] = 0 M) versus [SCN $^-$]. Different from the results at room temperature, their values for k'_7 are much higher than those for k'_8 at 277 K and 321 K, indicating faster decay of SCN than (SCN) $_2^-$. During our studies, it is very obvious that the decay rates of observed temporal

absorption profiles decrease with increasing SCN^- concentrations when SCN^- and H_2O_2 are the only species in the system (for example, curves a and d in Figure 28), which could only be explained by the different first order loss rates of SCN^- and $(\text{SCN})_2^-$. Different data analysis methods might account for the discrepancy and we believe that the results obtained from the method in this work are preferable.

Determination of k_3

Using the values of k_4 , k_5 , k'_7 and k'_8 obtained from the previous section and average literature k_2 (Table 17), values of a_1 and a_2 can be calculated from Equations (6-6) and (6-7) for each specific SCN^- and MSI concentration. Therefore, the four-parameter fitting routine is simplified to a two-parameter fit: only a_3 and a_4 are variable coefficients during the data analysis, which makes the output results more reliable. Figure 31 shows an example of a two-parameter fit of the data using Equation (6-1) at the SCN^- concentration of 3.3×10^{-6} M. Table 18 summarizes results from this fitting routine at all SCN^- and MSI concentrations, where a_1 and a_2 were calculated from Equations (6-6) and (6-7) using the above mentioned rate coefficients and the concentrations of SCN^- and MSI for each experiment; a_3 and a_4 were obtained from fitting the data for each experiment, as exemplified in Figure 31. As defined in Equation (6-5), a_4 is independent of [MSI]; therefore, for each set of data at a given [SCN^-], a_4 should theoretically remain unchanged for all [MSI]. The fitting results of a_4 for each data set at a given [SCN^-] vary by less than 5% (Table 18). The likely source of this difference includes fluctuations in laser power and random variations in solution concentrations or optical alignment.

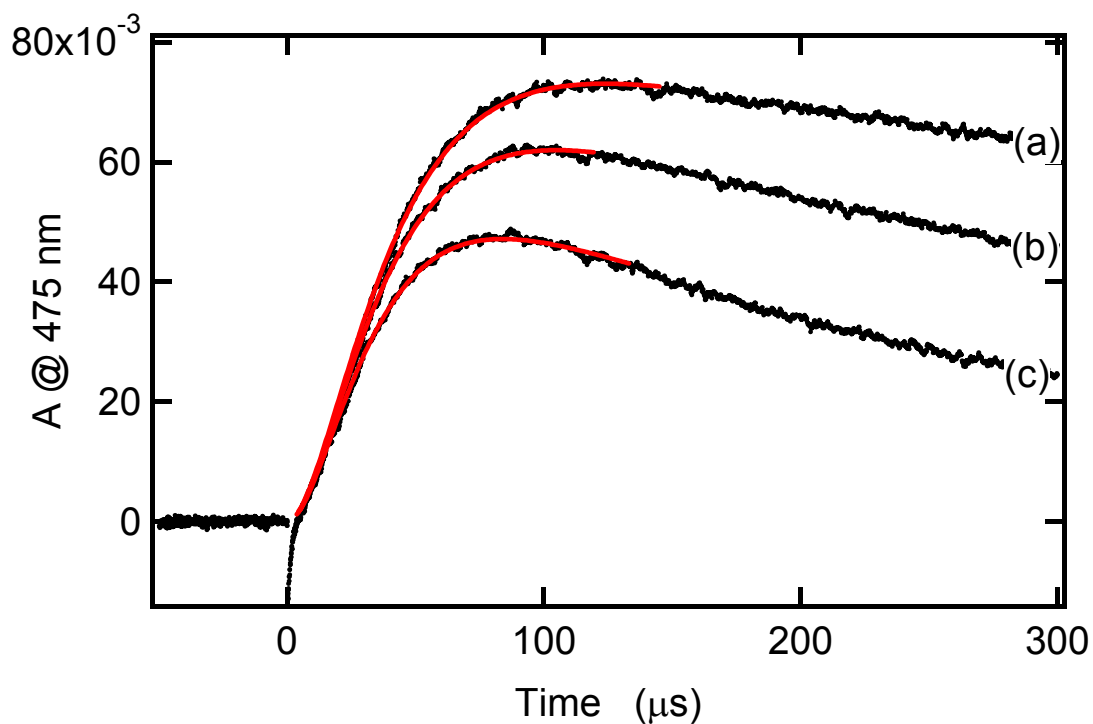


Figure 31 Analytical fits of $(\text{SCN})_2^-$ absorbance at 475 nm using the two-parameter fitting routine

Red curves are obtained from fitting the data with Equation (6-1), where a_1 and a_2 are held at the values listed in Table 19; a_3 and a_4 are derived from the red curves, which are also listed in Table 19. Experimental conditions: $[\text{H}_2\text{O}_2] = 1.27 \times 10^{-4} \text{ M}$, $[\text{SCN}^-] = 3.3 \times 10^{-6} \text{ M}$, $[\text{MSI}] =$ (a) 0 M, (b) $5.2 \times 10^{-7} \text{ M}$, and (c) $1.6 \times 10^{-6} \text{ M}$.

Table 18 Summary of the kinetics results from the two-parameter fitting routine

[SCN ⁻] (10 ⁻⁶ M)	[MSI] (10 ⁻⁶ M)	a_1 (s ⁻¹)	a_2 (10 ⁴ s ⁻¹)	a_3 (10 ⁴ s ⁻¹)	a_4 (10 ⁸ s ⁻¹)	*k_3 (10 ⁹ M ⁻¹ s ⁻¹)
3.32	0	1000	6.61	3.65	1.96	7.74±0.53
	0.523	1745	6.66	4.16	1.98	
	1.05	2475	6.70	4.59	2.00	
	1.57	3195	6.76	4.91	1.94	
	2.09	3905	6.81	5.27	1.97	
	2.62	4605	6.86	5.75	1.95	
3.54	0	980	6.79	3.92	2.16	7.60±0.26
	0.254	1330	6.81	4.07	2.14	
	0.508	1680	6.84	4.30	2.16	
	0.625	2030	6.86	4.53	2.15	
	1.27	2715	6.91	4.92	2.16	
	1.78	3395	6.96	5.27	2.14	
4.87	0	875	7.78	5.64	3.79	7.03±0.67
	0.604	1605	7.85	5.92	3.80	
	1.21	2325	7.92	6.51	3.78	
	2.12	3370	8.03	7.03	3.71	
	3.02	4405	8.13	7.74	3.65	
4.87	0	875	7.78	5.61	3.89	8.32±0.66
	1.27	2395	7.93	6.92	3.78	
	2.54	3865	8.08	7.86	3.84	
	3.81	5280	8.23	8.75	3.80	
	5.08	6645	8.39	9.98	3.76	
30.5	0	380	26.43	28.01	96.7	7.35±0.53
	1.21	855	26.66	29.28	97.6	
	2.42	1320	26.90	30.28	97.2	
	4.83	2225	27.37	31.99	96.2	
	7.25	3110	27.85	33.43	95.0	
	9.67	3965	28.32	35.39	96.2	
33.2	0	355	28.80	27.35	12.6	7.90±0.27
	2.42	1235	29.28	29.34	12.9	
	4.83	2080	29.75	31.28	12.6	
	7.25	2905	30.23	33.07	12.8	

* Error bars are 2σ and represent precision of the linear least squares analysis only.

From the definition in Equation (6-4), a_3 is the total first order loss rate of OH in the system, so a plot of a_3 vs. [MSI] at a given $[\text{SCN}^-]$ should show a linear relationship with a slope of k_3 (MS + OH rate coefficient) and an intercept of $k_1[\text{SCN}^-] + k'_6$. The first order loss rates of OH from reactions with SCN^- ($k_1[\text{SCN}^-]$), and with H_2O_2 and background impurities (k'_6) are both constant since all experimental conditions remain constant except the concentration of MSI. As an example, plots of a_3 vs. [MSI] at $[\text{SCN}^-] = 3.3 \times 10^{-6}$ and 3.0×10^{-5} M are shown in Figure 32, and rate coefficients for the OH + MSI reaction from this analysis at all $[\text{SCN}^-]$ are listed in Table 18. k_3 obtained from different $[\text{SCN}^-]$ vary by less than 15%, so the average of all data listed in Table 18 is reported as the final result for k_3 , i.e., $(7.7 \pm 0.7) \times 10^9 \text{ M}^{-1} \text{ s}^{-1}$.

This MS + OH rate coefficient falls in the middle of the values from Sehested and Holcman (1996), Flyunt et al. (2001) and Bardouki et al.(2002); it is closer to the first two studies where the pulse radiolysis technique with either UV absorption or conductometric detection methods were employed. Because these previous studies focused on mechanistic studies of the MSI + OH reaction and reactions of intermediate products, no valuable details concerning the kinetics analysis were provided in these papers. The third work employed a continuous photolysis technique with analysis of MSI and its oxidation products using UV-spectroscopy and ion-chromatography, and used benzoate as a competitor. They reported a rate coefficient of almost twice the value reported by the other two studies. While their approach provides useful mechanistic information (see below), rate coefficient determinations are subject to complications from slow secondary chemical and photochemical reactions that would not present a problem in flash photolysis or pulse radiolysis studies.

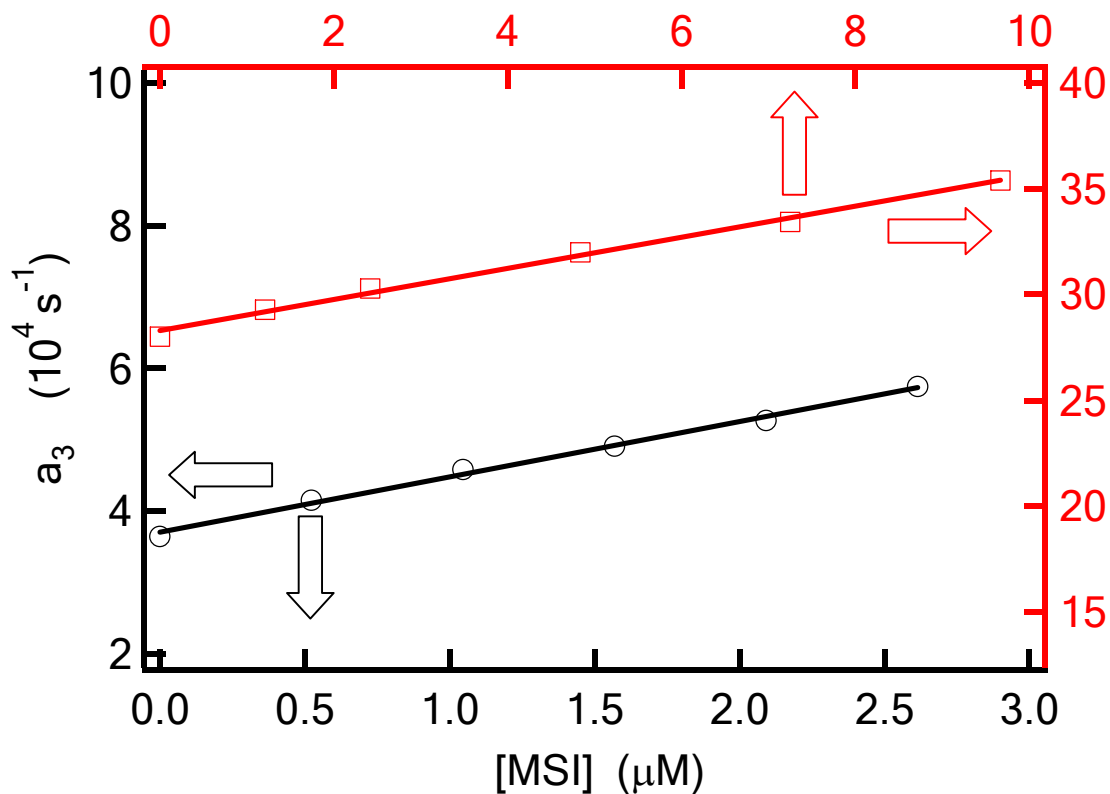


Figure 32 Plots of a_3 versus [MSI] at $[\text{SCN}^-] = 3.0 \times 10^{-5} \text{ M}$ (red) and $3.3 \times 10^{-6} \text{ M}$ (black)

Experimental conditions: $[\text{H}_2\text{O}_2] = 1.27 \times 10^{-4} \text{ M}$, $[\text{SCN}^-] = 3.3 \times 10^{-6} \text{ M}$ (black circles) and $[\text{H}_2\text{O}_2] = 1.08 \times 10^{-4} \text{ M}$, $[\text{SCN}^-] = 3.0 \times 10^{-5} \text{ M}$ (red squares). Slopes of the linear least squares analysis of each set of data are $(7.74 \pm 0.53) \times 10^9$ (black circles) and $(7.35 \pm 0.53) \times 10^9$ (red squares).

Possible Sources of Systematic Errors

The above data analysis is very complicated and each literature value used in the analysis brings along with it a potential systematic error, which contributes the largest source of systematic error in our reported value of k_3 .

In the determination of k_4 , k_5 , k'_7 and k'_8 , the most important source of systematic error comes from the equilibrium constant K_2 that was adopted for the two-parameter fitting procedure. The first order loss rates of the temporal profiles (Figure 28) were obtained with good accuracy and show very good linear relationships with MSI concentrations at any given $[\text{SCN}^-]$ (Figure 29); therefore, the errors from these two factors are estimated to be less than 5%. The adopted value for K_2 is an average of all literature values listed in Table 17 and has an estimated accuracy of $\pm 20\%$. Different values of K_2 were used to fit the data shown in Figure 30 to test the sensitivity of k_4 , k_5 , k'_7 and k'_8 to the choice of K_2 . It was found that k_4 and k'_7 (SCN reactions) varied by $<20\%$ as K_2 was adjusted by $\pm 20\%$, while k_5 and k'_8 ($(\text{SCN})_2^-$ reactions) changed by $\sim 60\%$ for the same adjustment in K_2 . The most plausible reason is that we were unable to collect data at higher SCN^- concentrations, because the photolysis of SCN^- at 248 nm became a problem (Matheson et al., 1963; Dogliotti and Hayon 1968; Luria and Treinin 1968; Fox et al., 1981; Iwata et al., 1993) at high SCN^- concentrations. Thus, the systematic error from the value of K_2 is estimated to be $\sim 20\%$ in k_4 and k'_7 and $\sim 60\%$ for k_5 and k'_8 , and the the uncertainties of these rate coefficients reported previously need to be adjusted upward accordingly.

The determination of the four parameters (a_1 , a_2 , a_3 , and a_4) in Equation (6-1) is key to obtaining k_3 , which involves the kinetics data of R6-1, R6-2 (literature values), R6-4, R6-5, R6-7, and R6-8 (obtained from this work). As mentioned previously, the errors are estimated to be around 20% for k_1 , k_2 , k'_{-2} , k_4 , and k'_7 , and $\sim 60\%$ for k_5 and k'_8 . When all these rate coefficients were adjusted by the amount of their uncertainties, variations of 30% in a_1 and 20% in a_2 were found when they were calculated from Equations (6-6) and (6-7). The values of a_1 and a_2 listed in Table 18 were adjusted by $\pm 30\%$ and $\pm 20\%$, respectively, to test their effect on uncertainties in a_3 and a_4 . It was found that a_3 and a_4 changes by $< 30\%$ for this adjustment of a_1 and a_2 . Therefore, the systematic error from using all the above kinetics data is estimated to be $\sim 30\%$.

Another possible source of error is from reactions with sample impurities. The purity of the MSI sample was labeled to be $\geq 97\%$ (the impurities are not specified). However, MSI is so reactive that minor impurities are not likely to affect the kinetics study, and the reactions of radicals with background impurities in solvent, photolyte, and competitor (R6-6, R6-7, R6-8) are included in the data analysis. Therefore, the error contribution by chemical impurities is not important in this work and is estimated to be less than 5%.

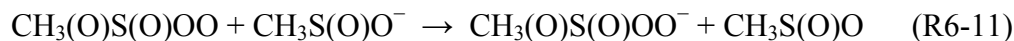
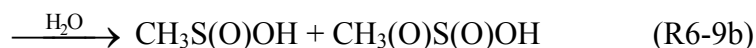
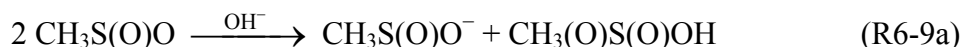
Considering all above possible systematic errors, the error bars were adjusted upward, and the rate coefficient of MSI + OH reaction obtained from this work is reported as $(7.7 \pm 3.0) \times 10^9 \text{ M}^{-1} \text{ s}^{-1}$ at 295 K. The largest source of uncertainty is from the uncertainties of the literature kinetics values adopted in the determinations of a_1 and a_2 .

Reaction Mechanisms

Although this work does not provide information about the reaction mechanism of MSI + OH, the very fast rate coefficient obtained for this reaction supports the one-electron transfer mechanism proposed by Sehested & Holcman (1996) and Flyunt et al. (2001):



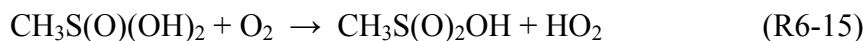
The $\text{CH}_3\text{S(O)}\text{O}$ transient radical was detected in both works by UV absorbance at its peak wavelength of ~ 330 nm, where the extinction coefficient of $\text{CH}_3\text{S(O)}\text{O}$ is reported to be $\sim 1000 \pm 100 \text{ M}^{-1} \text{ cm}^{-1}$. $\text{CH}_3\text{S(O)}\text{O}$ radical decays *via* either second order self-reaction or reaction with O_2 :



Therefore, the final stable product from the MSI + OH reaction is methane sulfonic acid (MSA) or its deprotonated anion, MS. In the presence of O_2 , the sum of R6-10, R6-11 and R6-12 results in a chain oxidation of MSI:

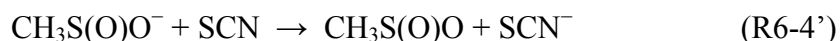


The studies by Bardouki et al. (2002) also claimed MSA to be the final end product for the MSI + OH reaction, but they proposed a different mechanism:



In our studies, methane sulfinate sodium salt was used as the source of MSI. Given the pK_a of ~ 2.2 for MSIA, it dissociates almost completely at $\text{pH} \sim 5.5$. Hence, in our studies, the intermediate adduct exists in the form $\text{CH}_3\text{S(O)}(\text{OH})\text{O}^-$, rather than $\text{CH}_3\text{S(O)}(\text{OH})_2$. According to Flyunt et al. (2001), $\sim 80\text{-}90\%$ of $\text{CH}_3\text{S(O)}(\text{OH})\text{O}^-$, dissociated to produce $\text{CH}_3\text{S(O)}\text{O} + \text{OH}^-$, and the other $\sim 10\text{-}20\%$ proceeds to release a methyl group. Therefore, the mechanism provided from their work, if correct, describes the reactions in our system better.

Our studies indicate that the $\text{SCN} + \text{MSI}$ reaction is about 50 times faster than the $(\text{SCN})_2^- + \text{MSI}$ reaction, which is consistent with generally observed reactivity trends in halogen and “pseudo-halogen” radicals. The most likely reason for this difference in reactivity is their different redox potentials: $E^0 \approx 1.64 \text{ V}$ for SCN/SCN^- (Nord et al., 1978; Stanbury et al., 1980; Martins 1982; Schwarz and Bielski 1986) and $E^0 \approx 1.32 \text{ V}$ for $(\text{SCN})_2^- / 2 \text{SCN}^-$ (Nord et al., 1978; Stanbury et al., 1980; Butler et al., 1982; Nord et al., 1982; Schwarz and Bielski 1986). By analogy with the $\text{MSI} + \text{OH}$ reaction, the following one electron transfer mechanism is proposed for both reactions:





Then reactions of the $\text{CH}_3\text{S(O)}\text{O}$ radical will proceed *via* the mechanism discussed above (R6-9 to R6-13).

In studies of $\text{DMSO} + \text{OH}$ kinetics, the $\text{DMSO} + \text{SCN}$ or $\text{DMSO} + (\text{SCN})_2^-$ reactions were found to be unimportant under our experimental conditions. The redox potential of DMSO is 1.8-2.0 V (Kishore and Asmus 1989), which is higher than the values for SCN and $(\text{SCN})_2^-$. Thus it is not likely for DMSO to be oxidized by SCN and $(\text{SCN})_2^-$. To the best knowledge of the author, there is no literature value of the redox potential of MSI available, while our kinetic data suggests that it is quite likely to be lower than that of SCN/SCN^- and $(\text{SCN})_2^-/2 \text{SCN}^-$.

Kinetics Studies of $\text{Cl} \leftrightarrow \text{Cl}_2^-$ Reactions with MSI

The kinetics of the $\text{Cl} \leftrightarrow \text{Cl}_2^- + \text{MSI}$ reactions at room temperature ($295 \pm 1 \text{ K}$) were studied by the method described in Chapter V. All experiments were carried out under pseudo-first order conditions with the concentrations of stable species in large excess over those of radicals. $\text{Cl} \leftrightarrow \text{Cl}_2^-$ radicals were monitored by their absorbance at 340 nm, and the absorption temporal profiles showed very good single exponential decay kinetics. An excellent linear relationship was observed in plots of the pseudo-first order decay rates (k') vs. $[\text{MSI}]$ at each Cl^- concentration.

Different from our studies of the DMSO, DMSO₂ and MS reactions with $\text{Cl} \leftrightarrow \text{Cl}_2^-$, the measured second order reaction rate coefficient for the $\text{Cl} \leftrightarrow \text{Cl}_2^- + \text{MSI}$ reactions is found to be independent of the concentration of Cl^- ($10^{-4} - 10^{-2} \text{ M}$). Measured second order rate coefficients at all Cl^- concentrations are listed in Table 19, and the data scatter was less than 10% from the average of all data, $\sim 8.25 \times 10^8 \text{ M}^{-1} \text{ s}^{-1}$.

To better compare the data, plots of $k' - k'_0$ versus $[\text{MSI}]$ at different $[\text{Cl}^-]$ are shown in Figure 33. k' is the pseudo-first order decay rate coefficient when MSI is present in the system, and k'_0 is the analogous rate coefficient when MSI is absent. Because of the equilibrium between Cl and Cl_2^- , k'_0 changes dramatically with Cl^- concentration, as discussed in Chapter V, and it was subtracted from k' to allow a better comparison of data at different Cl^- concentrations. The overall second order reaction rate coefficient was derived from least squares linear fits of all the data shown in Figure 33,

and has a value of $(8.22 \pm 0.38) \times 10^8 \text{ M}^{-1} \text{ s}^{-1}$, which is very close to the average of all results listed in Table 19.

Over the range of Cl^- concentrations investigated (10^{-4} to 10^{-2} M), the fraction of $\text{Cl} \leftrightarrow \text{Cl}_2^-$ that exists as Cl_2^- at equilibrium increased from $\sim 93\%$ to $> 99.9\%$. Therefore, $\text{Cl}_2^- + \text{MSI}$ is always the dominant reaction and it is primarily responsible for the measured rate coefficient. In that sense, no information on the $\text{Cl} + \text{MSI}$ reaction is obtainable from our data. Unfortunately, it is not possible to use even lower Cl^- concentrations to evaluate the $\text{MSI} + \text{Cl}$ reaction, because (a) the production rate of $\text{Cl} \leftrightarrow \text{Cl}_2^-$ radicals from the $\text{SO}_4^- + \text{Cl}^-$ reaction will be too slow when compared to the decay rate, which makes it impossible to derive of the first order decay rate of the radicals and (b) equilibrium between Cl and Cl^- is not maintained over the course of the decay if the Cl^- concentration is too low.

Because the $\text{MSI} + \text{Cl}_2^-$ reaction involves two negatively charged reactants, the measured reaction rate coefficient is expected to increase with increasing solution ionic strength (μ). Therefore, each measured first order decay rate ($k' - k'_0$) was converted to a value for the limit where $\mu \rightarrow 0$ using Equation (3-4). The corrected data are shown in the bottom plot of Figure 33, and a second order rate coefficient of $(8.00 \pm 0.35) \times 10^8 \text{ M}^{-1} \text{ s}^{-1}$ is derived for the zero ionic strength limit. Since the reaction is fast and very low concentrations of MSI were employed, the most important source of ionic strength is Cl^- . The difference between the results from the original (top plot) and corrected (bottom plot) is small.

Table 19 Measured rate coefficients for $\text{MSI} + \text{Cl} \leftrightarrow \text{Cl}_2^-$ at different $[\text{Cl}^-]$

$[\text{Cl}^-]$ (M)	1.0×10^{-4}	2.5×10^{-4}	5.0×10^{-4}	1.0×10^{-3}	3.0×10^{-3}	1.0×10^{-2}
k_{measured}	7.45	8.86	8.41	7.48	8.58	8.69
2σ ($10^8 \text{ M}^{-1} \text{ s}^{-1}$)	0.44	0.55	0.61	0.28	0.68	0.78

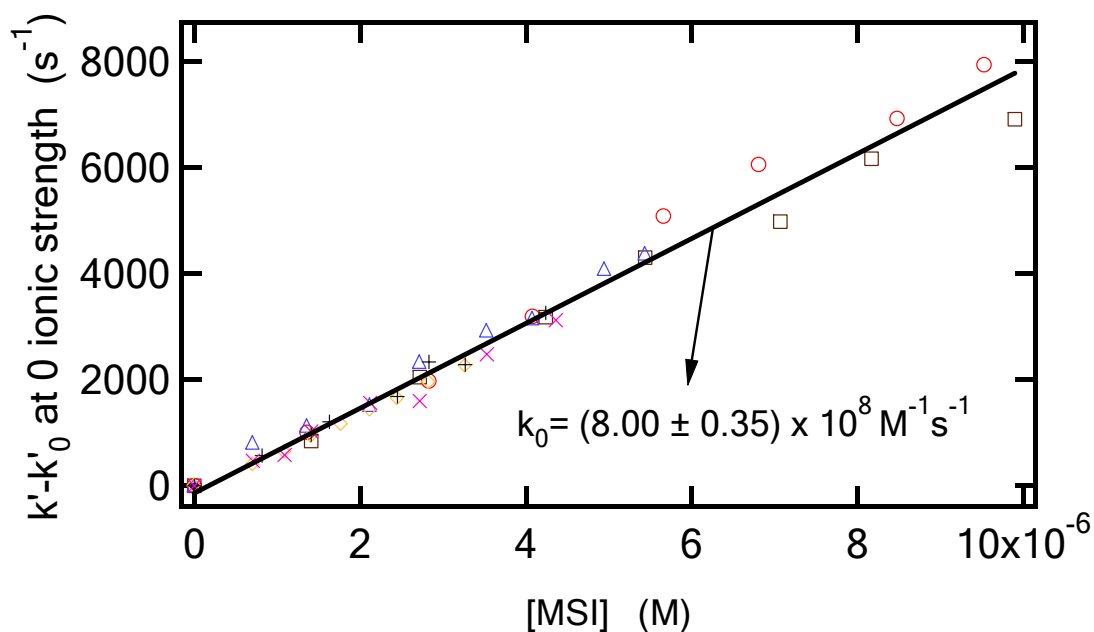
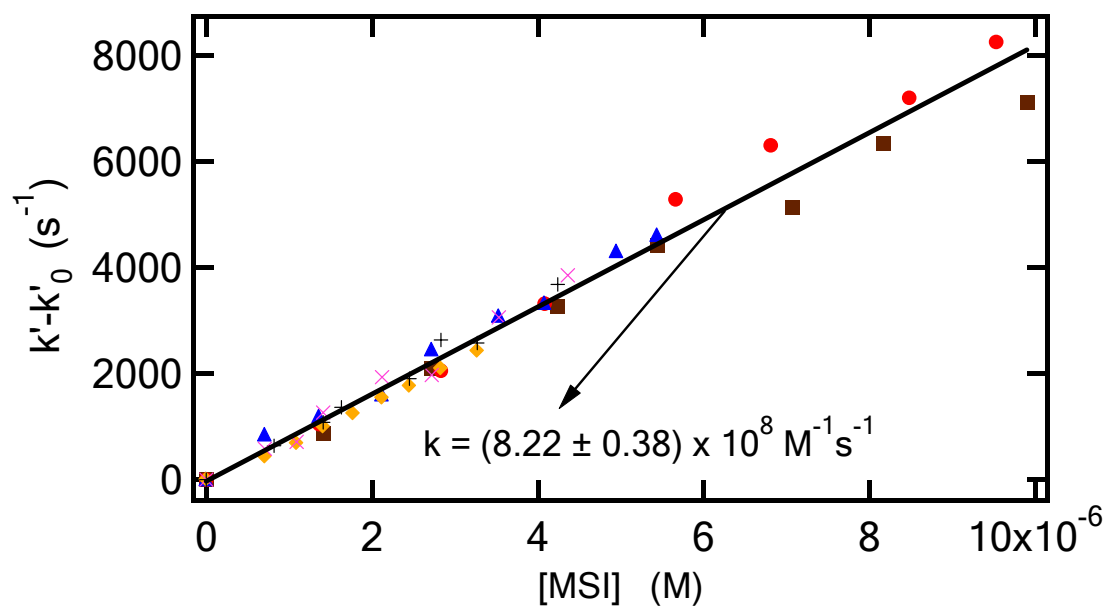
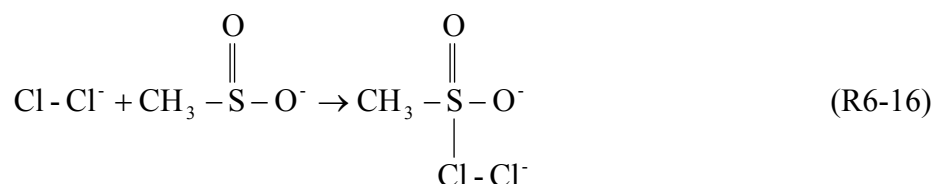


Figure 33 Plots of $k' - k'_0$ versus [MSI] at all $[Cl^-]$ studied

k' and k'_0 are defined in the text; the top plot is for the analysis of original data, and the bottom plot is for data corrected to 0 ionic strength. The solid lines are obtained from the least squares analysis of all data in each plot. Experimental conditions: $[S_2O_8^{2-}] = (1-3) \times 10^{-5}$ M, $[Cl^-] = 1.0 \times 10^{-4}$ (■ and □), 2.5×10^{-4} (●, ○), 5.0×10^{-4} (▲, △), 1.0×10^{-3} (◆, ◇), 3.0×10^{-3} (+, +), and 1.0×10^{-2} M (×, ×).

Analogous to the mechanism for the MSI + OH reaction (discussed above) (Sehested and Holcman 1996; Flyunt et al., 2001; Bardouki et al., 2002), the MSI + Cl₂⁻ reaction probably also proceeds *via* the one-electron transfer mechanism, because the redox potential of Cl₂⁻/2Cl⁻ is ~ 2.23 V (Malone and Endicott 1972; Thornton and Laurence 1973; Henglein 1980; Schwarz and Dodson 1984), higher than that of OH/OH⁻ (~1.90V) (Berdniko.Vm and Bazhin 1970; Koppenol and Liebman 1984; Schwarz and Dodson 1984; Klaning et al., 1985). Furthermore, the structure of MSI makes attack by Cl₂⁻ radicals very easy:



Such addition reactions normally occur at a diffusion controlled rate, followed by the electron exchange and release of two Cl⁻ anions. Therefore, the CH₃S(O)O radical is generated as an intermediate during the MSI + Cl₂⁻ reaction. As discussed above, the CH₃S(O)O radical absorbs at the wavelength we used to monitor Cl₂⁻ radical (340nm) with an extinction coefficient of ~ 900 M⁻¹ cm⁻¹, about one tenth of ε_{Cl₂⁻}. The absorbance signals obtained at 340 nm show excellent single exponential decay and indicate that the interference from CH₃S(O)O is not important in our studies. However, in order to check the possible impact of CH₃S(O)O radicals to the observed absorbance, a few experiments were carried out by monitoring the absorbance at 430 nm, where CH₃S(O)O absorbance is negligible. Single exponential decays of the temporal absorption profiles were observed, and the linear relationship between first order decay rates and [MSI] gives second order

rate coefficients of $(8.38 \pm 0.28) \times 10^8$, $(8.06 \pm 0.46) \times 10^8$, and $(7.71 \pm 0.43) \times 10^8 \text{ M}^{-1}\text{s}^{-1}$ for Cl^- concentrations of 10^{-4} , 10^{-3} and 10^{-2} M , respectively. Although a slightly decreasing trend in the rate coefficient was found as the Cl^- concentration increases, the change is most likely to be the random scatter of the data when error bars (two standard deviations) are considered. The average of the above results gives a rate coefficient of $(8.05 \pm 0.45) \times 10^8 \text{ M}^{-1}\text{s}^{-1}$, very close to the result from studies at 340 nm.

The most likely source of the systematic error in our study of $\text{Cl} \leftrightarrow \text{Cl}_2^- + \text{MSI}$ kinetics is from reactions of radicals with sample impurities. From the very slow decay rate of the radicals at high Cl^- concentrations when MSI is absent in the system, it can be concluded that the samples of Cl^- and $\text{S}_2\text{O}_8^{2-}$ are not important sources of impurities into the system. The MSI sample was labeled as $\geq 97\%$ purity and its impurities were not identified. Since MSI is very reactive, a small amount of even reactive impurities will not noticeably affect the kinetics. However, to allow for unidentified systematic errors, we increase the uncertainty somewhat over that due to precision only and report a rate coefficient for the $\text{MSI} + \text{Cl}_2^-$ reaction of $(8.0 \pm 1.0) \times 10^8 \text{ M}^{-1}\text{s}^{-1}$ at 295 K. Such a high reaction rate coefficient makes Cl_2^- a very important radical for oxidizing MSI in the atmospheric aqueous phase given typical Cl_2^- concentrations of 10 to 100 times higher than OH concentrations, and its contribution in MSI oxidation will be discussed in Chapter VIII.

CHAPTER VII

SUMMARY OF KINETICS STUDIES

In this work the kinetics of aqueous phase reactions of four important radicals, SO_4^- , OH, Cl and Cl_2^- , with four important organic sulfur compounds produced from atmospheric DMS oxidation, DMSO, DMSO₂, MSI and MS, were investigated using a Laser Flash Photolysis – Long Path UV-visible Absorption technique. Kinetic data for the reactions of SO_4^- , Cl and Cl_2^- with DMSO₂ and MS are reported for the first time, as are kinetic data for the reaction of Cl_2^- with MSI. In addition, the kinetics of reactions of OH and SO_4^- radicals with DMSO, DMSO₂, and MS have been studied as a function of temperature for the first time. The results at 295 ± 1 K are summarized in Table 30.

The reactivity of radicals at room temperature (295 ± 1 K) is observed to be in the order $\text{OH} > \text{Cl} > \text{SO}_4^- > \text{Cl}_2^-$, which is in agreement with most kinetic studies of reactions of these radicals with other organic compounds (Clifton and Huie 1989; Huie and Clifton 1989; Padmaja et al., 1992; Chin and Wine 1994; George et al., 2001; Martire et al., 2001; Ervens et al., 2003; George et al., 2003). The OH and Cl reactions with organic species could proceed *via* addition, H-abstraction, or electron transfer, while SO_4^- and Cl_2^- reactions proceed primarily through hydrogen abstraction or electron transfer processes. Typically, addition reactions are the fastest and abstraction reactions are the slowest. Therefore, SO_4^- and Cl_2^- are considerably less reactive than OH and Cl radicals toward most compounds. For a very reactive species, such as DMS, the rate coefficient for its reaction with OH ($1.9 \times 10^{10} \text{ M}^{-1} \text{ s}^{-1}$) (Bonifacic et al., 1975) is only

approximately a factor of 6 faster than the rate coefficient for its reaction with Cl_2^- ($3.0 \times 10^9 \text{ M}^{-1} \text{ s}^{-1}$) (Bonifacic and Asmus 1980). Our work also found that the $\text{MSI} + \text{OH}$ rate coefficient at room temperature ($7.7 \times 10^9 \text{ M}^{-1} \text{ s}^{-1}$) is about one order of magnitude faster than the $\text{MSI} + \text{Cl}_2^-$ rate coefficient ($8.0 \times 10^8 \text{ M}^{-1} \text{ s}^{-1}$). However, for DMSO, not as reactive as DMS but comparable to MSI, the OH reaction rate coefficient at room temperature obtained from this work, $6.3 \times 10^9 \text{ M}^{-1} \text{ s}^{-1}$, is approximately a factor of 400 faster than the Cl_2^- reaction rate coefficient ($1.6 \times 10^7 \text{ M}^{-1} \text{ s}^{-1}$, also from this work). For the less reactive species DMSO_2 and MS, the differences between OH and Cl_2^- reaction rate coefficients are even greater, i.e., factors of ~ 2000 and 3000 , respectively.

The reactivity order of sulfur species is $\text{DMSO} \approx \text{MSI} > \text{DMSO}_2 > \text{MS}$, which was determined from comparing our kinetics data at room temperature. For the most reactive OH radical, the rate coefficient of the $\text{DMSO} + \text{OH}$ reaction is about 500 times faster than that of the $\text{MS} + \text{OH}$ reaction; while for the least reactive Cl_2^- radical, the DMSO reaction is over 4000 times faster than the MS reaction (comparison from results reported at 295 K). The huge difference in reactivity is from the differences in molecular structures of the individual sulfur compound. For DMSO and MSI, there is a lone pair of electrons on the sulfur atom; for DMSO_2 and MS all electrons are bonded. The other reason is that the less oxidized sulfur species DMSO and MSI have lower electron affinities than the more oxidized DMSO_2 and MS. Therefore, addition to the sulfur atom is almost always the initial step of DMSO and MSI reactions, followed by either electron transfer or C-S bond cleavage. However, the dominant channel for DMSO_2 and MS reactions is probably *via* hydrogen abstraction from the methyl group.

Table 20 Summary of kinetic data at 295 ± 1 K

	k (M ⁻¹ s ⁻¹)			
	OH	SO ₄ ⁻	Cl	Cl ₂ ⁻
DMSO	(6.4 ± 0.5)×10 ⁹	(3.2 ± 0.3)×10 ⁹	(6.3 ± 0.6)×10 ⁹	(1.6 ± 0.8)×10 ⁷
DMSO ₂	(1.7 ± 0.2)×10 ⁷	(3.8 ± 0.4)×10 ⁶	(8.2 ± 1.6)×10 ⁵	(8.2 ± 5.5)×10 ³
MSI	(7.7 ± 0.7)×10 ⁹	—	—	(8.0 ± 1.0)×10 ⁸
MS	(1.2 ± 0.2)×10 ⁷	(1.0 ± 0.2)×10 ⁴	(4.9 ± 0.2)×10 ⁵	(3.9 ± 0.7)×10 ³

* all uncertainties are 2σ and represent precision only.

For the SO_4^- and OH reactions with DMSO, DMSO₂ and MS, temperature dependent kinetics were studied for the first time over a temperature range of atmospheric interest. The measured activation energies of very fast DMSO reactions with OH and SO_4^- , i.e., 10.6 ± 0.3 and 11.6 ± 0.3 kJ mol⁻¹, respectively, were found to be primarily from the diffusion of reactants in water. However, the much slower MS + OH and MS + SO_4^- reactions were found to have larger activation energies with values of 21.9 ± 0.3 and 20.7 ± 4.3 kJ mol⁻¹, respectively. Thus the rate coefficients for the latter two reactions change the most with temperature, which is potentially important in the atmosphere for explaining variations of observed MS/NSS ratios in atmospheric particulate matter at different temperatures.

In Chapter VIII, the kinetic data obtained in this work, are employed in a Trajectory Ensemble Model (TEM) to simulate DMS oxidation in the cloudy marine atmosphere to assess the importance of aqueous phase reactions in the production of MS and NSS from DMS oxidation as well as the observed MS/NSS ratios.

CHAPTER VIII

**EFFECTS OF UPDATED AQUEOUS ORGANO-SULFUR
CHEMISTRY ON SPECIATION AND PARTICULATE
MS-TO-NSS RATIOS**

Introduction

Understanding the contribution of biogenic emissions to the global sulfur burden has motivated extensive study of DMS oxidation in the marine boundary layer. Despite many laboratory studies, field measurements and model simulations, the atmospheric processes involved in the oxidation of DMS are still only partially understood and, as a result, it is not yet possible to fully understand field observations of DMS and its important oxidation products.

The modeling efforts of Yin et al. (1990a; 1990b) have been particularly important to the understanding of DMS chemistry. Subsequent studies are to a large extent based on modified versions of the large reaction scheme presented by Yin et al. (1990a; 1990b). The DMS oxidation mechanisms employed by most modeling studies can be classified as either “comprehensive” (or detailed) or “parameterized”. Comprehensive mechanisms (e.g., Yin et al., 1990a; 1990b; Koga and Tanaka 1993; Hertel et al., 1994; von Glasow and Crutzen 2004) describe elementary kinetic steps and

predict intermediate species. Parameterized mechanisms (e.g., Kreidenweis et al., 1991; Benkovitz et al., 1994; Pham et al., 1995; Davis et al., 1998; 1999; Chen et al., 2000; Chin et al., 2000a; Cosme et al., 2002; Gondwe et al., 2003; 2004) predict only the end products of the oxidation by assuming branching ratios between products. An evaluation and sensitivity analysis of several DMS mechanisms (from Yin et al.(1990a; 1990b), Koga and Tanaka (1993), Hertel et al. (1994), Benkovitz et al. (1994) and Pham et al. (1995)) has been published by Capaldo and Pandis (1997). Comparing results from these model simulations to field observations suggests that the variations in estimates of SO₂, NSS and MS production from DMS oxidation among these mechanisms are small. Their predicted SO₂ and MS concentrations depend more on the gas phase reactions, while NSS predictions are more sensitive to the uncertain parameterization of heterogeneous processes. However, in all mechanisms considered by Capaldo and Pandis (1997), uptake of SO₂ into the condensed phase and its subsequent oxidation by hydrogen peroxide and ozone is the primary source of NSS; MS originates solely from the uptake of gas-phase MSA into particles. In some later studies, mass transfer of organo-sulfur species, i.e., DMSO and MSIA, into the aqueous phase and their subsequent oxidation are proposed to play important roles in condensed phase MS production. For example, Davis et al. (1999) postulated that over 99% of MS in aerosols is generated by aqueous phase oxidation of DMSO or its oxidation intermediates. Studies from Sciare et al. (2000b), Legrand et al. (2001) and Cosme et al. (2002) found that the uptake of DMSO into the condensed phase and its subsequent oxidation have to be considered to reproduce observations of gas phase DMSO and condensed phase MS. It is well established that the H-abstraction channel of DMS oxidation leads primarily to production of SO₂ (Figure 1);

the addition channel leads to immediate production of DMSO, which is further oxidized to generate MSIA with a high yield (Barnes et al., 1989; Hynes and Wine 1996; Urbanski et al., 1998; Falbe-Hansen et al., 2000; Arsene et al., 2002; Kukui et al., 2003). Further gas phase oxidation of MSIA by OH appears to produce SO₂ with a yield close to 1 (Kukui et al., 2003). As a result, SO₂ is the dominant gas phase end sulfur product, while MS is primarily generated *via* aqueous phase reactions. Consequently, a significant fraction of DMSO is partitioned into the aqueous phase due to its high solubility, and the production yield of SO₂ may be reduced while MS production in the aqueous phase is increased.

In recent studies (e.g., Campolongo et al., 1999; von Glasow and Crutzen 2004), aqueous phase reactions of organo-sulfur species are considered in DMS oxidation simulations. Campolongo et al. (1999) studied the role of aqueous phase oxidation of SO₂, DMS, DMSO, and DMSO₂ by O₃, H₂O₂ and OH on MS and SO₄²⁻ production. In their work DMSO₂ is considered as an important precursor of MS and SO₄²⁻, which is a questionable assumption for several reasons. First, even though DMSO₂ is the primary product from DMSO + O₃ (H₂O₂), it is only a minor product from DMSO oxidation because reactions of DMSO with O₃ and H₂O₂ are insignificant compared to the DMSO + OH reaction in the aqueous phase (Lee and Zhou 1994; Bardouki et al., 2002). Second, the predominant product from DMSO + OH is MSI, which is further oxidized by OH to generate MS at about the same rate as the DMSO + OH reaction (Meissner et al., 1967; Veltwisch et al., 1980; Milne et al., 1989; Scaduto 1995; Sehested and Holcman 1996; Jahnke 1999; Flyunt et al., 2001; Bardouki et al., 2002). Third, in their chemistry model, the rate coefficients for DMSO₂ reactions with O₃ and H₂O₂ are assumed to be same as

those for the DMSO reactions. However, kinetics studies have found that the DMSO reactions with O₃ and H₂O₂ are much slower than the DMS reactions (Pryor et al., 1984; Lee and Zhou 1994; Amels et al., 1997; Gershenzon et al., 2001; Bardouki et al., 2002), and the more oxidized DMSO₂ is expected to be much less reactive than DMSO (DMSO₂ + OH is over two orders of magnitude slower than DMSO + OH (Milne et al., 1989; Zhu et al., 2003b)), therefore assuming that DMSO₂ reacts with O₃ and H₂O₂ at the same rates as DMSO reactions is not valid.

von Glasow and Crutzen (2004) investigated the effects of halogens on multiphase DMS oxidation and included OH-initiated aqueous oxidation of DMS, DMSO, MSI and MS in their model to simulate the production of MS and NSS. The authors concluded that the inclusion of gas phase halogen chemistry leads to higher DMS oxidation rates and smaller DMS → SO₂ conversion efficiencies, which are also drastically reduced under cloudy conditions due to efficient uptake of DMSO and other intermediates formed from the addition channel of DMS oxidation. They also found that gas phase reactions contribute about 2% to the total formation rate of MS, and, that the aqueous phase MSI + OH reaction is the primary source for MS. The same study claimed that the aqueous phase MS + OH reaction contributes about 10% to the NSS production (when the reaction rate coefficient of $1.2 \times 10^7 \text{ M}^{-1} \text{ s}^{-1}$ was adopted), indicating that aqueous MS + OH is an important contributor to the NSS production in the marine boundary layer.

OH is the only oxidant of DMSO and MSI in the aqueous phase mechanism of von Glasow and Crutzen (2004). However, from our kinetics studies, SO₄⁻ (chapter III), Cl and Cl₂⁻ (Chapter V and VI) can also play an important role in the oxidation of DMSO

and MSI. For instance, the $\text{MSI} + \text{Cl}_2^-$ reaction rate coefficient is found to be $\sim 8 \times 10^8 \text{ M}^{-1} \text{ s}^{-1}$; given the high concentration of Cl_2^- , the $\text{MSI} + \text{Cl}_2^-$ reaction is very likely to be an important source of MS. For the first time, the temperature dependence of $\text{MS} + \text{OH}$ was studied in our work and it was found that its rate coefficient increases with increasing temperature, which makes it more important in producing NSS and affecting MS/NSS at high temperatures. Including the new radical chemistry and temperature-dependent kinetics into the aqueous chemistry mechanism is important for a better understanding of MS and NSS production from DMS oxidation.

In the present work, DMS oxidation in the marine boundary layer is studied using the Trajectory Ensemble Model (here referenced as TEM) (Stevens et al., 1996). We emphasize the application of the aqueous phase kinetic data obtained from the work previously described in this dissertation. We focus on the contribution of aqueous phase reactions to MS and NSS production and total non-volatile sulfur mass growth, the temperature dependence of MS/NSS ratios, and effects of cloud dynamics on DMS oxidation. For the first time, aqueous phase oxidation of DMS and MSI by SO_4^- , Cl_2^- , and Cl in the aqueous phase are included in the model to assess the significance of these reactions in MS and NSS production.

Model Description and Chemical Mechanism

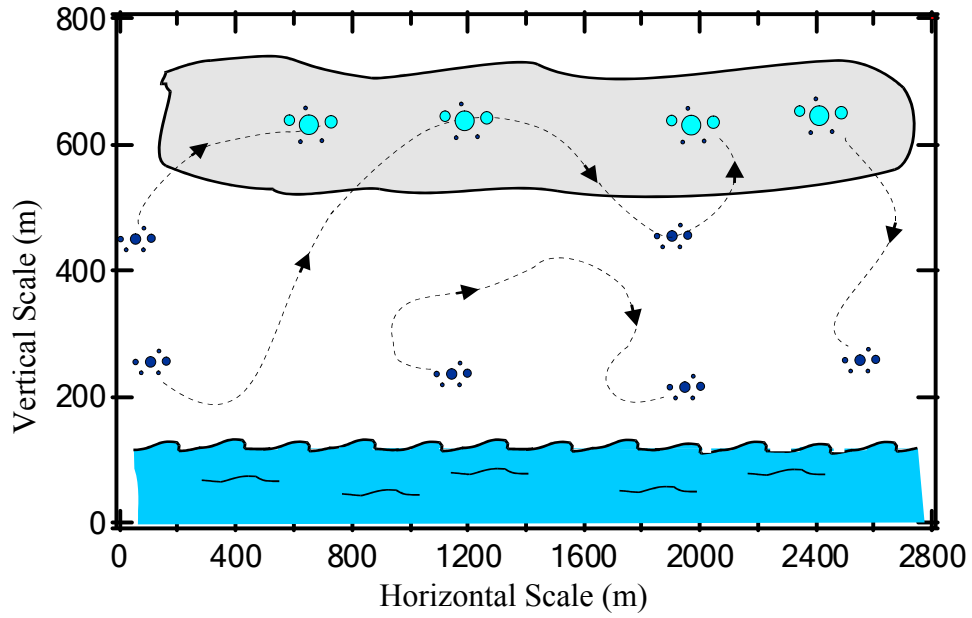
Physical Description

In this work DMS oxidation in the marine boundary layer was simulated using the Trajectory Ensemble Model (TEM) approach of Stevens et al. (1996). The TEM can be thought of as a host Lagrangian dynamical framework in which one can embed a variety of microphysical representations. This methodology employs a Large Eddy Simulation (LES) of a cloud field to generate a set of Lagrangian trajectories that describe the temporal evolution of the thermodynamic properties of the cloud field. The LES is one of the often used modeling methods to study turbulent flows; it allows all large scale turbulent eddies to be calculated explicitly, while smaller sub-grid-scale turbulence is accounted for using a parameterized closure scheme. A detailed description of the TEM and the LES is given by Stevens et al. (1996).

As illustrated in Figure 34, each trajectory travels in and out of clouds with their own residence time. Each trajectory is allowed to force a parcel model that simulates the chemical evolution and growth of cloud condensation nuclei within the parcel. A horizontal ensemble average concentration of each species of interest throughout the simulated vertical height is calculated. The important advantage of using TEM is that it captures the complex dynamics of clouds within the computationally efficient framework of a parcel model.

Each trajectory contains information that characterizes the thermodynamic state of the air parcel as it is advected throughout the flow field. The variables contained in the trajectories are time t , position x , y , and z , pressure p , potential temperature in moist air θ , and the total (e.g., liquid and vapor) water mass mixing ratio, w_t . The equations that describe the evolution of trajectory properties and water vapor supersaturation profiles have been described before by Medina and Nenes (2004), and will not be repeated here.

(a)



(b)

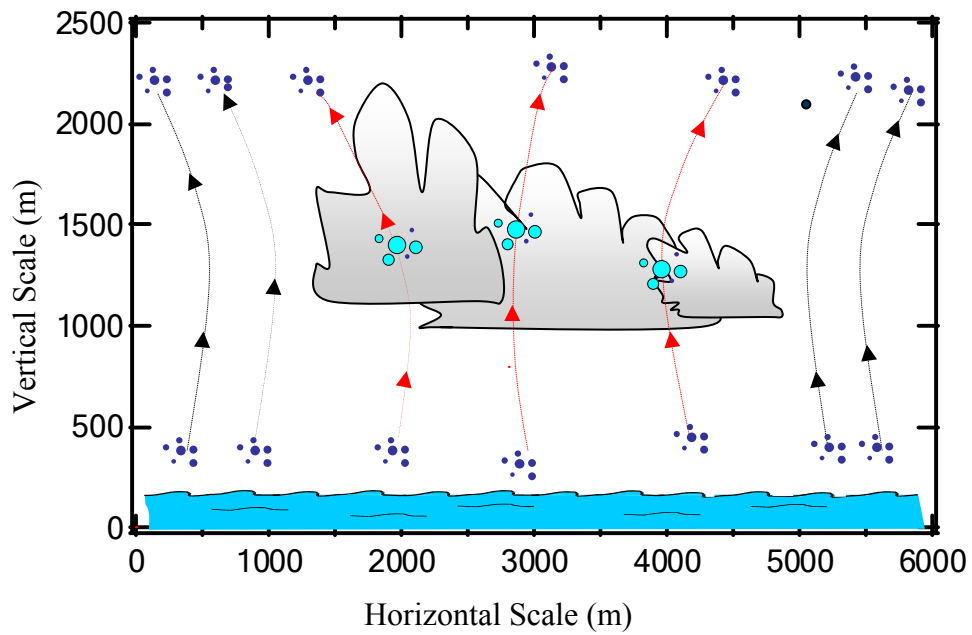


Figure 34 Lagrangian trajectories derived from the LES used to “drive” the cloud parcel model for (a) stratocumulus clouds and (b) cumulus clouds

Chemical Mechanism

A simplified chemical mechanism (Figure 1) including 12 gas phase reactions, 16 aqueous phase reactions, 10 aqueous phase equilibria and mass transfer of 12 species between the gas and the aqueous phase, is used to simulate DMS oxidation. Tables 21 to 24 contain the gas phase (Table 21) and aqueous phase (Table 22) reaction rate coefficients, equilibrium constants for aqueous species (Table 23), Henry's Law constants and mass accommodation coefficients (Table 24), as well as the temperature dependencies of these parameters (if available) that are used for the simulation. Sources for all above parameters are also listed in the Tables.

Important oxidants include OH, NO₃, BrO, Cl, NO and HO₂ in the gas phase and O₃, H₂O₂, OH, SO₄⁻, Cl₂⁻, and Cl in the aqueous phase. For the first time SO₄⁻, Cl₂⁻, and Cl initiated oxidation of sulfur species, especially DMSO and MSI, in the aqueous phase are included in a model simulation of DMS oxidation, because our kinetics studies (Chapters III to VI), have found that these reactions are potentially important in aqueous phase MS production to an extent comparable to, or even higher than OH reactions. To simplify the model calculation, all radicals are assumed to be in steady-state with a constant concentration throughout a simulation (Table 25). Given that free radical concentrations can vary over as much as two orders of magnitude, we choose daily average values representative of the remote marine atmosphere obtained from field measurements and model studies (references in Table 25).

Concentrations of sulfur compounds of atmospheric interest were calculated from a mass balance:

$$\frac{dX}{dt} = \sum_i P_i - \sum_j k'_j [X] + E_F [X] \pm V_T ([X]_g - [X]_{eq}) \quad (8-1)$$

Where P_i is the production rate of species X from reaction i in units of molecule $\text{cm}^{-3} \text{s}^{-1}$, k'_j is the pseudo-first order loss rate of X due to reaction j in units of s^{-1} , E_F is the expansion factor due to the ambient pressure change in units of s^{-1} :

$$E_F = \frac{dP}{P dt} \quad (8-2)$$

and V_T is the transport velocity of species X from the gas phase into the particles in units of s^{-1} :

$$V_T = \frac{D}{\frac{r^2}{3} \left[1 + \frac{D}{r\alpha} \sqrt{\frac{2\pi}{RT} M_X} \right]} \quad (8-3)$$

where D is the binary (gas –air) diffusion coefficient for species X in units of $\text{m}^2 \text{s}^{-1}$, r is the radius of particles in units of m, α is the mass accommodation coefficient, M_X is the molecular weight of X in units of kg mol^{-1} , R is the molar gas constant, and T is the temperature. For calculations of species X in the gas phase, the negative sign for the mass transfer term in Equation (8-1) was applied, and for aqueous phase concentration calculations the positive sign was applied.

It has been demonstrated that pH of cloud dropets can affect the production rate of sulfate from the oxidation of S(IV) by O_3 and H_2O_2 (Kreidenweis et al., 2003). In our kinetics studies of the organo-sulfur reactions, no significant pH dependence was found; therefore, a fixed pH of 5.0 was used in all simulations.

Table 21 Gas phase kinetic mechanism

#	Reaction	k (T) (cm ³ molecule ⁻¹ s ⁻¹)	Source
G1	$\text{CH}_3\text{SCH}_3 + \text{OH} \xrightarrow{\text{O}_2} \text{CH}_3\text{SCH}_2\text{O}_2 + \text{H}_2\text{O}$	$1.13 \times 10^{-11} \exp(-253/T)$	(Atkinson et al., 2001)
G2	$\text{CH}_3\text{SCH}_3 + \text{OH} \xrightarrow{\text{O}_2} 0.5\text{CH}_3\text{S(O)CH}_3 + 0.2\text{CH}_3\text{(O)S(O)CH}_3 + 0.3\text{CH}_3\text{(O)SOH}$	$1.0 \times 10^{-39} \exp(5820/T)[\text{O}_2]$ $(1 + 1.0 \times 10^{-30} \exp(6280/T)[\text{O}_2])$	(Hynes et al., 1986; Atkinson et al., 1997; Williams et al., 2001)
G3	$\text{CH}_3\text{SCH}_3 + \text{NO}_3 \xrightarrow{\text{O}_2} \text{CH}_3\text{SCH}_2\text{O}_2 + \text{HNO}_3$	$1.9 \times 10^{-13} \exp(520/T)$	(Atkinson et al., 2001)
G4	$\text{CH}_3\text{SCH}_3 + \text{Cl} \xrightarrow{\text{O}_2} \text{CH}_3\text{SCH}_2\text{O}_2 + \text{HCl}$	3.3×10^{-10}	(Atkinson et al., 2001)
G5	$\text{CH}_3\text{SCH}_3 + \text{BrO} \rightarrow \text{CH}_3\text{S(O)CH}_3 + \text{Br}$	$1.4 \times 10^{-14} \exp(940/T)$	(Atkinson et al., 1997; Ingham et al., 1999; Nakano et al., 2001)
G6	$\text{CH}_3\text{SCH}_2\text{O}_2 + \text{NO} \rightarrow \text{CH}_3\text{S} + \text{CH}_2\text{O} + \text{NO}_2$	$4.9 \times 10^{-12} \exp(260/T)$	(Urbanski et al., 1997; Atkinson et al., 2001)
G7	$2\text{CH}_3\text{SCH}_2\text{O}_2 \rightarrow 2\text{CH}_3\text{S} + 2\text{CH}_2\text{O} + \text{O}_2$	1.0×10^{-11}	(Urbanski et al., 1997; Atkinson et al., 2001)
G8	$\text{CH}_3\text{SCH}_2\text{O}_2 + \text{HO}_2 \rightarrow \text{CH}_3\text{S}$	$3.8 \times 10^{-13} \exp(780/T)$	¹ (Tyndall et al., 2001)
G9	$\text{CH}_3\text{S} \xrightarrow{\text{NO}_2, \text{O}_3, \text{HO}_2, \text{O}_2, \text{H}_2\text{O}} 0.9\text{SO}_2 + 0.1\text{H}_2\text{SO}_4$	5.0	(Barone et al., 1995; Atkinson et al., 2002)
G10	$\text{CH}_3\text{S(O)CH}_3 + \text{OH} \xrightarrow{\text{O}_2} 0.9\text{CH}_3\text{(O)SOH} + 0.1\text{CH}_3\text{(O)S(O)CH}_3$	9.0×10^{-11}	(Urbanski et al., 1998; Kukui et al., 2003)
G11	$\text{CH}_3\text{(O)SOH} + \text{OH} \xrightarrow{\text{O}_2} 0.9\text{SO}_2 + 0.1\text{CH}_3\text{(O)S(O)OH}$	9.0×10^{-11}	(Kukui et al., 2003)
G12	$\text{SO}_2 + \text{OH} + \text{O}_2 + \text{H}_2\text{O} \rightarrow \text{H}_2\text{SO}_4 + \text{HO}_2$	² $k_{12} = F \times k_0 \times k_{c_0} / (k_0 + k_{c_0})$	(Wine et al., 1984)

¹ by analogy to $\text{CH}_3\text{O}_2 + \text{HO}_2$

² $\log F = \log(0.525)/(1 + [\log(k_0/k_{c_0})]^2)$, $k_0 = 4.5 \times 10^{-31} (\text{T}/300)^{3.9} \times [\text{Air}]$, $k_{c_0} = 1.26 \times 10^{-12} (\text{T}/300)^{0.7}$.

Table 22 Aqueous phase kinetic mechanism

#	Reaction	$k(T)$ ($M^{-1} s^{-1}$)	Source
A1	$CH_3SCH_3 + O_3 \rightarrow CH_3S(O)CH_3 + O_2$	$5.3 \times 10^{12} \exp(-2600/T)$	(Gershenson et al., 2001)
A2	$CH_3SCH_3 + OH \rightarrow CH_3S(O)CH_3 + HO_2$	1.9×10^{10}	(Bonifacic et al., 1975)
A3	$CH_3S(O)CH_3 + O_3 \rightarrow CH_3(O)S(O)CH_3 + O_2$	5.7	(Lee and Zhou 1994)
A4	$CH_3S(O)CH_3 + OH \rightarrow CH_3(O)SOH + CH_3$	$4.7 \times 10^{11} \exp(-1270/T)$	This work
A5	$CH_3S(O)CH_3 + SO_4^- \xrightarrow{H_2O} CH_3(O)SO^- + SO_4^{2-}$	$3.7 \times 10^{11} \exp(-1440/T)$	This work
A6	$CH_3S(O)CH_3 + Cl^- \xrightarrow{H_2O} CH_3(O)SO^-$	6.3×10^9	This work
A7	$CH_3S(O)CH_3 + Cl_2^- \xrightarrow{H_2O} CH_3(O)SO^-$	1.6×10^7	This work
A8	$CH_3(O)S(O)CH_3 + OH \rightarrow 0.3 CH_3SO_3H + 0.7 SO_4^{2-}$	$5.1 \times 10^9 \exp(-1690/T)$	This work
A9	$CH_3(O)SO^- + OH \xrightarrow{O_2} CH_3(O)S(O)O^- + H^+$	7.7×10^9	This work
A10	$CH_3(O)SO^- + SO_4^- \xrightarrow{O_2} CH_3(O)S(O)O^- + SO_4^{2-}$	1.0×10^9	This work
A11	$CH_3(O)SO^- + Cl_2^- \xrightarrow{O_2} CH_3(O)S(O)O^- + 2Cl^-$	8.0×10^8	This work
A12	$CH_3(O)S(O)O^- + OH \rightarrow SO_4^{2-}$	$8.8 \times 10^{10} \exp(-2630/T)$	This work
A13	$SO_2 + O_3 \xrightarrow{H_2O} SO_4^{2-}$	2.4×10^4	(Kreidenweis et al., 2003)
A14	$HSO_3^- + O_3 \xrightarrow{H_2O} SO_4^{2-}$	$3.5 \times 10^5 \exp[-5530(1/T-1/298)]$	(Hoffmann 1986; Kreidenweis et al., 2003 and references therein)
A15	$SO_3^{2-} + O_3 \xrightarrow{H_2O} SO_4^{2-}$	$1.5 \times 10^9 \exp[-5280(1/T-1/298)]$	(Hoffmann 1986; Kreidenweis et al., 2003 and references therein)
A16	$HSO_3^- + H_2O_2 \rightarrow SO_4^{2-}$	$\frac{7.45 \times 10^7 \exp[-4430(1/T-1/298)]}{1+13[H^+]}$	(Hoffmann 1986; Kreidenweis et al., 2003 and references therein)

Table 23 Acid-base equilibria for aqueous phase species

#	Equilibrium Reaction	Equilibrium Constant (M)	Source
E1	$\text{H}_2\text{SO}_4 \leftrightarrow \text{HSO}_4^- + \text{H}^+$	1000	(Seinfeld and Pandis 1998)
E2	$\text{HSO}_4^- \leftrightarrow \text{SO}_4^{2-} + \text{H}^+$	$1.02 \times 10^{-2} \exp[2720(1/T-1/298)]$	(Weast 1980)
E3	$\text{SO}_2 + \text{H}_2\text{O} \leftrightarrow \text{HSO}_3^- + \text{H}^+$	$1.3 \times 10^{-2} \exp[1960(1/T-1/298)]$	(Chameides 1984)
E4	$\text{HSO}_3^- \leftrightarrow \text{SO}_3^{2-} + \text{H}^+$	$6.6 \times 10^{-8} \exp[1500(1/T-1/298)]$	(Chameides 1984)
E5	$\text{H}_2\text{O}_2 \leftrightarrow \text{HO}_2^- + \text{H}^+$	$2.2 \times 10^{-12} \exp[-3730(1/T-1/298)]$	(Kreidenweis et al., 2003)
E6	$\text{CO}_2 + \text{H}_2\text{O} \leftrightarrow \text{HCO}_3^- + \text{H}^+$	$4.3 \times 10^{-7} \exp[-1000(1/T-1/298)]$	(Chameides 1984)
E7	$\text{HCO}_3^- \leftrightarrow \text{CO}_3^{2-} + \text{H}^+$	$4.68 \times 10^{-11} \exp[-1760(1/T-1/298)]$	(Chameides 1984)
E8	$\text{NH}_3 + \text{H}_2\text{O} \leftrightarrow \text{NH}_4^+ + \text{OH}^-$	$1.7 \times 10^{-5} \exp[-4500(1/T-1/298)]$	(Chameides 1984)
E9	$\text{CH}_3\text{SO}_2\text{H} \leftrightarrow \text{CH}_3\text{SO}_2^- + \text{H}^+$	5.0×10^{-3}	(Wudl et al., 1967)
E10	$\text{CH}_3\text{S(O)}_3\text{H} \leftrightarrow \text{CH}_3\text{SO}_3^- + \text{H}^+$	73	(Clarke and Woodward 1966)

Table 24 Henry's Law's constant (H) and Mass Accommodation Coefficient (α) for semi-volatile species

Species	H (M atm ⁻¹) (Source)	Accommodation Coefficient (Source)
SO ₂	1.23 exp[3140(1/T-1/298)] (Seinfeld 1986)	0.035 (Kreidenweis et al., 2003)
O ₃	1.1×10 ⁻² exp[2540(1/T-1/298)] (Seinfeld 1986)	5.3×10 ⁻⁴ (Kreidenweis et al., 2003)
H ₂ O ₂	7.45×10 ⁴ exp[7300(1/T-1/298)] (Seinfeld 1986)	0.018 (Kreidenweis et al., 2003)
HNO ₃	2.1×10 ⁵ exp[8700(1/T-1/298)] (Lelieveld and Crutzen 1991)	0.05 (Kreidenweis et al., 2003)
CO ₂	3.4×10 ⁻² exp[2440(1/T-1/298)] (Seinfeld 1986)	0.05 (Kreidenweis et al., 2003)
NH ₃	62 exp[4110(1/T-1/298)] (Seinfeld 1986)	0.05 (Kreidenweis et al., 2003)
CH ₃ SCH ₃	0.56 exp[4480(1/T-1/298)] (Campolongo et al., 1999)	0.001 Estimated
CH ₃ S(O)CH ₃	1.0×10 ⁷ exp[2580(1/T-1/298)] (Campolongo et al., 1999)	0.1 (De Bruyn et al., 1994)
CH ₃ S(O) ₂ CH ₃	1.0×10 ⁷ exp[5390(1/T-1/298)] (Campolongo et al., 1999)	0.1 (De Bruyn et al., 1994)
CH ₃ SO ₂ H	1.0×10 ⁹ exp[1760(1/T-1/298)] (Campolongo et al., 1999)	0.1 Assumed same as MSA
CH ₃ SO ₃ H	1.0×10 ⁹ exp[1760(1/T-1/298)] (Campolongo et al., 1999)	0.1 (De Bruyn et al., 1994)
H ₂ SO ₄	∞ (Campolongo et al., 1999)	0.75 (Poschl et al., 1998)

Table 25 Concentrations of steady-state radicals used in the simulation

Radicals	Concentration (molecules cm ⁻³)	Source
OH(g)	1×10 ⁶	(Prinn et al., 1995)
NO ₃ (g)	1×10 ⁶	(Noxon 1983)
Cl(g)	1×10 ⁴	(Pszenny et al., 1993; Wingenter et al., 1996)
BrO(g)	1×10 ⁷	(Sander and Crutzen 1996; Vogt et al., 1996; von Glasow and Crutzen 2004)
NO (g)	1×10 ⁸	(Seinfeld and Pandis 1998)
HO ₂ (g)	1×10 ⁸	(Jaegle et al., 2000; Tan et al., 2001)
	(mol l ⁻¹)	
OH (aq)	6×10 ⁻¹³	(Herrmann et al., 2000)
SO ₄ ⁻ (aq)	1×10 ⁻¹²	(Herrmann et al., 2000)
Cl(aq)	1×10 ⁻¹³	*
Cl ₂ ⁻ (aq)	1×10 ⁻¹¹	(Herrmann et al., 2000)

*: Calculated from [Cl₂⁻], [Cl⁻], [Cl[•]] = 6.0×10⁻⁴ M (Herrmann et al., 1996), and K = 1.4×10⁵ M⁻¹ for Cl + Cl[•] ↔ Cl₂⁻ (Yu et al., 2004).

Simulations

Given the global importance and dynamic differences between cumulus and stratocumulus clouds, both are considered in our simulations. Stratocumulus clouds cover 20% to 40% of the earth surface (Lelieveld et al., 1989) and play an important climatic role as they are responsible for about one third of the shortwave planetary albedo (Barry and Chorley 1998). Because of their wide coverage and long lifetime in the atmosphere, stratocumulus provide an excellent environment for aqueous phase oxidation of organo-sulfur compounds. The aqueous phase reactions convert the relatively volatile species, i.e., DMS and DMSO, into non-volatile species, i.e., MS and NSS, which stay in particles after cloud droplets evaporate and contribute to particle growth. Cumulus clouds cover about 6-10% of the oceans and are radiatively neutral (Seinfeld and Pandis 1998), but they play a pivotal role in long range transport of water vapor and trace species (e.g., S) to the upper troposphere.

Lagrangian trajectories for stratocumulus clouds used in this study were derived from two simulations (non-drizzling “ASTEX-1” and heavy drizzling “ASTEX-2”) for conditions observed during the Atlantic Stratocumulus Transition Experiment (Albrecht et al., 1995), while those for cumulus clouds were derived from simulations of observed soundings (CRYSTAL-FACE) obtained during the Cirrus Regional Study of Tropical Anvils and Cirrus Layers - Florida Area Cirrus Experiment (Miao-Ling Liu, personal communication). 500 trajectories covering one hour of simulation time were used for both ASTEX-1 and ASTEX-2 clouds, while 61 trajectories were used in the simulation of

the cumulus cloud for 30 minutes. A time step of 2 s was used in the model calculation for stratocumulus clouds, therefore, 1800 total steps are needed to finish one simulation cycle (1 hour). For the cumulus cloud, the time step is 180 s in the computation, therefore, only 180 steps are necessary to finish one simulation cycle (30 minutes).

In Figure 35, vertical profiles of average liquid water content (LWC) within one simulation cycle of (a) stratocumulus clouds and (b) cumulus clouds are plotted. In Figure 35 (a), LWC of two types of stratocumulus clouds considered in simulations (ASTEX-1 and ASTEX-2) are compared. It is obvious that ASTEX-2 has a higher average LWC (0.6 g m^{-3}) and lower cloud base (200 m) than ASTEX-1 (0.4 g m^{-3} and 400 m, respectively). And cumulus clouds have a base of about 500 m and average LWC close to 1.0 g m^{-3} . The average updraft velocities of the cumulus cloud (2 m s^{-1}) are higher than that of the stratocumulus cloud (0.2 to 0.4 m s^{-1}). Another important difference between the stratocumulus and the cumulus cloud is the cloud droplet number concentration and size distribution. Stratocumulus clouds are energetic enough to maintain droplets of about $80 \text{ }\mu\text{m}$ in diameter, and droplet number concentrations for maritime stratocumulus clouds are usually low, i.e., $<20 - 400 \text{ cm}^{-3}$. For cumulus clouds, on the other hand, the droplet number concentration varies in a wide range from ~ 250 to $\sim 2300 \text{ cm}^{-3}$, while the average droplet diameters are usually in the range of $0.5 - 60 \text{ }\mu\text{m}$ (Albrecht et al., 1995; Stevens et al., 1996; Conant et al., 2004). An average field of 2.8 km (horizontal) \times 760 m (vertical) was simulated for the two stratocumulus clouds considered, while a much larger space of 6.0 km (horizontal) \times 2.3 km (vertical) was simulated for the cumulus cloud case. The stratocumulus clouds cover the whole simulation field while the cumulus clouds cover only part of it; and the stratocumulus

clouds last for the whole simulation period while the cumulus clouds do not. Instead, the latter form and dissipate throughout one simulation cycle.

Since non-drizzling stratocumulus clouds (here, the ASTEX-1 simulation) are the most abundant in the marine atmosphere, most studies in the present work will use this type of cloud to simulate DMS oxidation. For one simulation cycle of the ASTEX-1 cloud, horizontal ensemble average concentrations of the simulated compounds for every 12-minute and one-hour average are generated as the output. After the first cycle, the initial cloud and trajectory profiles and the last 12-minute average concentrations of all sulfur compounds are used as the input of the model to start a new simulation cycle. Thus, concentrations of sulfur species of interest for longer time scales can be modeled by continuous simulation using the same trajectory and cloud dataset.

Analysis of trajectories in the ASTEX-1 cloud field indicated that air parcels stay in cloud areas for about 30% of the simulation time; typical particles in the marine boundary layer spend about 3 hours per day in clouds (Katoshevski et al., 1999). As a result, ~ 15 simulation cycles of this model will cover 3 days of in-cloud processes assuming that the photochemical transformations occur only in the aqueous phase (cloud droplets) during daytime, and the meteorological conditions do not change much in this period of time. The average lifetime of aerosols in the marine boundary layer is ~ 6 days (see for example, Pham et al., 1995); given that we consider only cloudy conditions (which would reduce aerosol lifetime because of increased wet deposition), it is reasonable to assume that the modeled aqueous phase concentrations of MS and NSS after 15 simulation cycles represent those observed in the atmosphere for the average aerosol lifetime.

To focus on DMS chemistry, initial concentrations of SO₂ in the gas phase and NSS in the aqueous phase are always set to be zero, i.e., all SO₂ and NSS in the system are produced solely from DMS oxidation. The recommended average DMS concentration of 100 ppt in the marine atmosphere (Seinfeld and Pandis 1998) is used as the steady-state DMS concentration throughout the simulation. This DMS concentration and the DMS oxidation mechanism using the kinetics and thermodynamics data listed in Tables 21 to 24, as well as the steady-state concentrations of radical oxidants in Table 25 are used in the TEM to simulate the production of aqueous phase MS and NSS from DMS oxidation in the ASTEX-1 cloud, which will be called the “primary scenario” in this work.

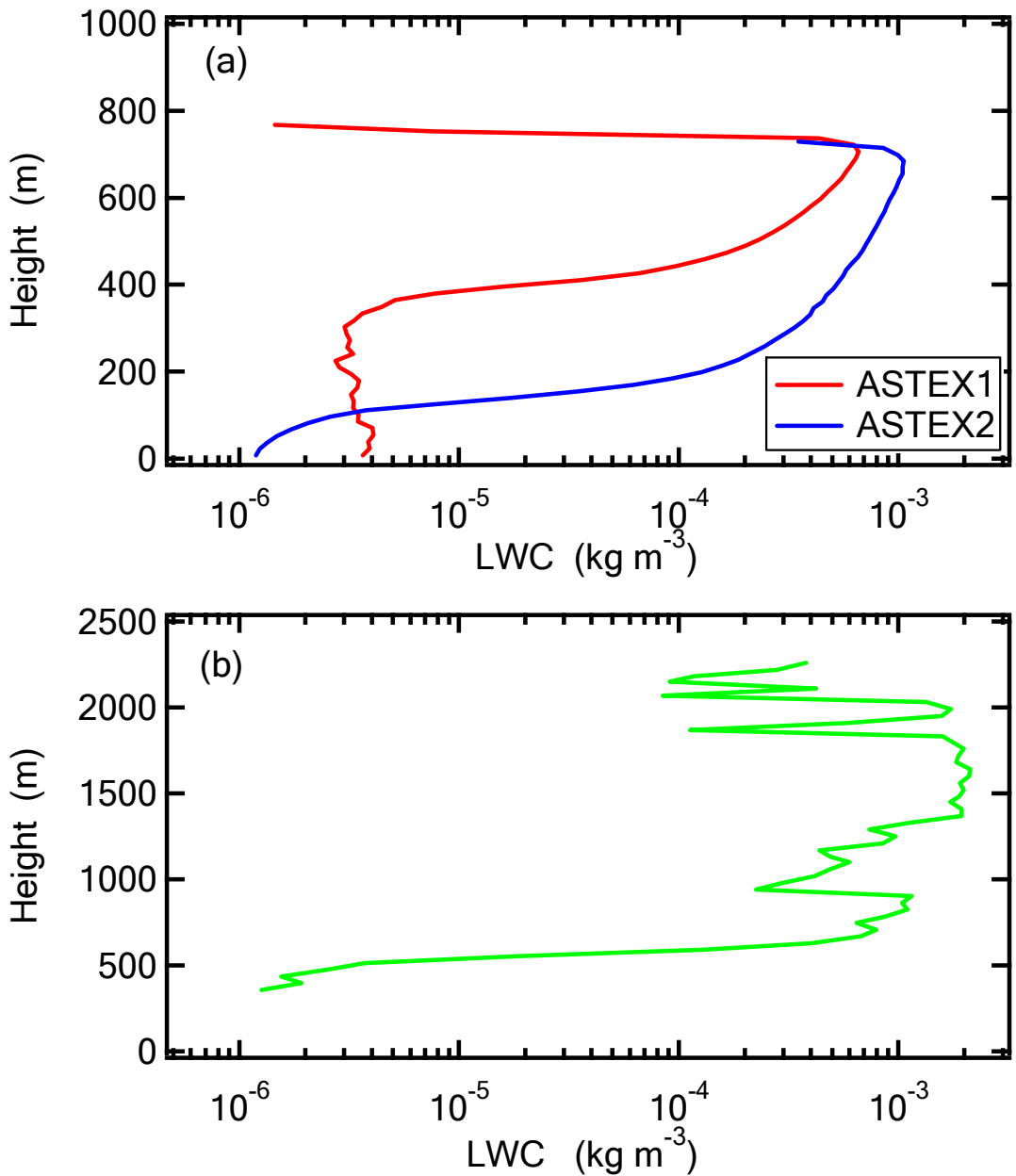


Figure 35 Average liquid water content for (a) 1-hour simulation of the stratocumulus cloud, and (b) 30-minute simulation of the cumulus cloud considered

Simulation of the “Primary Scenario”

Figure 36 compares the production of DMSO(g), SO₂(g), MS(aq) and NSS(aq) from DMS oxidation, after 1, 5, 10 and 15 simulation cycles of the “primary scenario”. Given the fast uptake of DMSO and SO₂ into the aqueous phase in the cloud and the release back into the gas phase under the cloud, all concentration profiles of SO₂(g) and DMSO(g) have an “S” shape, i.e., concentrations below the cloud area are higher than those within the cloud area. The uptake of DMSO into droplets is so efficient that equilibrium between the gas and aqueous phases is achieved in less than one hour and at the same time, fast oxidation of DMSO in both the gas and the aqueous phases make the concentrations of DMSO in both phases approach the steady state very quickly; therefore the four vertical profiles of DMSO(g) concentration in Figure 36 (a) have almost identical shape and overlap each other. Given the lower solubility and reactivity of SO₂, it is expected to take longer for SO₂ to achieve the equilibration between the gas and aqueous phases and for SO₂(g) to reach steady-state concentration. Indeed, as can be seen in Figure 36 (b), the difference between the in-cloud and the under-cloud SO₂(g) concentrations after 1 simulation is not as large as is obtained from longer simulation time. After about 10 simulation cycles, SO₂(g) profiles become independent of time, indicating a pseudo steady-state for SO₂.

Based on the MS and NSS profiles shown in Figure 36 (c) and (d), it seems that the production rate of MS is constant, so the MS concentration increases at a constant rate throughout 15 simulation cycles; while the NSS production rate increases with simulation

time and the NSS concentration grows faster if longer simulations are carried out. This trend can be clearly seen in the temporal evolution of the in-cloud average MS and NSS concentrations, as shown in Figure 37 (d) and (e). For completeness, the temporal evolution of below-cloud average $\text{SO}_2(\text{g})$ and $\text{DMSO}(\text{g})$, and in-cloud average $\text{DMSO}(\text{aq})$ and MS/NSS are also plotted in Figure 37. As discussed previously, concentrations of very reactive DMSO in both the gas and the aqueous phase become constant within 1-2 simulation cycles (Figure 37 (a) and (b)), and the less reactive SO_2 achieves the steady state only after about 10 cycles (Figure 37 (c)). Different from DMSO and SO_2 , concentrations of MS (Figure 37 (d)) and NSS (Figure 37 (e)) keep increasing after 15 simulation cycles. This is expected, because for the relatively non-volatile non-reactive sulfur species, i.e., MS and NSS, their main sink in the atmosphere is through wet/dry deposition of particles. However, the deposition of particles is not included in the mass balance equation (8-1) used in our model to calculate the concentration evolution of sulfur species, so MS and NSS continue to accumulate over time. In spite of the increase of MS and NSS concentrations, the MS/NSS ratio becomes almost constant with a value of ~ 0.35 after 15 simulation cycles (as shown in Figure 37 (f)). As discussed above, 15 simulation cycles represent about 3 days of cloud processing. The concentrations of MS and NSS obtained after 15 simulation cycles of the primary scenario (as shown in Figure 37 (d) and (e)) are used as the simulation results: 0.72 and 2.1 nmol m^{-3} , respectively.

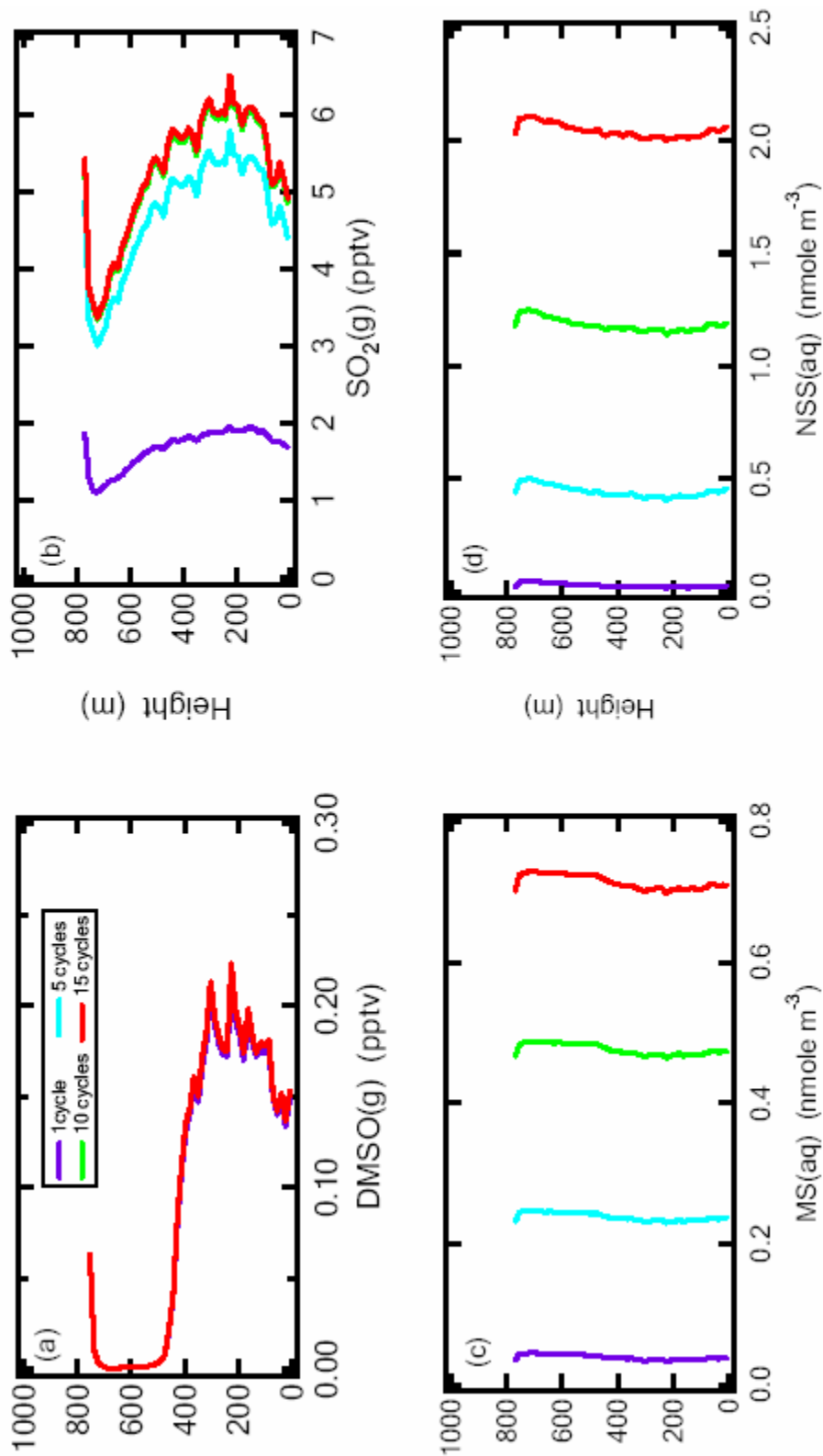


Figure 36 Vertical profiles of (a) DMSO(g), (b) SO₂(g), (c) MS(aq) and (d) NSS(aq) after 1, 5, 10, and 15 simulation cycles of the “primary scenario”

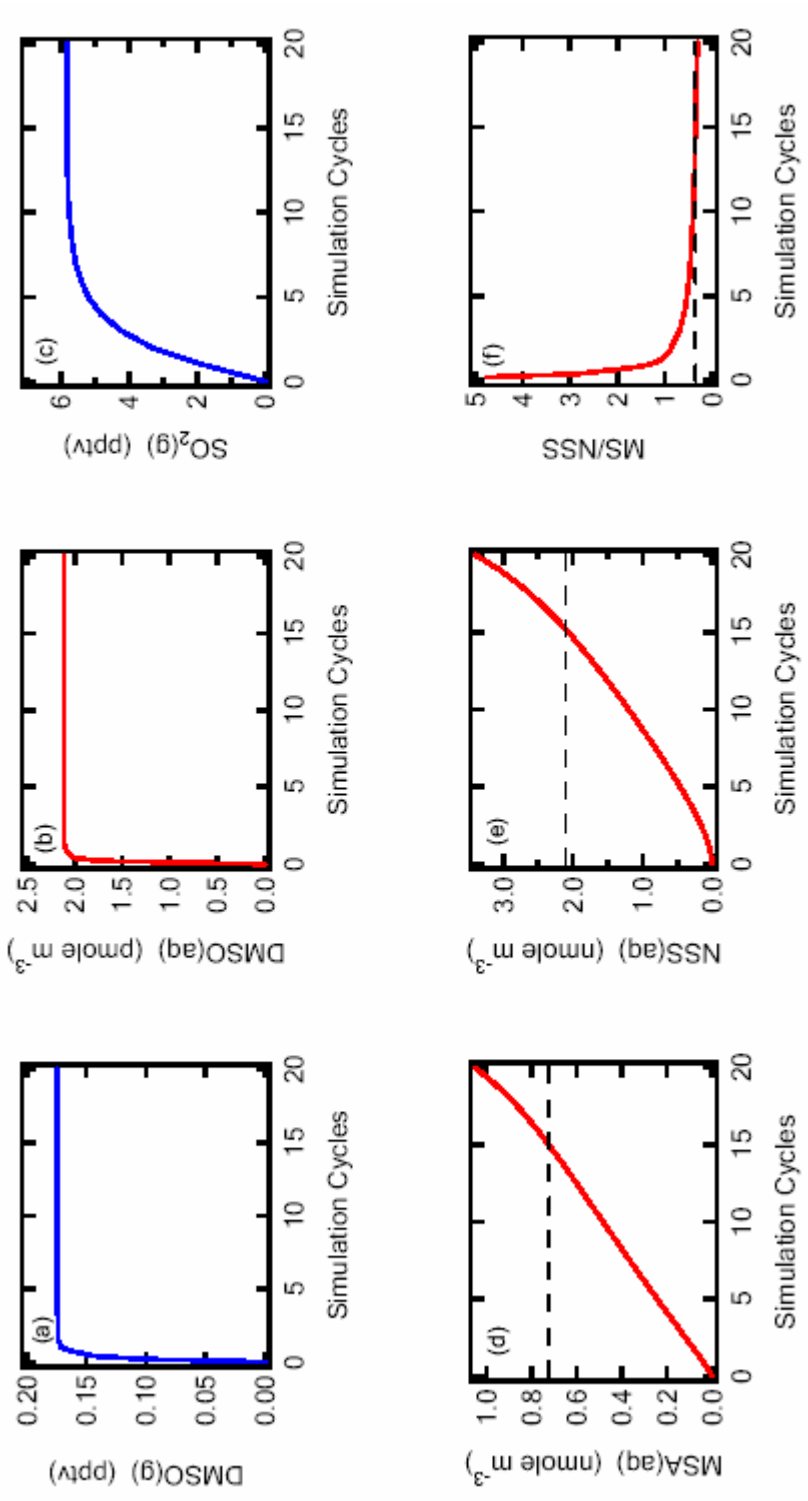


Figure 37 Temporal evolution of (a) DMSO(g), (b) DMSO(aq), (c) SO₂(g), (d) MSA(aq), (e) NSS(aq) and (f) MS/NSS from the simulations of the “primary scenario”

Contribution of Aqueous Phase Reactions to MS and NSS Production

In order to quantify the contribution of heterogeneous processes to MS and NSS production and particulate mass growth from DMS oxidation, as well as to the removal of $\text{SO}_2(\text{g})$ and $\text{DMSO}(\text{g})$, results are compared for four simulation scenarios: (1) including only gas phase reactions to produce DMSO and SO_2 , (2) including all gas phase reactions, (3) including all gas phase reactions and mass transfer to the aqueous phase, and (4) including all multi-phase physical and chemical transformations (the “primary scenario”).

The production of $\text{SO}_2(\text{g})$, $\text{DMSO}(\text{g})$, MS and NSS after 15 simulation cycles of all four scenarios are listed in Table 26, where both the concentration and the product yield of each species are compared. The product yield of $\text{SO}_2(\text{g})$ is ~64% for scenario 1 and ~75% for scenario 2, while the $\text{DMSO}(\text{g})$ yield decreases from ~27% for scenario 1 to ~6% for scenario 2. The different variation of SO_2 and DMSO product yield is because the OH-initiated oxidation of DMSO is faster than that of SO_2 , and SO_2 is the dominant gas phase product from $\text{DMSO} + \text{OH}$ through the intermediate MSIA. This estimate of the SO_2 product yield agrees well with the estimate from Davis et al. (1999) and falls within the range 50-100% estimated by De Bruyn et al. (2002) based on studies from Ayers et al. (1997), De Bruyn et al. (1998), Mari et al. (1999), Shon et al. (2001) and Chin et al. (2000b).

The concentration of SO_2 for scenario 3 is same as that for scenario 2, suggesting either that mass transfer of SO_2 into the aqueous phase is very slow, or that the SO_2 uptake rate is approximately the same as the SO_2 production rate from gas phase DMSO oxidation. The latter one is more likely because the fraction of $\text{SO}_2(\text{g})$ in the total sulfur

products for scenario 3 decreases dramatically compared to scenario 2. Given the high solubility of DMSO, concentrations of DMSO in both phases increase substantially before approaching saturation if there is no efficient removal in the aqueous phase (which is the case for scenario 3); DMSO then becomes the dominant end product from DMS oxidation for scenario 3. When all aqueous phase transformations are included in the simulation (scenario 4, or the “primary scenario”), MS and NSS become dominant and contribute about 23% and 67%, respectively, to the total sulfur products. The SO₂ product yield decreases to 8% because (1) efficient uptake of DMSO into the condensed phase and subsequent aqueous phase oxidation reduces the gas phase SO₂ product yield; and (2) the heterogeneous reactions of O₃ and H₂O₂ with S(IV) efficiently drive gaseous SO₂ into the aqueous phase to produce S(VI) (NSS).

Understanding the atmospheric fate of DMSO is central for quantifying the amount of sulfur species in the gas and condensed phases. This is clearly illustrated in our simulations, where heterogeneous processes contribute about 90% to the DMSO removal. This value is higher than current estimates of ~50% (Davis et al., 1998; Sciare et al., 2000b; Legrand et al., 2001; Cosme et al., 2002), suggesting that aqueous phase transformations are even more important than previously thought in understanding the sulfur cycle. Meanwhile, uptake from the gas phase is the primary source of DMSO in the aqueous phase and, our simulations suggest that oxidation of DMS in the aqueous phase is only a minor contribution to the total aqueous phase DMSO production, i.e., 10-15%. We have adopted the upper limit of the literature values of the Henry’s Law constant for DMSO(10^7 M atm⁻¹ at 298K, in Table 24), which is over 7000 times higher than the lowest literature value (Gmehling et al., 1982; Betterton 1992), to maximize the

production of MS. While when the very low Henry's law constant of DMSO (1400 M atm^{-1} at 298K) is used in the model, the production of MS and the MS/NSS ratio are reduced by only 15-20%, indicating that aqueous phase oxidation plays significant roles in driving DMSO from the gas into the aqueous phase. Of the four aqueous radicals studied, OH is the most efficient at scavenging DMSO and contributes ~55% to total aqueous DMSO loss. The $\text{DMSO} + \text{SO}_4^-$ reaction is the second most important aqueous phase DMSO sink and accounts for ~34% of total aqueous DMSO loss, and Cl_2^- consumes another 10% of DMSO in particles. This order in contributions of each radical to DMSO removal agrees fairly well with the estimate based on the rate coefficient of each reaction and the steady-state radical concentrations.

Clearly, scenario 3 would never occur in the atmosphere. However, by comparing MS and NSS production between scenarios 3 and 4, contributions of gas phase uptake to MS and NSS production can be evaluated. Our simulations indicate that uptake from the gas phase MSA accounts for $\leq 3\%$ of total MS production. This upper limit is slightly higher than the estimates of ~1% from Davis et al. (1999) and 2% from von Glasow and Crutzen (2004). MSA may be produced in the gas phase from the $\text{MSIA} + \text{OH}$ reaction; given the large measurement uncertainty for MSA product yield from $\text{MSIA} + \text{OH}$ (0-10% from Kukui et al., 2003), we adopted the upper limit (10%) in our simulations to maximize the effect of gas phase MSA production. If this yield is halved to 5% (a value used by von Glasow and Crutzen (2004)), the gas phase formation of MSA will account for only $< 2\%$ of total MS production, in good agreement with the estimate from von Glasow and Crutzen (2004). As shown in Figure 37 (d), the MS concentration in particles increases almost linearly with time, which also suggests that

MS has one dominant source, i.e., aqueous phase production. von Glasow and Crutzen (2004) postulated that the $\text{MSI} + \text{OH}$ reaction is the only important direct source of MS. While this reaction was found to contribute only about 25% to total MS production in our modified chemical mechanism; the $\text{MSI} + \text{Cl}_2^-$ reaction (not included in their studies) is found to be the dominant source of MS and contributes $\sim 65\%$ of total MS production. $\text{MSI} + \text{SO}_4^-$ and $\text{DMSO}_2 + \text{OH}$ account for $< 10\%$ of total MS.

As shown in Figure 37 (e), in contrast to MS, the NSS concentration increases non-linearly with simulation time, because gas phase uptake, heterogeneous oxidation of SO_2 and DMS, and aqueous phase oxidation of organo-sulfur species all contribute to NSS production. Our simulations suggest that gas phase production contributes $\sim 9\%$ of total NSS production. This value is very close to the value from von Glasow and Crutzen (2004), but is only about half of the value postulated by Davis et al. (1999). In our mechanism, there are two sources of gas phase H_2SO_4 : the CH_3S radical and SO_2 . As discussed earlier, the reaction of CH_3S in the atmosphere is a key to understanding the abstraction channel of DMS oxidation and SO_2 and H_2SO_4 production. Even though some studies have found that CH_3S can be oxidized by NO_2 , HO_2 and O_3 in the presence of O_2 and H_2O (Tyndall and Ravishankara 1989a; 1989b; Turnipseed et al., 1993; Martinez et al., 1999; 2000), the detailed mechanism leading to production of SO_2 and H_2SO_4 and their branching ratios from CH_3S are not well determined. So the branching ratios of SO_2 and H_2SO_4 from CH_3S oxidation specified here are our own estimates. If the branching ratio of H_2SO_4 in our model is doubled, i.e, 20%, the gas phase H_2SO_4 formation will contribute 17% to total NSS production, still a rather minor contribution.

In the marine atmosphere, the main components of non-seasalt aerosols are NSS and MS. From simulation of scenario 4 (“primary scenario”), DMS oxidation increases total non-seasalt mass by about 2.8 nmol m^{-3} , and MS accounts for about 25% this mass growth. Based on the results from simulations of scenarios 3 and 4, as well as a simulation where all aqueous reactions of organo-sulfur species are not considered (scenario 5, listed in Table 26), the contribution of aqueous phase organo-sulfur species reactions to the total growth of particle mass can be estimated. Oxidation of S(IV) in the aqueous phase by O_3 and H_2O_2 is found to be the most important source of the mass increase, and contributes over 60% of total non-volatile sulfur production from DMS oxidation. The aqueous phase oxidation of organo-sulfur compounds, i.e., DMS, DMSO and MSI, accounts for ~30% of total MS and NSS production from DMS, and the other 5-10% is due to mass transfer of MSA and H_2SO_4 from the gas phase.

The $\text{MS} + \text{OH}$ reaction is proposed to be potentially important in NSS production and in affecting the observed MS/NSS ratio. It is also the only removal pathway for MS in our chemical mechanism. von Glasow and Crutzen (2004) estimated a 10% contribution of this reaction to NSS production in particles. Our rate coefficient for the $\text{MS} + \text{OH}$ reaction at room temperature is in good agreement with the lowest of three literature values that differ by more than a factor of 100, and for the first time we report the temperature dependent kinetics of this reaction. To quantify the contribution of $\text{MS} + \text{OH}$ to NSS production and MS removal, we compared the results of MSA, NSS and MS/NSS obtained from scenario 4 (the “primary scenario”) with those from simulations without the $\text{MS} + \text{OH}$ reaction under identical conditions (scenario 6, listed in Table 26). It is found that the $\text{MS} + \text{OH}$ reaction consumes almost 20% of MS and accounts for 8%

of total NSS production; as a result, the simulated MS/NSS decreases by ~25% due to the oxidation of MS by OH radicals. This estimate agrees well with the value from von Glasow and Crutzen (2004), who adopted the lowest literature value for the MS + OH reaction rate coefficient, close to our room temperature data. These results indicate that even at this relatively slow reaction rate, the MS + OH reaction changes the MS/NSS ratio evidently due to the long lifetime of atmospheric aerosols in the marine boundary layer.

Table 26 Production yields of SO₂(g), DMSO(g) (pptv) and aqueous phase MS and NSS (pmol m⁻³) after 15 simulation cycles for scenarios (1), (2), (3), (4), (5) and (6)

Simulation #	(1)	(2)	(3)	(4)	(5)	(6)
SO ₂ (g)	40 (64%)	47 (75%)	47 (13%)	5.8 (8%)	8.3 (2%)	5.8 (8%)
DMSO(g)	17 (27%)	3.9 (6%)	95 (27%)	0.2 (0.3%)	104 (27%)	0.2 (0.3%)
MS	—	—	23 (0.15%)	720 (23%)	25 (12%)	890 (29%)
NSS	—	—	193 (1.2%)	2100 (67%)	1990 (0.2%)	1910 (61%)

Temperature Dependence of MS and NSS Production

Production of MS, NSS, MS/NSS, DMSO(g), DMSO(aq) and SO₂(g) obtained at different temperatures for the “primary scenario” simulation are depicted in Figures 38 and 39. MS production decreases with increasing temperature (Figure 38 (a)) for two reasons: (1) The production of gas phase DMSO decreases with increasing temperature (Figure 39 (a)) due to the negative temperature dependence of both DMSO production channels (DMS + OH (R2) and DMS + BrO (R5)); and (2) The solubility of DMSO in the aqueous phase decreases with increasing temperature (Table 24), which results in a very low concentration of DMSO in the aqueous phase at high temperatures (Figure 39 (b)). DMSO is the most important immediate source of MSI and oxidation of MSI in the aqueous phase is the primary source of MS (discussed previously). Although the rate of aqueous phase DMSO oxidation increases with increasing temperature (Table 22), it is limited by mass transfer of DMSO from the gas phase. As a result, the trend of MS production at different temperatures follows the temperature-dependence of the aqueous phase DMSO.

The temperature dependence of NSS production is not monotonic. Simulations suggest that for the first 3-4 cycles NSS production decreases with increasing temperature, but for simulations after that, it is the highest at 288 K and gets lower at both higher and lower temperatures, as shown in Figure 38 (b). Since the most important precursor of NSS is SO₂, temperature dependences of gas phase SO₂ production rate, mass transfer of SO₂ between the gas and aqueous phases, as well as the oxidation of S(IV) in the aqueous phase are all potentially important in understanding this result. As the main gas phase

end product from both the addition and the abstraction channels of DMS oxidation, the total SO_2 production rate increases with decreasing temperature according to our mechanism. However, as shown in Figure 39 (c), due to the decreased solubility of SO_2 in water at high temperatures, it is accumulated in the gas phase; therefore the simulated $\text{SO}_2(\text{g})$ increase with increasing temperature. Comparing the temporal evolution of SO_2 at different temperatures also found that it takes 2-3 simulation cycles to achieve the steady-state concentration for simulations at the lowest temperature considered, while it takes much longer to achieve the steady-state concentration at higher temperatures. Before the steady-state between the gas and aqueous phases was reached, uptake of SO_2 into the aqueous phase is rate-limiting for NSS production; and after that, aqueous phase oxidation of $\text{S}(\text{IV})$ becomes more important in determining the NSS production rate. Since all reactions of $\text{S}(\text{IV})$ with O_3 and H_2O_2 have positive temperature dependence, i.e., reaction rates increase with increasing temperature, which is opposite to the temperature dependence of SO_2 mass transfer into the aqueous phase, there is a transition point for each temporal evolution profile of NSS. For the simulation at 278K, production of NSS is fastest for the first few simulation cycles where gas SO_2 production rate and its uptake into the aqueous phase are rate-limiting for NSS production and gets slower after the steady-state has been achieved and the aqueous phase chemistry becomes rate limiting for NSS production. For the simulation at 298K, it apparently takes longer for $\text{SO}_2(\text{g})$ to approach the steady-state, so the NSS production for the first few simulation cycles is slow while the aqueous phase chemistry tends to compensate the NSS production after the steady-state is established. While for the higher temperatures, aqueous phase reactions can not compensate the slow production of NSS

due to slow SO₂ production rate and mass transfer into the aqueous phase within the time considered in our simulations. As a result, the NSS production from 278 K, 288 K and 298K are very close to each other, but are obviously lower at two higher temperatures.

As MS and NSS production each differ with temperature, the simulated MS/NSS exhibits a complex temperature dependence (Figure 38 ©). For all temperatures studied, MS/NSS ratios decrease with time and eventually approach a constant value representing the final MS/NSS at each temperature. It takes longer for MS/NSS at higher temperatures to reach the steady state than at lower temperatures. Except for the 318 K simulation (which needs more time to achieve the “pseudo-steady-state”), all MS/NSS ratios become almost independent of time after 15 cycles. For a consistent evaluation, all MS/NSS ratios after 15 simulation cycles are compared. The simulation at 278 K gives the highest MS/NSS with a value of ~ 0.8 ; this is expected since the MS production is the highest while the NSS production is moderate at this low temperature. The MS/NSS ratios are ~ 0.5 at 318K and 288K, and ~ 0.4 at 298K and 308K. This analysis suggests that the MS/NSS ratio obtained from our simulation of the “primary scenario” (which is ~ 300 K) is the lowest with a value of ~ 0.35 , and increases at both high and low temperatures. Especially at low temperatures, MS production becomes comparable to that of NSS, and this is potentially important in understanding variations in observed MS/NSS ratios at different latitudes. The studies carried out in the Antarctica for the austral summer by Berresheim et al. (1998) observed high concentrations of MS (1.9 nmol m⁻³) and a high MS/NSS ratio in the range of 0.49-0.96 with an average of 0.73. While the studies in the equatorial Pacific from Davis et al. (1999) found a much lower MS (0.7 nmol m⁻³) and MS/NSS (0.08), even though the DMS concentrations differ by

only 30% between these two sets of observations. Different temperatures appear to be at least partially responsible for the different MS levels and MS/NSS ratios observed from the two studies.

The contribution of aqueous-phase reactions to the total production of MS and NSS also depends on temperature. Simulations suggest that aqueous phase MS production decreases from 99% to 95% when temperature increases from 278K to 318K (Table 27). This result is expected, since total MS production decreases with increasing temperature (primarily due to decreased mass transfer of DMSO into the aqueous phase at high temperatures) while the partitioning of non-volatile MSA between the gas and the aqueous phase remains practically unchanged within the temperature range considered. Therefore, uptake of gas phase MSA into particles contributes more to total MS production at higher temperatures than at lower temperatures. For the same reason, aqueous phase reactions contribute less than 80% to total NSS production at 318K and over 90% at temperatures lower than 300K.

Our kinetic studies have found a high activation energy of the MS + OH reaction, i.e., $\sim 22 \text{ kJ mol}^{-1}$, which makes this reaction potentially more important in affecting the MS/NSS ratio at high temperatures than at low temperatures. As listed in Table 28, the MS + OH reaction scavenges 9% of MS and creates 8% of NSS at 278 K, while it can consume 27% of MS and produce 23% of NSS at 318 K; as a result, MS/NSS ratios decrease by 17% at 278 K and by 40% at 318 K due to MS + OH. In that sense, the temperature dependence of the MS + OH rate coefficient is another potentially important reason for the high value of observed MS/NSS at low temperatures, e.g., the measurement from Berresheim et al. (1998) in the Antarctica.

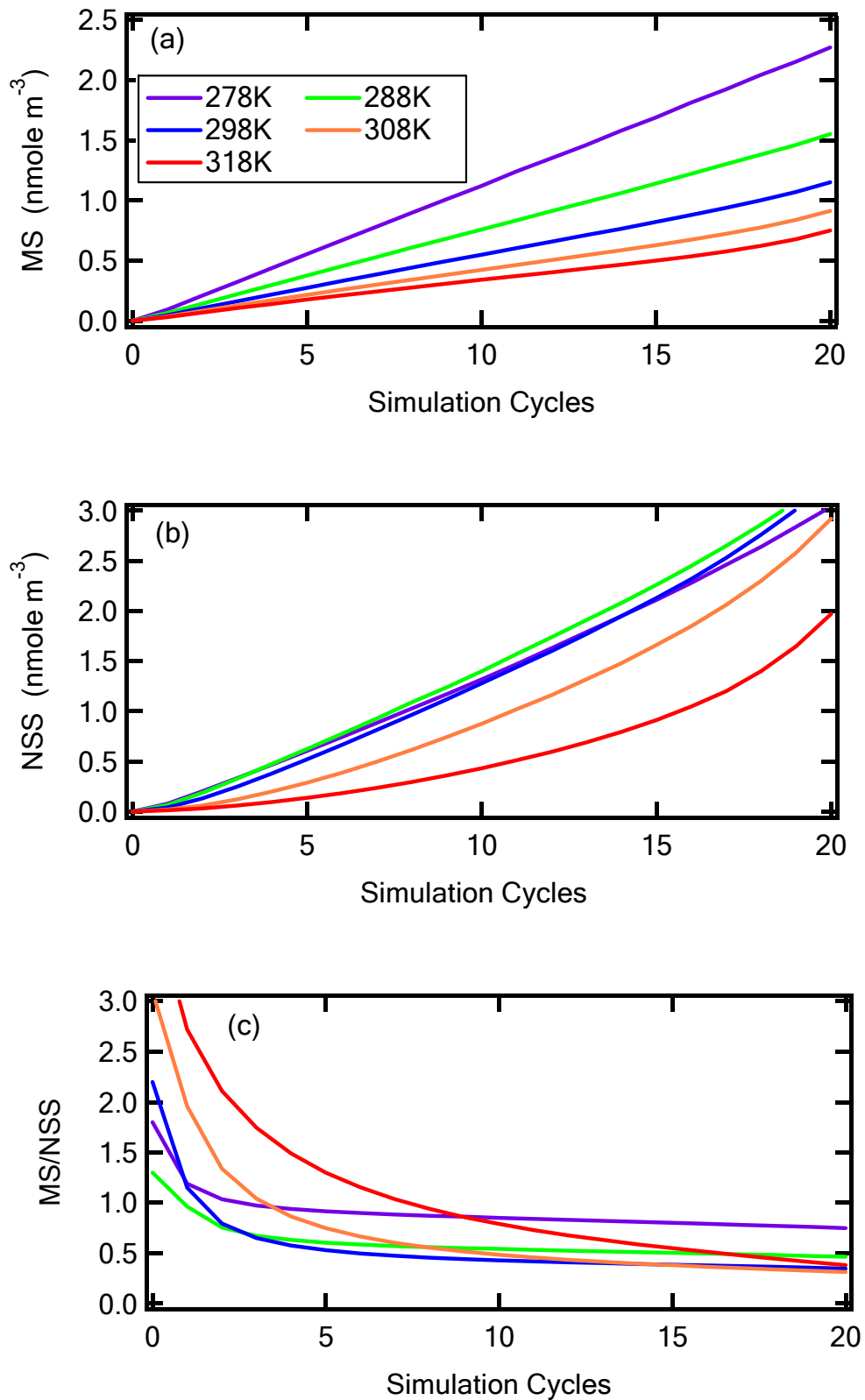


Figure 38 Temporal evolution of (a) MS, (b) NSS and (c) MS/NSS for simulations of the “primary scenario” at different temperatures

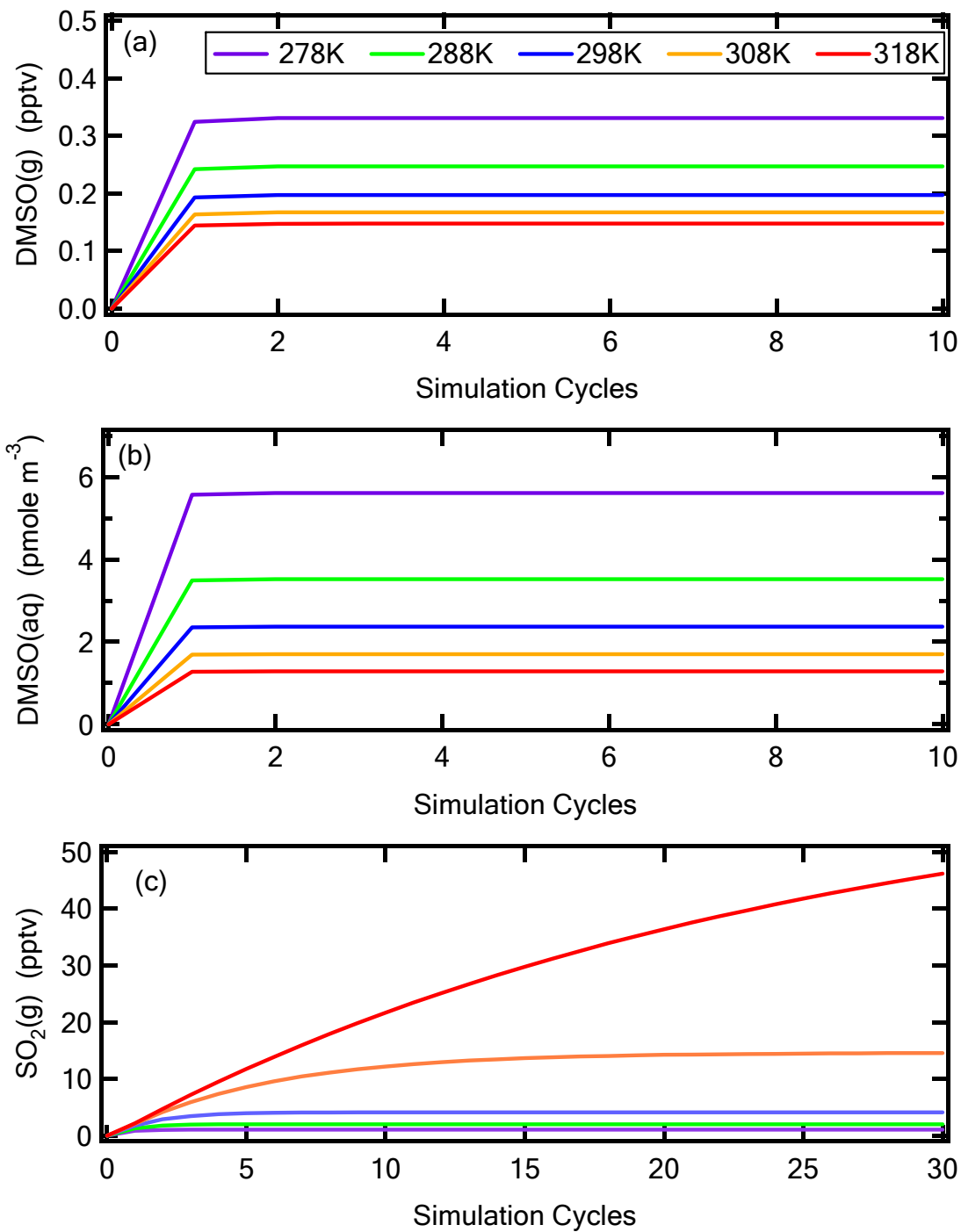


Figure 39 Temporal evolution of (a) DMSO(g), (b) DMSO(aq) and (c) SO₂(g) for simulations of the “primary scenario” at different temperatures

Table 27 Contributions of aqueous phase reactions to MS and NSS production for simulations of the “primary scenario” at different temperatures

T (K)	278	288	298	308	318
MS	99%	98%	97%	96%	95%
NSS	91%	91%	91%	88%	79%

Table 28 Change of of MS, NSS and MS/NSS due to the MS + OH reaction for simulations of the “primary scenario” at different temperatures

T (K)	278	288	298	308	318
MS	-9%	-12%	-20%	-21%	-27%
NSS	+8%	+7%	+ 8%	+11%	+23%
P(MS)/P(NSS)	-17%	-19%	-26%	-28%	-40%

Comparison of Stratocumulus and Cumulus Clouds

All simulations discussed before are done for the non-drizzling stratocumulus cloud (ASTEX-1), which is a frequent occurrence in the marine atmosphere. We also considered a heavy drizzling stratocumulus cloud (ASTEX-2) and cumulus cloud (CF) to examine how DMS oxidation occurs in these cloud regimes, using the same chemical mechanism as before.

Comparison of ASTEX-1 and ASTEX-2 Simulations

The ASTEX-2 cloud has higher liquid water content and a lower cloud base than the ASTEX-1 cloud (Figure 35 (a)). Therefore it is expected that the vertical distribution profiles of sulfur species in these two cloud fields are different. Figure 40 compares the vertical distribution profiles of MS, NSS and MS/NSS after 15 simulation cycles of ASTEX-1 and ASTEX-2 when the same full chemistry and mass transfer are allowed. As expected, simulated results from two cloud fields follow their own LWC profiles, and productions of both MS and NSS in ASTEX-2 are higher than those in ASTEX-1. In Figure 41, the temporal evolutions of MS, NSS and MS/NSS from the simulations of the “primary scenario” using the ASTEX-1 and AXTEX-2 clouds are compared. It can be seen that MS production from the two cloud fields are about same for the first 15 cycles, while the production from the ASTEX-2 cloud apparently becomes faster than that from the ASTEX-1 cloud after 15 simulation cycles. The reason for this difference is not clear yet; since for both cloud fields 15 simulation cycles are enough to follow the evolution of MS and NSS production, all comparison will be made based on results from 15 simulation cycles.

The difference between the two types of clouds for NSS production is more evident than that for MS production (Figure 40 (b) and 41(b)). The aqueous phase production of NSS is more important for the ASTEX-2 case due to its higher LWC than the ASTEX-1 cloud. As discussed earlier, uptake from the gas phase accounts for $\leq 3\%$ of MS and 9% of NSS production in the aqueous phase for the ASTEX-1 cloud. By comparing identical simulations of scenarios 3 and 4 for the ASTEX-2 cloud, it is found that that gas phase MSA production could contribute as much as 7% to total MS production, while uptake of gas phase H_2SO_4 accounts for only 6% of total NSS production.

The change of MS/NSS ratios with time is also different between the two stratocumulus clouds. As shown in Figure 41 (c), MS/NSS in the ASTEX-2 case is higher than the ASTEX-1 cloud for the first 5-6 cycles and becomes lower than ASTEX-1 after that. Mass transfer of DMSO and SO_2 into the aqueous phase is important in determining the production rate of MS and NSS for a short period of time when total concentrations of sulfur species in particles are relatively low. Since DMSO is much more soluble than SO_2 in water, production of MS is dramatically higher than NSS at the beginning of the simulation (first 5-6 cycles), especially for the ASTEX-2 cloud where high surface areas of droplets are available. After DMSO and SO_2 have achieved equilibration between the gas and the aqueous phases, aqueous phase reactions become rate limiting for MS and NSS production; hence accumulation of NSS exceeds MS due to its fast production from oxidation of both SO_2 and organo-sulfur species. As a result, the MS/NSS ratio reaches a constant value of ~ 0.21 after 15 cycles of ASTEX-2 simulations, which is about 40% lower than the estimate for the ASTEX-1 cloud.

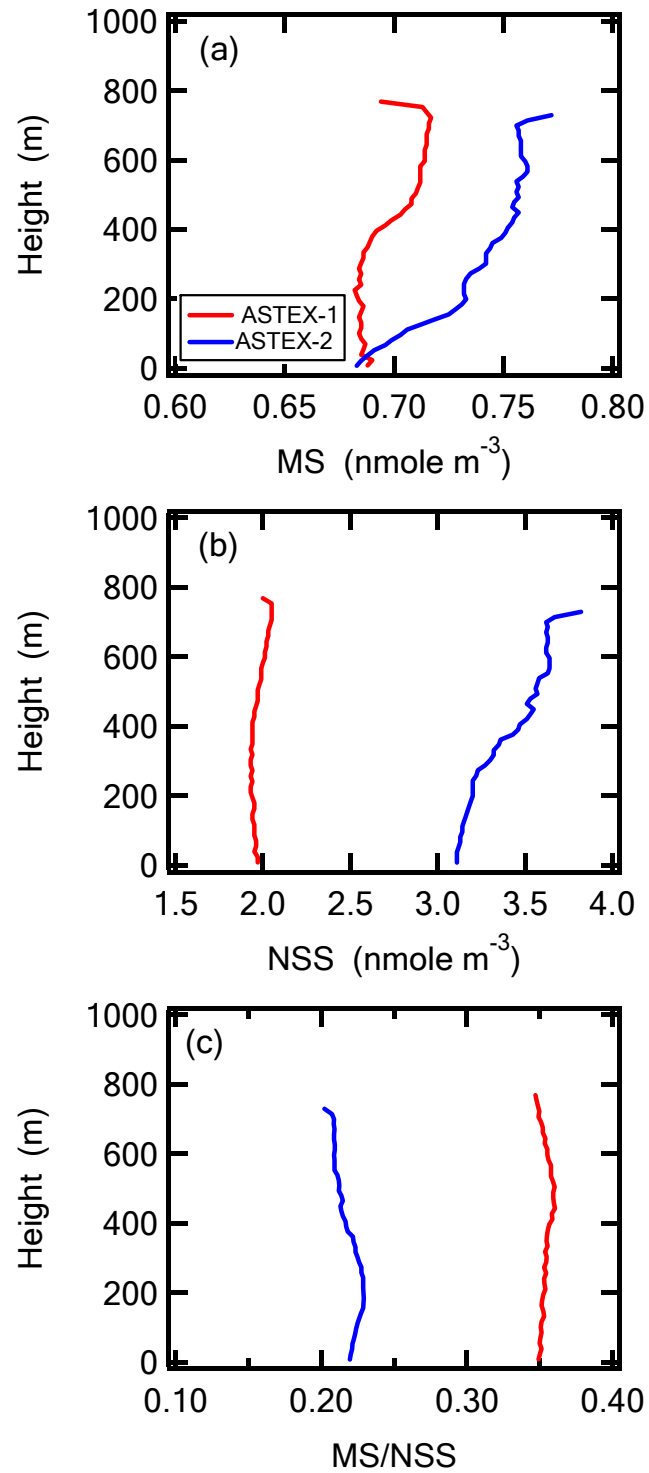


Figure 40 Vertical distribution of (a) MS, (b) NSS and (c) MS/NSS after 15 simulation cycles of the ASTEX-1(red) and the ASTEX-2 (blue) cloud

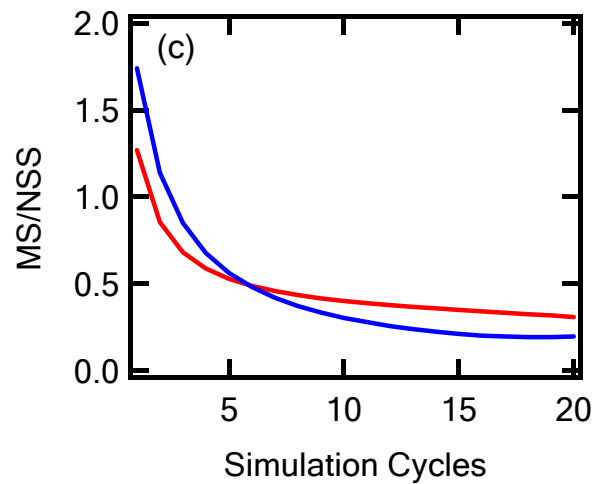
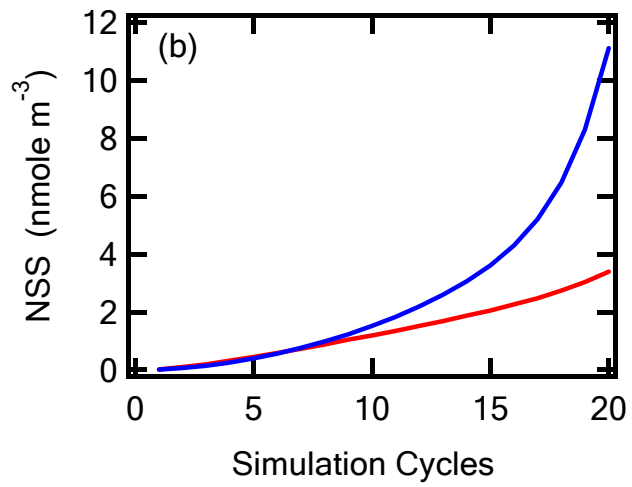
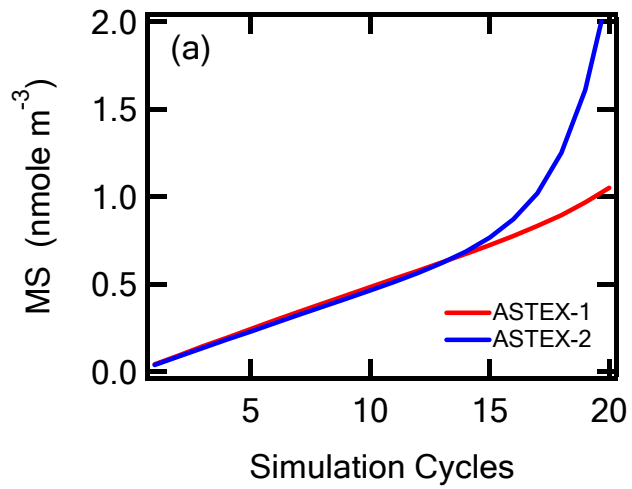


Figure 41 Temporal evolution of (a) MS, (b) NSS and (c) MS/NSS for simulations of ASTEX-1 (red) and ASTEX-2 (blue)

Our simulations suggest that heavy drizzling stratocumulus clouds favor the production of NSS and lower the MS/NSS ratio compared to the non-drizzling cloud case. The MS + OH reaction is a potentially important reason for the lower MS/NSS ratio for the ASTEX-2 cloud due to the higher liquid water content in the ASTEX-2 cloud than in the ASTEX-1 cloud. However, since the ASTEX-2 system should experience a significant wet deposition rate, how significantly drizzling clouds affect global MS/NSS ratios cannot be properly quantified unless wet deposition of particles is considered in the mass balance equation.

Comparison of Cumulus and Stratocumulus Simulations

Cumulus clouds are a primary mechanism for placing sulfur species into the upper troposphere and affect their long-range transport. A schematic plot of the trajectory dynamics in the cumulus cloud field is shown in Figure 35 (b). There are two important features of cumulus clouds that are different from stratocumulus clouds (in Figure 35 (a)): (1) cumulus clouds do not cover the whole simulation field, and (2) they do not last for the whole simulation time, i.e., the clouds form and dissipate throughout one simulation cycle. Also, only 14 out of 61 total trajectories in the cumulus cloud field go through the cloud and affect DMS oxidation through in-cloud chemistry; therefore, two trajectory sets are considered: “CF-All” contains all of 61 trajectories in the cloud field (in cloud and out of cloud); “CF-Cloud” contains only the 14 trajectories that pass through the cloud area. Analysis of trajectories in the cumulus cloud field indicates that particles stay in cloud as cloud droplets for about 23% of simulation time for “CF-Cloud”, but for only

about 5% of the time for “CF-All”. By simulating these two cumulus cloud scenarios, we can separately treat chemistry in the combined cloudy + clear sky between clouds (CF-All) vs. only in-cloud trajectories (CF-Cloud) and assess how significant the in-cloud chemistry is compared to the overall average of the simulation field for MS and NSS production. Our simulations suggest that in-cloud processes account for about 60% of MS and 56% of NSS production in the aqueous phase. These values are much lower than the estimate for the stratocumulus clouds (ASTEX-1 and ASTEX-2).

Since the main purpose of this work is to evaluate the importance of in-cloud chemistry to MS and NSS production from DMS oxidation, results from the “CF-Cloud” will be used primarily to represent the in-cloud simulations for the cumulus cloud case and to compare to results from the stratocumulus. One simulation cycle for the CF-Cloud scenario represents ~ 30 minutes in-cloud processing, and the trajectories stay in cloud for only 23% of the simulation time. Therefore, 40 simulation cycles are needed to represent 3 days of atmospheric in-cloud processing, that is simulated by only 15 cycles of the stratocumulus cloud (ASTEX-1 and ASTEX-2). However, our simulations indicate that MS and NSS production in the cumulus clouds will be very high after 40 simulation cycles (because no deposition is considered in the model), which is not possible in the atmosphere. Instead, MS and NSS obtained from 20 simulation cycles for the cumulus cloud (CF-Cloud scenario) are compared to the results obtained from 8 simulation cycles of stratocumulus (ASTEX-1), and both results represent about 1.5 days of atmospheric in-cloud processing.

In Figure 42, the temporal evolution of MS, NSS and MS/NSS from simulations of CF-Cloud and ASTEX-1 are compared. It is clear that both MS (Figure 42 (a)) and

NSS (Figure 42 (b)) production from the ASTEX-1 scenario are higher than from the CF-Cloud scenario, while the difference of NSS production between the two simulations is apparently more significant than that of MS production. As a result, MS/NSS from CF-Cloud is higher than ASTEX-1 (in Figure 42 (c)). As discussed above, the total liquid water content of the cumulus cloud is more than twice that of the ASTEX-1 (as shown in Figure 35), while the average droplet size of cumulus clouds is lower than stratocumulus; thus the total air-liquid surface area is significantly higher in cumulus clouds than in stratocumulus. Meanwhile, cumulus clouds form and dissipate during one simulation cycle, while stratocumulus clouds do not; therefore, evaporation/condensation processes occur more frequently in the cumulus trajectories than in stratocumulus. This frequent evaporation/condensation cycling favors mass transfer of DMSO into the aqueous phase over SO₂, because it takes less time for the more soluble and more reactive DMSO to achieve a pseudo-steady-state between the gas and aqueous phases. Thus, mass transfer is more important than aqueous phase reactions in affecting NSS production in particles for the cumulus cloud scenario. As a result, cumulus clouds favor the production of MS and the MS/NSS ratio obtained after 1.5 days of in-cloud processing in the CF-Cloud (0.95) is higher than that from ASTEX-1 (0.44). Our simulations suggest that aqueous phase transformations in the cumulus cloud, which often occur at the altitude defined as the “Buffer Layer” by Davis et al. (1998), play a potentially important role in controlling the high concentration of MS and the MS/NSS ratios observed in their studies.

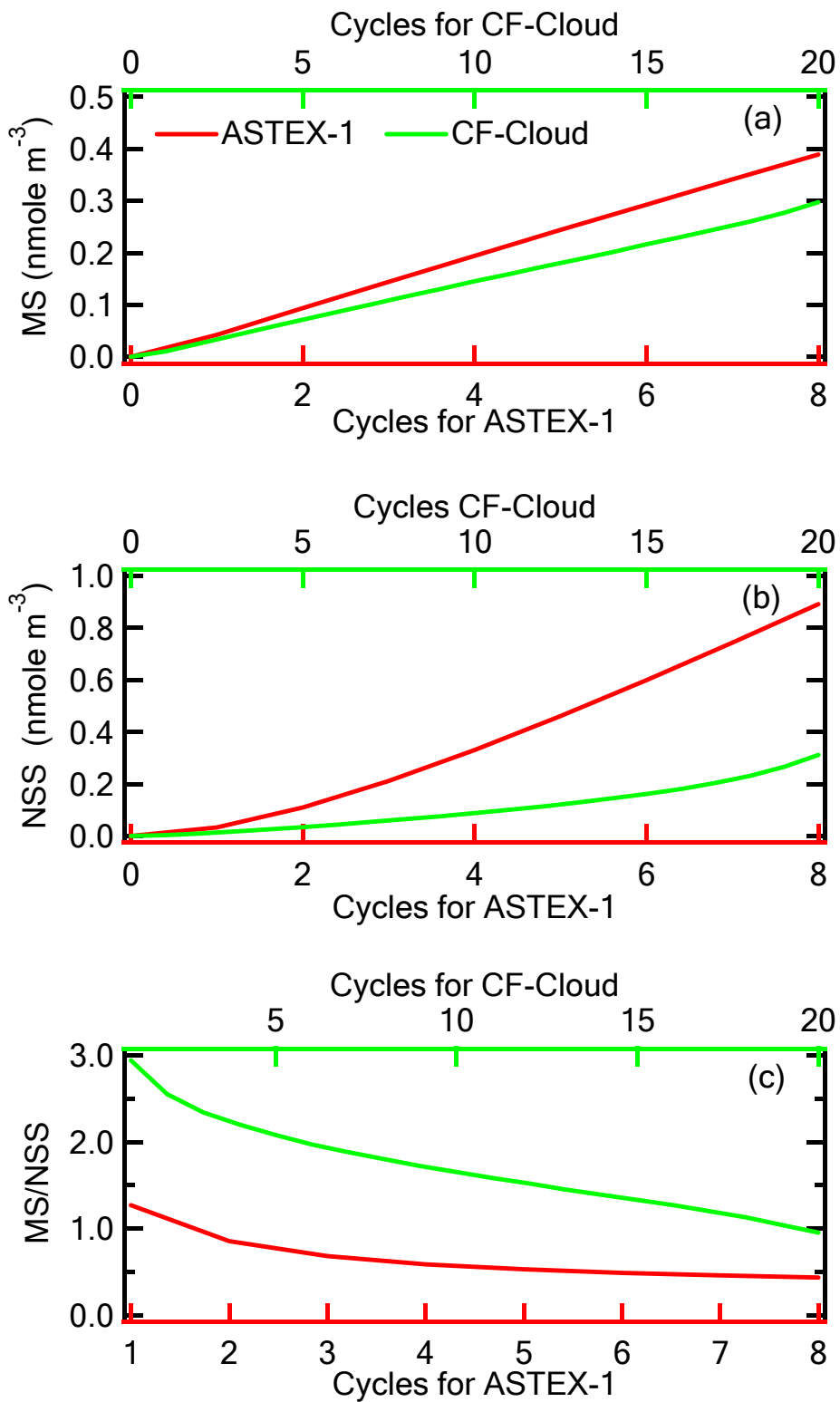


Figure 42 Temporal evolution of MS (a), NSS (b) and MS/NSS (c) for simulations of CF-Cloud (green) and ASTEX-1 (red)

Comparison with Field Observations

Although the purpose of this work is not to reproduce any observations, comparing our results with field observations could provide important information to understand the application of our simulation in the atmosphere, as well as a “sanity check” on our approach. Several representative field measurements of MS and NSS as well as MS/NSS in marine atmospheric aerosols are summarized in Table 29, and it is very obvious that the observations vary significantly with location and season, because temperature, solar radiation, radical concentrations, and dynamics of the atmosphere are all potentially important in affecting DMS oxidation and the production of MS and NSS. Also listed in the table are our results from 15 simulation cycles for the non-drizzling stratocumulus cloud field (primary scenario).

Our simulated MS concentration of 0.72 nmol m^{-3} (Figure 37 (d), after 15 simulation cycles) agrees very well with measurements in the equatorial Pacific by Davis et al. (1999) and in coastal Antarctica (summer) by Jourdain and Legrand (2001). Our estimate of MS falls well within the observation range except for the extremely low MS levels observed at coastal Antarctica during austral winter (Jourdain and Legrand 2001) and in the South Pole (Arimoto et al., 2001; Davis et al., 2004), and is $\sim 20\%$ higher than the average value of all observations in Table 29. On the other hand, our estimate of $\sim 2.1 \text{ nmol m}^{-3}$ for NSS (Figure 37 (e)) is at the lower end of field measurements, such as

those at relatively unpolluted Antarctica. The two observations from Putaud et al. (1999) and Bardouki et al. (2003) (in coastal areas where anthropogenic effects are significant) are about 15 to 30 times higher than our simulation of NSS production. Even if these two values are not considered, our NSS concentration is still about 40% lower than the average of observations listed in the table. As discussed above, the only source of NSS in our simulation is DMS oxidation, while production of NSS from other sources cannot be completely ruled out in any field measurements. Even at the South Pole, which is thought to be the least polluted place on Earth, it has been suggested that non-biogenic contributions to NSS, mainly from volcanoes as well as transport of materials from the upper troposphere and stratosphere, could be as high as 35% (Arimoto et al., 2001). As shown in Figure 37 (c), our simulated $\text{SO}_2(\text{g})$ achieves a steady-state concentration of ~ 5.8 pptv after ~ 10 simulation cycles, which is much lower than the average of ~ 40 pptv in the unpolluted marine atmosphere (see Table 29). Simulated MS/NSS after 15 simulation cycles is reduced to 0.19 when an initial concentration of 40 pptv for SO_2 is used in the simulation, and this value will further decrease to about 0.10 when 60 pptv SO_2 is used. These results further demonstrate that production of NSS from sources other than DMS oxidation is an important reason for the difference between our simulations and field observations.

As shown in Figure 37 (f), the simulated MS/NSS becomes constant with a value of ~ 0.35 after 15 simulation cycles, independent of MS and NSS concentration. This

value for MS/NSS is over twice the average of all observations listed in Table 29; when the three measurements in coastal areas are not considered, the difference between our simulation and the observation average is reduced to ~55%. In a recent study by Gondwe et al. (2004), over 50 observed MS/NSS ratios resulting from solely oceanic DMS source of MS and NSS were listed and an average value of ~ 0.25 was obtained from all these observations, which is close to the average value listed in Table 29 and is about 30% lower than our result. This comparison suggests that our model overestimates the MS/NSS ratio even if the production of NSS from other sources is excluded.

As mentioned earlier, deposition is not considered in our model, which could also lead to a higher estimate of MS/NSS. In the studies of Berresheim et al. (1998), it was found that nearly all of the NSS mass ($\sim 96\%$) occurred in the fine-particle mode while $\sim 25\%$ of MS were in the coarse-mode particles because of the lower vapor pressure of $\text{H}_2\text{SO}_4(\text{g})$ compared to $\text{MSA}(\text{g})$. Given the higher deposition rate of coarse particles vs. fine particles, the MS loss rate in the atmosphere is expected to be faster than the NSS removal rate, which would decrease observed MS/NSS ratios; this effect cannot be accounted for in our model.

An important factor determining the simulated MS/NSS ratio is the gas phase DMS oxidation mechanism. As discussed above, the detailed DMS oxidation mechanism is not well established yet, therefore, each branching ratio speculated in our chemistry mechanism (Table 21) brings with it an uncertainty to the simulation results. The DMSO

distribution between the gas and aqueous phases plays a key role in determining the MS/NSS ratio in the aqueous phase, while large uncertainties in the product yield of DMSO from the addition channel of DMS oxidation, the Henry's Law constant for DMSO as well as the oxidation mechanism of DMSO in both the gas and the aqueous phases make it impossible to assess the fate of DMSO in the atmosphere accurately. In our chemistry mechanism, SO₂ is the main gas phase end product from both the addition and the abstraction channels of DMS oxidation. However, the detailed mechanism and product yield of SO₂ from CH₃S and MSIA are far from enough to estimate the conversion efficiency of SO₂ from DMS more accurately. These uncertainties make our simulations only an approximate method for evaluating MS and NSS production under the conditions in our model when the chemistry mechanism shown in Figure 1 is applied.

We also found that the simulated MS/NSS ratio is very sensitive to the steady-state concentration of gas phase radicals. As BrO increases from 10⁶ to 10⁷ to 10⁸ molecules cm⁻³, MS/NSS increases from 0.13 to 0.35 to 1.70. This trend supports the assessment of von Glasow and Crutzen (2004), and suggests that BrO can strongly influence the yield of SO₂ from DMS as well as the MS/NSS ratio. Because the BrO + DMS reaction produces primarily DMSO, which is quite efficiently taken-up by particles/droplets, this reaction affects the distribution of sulfur species between the gas and aqueous phases. Based on the above results, the lower limit of BrO concentrations from several studies (Sander and Crutzen 1996; Vogt et al., 1996; von Glasow and

Crutzen 2004) was chosen in our “primary scenario”. The steady-state concentrations of OH(g), NO₃(g) and Cl(g) also affect MS/NSS and the SO₂ yield, but to a much smaller extent than BrO(g): as the concentration of OH(g) increases from 10⁵ to 10⁷ molecules cm⁻³, MS/NSS decreases from 0.55 to 0.16; for the same adjustment of NO₃(g) concentration, MS/NSS decreases from 0.39 to 0.18; and when Cl increases from 10³ to 10⁵ molecules cm⁻³, MS/NSS decreases from 0.49 to 0.10. These results indicate that OH(g), NO₃(g) and Cl(g) all favor the production of NSS because the DMS reactions with these radicals proceed primarily (exclusively for NO₃) *via* the abstraction channel at the temperature used in the simulations (~300 K). Typical average concentrations in the marine boundary layer atmosphere are used as the steady-state concentrations of radicals in our model. Given the large variations in radical speciation and concentration with location and altitude, our simulation results can be used only as an average assessment, and could deviate from some measurements under conditions quite different from those in our model. As an example, it was proposed that the only important oxidant of DMS in the Antarctica area is the OH radical (Arimoto et al., 2001; Davis et al., 2004). When OH is the only radical, with an average concentration of 10⁶ molecule cm⁻³, in our model, the simulated MS/NSS ratio decreases to <0.2, which is over 45% lower than the result from the simulation of the primary scenario.

It is also worth noting that the MS/NSS ratio simulated from our model represents the value that will be observed when the oxidation of local oceanic DMS is the only

source of MS and NSS under the conditions considered. However, in the field observations, both vertical and horizontal transport of sulfur compounds play important roles in the observed levels of the DMS oxidation products. In two recent missions to investigate sulfur chemistry in the Antarctic Troposphere (ISCAT), MS/NSS ratios of 0.06 and 0.05 were observed at the South Pole (Arimoto et al., 2001; Davis et al., 2004), close to the value of 0.07-0.08 observed in the tropical areas (Saltzman et al., 1983; Davis et al., 1999), as listed in Table 29. These observations are in conflict with our simulations at different temperatures. Our simulations suggest that the MS/NSS ratio increases with decreasing temperature, so it is expected that the MS/NSS ratio in the South Pole is lower than that observed in the equatorial areas. However, the very low DMS concentrations observed in the South Pole suggest that both DMS and its oxidation products are from the long range transport of oceanic emissions. Thus, oxidation of DMS at different locations and altitudes are potentially responsible for the observed levels of MS and NSS, and it is quite likely that the chemistry mechanism of DMS oxidation varies with locations and altitude. In the studies from Davis et al. (1998) in the Antarctic, numerous abrupt enhancements were seen in the mixing ratios of gas phase DMSO and DMSO₂, which were speculated to be from the frequent episodes of rapid vertical transport between the very shallow boundary layer and the overlying “Buffer layer”. Due to the combination of long photochemical lifetime of DMS and the frequency of shallow convective events, a large fraction of oceanic DMS is transported into the “buffer layer” before being oxidized. In the “buffer layer”, oxidized sulfur compounds accumulate due

to lower humidity and aerosol concentration. Meanwhile, photo-oxidation becomes the dominant sink for DMSO, leading to higher production rate of SO₂ and H₂SO₄; thus nucleation of H₂SO₄ is possible to form fine particles within the “buffer layer”. On the other hand, given the very low water vapor pressure in the “buffer layer”, MSA is more likely to evaporate from the dry particles than H₂SO₄ when they are transported into the “buffer layer” from the boundary layer (private communications, Rodney Weber). As a result, when these particles are re-entrained into the boundary layer, the MS/NSS ratio in the particles is evidently reduced while higher levels of DMSO, DMSO₂ and MSA in the gas phase are observed.

In summary, our simulations represent the product distribution from the oxidation of DMS in the marine boundary layer atmosphere under cloudy conditions when the local oceanic DMS is the only sulfur source and the chemistry mechanism shown in Figure 1 is applied. Production of NSS from other sulfur sources, deposition of particles to the surface, variations in DMS oxidation mechanism and radical speciation and concentration with location and altitude, as well as vertical and horizontal transport all play significant roles in the wide range of observed levels of DMS oxidation products, as shown in Table 29; and they are all potentially important in explaining the difference between these field observations with our simulations.

Table 29 Examples of field measurements of DMS, SO₂ (pptv), MS, NSS (nmol m⁻³) and MS/NSS in the marine atmosphere

DMS	SO ₂	MS	NSS	MS/NSS	Location, Season	Source
—	—	0.4±0.3	5.9±3.5	0.07	the Pacific and Indian oceans and Sourthern Florida, multi-year	(Saltzman et al., 1983)
75±15	65±15	0.7±0.07	8.5±1.0	0.08	Equatorial Pacific, August	(Davis et al., 1999)
60±40	—	0.5±0.4	2.5±3.0	0.2	Sourthern Austrilian Baseline, multi-year	(Ayers and Gillett 2000)
119±94	—	1.9±1.5	2.5±2.1	0.73	Palmer Station, Antarctica, austral summer	(Berresheim et al., 1998)
290±140	63±20	0.6±0.3	3.8±1.4	0.16	Coastal Antarctica, austral summer	(Jourdain and Legrand 2001)
1.7±3.9	—	0.13±0.01	2.2±0.1	0.06	South Pole, austral summer	(Arimoto et al., 2001)
4.2±3.0	7.8±10	0.05±0.03	1.0±0.2	0.05	South Pole, austral summer	(Davis et al., 2004)
—	—	0.2±0.3	0.9±0.9	0.26	Three Antarctic sites, multi-year	(Savoie et al., 1993)
87±29	5.6	0.01±0.004	0.2±0.2	0.05	Coastal Antarctica, austral winter	(Jourdain and Legrand 2001)
50±30	30±10	0.20±0.15	4.2±3.2	0.032	The Northeastern Pacific coast, April	(Berresheim et al., 1993)
570±560	540±300	1.1±0.7	33±37	0.034	France coast, May-June	(Putaud et al., 1999)
22±22	1030±600	0.5±0.26	64±34	0.008	Eastern Mediterranean coast, July-August	(Bardouki et al., 2003)
Our results						
100	5.8	0.72	2.1	0.35		

CHAPTER IX

SUMMARY AND CONCLUSIONS

In this dissertation a Laser Flash Photolysis – Long Path UV-visible Absorption technique was employed to investigate the kinetics of aqueous phase reactions of SO_4^- , OH, Cl and Cl_2^- with DMSO, DMSO₂, MSI and MS. Reactivity ($295 \pm 1 \text{ K}$) in the order of $\text{OH} > \text{Cl} > \text{SO}_4^- > \text{Cl}_2^-$ for radicals and $\text{DMSO} \approx \text{MSI} > \text{DMSO}_2 > \text{MS}$ for organo-sulfur compounds were found, in agreement with most previous kinetic studies of reactions of the above radicals with a variety of organics (Clifton and Huie 1989; Huie and Clifton 1989; Padmaja et al., 1992; Chin and Wine 1994; George et al., 2001; Martire et al., 2001; Ervens et al., 2003; George et al., 2003) and also in agreement with the limited data base on radical reactions with the sulfur compounds of interest (Meissner et al., 1967; Veltwisch et al., 1980; Kishore and Asmus 1989, 1991; Milne et al., 1989; Sehested and Holcman 1996; Flyunt et al., 2001; Bardouki et al., 2002). For SO_4^- and OH reactions with DMSO, DMSO₂ and MS, temperature dependent kinetics were studied for the first time over a temperature range of atmospheric interest. The activation energies of the $\text{MS} + \text{OH}$ and $\text{MS} + \text{SO}_4^-$ reactions were found to be the largest; thus the rate coefficients for these reactions change the most with temperature, which is potentially important in the atmosphere. A summary of kinetics studies was given in Chapter VII.

Summarized in Table 30 are estimated lifetimes of DMSO, DMSO₂, MSI and MS toward (a) loss from the gas phase by uptake into particles and/or aqueous droplets and (b)

aqueous phase destruction *via* reactions with OH, Cl, SO₄⁻ and Cl₂⁻ radicals at room temperature (T = 295 ± 1 K). The diurnally averaged radical concentrations are obtained from photochemical modeling studies (Jacob et al., 1989; Lelieveld and Crutzen 1991; Herrmann et al., 2000). It is worth noting that while the radical concentrations given in Table 30 are reasonable estimates for the specified environments (see footnotes in the Table), these concentrations are subject to considerable variability depending upon the average solar zenith angle and the chemical composition of the environment; as a result, the lifetimes in Table 30 should be considered rough estimates. The estimate of the aqueous phase lifetime was based on our kinetic data and on the assumptions that (1) aerosol particles spend about 3 hours per day as cloud droplets and (2) oxidation by the radicals occurs only during the aqueous droplet phase of the particle/droplet cycle (Katoshevski et al., 1999).

It is typically the case for aqueous phase radical-molecule reactions that ratios of rate coefficients for reactions of a pair of radicals with the same molecular reactant increase in favor of the more reactive radical as the reactivity of the molecular reactant decreases (Neta et al., 1988). Therefore, in spite of the extremely high concentration of Cl₂⁻, very slow reaction rates make it highly unlikely to compete with OH as a sink for the relatively unreactive species DMSO₂ and MS. Indeed, our simulations have found that the only significant loss of DMSO₂ and MS is reaction with OH. For the very reactive DMSO and MSI, however, reactions with all these radicals are potentially important for removing them from the atmosphere. Our simulations indicate that MSI + Cl₂⁻ dominates MSI + OH as a MSI loss pathway, while OH is more efficient in removing DMSO than either SO₄⁻ or Cl₂⁻.

Table 30 Estimated lifetimes of DMSO, DMSO₂, MSI and MS at 295 K
toward (a) uptake into aerosols under remote tropospheric conditions and
(b) aqueous phase destruction *via* reactions with SO₄⁻, OH, Cl and Cl₂⁻
radicals.

Process	Radical* Conc. (M)	τ_x (hrs)			
		DMSO	DMSO ₂	MSI	MS
X(g) → R(aq) [†]		1–15 ^c	1–15 ^c	1–15 ^c	1–15 ^c
SO ₄ ⁻ (aq) + R(aq) [‡]	1 × 10 ⁻¹² a	0.7 ^d	>580 ^d	1.2 ^m	2.2 × 10 ⁴ d
OH(aq) + R(aq) [‡]	6 × 10 ⁻¹³ a	0.6 ^d	>220 ^d	0.5 ^e	310 ^d
Cl(aq) + R(aq) [‡]	1 × 10 ⁻¹³ b	0.4 ^d	>2720 ^d	—	4520 ^d
Cl ₂ ⁻ (aq) + R(aq) [‡]	1 × 10 ⁻¹¹ a	14 ^d	>2.7 × 10 ⁴ d	0.3 ^d	5.7 × 10 ⁴ d

* The radical concentrations refer to: ^a Global diurnally averaged ^a Typical diurnally averaged concentration in marine boundary layer cloud droplets (Lelieveld and Crutzen 1991; Herrmann et al., 2000); ^b Calculated from [Cl₂⁻], typical [Cl⁻] = 6.0 × 10⁻⁴ M (Herrmann et al., 1996), and equilibrium constant of Cl + Cl⁻ ↔ Cl₂⁻, K = 1.4 × 10⁵ M⁻¹ (Yu et al., 2004).

[†] From field observations in the Antarctic troposphere by: ^c (Jefferson et al., 1998).

[‡] Calculated based on kinetic data from: ^d This work; ^e (Flyunt et al., 2001); and the assumption that marine boundary layer aerosol particles spend about 3 hours per day as cloud droplets (Katoshevski et al., 1999).

All the studied reactions convert the relatively volatile sulfur species such as DMSO and DMSO₂ to the less volatile product(s), MSI, MS and SO₄²⁻, which are less likely to return to the gas phase upon particle evaporation. Therefore aqueous phase oxidation of organic sulfur compounds may contribute to particle growth during droplet formation/evaporation cycling. In order to quantitatively address these issues, a DMS oxidation mechanism was proposed in this work based on our kinetics studies and a variety of literature concerning gas phase kinetics and gas phase-to-aqueous phase mass transfer. For the first time, aqueous phase oxidation of organo-sulfur compounds by SO₄⁻, Cl and Cl₂⁻ is included in a model to simulate DMS oxidation. Incorporation of this chemistry mechanism (Figure 1 and Tables 21 and 22) into the Trajectory Ensemble Model (TEM) allows simulation of MS and NSS production as well as MS/NSS ratios in both stratocumulus and cumulus clouds.

Our simulations have found that the MS and NSS production rates are proportional to the initial DMS concentration, while the MS/NSS ratio is independent of the DMS concentration employed. The steady state concentration of BrO(g) plays an important role in determining the conversion yield of SO₂ from DMS and the MS/NSS ratio. Using the best estimates of all parameters in the model, MS and NSS production after 3 days of in-cloud processings are estimated to be 0.7 and 2.1, respectively, for non-drizzling stratocumulus clouds (ASTEX-1) and 0.8 and 3.6, respectively, for heavy-drizzling stratocumulus clouds (ASTEX-2), in units of nmol m⁻³, at 300 K assuming an ambient DMS concentration of 100 ppt. These results give MS/NSS ratios of 0.35 and 0.2 for the above two types of clouds. The higher production of NSS in the ASTEX-2 cloud is because of its higher liquid water content compared to the ASTEX-1 cloud. Our

estimate of the MS/NSS ratio is somewhat higher than the average value obtained from field observations (Table 26); addition of NSS from sources other than DMS oxidation, and incorporation of deposition of MS and NSS in the atmosphere would apparently account for the difference between our estimate and field observations.

Simulations of the ASTEX-1, the most abundant cloud form in the marine boundary layer, have found that aqueous phase oxidation of organo-sulfur compounds contributes 30% of total particulate mass growth due to DMS oxidation, while oxidation of S(IV) to S(VI) is the most important source of non-volatile sulfur species in the condensed phase and accounts for 63% of this mass increase. The other 7% is from mass transfer of gas phase MSA and H₂SO₄. Uptake from the gas phase accounts for only about 3% of MS and 9% of NSS total production in particles at 300 K and these contributions tend to increase with increasing temperature.

For the first time, temperature dependent kinetics of the MS + OH reaction are considered in a DMS chemistry model. Our simulations at 300 K for the ASTEX-1 cloud found that the MS + OH reaction could scavenge ~ 20% of MS and contribute 8% of total NSS production in 3 days, thereby decreasing the MS/NSS ratio by ~ 25%. The contribution of the MS + OH reaction to NSS production increases with increasing temperature due to the high activation energy of this reaction and decreased production rate of MS and NSS at high temperatures.

The TEM approach was also used to simulate DMS oxidation in cumulus clouds. Simulations indicate that in-cloud chemistry accounts for about 35% of MS and 26 % of NSS total production and produces 0.53 nmol m⁻³ MS and 1.14 nmol m⁻³ NSS after three

days of in-cloud processing, for a typical marine boundary layer DMS concentration of 100 pptv. Higher liquid water content, smaller droplet size and the shorter lifetime of cumulus clouds result in the higher MS production compared to the stratocumulus cloud for the same in-cloud time. Frequent condensation/evaporation cycles in the cumulus cloud area make mass transfer of DMSO and SO₂ into the aqueous phase the rate-limiting step for MS and NSS production. Given the higher solubility and reactivity of DMSO compared to SO₂, cumulus clouds favor the production of MS. Hence estimated MS/NSS ratios for cumulus clouds are higher than for stratocumulus clouds, which is potentially important in explaining differences in MS/NSS ratios observed in the marine boundary layer and the “buffer layer”.

Recommendations for Future Kinetics Studies

Given the fast $\text{MSI} + \text{Cl}_2^-$ reaction rate coefficient and the high concentration of Cl_2^- , our simulations suggest that $\text{MSI} + \text{Cl}_2^-$ is the most important direct source of MS, and contributes $\sim 65\%$ of total MS production. Using the $\text{MSI} + \text{OH}$ rate coefficient obtained from this work, the $\text{MSI} + \text{OH}$ reaction was found to account for only about 25% of total MS production. Since a very complicated data analysis method was employed to obtain the $\text{MSI} + \text{OH}$ reaction kinetics because of the reaction of MSI with SCN and $(\text{SCN})_2^-$, studies of this reaction using a different competitor, such as ferricyanide ($\text{Fe}(\text{SCN})_6^{2-}$), might provide more evidence on the viability of the results from this kinetics study. In addition, temperature dependent studies of these two reactions are necessary given their importance in MS production.

$\text{MSI} + \text{SO}_4^-$ was not included in this dissertation, although some preliminary results obtained from studies of this reaction found a rate coefficient of about $1.0 \times 10^9 \text{ M}^{-1} \text{ s}^{-1}$ at room temperature, which is $\sim 40\%$ lower than the only literature value (Flyunt et al., 2001). Further studies of this reaction and studies of oxidation of organic sulfur compounds by other aqueous phase radicals of potential atmospheric importance, i.e., NO_3 , Br/Br_2^- , and CO_3^- radicals, would also be desirable.

Finally, additional detailed mechanistic studies of the oxidation of the organic sulfur compounds and the production of MS and SO_4^{2-} would be useful for furthering our understanding of DMS oxidation in the atmosphere and observed MS/NSS ratios in the atmospheric condensed phase.

References

- Akiho, S., O. Ito and M. Iino (1989). "Flash-Photolysis Study for Reactions of NO₃. With Sulfur-Compounds in Acetonitrile Solution." *International Journal of Chemical Kinetics* **21**(8): 667-676.
- Albrecht, B. A. (1989). "Aerosols, Cloud Microphysics, and Fractional Cloudiness." *Science* **245**(4923): 1227-1230.
- Albrecht, B. A., C. S. Bretherton, D. Johnson, W. H. Scubert and A. S. Frisch (1995). "The Atlantic Stratocumulus Transition Experiment - Astex." *Bulletin of the American Meteorological Society* **76**(6): 889-904.
- Amels, P., H. Elias and K. J. Wannowius (1997). "Kinetics and mechanism of the oxidation of dimethyl sulfide by hydroperoxides in aqueous medium - Study on the potential contribution of liquid-phase oxidation of dimethyl sulfide in the atmosphere." *Journal of the Chemical Society-Faraday Transactions* **93**(15): 2537-2544.
- Andreae, M. O. and W. Jaeschke (1992). Exchange of sulfur between biosphere and atmosphere over temperate and tropical regions. *Sulfur cycle on the continents*. R. W. Howarth, J. W. B. Stewart and M. V. Ivanov. Chichester, John Wiley & Sons: 27-61.
- Andreae, M. O. and P. J. Crutzen (1997). "Atmospheric aerosols: Biogeochemical sources and role in atmospheric chemistry." *Science* **276**(5315): 1052-1058.
- Anklam, E., H. Mohan and K. D. Asmus (1988). "2σ-1σ* 3-Electron-Bonded Radical Cations from Alkylthio(Halogeno)Alkanes." *Journal of the Chemical Society-Perkin Transactions* **2**(7): 1297-1302.
- Anklam, E., K. D. Asmus and H. Mohan (1990). "Structure and Stability of 2σ/1σ* 3-Electron-Bonded Radical Cations from 1,N-Bis(Alkylthio)Alkanes in Aqueous-Solutions." *Journal of Physical Organic Chemistry* **3**(1): 17-22.
- Arimoto, R., A. S. Nottingham, J. Webb, C. A. Schloesslin and D. D. Davis (2001). "Non-sea salt sulfate and other aerosol constituents at the South Pole during ISCAT." *Geophysical Research Letters* **28**(19): 3645-3648.
- Arsene, C., I. Barnes and K. H. Becker (1999). "FT-IR product study of the photo-oxidation of dimethyl sulfide: Temperature and O₂ partial pressure dependence." *Physical Chemistry Chemical Physics* **1**(24): 5463-5470.

- Arsene, C., I. Barnes, K. H. Becker and R. Mocanu (2001). "FT-IR product study on the photo-oxidation of dimethyl sulphide in the presence of NO_x - temperature dependence." *Atmospheric Environment* **35**(22): 3769-3780.
- Arsene, C., I. Barnes, K. H. Becker, W. F. Schneider, T. T. Wallington, N. Mihalopoulos and I. V. Patroescu-Klotz (2002). "Formation of methane sulfinic acid in the gas-phase OH-radical initiated oxidation of dimethyl sulfoxide." *Environmental Science & Technology* **36**(23): 5155-5163.
- Atkinson, R., D. L. Baulch, R. A. Cox, R. F. Hampson, J. A. Kerr, M. J. Rossi and J. Troe (1997). "Evaluated kinetic and photochemical data for atmospheric chemistry: Supplement VI - IUPAC subcommittee on gas kinetic data evaluation for atmospheric chemistry." *Journal of Physical and Chemical Reference Data* **26**(6): 1329-1499.
- Atkinson, R., D. L. Baulch, R. A. Cox, J. N. Crowley, R. F. J. Hampson, J. A. Kerr, M. J. Rossi and J. Troe (2001). "Summary of Evaluated Kinetic and Photochemical Data for Atmospheric Chemistry: IUPAC Subcommittee on Gas Kinetic Data Evaluation for Atmospheric Chemistry Web Version December 2001." 1-56.
- Atkinson, R., D. L. Baulch, R. A. Cox, J. N. Crowley, R. F. Hampson, J. A. Kerr, M. J. Rossi and J. Troe (2002). "Summary of Evaluated Kinetic and Photochemical Data for Atmospheric Chemistry." *Web Version*.
- Ayers, G. P., J. M. Cainey, R. W. Gillett, E. S. Saltzman and M. Hooper (1997). "Sulfur dioxide and dimethyl sulfide in marine air at Cape Grim, Tasmania." *Tellus Series B-Chemical and Physical Meteorology* **49**(3): 292-299.
- Ayers, G. P. and R. W. Gillett (2000). "DMS and its oxidation products in the remote marine atmosphere: implications for climate and atmospheric chemistry." *Journal of Sea Research* **43**(3-4): 275-286.
- Bao, Z. C. and J. R. Barker (1996). "Temperature and ionic strength effects on some reactions involving sulfate radical [SO₄⁻(aq)]." *Journal of Physical Chemistry* **100**(23): 9780-9787.
- Bardouki, H., M. B. da Rosa, N. Mihalopoulos, W. U. Palm and C. Zetzsch (2002). "Kinetics and mechanism of the oxidation of dimethylsulfoxide (DMSO) and methanesulfinate (MSI) by OH radicals in aqueous medium." *Atmospheric Environment* **36**(29): 4627-4634.
- Bardouki, H., H. Berresheim, M. Vrekoussis, J. Sciare, G. Kouvarakis, K. Oikonomou, J. Schneider and N. Mihalopoulos (2003). "Gaseous (DMS, MSA, SO₂, H₂SO₄ and DMSO) and particulate (sulfate and methanesulfonate) sulfur species over the northeastern coast of Crete." *Atmospheric Chemistry and Physics* **3**: 1871-1886.

- Barnes, I., V. Bastian, K. H. Becker and D. Martin (1989). "Fourier-Transform IR Studies of the Reactions of Dimethyl-Sulfoxide with OH, NO₃, and Cl Radicals." *Acs Symposium Series* **393**: 476-488.
- Barnes, I., V. Bastian, K. H. Becker and R. D. Overath (1991). "Kinetic-Studies of the Reactions of IO, BrO, and ClO with Dimethylsulfide." *International Journal of Chemical Kinetics* **23**(7): 579-591.
- Barnes, I., K. H. Becker and I. Patroescu (1994). "The Tropospheric Oxidation of Dimethyl Sulfide - a New Source of Carbonyl Sulfide." *Geophysical Research Letters* **21**(22): 2389-2392.
- Barone, S. B., A. A. Turnipseed and A. R. Ravishankara (1995). "Role of adducts in the atmospheric oxidation of dimethyl sulfide." *Faraday Discussions*(100): 39-54.
- Barone, S. B., A. A. Turnipseed and A. R. Ravishankara (1996). "Reaction of OH with dimethyl sulfide (DMS) .1. Equilibrium constant for OH+DMS reaction and the kinetics of the OH-DMS+O₂ reaction." *Journal of Physical Chemistry* **100**(35): 14694-14702.
- Barry, R. G. and R. J. Chorley (1998). *Atmosphere, Weather & Climate*. Routledge.
- Bates, T. S., J. D. Cline, R. H. Gammon and S. R. Kellyhansen (1987). "Regional and Seasonal-Variations in the Flux of Oceanic Dimethylsulfide to the Atmosphere." *Journal of Geophysical Research-Oceans* **92**(C3): 2930-2938.
- Bates, T. S., B. K. Lamb, A. Guenther, J. Dignon and R. E. Stoiber (1992). "Sulfur Emissions to the Atmosphere from Natural Sources." *Journal of Atmospheric Chemistry* **14**(1-4): 315-337.
- Baxendale, J. H., P. T. Bevan and D. A. Stott (1968). "Pulse radiolysis of aqueous thiocyanate and iodide solutions." *Trans. Far. Soc.* **64**: 2389-2397.
- Baxendale, J. H. and P. L. T. Bevan (1969). "Energetics of formation of I₂⁻ and (CNS)₂⁻ in aqueous solution." *J. Chem. Soc. A*: 2240-2241.
- Bedjanian, Y., G. Poulet and G. LeBras (1996). "Kinetic study of the reaction of BrO radicals with dimethylsulfide." *International Journal of Chemical Kinetics* **28**(5): 383-389.
- Behar, D., P. L. T. Bevan and G. Scholes (1972). "Pulse Radiolysis of Aqueous Thiocyanate Solutions - Nature of Intermediate Transient Species." *Journal of Physical Chemistry* **76**(11): 1537-1542.
- Benkovitz, C. M., C. M. Berkowitz, R. C. Easter, S. Nemesure, R. Wagener and S. E. Schwartz (1994). "Sulfate over the North-Atlantic and Adjacent Continental

- Regions - Evaluation for October and November 1986 Using a 3-Dimensional Model-Driven by Observation-Derived Meteorology." *Journal of Geophysical Research-Atmospheres* **99**(D10): 20725-20756.
- Berdniko.Vm and N. M. Bazhin (1970). "Oxidation-Reduction Potentials of Certain Inorganic Radicals in Aqueous Solutions." *Russian Journal of Physical Chemistry, Ussr* **44**(3): 395-398.
- Berresheim, H., M. O. Andreae, R. L. Iverson and S. M. Li (1991). "Seasonal-Variations of Dimethylsulfide Emissions and Atmospheric Sulfur and Nitrogen Species over the Western North-Atlantic Ocean." *Tellus Series B-Chemical and Physical Meteorology* **43**(5): 353-372.
- Berresheim, H., F. L. Eisele, D. J. Tanner, L. M. McInnes, D. C. Ramseybell and D. S. Covert (1993). "Atmospheric Sulfur Chemistry and Cloud Condensation Nuclei (CCN) Concentrations over the Northeastern Pacific Coast." *Journal of Geophysical Research-Atmospheres* **98**(D7): 12701-12711.
- Berresheim, H., P. H. Wine and D. Davis (1995). Sulfur in the Atmosphere. *Composition, Chemistry and Climate of the Atmosphere*. R. K. Singh. New York, Van Nostrand Reinhold: 251-307.
- Berresheim, H. and F. L. Eisele (1998). "Sulfur Chemistry in the Antarctic Troposphere Experiment: An overview of project SCATE." *Journal of Geophysical Research-Atmospheres* **103**(D1): 1619-1627.
- Berresheim, H., J. W. Huey, R. P. Thorn, F. L. Eisele, D. J. Tanner and A. Jefferson (1998). "Measurements of dimethyl sulfide, dimethyl sulfoxide, dimethyl sulfone, and aerosol ions at Palmer Station, Antarctica." *Journal of Geophysical Research-Atmospheres* **103**(D1): 1629-1637.
- Betterton, E. A. (1992). "Henry's law constants of soluble and moderately soluble organic gases: Effects on aqueous phase chemistry." *Advances in Environmental Science and Technology* **24**: 1-50.
- Bonifacic, M., H. Mockel, D. Bahnemann and K. D. Asmus (1975). "Formation of Positive-Ions and Other Primary Species in Oxidation of Sulfides by Hydroxyl Radicals." *Journal of the Chemical Society-Perkin Transactions* **2**(7): 675-685.
- Bonifacic, M. and K. D. Asmus (1980). "Stabilization of Oxidized Sulfur Centers by Halide-Ions - Formation and Properties of R₂S-X Radicals in Aqueous-Solutions." *Journal of the Chemical Society-Perkin Transactions* **2**(5): 758-762.
- Brimblecombe, P. and S. L. Clegg (1988). "The Solubility and Behavior of Acid Gases in the Marine Aerosol." *Journal of Atmospheric Chemistry* **7**(1): 1-18.

- Butkovskaya, N. I. and G. Lebras (1994). "Mechanism of the NO_3 +DMS Reaction by Discharge Flow Mass-Spectrometry." *Journal of Physical Chemistry* **98**(10): 2582-2591.
- Butkovskaya, N. I., G. Poulet and G. Lebras (1995). "Discharge Flow Study of the Reactions of Chlorine and Fluorine-Atoms with Dimethyl Sulfide." *Journal of Physical Chemistry* **99**(13): 4536-4543.
- Butler, J., E. J. Land, W. A. Prutz and A. J. Swallow (1982). "Charge-Transfer between Tryptophan and Tyrosine in Proteins." *Biochimica Et Biophysica Acta* **705**(2): 150-162.
- Buxton, G. V., S. McGowan, G. A. Salmon, J. E. Williams and N. D. Woods (1996). "A study of the spectra and reactivity of oxysulphur-radical anions involved in the chain oxidation of S(IV): A pulse and gamma-radiolysis study." *Atmospheric Environment* **30**(14): 2483-2493.
- Buxton, G. V., M. Bydder and G. A. Salmon (1998). "Reactivity of chlorine atoms in aqueous solution - Part 1 The equilibrium $\text{Cl} + \text{Cl}^- \rightleftharpoons \text{Cl}_2^-$." *Journal of the Chemical Society-Faraday Transactions* **94**(5): 653-657.
- Buxton, G. V., M. Bydder and G. A. Salmon (1999). "The reactivity of chlorine atoms in aqueous solution - Part II. The equilibrium $\text{SO}_4^- + \text{Cl}^- \rightleftharpoons \text{Cl} + \text{SO}_4^{2-}$." *Physical Chemistry Chemical Physics* **1**(2): 269-273.
- Buxton, G. V. and G. A. Salmon (2003). "On the chemistry of inorganic free radicals in cloud water." *Progress in Reaction Kinetics and Mechanism* **28**(3): 257-297.
- Cabelli, D. E. and B. H. J. Bielski (1985). "A Pulse-Radiolysis Study of Some Dicarboxylic-Acids of the Citric-Acid Cycle - the Kinetics and Spectral Properties of the Free-Radicals Formed by Reaction with the OH Radical." *Zeitschrift Fur Naturforschung Section B-a Journal of Chemical Sciences* **40**(12): 1731-1737.
- Campolongo, F., A. Saltelli, N. R. Jensen, J. Wilson and J. Hjorth (1999). "The role of multiphase chemistry in the oxidation of dimethylsulphide (DMS). A latitude dependent analysis." *Journal of Atmospheric Chemistry* **32**(3): 327-356.
- Capaldo, K. P. and S. N. Pandis (1997). "Dimethylsulfide chemistry in the remote marine atmosphere: Evaluation and sensitivity analysis of available mechanisms." *Journal of Geophysical Research-Atmospheres* **102**(D19): 23251-23267.
- Carshaw, N., L. J. Carpenter, J. M. C. Plane, B. J. Allan, R. A. Burgess, K. C. Clemitshaw, H. Coe and S. A. Penkett (1997). "Simultaneous observations of nitrate and peroxy radicals in the marine boundary layer." *Journal of Geophysical Research-Atmospheres* **102**(D15): 18917-18933.

- Challenger, F. and M. I. Simpson (1948). "Studies on biological methylation. Part XII. A precursor of the dimethylsulfide evolved by *Polysiphonia fastigiata*. Dimethyl-2-carboxyethyl sulphonium hydroxide and its salts." *J. Chem. Soc.*: 1591-1597.
- Chameides, W. L. and D. D. Davis (1982). "The Free-Radical Chemistry of Cloud Droplets and Its Impact Upon the Composition of Rain." *Journal of Geophysical Research-Oceans and Atmospheres* **87**(NC7): 4863-4877.
- Chameides, W. L. (1984). "The Photochemistry of a Remote Marine Stratiform Cloud." *Journal of Geophysical Research-Atmospheres* **89**(ND3): 4739-4755.
- Chameides, W. L. (1986). "Possible Role of NO₃ in the Nighttime Chemistry of a Cloud." *Journal of Geophysical Research-Atmospheres* **91**(D5): 5331-5337.
- Chameides, W. L. and A. W. Stelson (1992). "Aqueous-Phase Chemical Processes in Deliquescent Seasalt Aerosols." *Berichte Der Bunsen-Gesellschaft-Physical Chemistry Chemical Physics* **96**(3): 461-470.
- Charlson, R. J., J. E. Lovelock, M. O. Andreae and S. G. Warren (1987). "Oceanic Phytoplankton, Atmospheric Sulfur, Cloud Albedo and Climate." *Nature* **326**(6114): 655-661.
- Charlson, R. J., J. Langner, H. Rodhe, C. B. Leovy and S. G. Warren (1991). "Perturbation of the Northern-Hemisphere Radiative Balance by Backscattering from Anthropogenic Sulfate Aerosols." *Tellus Series a-Dynamic Meteorology and Oceanography* **43**(4): 152-163.
- Chawla, O. P. and R. W. Fessenden (1975). "Electron-Spin Resonance and Pulse-Radiolysis Studies of Some Reactions of SO₄⁻." *Journal of Physical Chemistry* **79**(24): 2693-2700.
- Chen, G., D. D. Davis, P. Kasibhatla, A. R. Bandy, D. C. Thornton, B. J. Huebert, A. D. Clarke and B. W. Blomquist (2000). "A study of DMS oxidation in the tropics: Comparison of Christmas Island field observations of DMS, SO₂, and DMSO with model simulations." *Journal of Atmospheric Chemistry* **37**(2): 137-160.
- Chin, M. and P. H. Wine (1992). "A Temperature-Dependent Kinetics Study of the Aqueous Phase Reactions OH+SCN⁻ → SCNOH⁻ and SCN+SCN⁻ ↔ (SCN)₂⁻." *Journal of Photochemistry and Photobiology a-Chemistry* **69**(1): 17-25.
- Chin, M. and D. D. Davis (1993). "Global Sources and Sinks of OCS and CS₂ and Their Distributions." *Global Biogeochemical Cycles* **7**(2): 321-337.
- Chin, M. and P. H. Wine (1994). "A temperature-dependent competitive kinetics study of the aqueous-phase reactions of OH radicals with formate, formic acid, acetate, acetic acid, and hydrated formaldehyde." *In: Helz, G.R., R.G. Zepp, and D.G.*

Crosby (eds.), Aquatic and Surface Photochemistry, Lewis Publishers, CRC Press, pp. 85-96.

- Chin, M., R. B. Rood, S. J. Lin, J. F. Muller and A. M. Thompson (2000a). "Atmospheric sulfur cycle simulated in the global model GOCART: Model description and global properties." Journal of Geophysical Research-Atmospheres **105**(D20): 24671-24687.
- Chin, M., D. L. Savoie, B. J. Huebert, A. R. Bandy, D. C. Thornton, T. S. Bates, P. K. Quinn, E. S. Saltzman and W. J. De Bruyn (2000b). "Atmospheric sulfur cycle simulated in the global model GOCART: Comparison with field observations and regional budgets." Journal of Geophysical Research-Atmospheres **105**(D20): 24689-24712.
- Chin, M. A. and D. J. Jacob (1996). "Anthropogenic and natural contributions to tropospheric sulfate: A global model analysis." Journal of Geophysical Research-Atmospheres **101**(D13): 18691-18699.
- Clarke, J. H. R. and L. A. Woodward (1966). "Raman Spectrophotometric Determination of Degrees of Dissociation of Methanesulphonic Acid in Aqueous Solution at 25 Degrees C." Transactions of the Faraday Society **62**(524P): 2226-2233.
- Clegg, S. L. and P. Brimblecombe (1985). "The Solubility of Methanesulfonic Acid and Its Implications for Atmospheric Chemistry." Environmental Technology Letters **6**(7): 269-278.
- Clifton, C. L. and R. E. Huie (1989). "Rate Constants for Hydrogen Abstraction Reactions of the Sulfate Radical, SO_4^- - Alcohols." International Journal of Chemical Kinetics **21**(8): 677-687.
- Conant, W. C., T. M. VanReken, T. A. Rissman, V. Varutbangkul, H. H. Jonsson, A. Nenes, J. L. Jimenez, A. E. Delia, R. Bahreini, G. C. Roberts, R. C. Flagan and J. H. Seinfeld (2004). "Aerosol-cloud drop concentration closure in warm cumulus." Journal of Geophysical Research-Atmospheres **109**: D13204, doi: 10.1029/2003JD004324.
- Cosme, E., C. Genthon, P. Martinerie, O. Boucher and M. Pham (2002). "The sulfur cycle at high-southern latitudes in the LMD-ZT General Circulation Model." Journal of Geophysical Research-Atmospheres **107**(D23): 4690-4708.
- Dacey, J. W. H., F. A. Howse, A. F. Michaels and S. G. Wakeham (1998). "Temporal variability of dimethylsulfide and dimethylsulfoniopropionate in the Sargasso Sea." Deep-Sea Research Part I-Oceanographic Research Papers **45**(12): 2085-2104.

- Davis, D., G. Chen, P. Kasibhatla, A. Jefferson, D. Tanner, F. Eisele, D. Lenschow, W. Neff and H. Berresheim (1998). "DMS oxidation in the Antarctic marine boundary layer: Comparison of model simulations and field observations of DMS, DMSO, DMSO₂, H₂SO₄(g), MSA(g), and MSA(p)." *Journal of Geophysical Research-Atmospheres* **103**(D1): 1657-1678.
- Davis, D., G. Chen, A. Bandy, D. Thornton, F. Eisele, L. Mauldin, D. Tanner, D. Lenschow, H. Fuelberg, B. Huebert, J. Heath, A. Clarke and D. Blake (1999). "Dimethyl sulfide oxidation in the equatorial Pacific: Comparison of model simulations with field observations for DMS, SO₂, H₂SO₄(g), MSA(g), MS, and NSS." *Journal of Geophysical Research-Atmospheres* **104**(D5): 5765-5784.
- Davis, D. D., F. Eisele, G. Chen, J. Crawford, G. Huey, D. Tanner, D. Slusher, L. Mauldin, S. Oncley, D. Lenschow, S. Semmer, R. Shetter, B. Lefer, R. Arimoto, A. Hogan, P. Grube, M. Lazzara, A. Bandy, D. Thornton, H. Berresheim, H. Bingemer, M. Hutterli, J. McConnell, R. Bales, J. Dibb, M. Buhr, J. Park, P. McMurry, A. Swanson, S. Meinardi and D. Blake (2004). "An overview of ISCAT 2000." *Atmospheric Environment* **38**(32): 5363-5373.
- Daykin, E. P. and P. H. Wine (1990). "A Study of the Reactions of NO₃ Radicals with Organic Sulfides - Reactivity Trend at 298-K." *International Journal of Chemical Kinetics* **22**(10): 1083-1094.
- De Bruyn, W. J., J. A. Shorter, P. Davidovits, D. R. Worsnop, M. S. Zahniser and C. E. Kolb (1994). "Uptake of Gas-Phase Sulfur Species Methanesulfonic-Acid, Dimethylsulfoxide, and Dimethyl Sulfone by Aqueous Surfaces." *Journal of Geophysical Research-Atmospheres* **99**(D8): 16927-16932.
- De Bruyn, W. J., E. Swartz, J. H. Hu, J. A. Shorter, P. Davidovits, D. R. Worsnop, M. S. Zahniser and C. E. Kolb (1995). "Henry's Law Solubilities and Setchenow Coefficients for Biogenic Reduced Sulfur Species Obtained from Gas-Liquid Uptake Measurements." *Journal of Geophysical Research-Atmospheres* **100**(D4): 7245-7251.
- De Bruyn, W. J., T. S. Bates, J. M. Cainey and E. S. Saltzman (1998). "Shipboard measurements of dimethyl sulfide and SO₂ southwest of Tasmania during the First Aerosol Characterization Experiment (ACE 1)." *Journal of Geophysical Research-Atmospheres* **103**(D13): 16703-16711.
- De Bruyn, W. J., M. Harvey, J. M. Cainey and E. S. Saltzman (2002). "DMS and SO₂ at Baring Head, New Zealand: Implications for the yield of SO₂ from DMS." *Journal of Atmospheric Chemistry* **41**(2): 189-209.
- Diaz-de-Mera, Y., A. Aranda, D. Rodriguez, R. Lopez, B. Cabanas and E. Martinez (2002). "Gas-phase reactions of chlorine atoms and ClO radicals with dimethyl

- sulfide. Rate coefficients and temperature dependences." *Journal of Physical Chemistry A* **106**(37): 8627-8633.
- Dlugokencky, E. J. and C. J. Howard (1988). "Laboratory Studies of NO₃ Radical Reactions with Some Atmospheric Sulfur-Compounds." *Journal of Physical Chemistry* **92**(5): 1188-1193.
- Dogliotti, L. and E. Hayon (1967a). "Flash photolysis of persulfate ion in aqueous solutions: study of the sulfate and ozonide radical anions." *J. Phys. Chem.* **71**: 2511-2516.
- Dogliotti, L. and E. Hayon (1967b). "Transient species produced in the photochemical decomposition of ceric salts in aqueous solution. Reactivity of nitrogen oxide and hydrogen compd. with oxygen and sulfur (HSO₄) free radicals." *J. Phys. Chem.* **71**(12): 3802-3808.
- Dogliotti, L. and a. E. Hayon (1968). "Flash photolysis study of sulfite, thiocyanate and thiosulphate ions in solution." *J. Phys. Chem.* **72**: 1800-1807.
- Eisele, F. L. and D. J. Tanner (1993). "Measurement of the Gas-Phase Concentration of H₂SO₄ and Methane Sulfonic-Acid and Estimates of H₂SO₄ Production and Loss in the Atmosphere." *Journal of Geophysical Research-Atmospheres* **98**(D5): 9001-9010.
- Elliot, A. J. and A. S. Simsons (1984). "Rate Constants for Reactions of Hydroxyl Radicals as a Function of Temperature." *Radiation Physics and Chemistry* **24**(2): 229-231.
- Elliot, A. J. and F. C. Sopchyshyn (1984). "A Pulse-Radiolysis Study of I₂⁻ and (SCN)₂⁻ in Aqueous-Solutions over the Temperature-Range 15-90 °C." *International Journal of Chemical Kinetics* **16**(10): 1247-1256.
- Elliot, A. J., D. R. Mccracken, G. V. Buxton and N. D. Wood (1990). "Estimation of Rate Constants for near-Diffusion-Controlled Reactions in Water at High-Temperatures." *Journal of the Chemical Society-Faraday Transactions* **86**(9): 1539-1547.
- Enami, S., Y. Nakano, S. Hashimoto, M. Kawasaki, S. Aloisio and J. S. Francisco (2004). "Reaction of Cl Atoms with Dimethyl Sulfide: A Theoretical Calculation and an Experimental Study with Cavity Ring-Down Spectroscopy." *J. Phys. Chem. A* **108**: in press.
- Erickson, D. J., S. J. Ghan and J. E. Penner (1990). "Global Ocean-to-Atmosphere Dimethyl Sulfide Flux." *Journal of Geophysical Research-Atmospheres* **95**(D6): 7543-7552.

- Ervens, B., S. Gligorovski and H. Herrmann (2003). "Temperature-dependent rate constants for hydroxyl radical reactions with organic compounds in aqueous solutions." *Physical Chemistry Chemical Physics* **5**(9): 1811-1824.
- Espenson, J. H. (1981). *Chemical Kinetics and Reaction Mechanisms*. New York, McGraw-Hill.
- Falbe-Hansen, H., S. Sorensen, N. R. Jensen, T. Pedersen and J. Hjorth (2000). "Atmospheric gas-phase reactions of dimethylsulphoxide and dimethylsulphone with OH and NO₃ radicals, Cl atoms and ozone." *Atmospheric Environment* **34**(10): 1543-1551.
- Flyunt, R., O. Makogon, M. N. Schuchmann, K. D. Asmus and C. von Sonntag (2001). "OH-Radical-induced oxidation of methanesulfinic acid. The reactions of the methanesulfonyl radical in the absence and presence of dioxygen." *Journal of the Chemical Society-Perkin Transactions 2*(5): 787-792.
- Fox, M. F., C. B. Smith and E. Hayon (1981). "Far-Ultraviolet Solution Spectroscopy of Thiocyanate." *Journal of the Chemical Society-Faraday Transactions I* **77**: 1497-1502.
- George, C., H. El Rassy and J. M. Chovelon (2001). "Reactivity of selected volatile organic compounds (VOCs) toward the sulfate radical (SO₄⁻)." *International Journal of Chemical Kinetics* **33**(9): 539-547.
- George, C. and J. M. Chovelon (2002). "A laser flash photolysis study of the decay of SO₄⁻ and Cl₂⁻ radical anions in the presence of Cl⁻ in aqueous solutions." *Chemosphere* **47**(4): 385-393.
- George, C., D. Rouse, E. Perraudin and R. Strekowski (2003). "A new approach for studying aqueous phase OH kinetics: application of Teflon waveguides." *Physical Chemistry Chemical Physics* **5**(8): 1562-1569.
- Gershenzon, M., P. Davidovits, J. T. Jayne, C. E. Kolb and D. R. Worsnop (2001). "Simultaneous uptake of DMS and ozone on water." *Journal of Physical Chemistry A* **105**(29): 7031-7036.
- Gmehling, J., P. Rasmussen and A. Fredenslund (1982). "Vapor-Liquid-Equilibria by Unifac Group Contribution - Revision and Extension .2." *Industrial & Engineering Chemistry Process Design and Development* **21**(1): 118-127.
- Gmitro, J. I. and T. Vermeulen (1964). "Vapor-liquid equilibria for aqueous sulfuric acid." *AIChE. J.* **10**: 740-746.
- Gondwe, M., M. Krol, W. Gieskes, W. Klaassen and H. de Baar (2003). "The contribution of ocean-leaving DMS to the global atmospheric burdens of DMS,

- MSA, SO₂, and NSS SO₄⁻." *Global Biogeochemical Cycles* **17**(2): 1056, doi: 10.1029/2002GB001937.
- Gondwe, M., M. Krol, W. Klaassen, W. Gieskes and H. de Baar (2004). "Comparison of modeled versus measured MSA : nss SO₄⁻ ratios: A global analysis." *Global Biogeochemical Cycles* **18**(2): GB2006, doi: 10.1029/2003GB002144.
- Harvey, G. R. and R. F. Lang (1986). "Dimethylsulfoxide and Dimethylsulfone in the Marine Atmosphere." *Geophysical Research Letters* **13**(1): 49-51.
- Hayon, E. and J. J. McGarvey (1967). "Flash photolysis in the vacuum ultraviolet region of SO₄²⁻, CO₃²⁻, and OH⁻ ions in aqueous solution." *J. Phys. Chem.* **70**(1472-1477).
- Hayon, E., A. Treinin and J. Wilf (1972). "Electronic spectra, photochemistry, and autoxidation mechanism of the sulfite-bisulfite, pyrosulfite systems: The SO₂⁻, SO₃⁻, SO₄⁻, and SO₅⁻ radicals." *J. Am. Chem. Soc.* **94**: 47-57.
- Heckel, E., A. Henglein and G. Beck (1966). "Pulse radiolytic investigation of the radical anion SO₄⁻." *Ber. Bunsenges. Phys. Chem.* **70**(149-154).
- Henglein, A. (1980). "Energetics of Reactions of O-Aq(-) and of O(-)-Transfer Reactions between Radicals." *Radiation Physics and Chemistry* **15**(2-3): 151-158.
- Herrmann, H., M. Exner, H. W. Jacobi, G. Raabe, A. Reese and R. Zellner (1995a). "Laboratory studies of atmospheric aqueous-phase free-radical chemistry: Kinetic and spectroscopic studies of reactions of NO₃ and SO₄⁻ radicals with aromatic compounds." *Faraday Discussions*(100): 129-153.
- Herrmann, H., A. Reese and R. Zellner (1995b). "Time-Resolved UV/Vis Diode-Array Absorption-Spectroscopy of SO_x⁻(X=3, 4, 5) Radical-Anions in Aqueous-Solution." *Journal of Molecular Structure* **348**: 183-186.
- Herrmann, H., H. W. Jacobi, G. Raabe, A. Reese and R. Zellner (1996). "Laser-spectroscopic laboratory studies of atmospheric aqueous phase free radical chemistry." *Fresenius Journal of Analytical Chemistry* **355**(3-4): 343-344.
- Herrmann, H., B. Ervens, H. W. Jacobi, R. Wolke, P. Nowacki and R. Zellner (2000). "CAPRAM2.3: A chemical aqueous phase radical mechanism for tropospheric chemistry." *Journal of Atmospheric Chemistry* **36**(3): 231-284.
- Hertel, O., J. Christensen and O. Hov (1994). "Modeling of the End-Products of the Chemical Decomposition of DMS in the Marine Boundary-Layer." *Atmospheric Environment* **28**(15): 2431-2449.
- Hoffmann, M. R. and D. J. Jacob (1984). kinetics and mechanisms of the catalytic oxidation of dissolved sulfur dioxide in aqueous solution: An application to

- nighttime fog water chemistry. *SO₂, NO and NO₂ oxidation mechanisms: Atmospheric Considerations*. J. G. Calvert. Boston, MA, Butterworth Publisher: 101-172.
- Hoffmann, M. R. (1986). "On the Kinetics and Mechanism of Oxidation of Aqueated Sulfur-Dioxide by Ozone." *Atmospheric Environment* **20**(6): 1145-1154.
- Holligan, P. M., S. M. Turner and P. S. Liss (1987). "Measurements of Dimethyl Sulfide in Frontal Regions." *Continental Shelf Research* **7**(2): 213-224.
- Hug, G. L. (1981). *Optical Spectra of Nonmetallic Inorganic Transient Species in Aqueous Solutions*, U.S. Dept. of Commerce.
- Huie, R. E. and C. L. Clifton (1989). "Rate Constants for Hydrogen Abstraction Reactions of the Sulfate Radical, SO₄⁻ - Alkanes and Ethers." *International Journal of Chemical Kinetics* **21**(8): 611-619.
- Huie, R. E., C. L. Clifton and N. Altstein (1989). "A Pulse-Radiolysis and Flash-Photolysis Study of the Radicals SO₂⁻, SO₃⁻, SO₄⁻ and SO₅⁻." *Radiation Physics and Chemistry* **33**(4): 361-370.
- Huie, R. E. and C. L. Clifton (1990). "Temperature-Dependence of the Rate Constants for Reactions of the Sulfate Radical, SO₄⁻, with Anions." *Journal of Physical Chemistry* **94**(23): 8561-8567.
- Huie, R. E., C. L. Clifton and P. Neta (1991). "Electron-Transfer Reaction-Rates and Equilibria of the Carbonate and Sulfate Radical-Anions." *Radiation Physics and Chemistry* **38**(5): 477-481.
- Hynes, A. J., P. H. Wine and D. H. Semmes (1986). "Kinetics and Mechanism of OH Reactions with Organic Sulfides." *Journal of Physical Chemistry* **90**(17): 4148-4156.
- Hynes, A. J. and P. H. Wine (1988). "Time-Resolved Resonance Raman Study of the Spectroscopy and Kinetics of the Cl₂⁻ Radical Anion in Aqueous Solution." *J. Chem. Phys.* **89**: 3565 - 3572.
- Hynes, A. J. and P. H. Wine (1989). "OH-Initiated Oxidation of Biogenic Sulfur-Compounds - Kinetics and Mechanisms under Atmospheric Conditions." *ACS Symposium Series* **393**: 424-436.
- Hynes, A. J., R. E. Stickel, A. J. Pounds, Z. Zhao, T. McKay, J. D. Bradshaw and P. H. Wine (1993). Mechanistic Studies of the OH-Initiated Oxidation of Dimethylsulfide. *Dimethylsulfide: Oceans, Atmosphere and Climate*. G. Restelli and G. Angeletti, Kluwer Academic Publishers: 211-221.

- Hynes, A. J., R. B. Stoker, A. J. Pounds, T. McKay, J. D. Bradshaw, J. M. Nicovich and P. H. Wine (1995). "A Mechanistic Study of the Reaction of OH with Dimethyl-D(6) Sulfide - Direct Observation of Adduct Formation and the Kinetics of the Adduct Reaction with O₂." *Journal of Physical Chemistry* **99**(46): 16967-16975.
- Hynes, A. J. and P. H. Wine (1996). "The atmospheric chemistry of dimethylsulfoxide (DMSO) kinetics and mechanism of the OH+DMSO reaction." *Journal of Atmospheric Chemistry* **24**(1): 23-37.
- Ingham, T., D. Bauer, R. Sander, P. J. Crutzen and J. N. Crowley (1999). "Kinetics and products of the reactions BrO+DMS and Br+DMS at 298 K." *Journal of Physical Chemistry A* **103**(36): 7199-7209.
- Iwata, A., N. Nakashima, M. Kusaba, Y. Izawa and C. Yamanaka (1993). "Quantum Yields of Hydrated Electrons by UV Laser Irradiation." *Chemical Physics Letters* **207**(2-3): 137-142.
- Jacob, D. J. (1986). "Chemistry of OH in Remote Clouds and Its Role in the Production of Formic-Acid and Peroxymonosulfate." *Journal of Geophysical Research-Atmospheres* **91**(D9): 9807-9826.
- Jacob, D. J., E. W. Gottlieb and M. J. Prather (1989). "Chemistry of a Polluted Cloudy Boundary-Layer." *Journal of Geophysical Research-Atmospheres* **94**(D10): 12975-13002.
- Jaegle, L., D. J. Jacob, W. H. Brune, I. Faloon, D. Tan, B. G. Heikes, Y. Kondo, G. W. Sachse, B. Anderson, G. L. Gregory, H. B. Singh, R. Poeschel, G. Ferry, D. R. Blake and R. E. Shetter (2000). "Photochemistry of HO_x in the upper troposphere at northern midlatitudes." *Journal of Geophysical Research-Atmospheres* **105**(D3): 3877-3892.
- Jahnke, L. S. (1999). "Measurement of hydroxyl radical-generated methane sulfinic acid by high-performance liquid chromatography and electrochemical detection." *Analytical Biochemistry* **269**(2): 273-277.
- Jayson, G. G., B. J. Parson and A. J. Swallow (1973). "Some simple, highly reactive, inorganic chlorine derivatives in aqueous solution." *J. Chem. Soc. Faraday Trans.* **69**: 1597-1607.
- Jefferson, A., F. L. Eisele, P. J. Ziemann, R. J. Weber, J. J. Marti and P. H. McMurry (1997). "Measurements of the H₂SO₄ mass accommodation coefficient onto polydisperse aerosol." *Journal of Geophysical Research-Atmospheres* **102**(D15): 19021-19028.
- Jefferson, A., D. J. Tanner, F. L. Eisele, D. D. Davis, G. Chen, J. Crawford, J. W. Huey, A. L. Torres and H. Berresheim (1998). "OH photochemistry and methane

- sulfonic acid formation in the coastal Antarctic boundary layer." *Journal of Geophysical Research-Atmospheres* **103**(D1): 1647-1656.
- Jensen, N. R., J. Hjorth, C. Lohse, H. Skov and G. Restelli (1992). "Products and Mechanisms of the Gas-Phase Reactions of NO₃ with CH₃SCH₃, CD₃SCD₃, CH₃SH and CH₃SSCH₃." *Journal of Atmospheric Chemistry* **14**(1-4): 95-108.
- Jiang, P. Y., Y. Katsumura, R. Nagaishi, M. Domae, K. Ishikawa, K. Ishigure and Y. Yoshida (1992). "Pulse-Radiolysis Study of Concentrated Sulfuric-Acid-Solutions - Formation Mechanism, Yield and Reactivity of Sulfate Radicals." *Journal of the Chemical Society-Faraday Transactions* **88**(12): 1653-1658.
- Jourdain, B. and M. Legrand (2001). "Seasonal variations of atmospheric dimethylsulfide, dimethylsulfoxide, sulfur dioxide, methanesulfonate, and non-sea-salt sulfate aerosols at Dumont d'Urville (coastal Antarctica) (December 1998 to July 1999)." *Journal of Geophysical Research-Atmospheres* **106**(D13): 14391-14408.
- Katoshevski, D., A. Nenes and J. H. Seinfeld (1999). "A study of processes that govern the maintenance of aerosols in the marine boundary layer." *Journal of Aerosol Science* **30**(4): 503-532.
- Kettle, A. J., M. O. Andreae, D. Amouroux, T. W. Andreae, T. S. Bates, H. Berresheim, H. Bingemer, R. Boniforti, M. A. J. Curran, G. R. DiTullio, G. Helas, G. B. Jones, M. D. Keller, R. P. Kiene, C. Leck, M. Levasseur, G. Malin, M. Maspero, P. Matrai, A. R. McTaggart, N. Mihalopoulos, B. C. Nguyen, A. Novo, J. P. Putaud, S. Rapsomanikis, G. Roberts, G. Schebeske, S. Sharma, R. Simo, R. Staubes, S. Turner and G. Uher (1999). "A global database of sea surface dimethylsulfide (DMS) measurements and a procedure to predict sea surface DMS as a function of latitude, longitude, and month." *Global Biogeochemical Cycles* **13**(2): 399-444.
- Kiehl, J. T. and K. E. Trenberth (1997). "Earth's annual global mean energy budget." *Bulletin of the American Meteorological Society* **78**(2): 197-208.
- Kim, K. J. and W. H. Hamill (1976). "Direct and Indirect Effects in Pulse Irradiated Concentrated Aqueous-Solutions of Chloride and Sulfate-Ions." *Journal of Physical Chemistry* **80**(21): 2320-2325.
- Kishore, K. and K. D. Asmus (1989). "Radical Cations from One-Electron Oxidation of Aliphatic Sulfoxides in Aqueous-Solution - a Radiation Chemical Study." *Journal of the Chemical Society-Perkin Transactions* **2**(12): 2079-2084.
- Kishore, K. and K. D. Asmus (1991). "Nature of 2σ/1σ* 3-Electron-Bonded Chlorine Adducts to Sulfoxides." *Journal of Physical Chemistry* **95**(19): 7233-7239.
- Klaning, U. K., K. Sehested and J. Holcman (1985). "Standard Gibbs Energy of Formation of the Hydroxyl Radical in Aqueous-Solution - Rate Constants for the

Reaction $\text{ClO}_2^- + \text{O}_3 \rightleftharpoons \text{O}_3^- + \text{ClO}_2$." *Journal of Physical Chemistry* **89**(5): 760-763.

- Klaning, U. K. and T. Wolff (1985). "Laser Flash-Photolysis of HClO, ClO⁻, HBrO, and BrO⁻ in Aqueous-Solution - Reactions of Cl Atoms and Br Atoms." *Berichte Der Bunsen-Gesellschaft-Physical Chemistry Chemical Physics* **89**(3): 243-245.
- Koga, S. and H. Tanaka (1993). "Numerical Study of the Oxidation Process of Dimethylsulfide in the Marine Atmosphere." *Journal of Atmospheric Chemistry* **17**(3): 201-228.
- Koppenol, W. H. and J. F. Liebman (1984). "The Oxidizing Nature of the Hydroxyl Radical - a Comparison with the Ferryl Ion (FeO₂⁺)." *Journal of Physical Chemistry* **88**(1): 99-101.
- Kraljic, I. (1970). "Photolytic determination of SO₄⁻ rate constant." *Int. J. Radiat. Phys. Chem.* **2**: 59.
- Kreidenweis, S. M., J. E. Penner, F. Yin and J. H. Seinfeld (1991). "The Effects of Dimethylsulfide Upon Marine Aerosol Concentrations." *Atmospheric Environment Part a-General Topics* **25**(11): 2501-2511.
- Kreidenweis, S. M., C. J. Walcek, G. Feingold, W. M. Gong, M. Z. Jacobson, C. H. Kim, X. H. Liu, J. E. Penner, A. Nenes and J. H. Seinfeld (2003). "Modification of aerosol mass and size distribution due to aqueous-phase SO₂ oxidation in clouds: Comparisons of several models." *Journal of Geophysical Research-Atmospheres* **108**(D7): 4213, doi:10.1029/2002JD002697.
- Kukui, A., D. Borissenko, G. Laverdet and G. Le Bras (2003). "Gas-phase reactions of OH radicals with dimethyl sulfoxide and methane sulfinic acid using turbulent flow reactor and chemical ionization mass spectrometry." *Journal of Physical Chemistry A* **107**(30): 5732-5742.
- Langer, S., B. T. McGovney, B. J. FinlaysonPitts and R. M. Moore (1996). "The dimethyl sulfide reaction with atomic chlorine and its implications for the budget of methyl chloride." *Geophysical Research Letters* **23**(13): 1661-1664.
- Langner, J. and H. Rodhe (1991). "A Global 3-Dimensional Model of the Tropospheric Sulfur Cycle." *Journal of Atmospheric Chemistry* **13**(3): 225-263.
- Leck, C., U. Larsson, L. E. Bagander, S. Johansson and S. Hajdu (1990). "Dimethyl Sulfide in the Baltic Sea - Annual Variability in Relation to Biological-Activity." *Journal of Geophysical Research-Oceans* **95**(C3): 3353-3363.

- Lee, Y. N. and X. L. Zhou (1994). "Aqueous Reaction-Kinetics of Ozone and Dimethylsulfide and Its Atmospheric Implications." *Journal of Geophysical Research-Atmospheres* **99**(D2): 3597-3605.
- Legrand, M., J. Sciare, B. Jourdain and C. Genthon (2001). "Subdaily variations of atmospheric dimethylsulfide, dimethylsulfoxide, methanesulfonate, and non-sea-salt sulfate aerosols in the atmospheric boundary layer at Dumont d'Urville (coastal Antarctica) during summer." *Journal of Geophysical Research-Atmospheres* **106**(D13): 14409-14422.
- Lelieveld, J., P. J. Crutzen and H. Rodhe (1989). "Zonal average cloud characteristics for global atmospheric chemistry modelling." *Tech. Rep. CM-76, Dep. of Meteorology, Univ. of Stockholm (MISU)*.
- Lelieveld, J. and P. J. Crutzen (1991). "The Role of Clouds in Tropospheric Photochemistry." *Journal of Atmospheric Chemistry* **12**(3): 229-267.
- Lelieveld, J., G. J. Roelofs, L. Ganzeveld and J. Feichter (1997). "Terrestrial sources and distribution of atmospheric sulfur." *Phil. Tran. R. Soc. Lond. B* **352**(1350): 149-158.
- Lightfoot, P. D., R. A. Cox, J. N. Crowley, M. Destriau, G. D. Hayman, M. E. Jenkin, G. K. Moortgat and F. Zabel (1992). "Organic Peroxy-Radicals - Kinetics, Spectroscopy and Tropospheric Chemistry." *Atmospheric Environment Part a-General Topics* **26**(10): 1805-1961.
- Lind, J. and a. T. E. Eriksen (1975). "Pulse radiolysis of methanesulfonic acid." *Radiochem. Radioanal. Lett.* **21**: 177-181.
- Liss, P. S. and L. Merlivat (1986). Air-sea gas exchange rates: introduction and synthesis. *The Role of Air-Sea Exchange in Geochemical Cycling*. H. Reidel. MA, Boat-Menard: 113-127.
- Liss, P. S., A. D. Hatton, G. Malin, P. D. Nightingale and S. M. Turner (1997). "Marine sulphur emissions." *Philosophical Transactions of the Royal Society of London Series B-Biological Sciences* **352**(1350): 159-168.
- Logan, S. R. and a. G. A. Salmon (1984). "Discrepancies between the rate constants for the reactions of hydroxyl radicals with ferrocenyl-substituted carboxylic acids determined by direct measurement and by competition with thiocyanate-ion." *Radiat. Phys. Chem.* **24**: 593-595.
- Logan, S. R. (1989). "Redox Reactions of Organic Radicals with Ferrocene Ferricenium Species in Aqueous-Solution .1. Radicals Derived from Carboxylic-Acids." *Journal of the Chemical Society-Perkin Transactions* **2**(7): 751-754.

- Lohmann, U. and J. Feichter (1997). "Impact of sulfate aerosols on albedo and lifetime of clouds: A sensitivity study with the ECHAM4 GCM." *Journal of Geophysical Research-Atmospheres* **102**(D12): 13685-13700.
- Lovelock, J. E., R. J. Maggs and Rasmussen, R. (1972). "Atmospheric Dimethyl Sulfide and Natural Sulfur Cycle." *Nature* **237**(5356): 452-453.
- Luria, M. and A. A. Treinin (1968). "The photochemistry of NCS^- in solution." *J. Phys. Chem.* **72**: 305-308.
- Madhavan, V., H. Levanon and P. Neta (1978). "Decarboxylation by SO_4^- Radicals." *Radiation Research* **76**(1): 15-22.
- Malone, S. D. and J. F. Endicott (1972). "Photochemical Behavior of Cobalt Complexes Containing Macrocyclic (N-4) Ligands - Oxidation-Reduction Chemistry of Dihalogen Radical Anions." *Journal of Physical Chemistry* **76**(16): 2223-2229.
- Manov, G. G., R. G. Bates, W. J. Hamer and S. F. Acree (1943). "Values of the constants in the Debye-Huckel equation for activity coefficients." *J. Am. Chem. Soc.* **65**: 1765-1767.
- Mari, C., K. Suhre, R. Rosset, T. S. Bates, B. J. Huebert, A. R. Bandy, D. C. Thornton and S. Businger (1999). "One-dimensional modeling of sulfur species during the First Aerosol Characterization Experiment (ACE 1) Lagrangian B." *Journal of Geophysical Research-Atmospheres* **104**(D17): 21733-21749.
- Martinez, E., J. Albaladejo, E. Jimenez, A. Notario and A. Aranda (1999). "Kinetics of the reaction of CH_3S with NO_2 as a function of temperature." *Chemical Physics Letters* **308**(1-2): 37-44.
- Martinez, E., J. Albaladejo, A. Notario and E. Jimenez (2000). "A study of the atmospheric reaction of CH_3S with O_3 as a function of temperature." *Atmospheric Environment* **34**(29-30): 5295-5302.
- Martins, L. J. A. (1982). "Electron-Transfer Reactions of the 2-Nitrothiophen Triplet-State Studied by Laser Flash-Photolysis." *Journal of the Chemical Society-Faraday Transactions I* **78**: 533-543.
- Martire, D. O., J. A. Rosso, S. Bertolotti, G. C. Le Roux, A. M. Braun and M. C. Gonzalez (2001). "Kinetic study of the reactions of chlorine atoms and Cl_2^- radical anions in aqueous solutions. II. Toluene, benzoic acid, and chlorobenzene." *Journal of Physical Chemistry A* **105**(22): 5385-5392.
- Matheson, M. S., W. A. Mulac and J. Rabani (1963). "Formation of Hydrated Electron in Flash Photolysis of Aqueous Solutions." *Journal of Physical Chemistry* **67**(12): 2613-2617.

- McElroy, W. J. (1990). "A Laser Photolysis Study of the Reaction of SO_4^- with Cl^- and the Subsequent Decay of Cl_2^- in Aqueous-Solution." *Journal of Physical Chemistry* **94**(6): 2435-2441.
- McElroy, W. J. and S. J. Waygood (1990). "Kinetics of the Reactions of the SO_4^- Radical with SO_4^- , $\text{S}_2\text{O}_8^{2-}$, H_2O and Fe^{2+} ." *Journal of the Chemical Society-Faraday Transactions* **86**(14): 2557-2564.
- Medina, J. A. and A. Nenes (2004). "Effects of Film Forming Compounds on the growth of Giant CCN: Implications for cloud microphysics and the aerosol indirect effect." *J. Geophys. Res.* **109**: D20207, doi:10.1029/2004JD004666.
- Meissner, G., A. Henglein and G. Beck (1967). "Pulsradiolytische Untersuchung Von Dimethylthioether Und Dimethylsulfoxyd in Wassriger Losung." *Zeitschrift Fur Naturforschung Part B-Chemie Biochemie Biophysik Biologie Und Verwandten Gebiete* **B 22**(1): 13-19.
- Milne, P. L., R. G. Zika and E. S. Saltzman (1989). Rate of reaction of methanesulfonic acid, dimethyl sulfoxide, and dimethyl sulfone with hydroxyl radical in aqueous solution. *Biogenic Sulfur in the Environment*. E. S. Saltzman and W. J. Cooper. **ACS. Symp. Ser 393**: 518-528.
- Molina, M. J., L. T. Molina and C. E. Kolb (1996). "Gas-phase and heterogeneous chemical kinetics of the troposphere and stratosphere." *Annual Review of Physical Chemistry* **47**: 327-367.
- Mozurkewich, M. (1986). "Comment on "Possible role of NO_3 in the nighttime chemistry of a cloud: by William L. Chameides." *J. Geophys. Res.* **91**: 14,569-14,570.
- Nagarajan, V. and R. W. Fessenden (1985). "Flash-Photolysis of Transient Radicals .1. Cl_2^- , Br_2^- , I_2^- and SCN_2^- ." *Journal of Physical Chemistry* **89**(11): 2330-2335.
- Nakano, Y., M. Goto, S. Hashimoto, M. Kawasaki and T. J. Wallington (2001). "Cavity ring-down spectroscopic study of the reactions of Br atoms and BrO radicals with dimethyl sulfide." *Journal of Physical Chemistry A* **105**(49): 11045-11050.
- Neta, P., R. E. Huie and A. B. Ross (1988). "Rate Constants for Reactions of Inorganic Radicals in Aqueous-Solution." *Journal of Physical and Chemical Reference Data* **17**(3): 1027-1284.
- Nguyen, B. C., N. Mihalopoulos and S. Belviso (1990). "Seasonal-Variation of Atmospheric Dimethylsulfide at Amsterdam Island in the Southern Indian-Ocean." *Journal of Atmospheric Chemistry* **11**(1-2): 123-141.

- Nord, G., B. Pedersen and O. Farver (1978). "Outer-Sphere Oxidation of Iodide and Thiocyanate by Tris(2,2'-Bipyridyl) Osmium(Iii) and Tris(1,10-Phenanthroline) Osmium(Iii) in Aqueous-Solutions." *Inorganic Chemistry* **17**(8): 2233-2238.
- Nord, G., B. Pedersen, E. Floryanlovborg and P. Pagsberg (1982). "Outer-Sphere Oxidation .2. Pulse-Radiolysis Study of the Rates of Reaction of the I_2^- and SCN_2^- Radical-Anions with the Tris(2,2'-Bipyridyl)₂ Complexes of Os(Ii) and Os(Iii)." *Inorganic Chemistry* **21**(6): 2327-2330.
- North, A. M. (1964). *The Collision Theory of Chemical Reactions in Liquids*. London, Methuen.
- Nowak, J. B., D. D. Davis, G. Chen, F. L. Eisele, R. L. Mauldin, D. J. Tanner, C. Cantrell, E. Kosciuch, A. Bandy, D. Thornton and A. Clarke (2001). "Airborne observations of DMSO, DMS, and OH at marine tropical latitudes." *Geophysical Research Letters* **28**(11): 2201-2204.
- Noxon, J. F. (1983). "NO₃ and NO₂ in the Mid-Pacific Troposphere." *Journal of Geophysical Research-Oceans and Atmospheres* **88**(NC15): 1017-1021.
- Noyes, R. M. (1961). Effects of diffusion rates on chemical kinetics. *Progress in Reaction Kinetics*. G. Porter, F.R.S., B. Stevens, M.A. and D.Phil. London. **1**: 129-160.
- Olson, T. M. and R. W. Fessenden (1992). "Pulse-Radiolysis Study of the Reaction of OH-Bullet Radicals with Methanesulfonate and Hydroxymethanesulfonate." *Journal of Physical Chemistry* **96**(8): 3317-3320.
- Padmaja, S., P. Neta and R. E. Huie (1992). "Rate Constants and Temperature Effects for Reactions of Cl₂⁻ with Unsaturated Alcohols and Hydrocarbons in Aqueous and Acetonitrile Water Solutions." *Journal of Physical Chemistry* **96**(8): 3354-3359.
- Pandis, S. N. and J. H. Seinfeld (1989). "Sensitivity Analysis of a Chemical Mechanism for Aqueous-Phase Atmospheric Chemistry." *Journal of Geophysical Research-Atmospheres* **94**(D1): 1105-1126.
- Patroescu, I. V., I. Barnes, K. H. Becker and N. Mihalopoulos (1999). "FT-IR product study of the OH-initiated oxidation of DMS in the presence of NO_x. (vol 33, pg 25, 1999)." *Atmospheric Environment* **33**(18): 3083-3084.
- Penner, J. E., C. A. Atherton and T. E. Graedel (1994). Global emissions and models of photochemically active compounds. *Global atmospheric-biospheric chemistry*. R. Prinn. New York, Plenum Press: 223-248.

- Pham, M., J. F. Muller, G. P. Brasseur, C. Granier and G. Megie (1995). "A three-dimensional study of the tropospheric sulfur cycle." *Journal of Geophysical Research-Atmospheres* **100**(D12): 26061-26092.
- Poschl, U., M. Canagaratna, J. T. Jayne, L. T. Molina, D. R. Worsnop, C. E. Kolb and M. J. Molina (1998). "Mass accommodation coefficient of H₂SO₄ vapor on aqueous sulfuric acid surfaces and gaseous diffusion coefficient of H₂SO₄ in N₂/H₂O." *Journal of Physical Chemistry A* **102**(49): 10082-10089.
- Prinn, R. G., R. F. Weiss, B. R. Miller, J. Huang, F. N. Alyea, D. M. Cunnold, P. J. Fraser, D. E. Hartley and P. G. Simmonds (1995). "Atmospheric Trends and Lifetime of CH₃CCl₃ and Global OH Concentrations." *Science* **269**(5221): 187-192.
- Pryor, W. A., D. H. Giamalva and D. F. Church (1984). "Kinetics of Ozonation .2. Amino-Acids and Model Compounds in Water and Comparisons to Rates in Nonpolar-Solvents." *Journal of the American Chemical Society* **106**(23): 7094-7100.
- Pszenny, A. A. P., W. C. Keene, D. J. Jacob, S. Fan, J. R. Maben, M. P. Zetwo, M. Springeryoung and J. N. Galloway (1993). "Evidence of Inorganic Chlorine Gases Other Than Hydrogen-Chloride in Marine Surface Air." *Geophysical Research Letters* **20**(8): 699-702.
- Putaud, J. P., B. M. Davison, S. F. Watts, N. Mihalopoulos, B. C. Nguyen and C. N. Hewitt (1999). "Dimethylsulfide and its oxidation products at two sites in Brittany (France)." *Atmospheric Environment* **33**(4): 647-659.
- Reuvers, A. P., Greensto.Cl, J. Borsa and J. D. Chapman (1973). "Studies on Mechanism of Chemical Radioprotection by Dimethyl Sulfoxide." *International Journal of Radiation Biology* **24**(5): 533-536.
- Robke, W., M. Renz and A. Henglein (1969). "Pulseradiolyse der anionen S₂O₈²⁻ und HSO₅⁻ in wassriger losung." *Int. J. Radiat. Phys. Chem* **1**: 39-44.
- Saltzman, E. S., D. L. Savoie, R. G. Zika and J. M. Prospero (1983). "Methane Sulfonic-Acid in the Marine Atmosphere." *Journal of Geophysical Research-Oceans and Atmospheres* **88**(NC15): 897-902.
- Sander, R. and P. J. Crutzen (1996). "Model study indicating halogen activation and ozone destruction in polluted air masses transported to the sea." *Journal of Geophysical Research-Atmospheres* **101**(D4): 9121-9138.
- Savoie, D. I., J. M. Prospero, R. J. Larsen, F. Huang, M. A. Izaguirre, T. Huang, T. H. Snowdon, L. Custals and C. G. Sanderson (1993). "Nitrogen and Sulfur Species in

- Antarctic Aerosols at Mawson, Palmer Station, and Marsh (King George Island)." *Journal of Atmospheric Chemistry* **17**(2): 95-122.
- Scaduto, R. C. (1995). "Oxidation of DMSO and Methanesulfinic Acid by the Hydroxyl Radical." *Free Radical Biology and Medicine* **18**(2): 271-277.
- Schoneich, C. and K. Bobrowski (1993). "Intramolecular Hydrogen-Transfer as the Key Step in the Dissociation of Hydroxyl Radical Adducts of (Alkylthio)Ethanol Derivatives." *Journal of the American Chemical Society* **115**(15): 6538-6547.
- Schwarz, H. A. and R. W. Dodson (1984). "Equilibrium between Hydroxyl Radicals and Thallium(I) and the Oxidation Potential of OH(Aq)." *Journal of Physical Chemistry* **88**(16): 3643-3647.
- Schwarz, H. A. and B. H. J. Bielski (1986). "Reactions of HO₂ and O₂⁻ with Iodine and Bromine and the I₂⁻ and I Atom Reduction Potentials." *Journal of Physical Chemistry* **90**(7): 1445-1448.
- Sciare, J., E. Baboukas, M. Kanakidou, U. Krischke, S. Belviso, H. Bardouki and N. Mihalopoulos (2000a). "Spatial and temporal variability of atmospheric sulfur-containing gases and particles during the Albatross campaign." *Journal of Geophysical Research-Atmospheres* **105**(D11): 14433-14448.
- Sciare, J., M. Kanakidou and N. Mihalopoulos (2000b). "Diurnal and seasonal variation of atmospheric dimethylsulfoxide at Amsterdam Island in the southern Indian Ocean." *Journal of Geophysical Research-Atmospheres* **105**(D13): 17257-17265.
- Sciare, J., N. Mihalopoulos and F. J. Dentener (2000c). "Interannual variability of atmospheric dimethylsulfide in the southern Indian Ocean." *Journal of Geophysical Research-Atmospheres* **105**(D21): 26369-26377.
- Sciare, J., E. Baboukas and N. Mihalopoulos (2001). "Short-term variability of atmospheric DMS and its oxidation products at Amsterdam Island during summer time." *Journal of Atmospheric Chemistry* **39**(3): 281-302.
- Sehested, K., J. Holcman and E. J. Hart (1983). "Rate Constants and Products of the Reactions of e_{aq}⁻, O₂⁻, and H with Ozone in Aqueous-Solutions." *Journal of Physical Chemistry* **87**(11): 1951-1954.
- Sehested, K. and J. Holcman (1996). "A pulse radiolysis study of the OH radical induced autoxidation of methanesulfinic acid." *Radiation Physics and Chemistry* **47**(3): 357-360.
- Seinfeld, J. H. (1986). *Air Pollution*. New York, Wiley and Sons.

- Seinfeld, J. H. and S. N. Pandis (1998). *Atmospheric Chemistry and Physics: From air pollution to climate change*. New York, John Wiley & Sons.
- Shaw, G. E. (1983). "Bio-Controlled Thermostasis Involving the Sulfur Cycle." *Climatic Change* **5**(3): 297-303.
- Shaw, G. E. (1987). "Aerosols as Climate Regulators - a Climate Biosphere Linkage." *Atmospheric Environment* **21**(4): 985-986.
- Shon, Z. H., D. Davis, G. Chen, G. Grodzinsky, A. Bandy, D. Thornton, S. Sandholm, J. Bradshaw, R. Stickel, W. Chameides, G. Kok, L. Russell, L. Mauldin, D. Tanner and F. Eisele (2001). "Evaluation of the DMS flux and its conversion to SO₂ over the southern ocean." *Atmospheric Environment* **35**(1): 159-172.
- Singh, H. B., A. N. Thakur, Y. E. Chen and M. Kanakidou (1996). "Tetrachloroethylene as an indicator of low Cl atom concentrations in the troposphere." *Geophysical Research Letters* **23**(12): 1529-1532.
- Sorensen, S., H. FalbeHansen, M. Mangoni, J. Hjorth and N. R. Jensen (1996). "Observation of DMSO and CH₃S(O)OH from the gas phase reaction between DMS and OH." *Journal of Atmospheric Chemistry* **24**(3): 299-315.
- Spicer, C. W., E. G. Chapman, B. J. Finlayson-Pitts, R. A. Plastridge, J. M. Hubbe, J. D. Fast and C. M. Berkowitz (1998). "Unexpectedly high concentrations of molecular chlorine in coastal air." *Nature* **394**(6691): 353-356.
- Spiro, P. A., D. J. Jacob and J. A. Logan (1992). "Global Inventory of Sulfur Emissions with 1-Degrees-X1-Degrees Resolution." *Journal of Geophysical Research-Atmospheres* **97**(D5): 6023-6036.
- Stanbury, D. M., W. K. Wilmarth, S. Khalaf, H. N. Po and J. E. Byrd (1980). "Oxidation of Thiocyanate and Iodide by Iridium(Iv)." *Inorganic Chemistry* **19**(9): 2715-2722.
- Stevens, B., G. Feingold, W. R. Cotton and R. L. Walko (1996). "Elements of the microphysical structure of numerically simulated nonprecipitating stratocumulus." *Journal of the Atmospheric Sciences* **53**(7): 980-1006.
- Stickel, R. E., J. M. Nicovich, S. Wang, Z. Zhao and P. H. Wine (1992). "Kinetic and Mechanistic Study of the Reaction of Atomic Chlorine with Dimethyl Sulfide." *Journal of Physical Chemistry* **96**(24): 9875-9883.
- Sumiyoshi, T. and M. Katayama (1987). "Novel Transient Absorption of Irradiated DMSO in Carbon-Tetrachloride as Studied by Pulse-Radiolysis." *Chemistry Letters*(6): 1125-1126.

- Tan, D., I. Faloon, J. B. Simpas, W. Brune, J. Olson, J. Crawford, M. Avery, G. Sachse, S. Vay, S. Sandholm, H. W. Guan, T. Vaughn, J. Mastromarino, B. Heikes, J. Snow, J. Podolske and H. Singh (2001). "OH and HO₂ in the tropical Pacific: Results from PEM-Tropics B." *Journal of Geophysical Research-Atmospheres* **106**(D23): 32667-32681.
- Tang, Y., R. P. Thorn, R. L. Mauldin and P. H. Wine (1988). "Kinetics and Spectroscopy of the SO₄⁻ Radical in Aqueous-Solution." *Journal of Photochemistry and Photobiology a-Chemistry* **44**(3): 243-258.
- Thornton, A. T. and G. S. Laurence (1973). "Kinetics of Oxidation of Transition-Metal Ions by Halogen Radical-Anions .2. Oxidation of Cobalt(Ii) by Dichloride Ions Generated by Flash-Photolysis." *Journal of the Chemical Society-Dalton Transactions*(16): 1632-1636.
- Toumi, R. (1994). "BrO as a Sink for Dimethylsulfide in the Marine Atmosphere." *Geophysical Research Letters* **21**(2): 117-120.
- Tuazon, E. C., S. M. Aschmann and R. Atkinson (1999). "Products of the gas-phase reaction of the OH radical with the dibasic ester CH₃OC(O)CH₂CH₂CH₂C(O)OCH₃." *Environmental Science & Technology* **33**(17): 2885-2890.
- Turner, S. M., G. Malin, P. S. Liss, D. S. Harbour and P. M. Holligan (1988). "The Seasonal-Variation of Dimethyl Sulfide and Dimethylsulfoniopropionate Concentrations in Nearshore Waters." *Limnology and Oceanography* **33**(3): 364-375.
- Turner, S. M., G. Malin, P. D. Nightingale and P. S. Liss (1996a). "Seasonal variation of dimethyl sulphide in the North Sea and an assessment of fluxes to the atmosphere." *Marine Chemistry* **54**(3-4): 245-262.
- Turner, S. M., P. D. Nightingale, L. J. Spokes, M. I. Liddicoat and P. S. Liss (1996b). "Increased dimethyl sulphide concentrations in sea water from in situ iron enrichment." *Nature* **383**(6600): 513-517.
- Turnipseed, A. A., S. B. Barone and A. R. Ravishankara (1993). "Reactions of CH₃S and CH₃SOO with O₃, NO₂, and NO." *Journal of Physical Chemistry* **97**(22): 5926-5934.
- Turnipseed, A. A., S. B. Barone and A. R. Ravishankara (1996). "Reaction of OH with dimethyl sulfide 2. Products and mechanisms." *Journal of Physical Chemistry* **100**(35): 14703-14713.
- Tyndall, G. S. and A. R. Ravishankara (1989a). "Atmospheric Reactions of CH₃S Radicals." *Acs Symposium Series* **393**: 450-458.

- Tyndall, G. S. and A. R. Ravishankara (1989b). "Kinetics of the Reaction of CH₃S with O₃ at 298-K." *Journal of Physical Chemistry* **93**(12): 4707-4710.
- Tyndall, G. S. and A. R. Ravishankara (1991). "Atmospheric Oxidation of Reduced Sulfur Species." *International Journal of Chemical Kinetics* **23**(6): 483-527.
- Tyndall, G. S., R. A. Cox, C. Granier, R. Lesclaux, G. K. Moortgat, M. J. Pilling, A. R. Ravishankara and T. J. Wallington (2001). "Atmospheric chemistry of small organic peroxy radicals." *Journal of Geophysical Research-Atmospheres* **106**(D11): 12157-12182.
- Urbanski, S. P., R. E. Stickel, Z. Z. Zhao and P. H. Wine (1997). "Mechanistic and kinetic study of formaldehyde production in the atmospheric oxidation of dimethyl sulfide." *Journal of the Chemical Society-Faraday Transactions* **93**(16): 2813-2819.
- Urbanski, S. P., R. E. Stickel and P. H. Wine (1998). "Mechanistic and kinetic study of the gas-phase reaction of hydroxyl radical with dimethyl sulfoxide." *Journal of Physical Chemistry A* **102**(51): 10522-10529.
- Urbanski, S. P. and P. H. Wine (1999). "Spectroscopic and kinetic study of the Cl-S(CH₃)₂ adduct." *Journal of Physical Chemistry A* **103**(50): 10935-10944.
- Veltwisch, D., E. Janata and K. D. Asmus (1980). "Primary Processes in the Reaction of OH-Radicals with Sulfoxides." *Journal of the Chemical Society-Perkin Transactions* **2**(1): 146-153.
- Vogt, R., P. J. Crutzen and R. Sander (1996). "A mechanism for halogen release from sea-salt aerosol in the remote marine boundary layer." *Nature* **383**(6598): 327-330.
- von Glasow, R. and P. J. Crutzen (2004). "Model study of multiphase DMS oxidation with a focus on halogens." *Atmospheric Chemistry and Physics* **4**: 589-608.
- Vrekoussis, M., M. Kanakidou, N. Mihalopoulos, P. J. Crutzen, J. Lelieveld, D. Perner, H. Berresheim and E. Baboukas (2004). "Role of the NO₃ radicals in oxidation processes in the eastern Mediterranean troposphere during the MINOS campaign." *Atmospheric Chemistry and Physics* **4**: 169-182.
- Walling, C. and G. M. El-Taliawi (1973). "Fentons Reagent .2. Reactions of Carbonyl-Compounds and Alpha,Beta-Unsaturated Acids." *Journal of the American Chemical Society* **95**(3): 844-847.
- Wallington, T. J., P. Dagaut and M. J. Kurylo (1992). "Ultraviolet-Absorption Cross-Sections and Reaction-Kinetics and Mechanisms for Peroxy-Radicals in the Gas-Phase." *Chemical Reviews* **92**(4): 667-710.

- Wallington, T. J., T. Ellermann and O. J. Nielsen (1993). "Atmospheric Chemistry of Dimethyl Sulfide - UV Spectra and Self-Reaction Kinetics of CH_3SCH_2 and $\text{CH}_3\text{SCH}_2\text{O}_2$ Radicals and Kinetics of the Reactions $\text{CH}_3\text{SCH}_2 + \text{O}_2 \rightarrow \text{CH}_3\text{SCH}_2\text{O}_2$ and $\text{CH}_3\text{SCH}_2\text{O}_2 + \text{NO} \rightarrow \text{CH}_3\text{SCH}_2\text{O} + \text{NO}_2$." *Journal of Physical Chemistry* **97**(32): 8442-8449.
- Wanninkhof, R. (1992). "Relationship between Wind-Speed and Gas-Exchange over the Ocean." *Journal of Geophysical Research-Oceans* **97**(C5): 7373-7382.
- Warneck, P. (1988). *Chemistry of the natural atmosphere*. San Diego, Academic Press.
- Watts, S. F., A. Watson and P. Brimblecombe (1987). "Measurements of the Aerosol Concentrations of Methanesulfonic Acid, Dimethyl-Sulfoxide and Dimethyl Sulfone in the Marine Atmosphere of the British-Isles." *Atmospheric Environment* **21**(12): 2667-2672.
- Watts, S. F., P. Brimblecombe and A. J. Watson (1990). "Methanesulfonic-Acid, Dimethyl-Sulfoxide and Dimethyl Sulfone in Aerosols." *Atmospheric Environment Part a-General Topics* **24**(2): 353-359.
- Weast, R. C. (1980). *CRC Handbook of Chemistry and Physics, 61 st Edition*. Boca Raton, FL, CRC Press, Inc.
- Weingartner, H. (1982). "Self diffusion in liquid water. A reassessment." *Zeitschrift fur Phys. Chem.* **132**: 129-149.
- White, J. U. (1942). "Long optical paths of large aperture." *J. Opt. Soc. Am* **32**: 285-288.
- Wicktor, F., A. Donati, H. Herrmann and R. Zellner (2003). "Laser based spectroscopic and kinetic investigations of reactions of the Cl atom with oxygenated hydrocarbons in aqueous solution." *Physical Chemistry Chemical Physics* **5**(12): 2562-2572.
- Williams, M. B., P. Campuzano-Jost, D. Bauer and A. J. Hynes (2001). "Kinetic and mechanistic studies of the OH-initiated oxidation of dimethylsulfide at low temperature - A reevaluation of the rate coefficient and branching ratio." *Chemical Physics Letters* **344**(1-2): 61-67.
- Wine, P. H., R. J. Thompson, A. R. Ravishankara, D. H. Semmes, C. A. Gump, A. Torabi and J. M. Nicovich (1984). "Kinetics of the Reaction $\text{OH} + \text{SO}_2 + \text{M} \rightarrow \text{HOSO}_2 + \text{M}$. Temperature and Pressure-Dependence in the Falloff Region." *Journal of Physical Chemistry* **88**(10): 2095-2104.
- Wine, P. H., R. L. Mauldin and R. P. Thorn (1988). "Kinetics and Spectroscopy of the NO_3 Radical in Aqueous Ceric Nitrate Nitric-Acid Solutions." *Journal of Physical Chemistry* **92**(5): 1156-1162.

- Wine, P. H., Y. Tang, R. P. Thorn, J. R. Wells and D. D. Davis (1989). "Kinetics of Aqueous Phase Reactions of the SO_4^- Radical with Potential Importance in Cloud Chemistry." *Journal of Geophysical Research-Atmospheres* **94**(D1): 1085-1094.
- Wingenter, O. W., M. K. Kubo, N. J. Blake, T. W. Smith, D. R. Blake and F. S. Rowland (1996). "Hydrocarbon and halocarbon measurements as photochemical and dynamical indicators of atmospheric hydroxyl, atomic chlorine, and vertical mixing obtained during Lagrangian flights." *Journal of Geophysical Research-Atmospheres* **101**(D2): 4331-4340.
- Wu, G.-Z., Y. Katsumura, Y. Muroya, M. Lin and T. Morioka (2001). "Temperature dependence of $(\text{SCN})_2^-$ in water at 25 - 400 °C: Absorption spectrum, equilibrium constant, and decay." *J. Phys. Chem. A* **105**: 4933-4939.
- Wudl, F., D. A. Lightner and D. J. Cram (1967). "Methanesulfinic Acid and Its Properties." *J. American Chem. Soc.* **89**(16): 4099-4101.
- Yin, F. D., D. Grosjean, R. C. Flagan and J. H. Seinfeld (1990a). "Photooxidation of Dimethyl Sulfide and Dimethyl Disulfide .2. Mechanism Evaluation." *Journal of Atmospheric Chemistry* **11**(4): 365-399.
- Yin, F. D., D. Grosjean and J. H. Seinfeld (1990b). "Photooxidation of Dimethyl Sulfide and Dimethyl Disulfide .1. Mechanism Development." *Journal of Atmospheric Chemistry* **11**(4): 309-364.
- Yu, X. Y. and J. R. Barker (2003a). "Hydrogen peroxide photolysis in acidic aqueous solutions containing chloride ions. II. Quantum yield of $\text{HO}(\text{Aq})$ radicals." *Journal of Physical Chemistry A* **107**(9): 1325-1332.
- Yu, X. Y. and J. R. Barker (2003b). "Hydrogen peroxide photolysis in acidic aqueous solutions containing chloride ions. I. Chemical mechanism." *Journal of Physical Chemistry A* **107**(9): 1313-1324.
- Yu, X. Y., Z. C. Bao and J. R. Barker (2004). "Free radical reactions involving Cl , Cl_2^- , and SO_4^- in the 248 nm photolysis of aqueous solutions containing $\text{S}_2\text{O}_8^{2-}$ and Cl^- ." *Journal of Physical Chemistry A* **108**(2): 295-308.
- Zhao, Z., R. E. Stickel and P. H. Wine (1996). "Branching ratios for methyl elimination in the reactions of OD radicals and Cl atoms with CH_3SCH_3 ." *Chemical Physics Letters* **251**(1-2): 59-66.
- Zhu, L., J. M. Nicovich and P. H. Wine (2003a). "Temperature-dependent kinetics studies of aqueous phase reactions of SO_4^- radicals with dimethylsulfoxide, dimethylsulfone, and methanesulfonate." *Journal of Photochemistry and Photobiology a-Chemistry* **157**(2-3): 311-319.

Zhu, L., J. M. Nicovich and P. H. Wine (2003b). "Temperature-dependent kinetics studies of aqueous phase reactions of hydroxyl radicals with dimethylsulfoxide, dimethylsulfone, and methanesulfonate." *Aquatic Sciences* **65**(4): 425-435.